Use Authorization

In presenting this thesis in partial fulfillment of the requirements for an advanced degree at Idaho State University, I agree that the Library shall make it freely available for inspection. I further state that permission for extensive copying of my thesis for scholarly purposes may be granted by the Dean of Graduate School, Dean of my academic division, or by the University Librarian. It is understood that any copying or publication of this thesis for financial gain shall not be allowed without my written permission.

Signature ___________________________

Date_______________________________

Experimental Investigations of Full-Scale MetRock Structural Concrete Insulated Panels (SCIPs)

by

Karma Tenzing Gurung

A thesis

submitted in partial fulfillment

of the requirements for the degree of

Master of Science in the Department of Civil and Environmental Engineering

Idaho State University

Summer 2019

Committee Approval

To the Graduate Faculty:

The members of the committee appointed to examine the thesis of Karma Tenzing Gurung find it satisfactory and recommended that it be accepted.

Major Advisor

Dr. Mustafa Mashal

Committee Member

Dr. Arya Ebrahimpour

Graduate Faculty Representative

Dr. Steve Chiu

Acknowledgments

I would like to acknowledge all those who helped throughout this project. I could not have done it without the support of my family, colleagues, and advisors.

Firstly, I would like to express my deepest gratitude to my primary advisor and mentor Dr. Mustafa Mashal, for his guidance and continuous support. I would like to acknowledge Dr. Arya Ebrahimpour the committee member and Dr. Steve Chiu the Graduate Faculty Representative. A thank you to Jared Cantrell, Mahesh Acharya and the entire structural team at Idaho State University for helping me execute this project. I would also like to acknowledge Dr. Irene van Woerden and Ali Shokrgozar for their help with the data analysis. A thank you to MetRock SCIP Inc. and its parent company Blastcrete Equipment Company, and to Pocatello Ready Mix for their generosity in providing material and supplies used for the experimental program. Lastly and most importantly, I would like to thank my parents Sunil and Sonam Gurung and my entire family, for their continuous love and support.

Table of Contents

List of Figures

List of Tables

THESIS ABSTRACT

Experimental Investigations of Full-Scale MetRock Structural Concrete Insulated Panels (SCIPs)

Idaho State University (2019)

The Structural Concrete Insulated Panel or SCIP is an alternative construction to tradational wood framing. This research includes a full-scale investigate of the in–plane and out-of-plane flexural properties of MetRock SCIPs. MR panels are a variation of SCIPs that are commercially available in the US. For this experiment 12 full-scale MR panels were tested as floor slabs and structural walls.

The out-of-plane testing of MR slabs showed that the short span (10 feet) panels are a good alternative for floors in residential housing. The short span panel behaved as a semi-composite section and achieved 66% capacity of a fully-composite panel. They exhibited an out-of-plane elastic stiffness of 58.6 kip/in and an average yield moment capacity was 8.1 kip-ft. On the other hand, the 14 and 18 feet spans, did not meet the standards for a floor but could still be used as roof slabs. The results from the in-plane cyclic testing of cantilever walls showed that the panels had an average in-plane stiffness of 14.8 kip/in and had a yield moment capacity of 63.3 kip-ft. at a drift ratio of 0.082%. Similarly the ultimate moment capacity was 146.8 kip-ft. at 0.9% drift.

Key Words: Structural Concrete Insulated Panels; MetRock SCIPs; Out-of-plane testing, In-plane cyclic test; Fully composite; Partially composite; Yield moment capacity; Ultimate moment capacity; Drift ratio.

CHAPTER 1. INTRODUCTION

1.1 Background

The population in the United States is growing at a rapid rate; projections show that the population will grow by another 78 million reaching a staggering 404 million in the next four decades (Vespa et al, 2018). With the increase in the population, the demand for new residential housing has also increased vastly. Billions of dollars are spent every year in developing and restoring residential housing to properly accommodate the increasing population. Despite being vulnerable to moisture, fire, decay, and termite damage, traditional wood framing is still the most popular method of construction used. This results in the homes that have high mantainance cost and a reduced service life. The use of alternative construction methods such as Structural Concrete Insulated Panels (SCIPs) that ultizes monolothically poured insulated concrete components, can offer building that have great strutural integrity, energy efficiency, and durability.

SCIP utilizes the concept of panel construction in which that the majority of the structural component is standardized and produced in plants away from the construction site, which is then transported to the site for assembly (Brzev, 2010). SCIPs are panels that are composed of an insulated core flanked on both sides with galvanized steel mesh held together using diagonal steel shear connectors. After assembly, a one-inch layer of concrete ‘wythes’ is applied to both sides of the panel. Using only commonly available resources like recycled Expanded Polyester Styrofoam (EPS), steel ,and concrete, the SCIP system offers buildings that are structurally sound, energy efficient, and economical.

Since its introduction in the late 1960s, SCIP technology has been used in several countries. Characteristics like superior thermal/sound insulation, structural stability, and sustainability make SCIPs very appealing especially in areas that are prone to high wind and seismic activity. The performance of well detailed structure with concrete floors and shear walls subjected to high lateral loads produced during hurrican and storms have been observed to be great. Since SCIPs are very similar to reinforced concrete but are significantly lighter, they have the potential to offer structure that are great for costal areas. Addationally, SCIPs structures are significantly lighter than traditional reinforced concrete and masonry buildings and hence they can also have improved performance in seismically active areas. Study show that SCIP structure have great reserve strength and ductily when exposed to seismic activity (Mashal, 2011). Monolithic concrete continuously poured over the building floors and walls delivers a structure that is composite and has adquate structural integrity. This is backed by record like the SCIP home outperforming traditional timber homes during the devastating hurricane Ike at Crystal Beach, Texas (ASPI,2019). But due to the lack of systematic research conducted on the product and the absence of proper design guidelines, structural engineers in the United States still hesitate to consider SCIPs in their design. Hence the purpose of this study was to contribute in filling the existing gap in the research on the structural behavior of SCIPs. The study includes a full-scale experimental program to study the flexural and seismic behavior of SCIPs.

1.2 Problem Statement and Scope

Ever since the industrial revolution, there has been a huge surge of innovations and technologies. Science and research have enabled the engineers to break traditional norms and achieve a height of success never thought possible. Unfortunately, the construction industry has still been lagging behind in finding a new innovative and efficient method of construction. Although innovations like the SCIP construction provide structurally sound sustainable buildings that are excellent for areas prone to seismic activity and wind, it is rarely considered by the design engineers due to the lack of proper understanding of the material and construction technology (Mashal, 2011). This results in the engineers relying on conventional timber or masonary construction techniques.

1.3 Objectives

For SCIPs to be broadly used in the construction industry and accepted by engineers, a reliable design procedure for predicting the panel strength properties must be developed. The information obtained for this investigation regarding the flexural and seismic properties for MetRock SCIPs could be used to define the structural behavior of MR panels used as slabs and wall and to check their effectiveness under various loading conditions. Additionally, the results obtained for this investigation will help to verify theories proposed regarding SCIPs elements and ultimately contribute towards a production of a design manual for MetRockSCIP construction. Some of the key objectives for this investigation are listed below:

1. Introduce the Structural Concrete Insulated Panel (SCIP) technology and its application in the civil engineering and industry.
2. Explain the principle mechanism of the SCIP technology and its construction
3. Define the material properties for SCIP components.
4. Conduct a full-scale experimental study of the MR SCIP slabs subjected to four point bending test.
5. Utilize the slab test results to define the out-of- plane flexural stiffness properties for the MR panels and check the effectiveness of the panels used as floor and roof slabs for residential construction.
6. Check the adequacy of mesh splice for MR slab panels and provide detailing and modification for better performance.

7. Define the composite action achieved by the MR panels when subjected to out-of-plane bending.
8. Conduct a full-scale experimental study of the MR wall panels subjected to quasi-static cyclic loading.
9. Utilize the results obtained from the testing of the wall specimens to define the in-plane flexural property and seismic faliure pattern of the MR panels.
10. Document and study the non-linear behavior of both the slab and wall specimens.

1.4 Thesis Structure

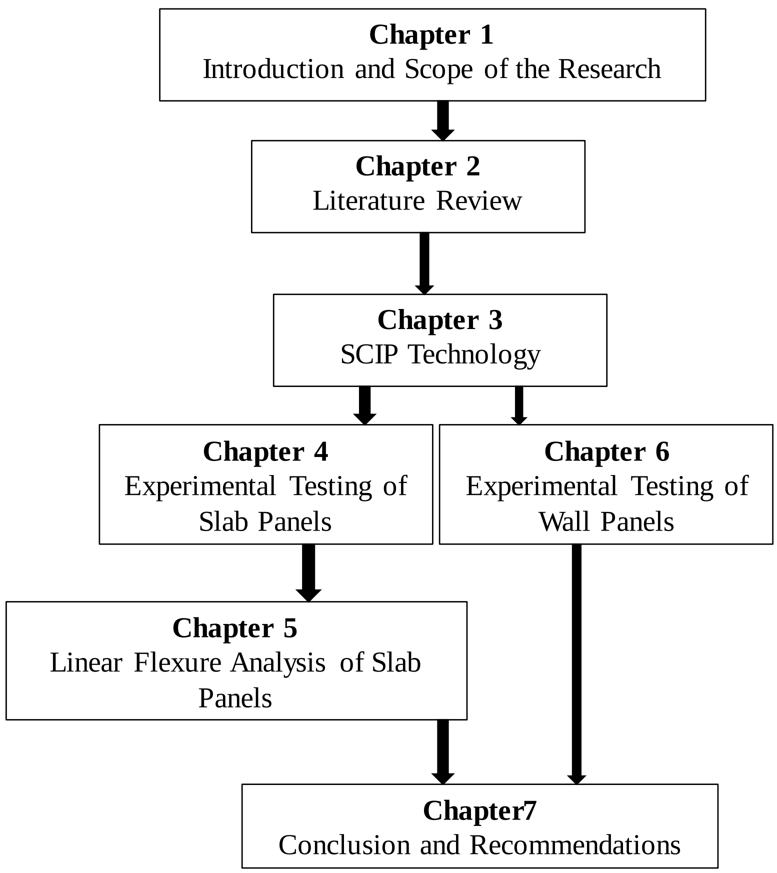

Figure 1-1: Thesis structure

1.5 Overview

Chapter 1 provides a brief introduction to the research. In this chapter the research background, problem statement, and objectives of the thesis are discussed.

Chapter 2 presents a literature review conducted on the sandwich panel system and its application in the civil engineering industry. An introduction of the SCIPs construction technology and its benefits are also described along with a brief material characterization. This chapter also provides a summary of similar research conducted on SCIPs. It further explains the testing methodology that can be used to define the structural properties of SCIPs.

Chapter 3 introduces the MR SCIPs technology and discusses how the SCIPs system can be used in the construction of residential homes; it breaks the construction process into different steps and describes them individually.This chapter also includes the details of the fabrication process used to prepare the test specimens used for the full-scale experimental program.

Chapter 4 describes the experimental testing and strength analysis conducted to determine the out-of-plane flexural behavior of SCIP used as floor and roof slabs. The experimental program and the test results are described in detail. Results such as the average load-deflection curve, ultimate moment capacity, and the elastic stiffness of the MR panels are discussed in this chapter.Furthermore, the adeqacy of the splice in the slab panels are tested experimentally and proper detailing considerations are presented. The results obtained from the testing are then used to compare the strength property of a the slab to various standards stated in the ASEC 7-16 and ACI 318-14.

In Chapter 5, a simplified ACI flexural analysis is conducted on shortsapn (10 ft) MR slab panel. Utilizing basic assumptions and the analysis method stated in ACI 318-14, the flexural strength of the slab are predicted and compared to the experimental results.

Chapter 6 presents the experimental testing conducted to determine the seismic performance of SCIPs used as structural walls. The experimental program and the test results are discussed in detail. Findings such as the average load-deflection hysteresis, back bone curve, yield drift ratio, displacment ductility, overstrength factor and the in-plane flexural capacities are described in this chapter. A study of the non-linear behavior of the walls is also conducted, which includes the stiffness degradation, crack propogation, and failure modes.

Chapter 7 summarizes the experimental results that were presented in chapters 5 and 6. Conclusions about the out-of-plane and in-plane structural behavior of SCIPs are presented. Future work involving modeling of SCIPs and producing design guidelines for SCIPs are also provided.

Also included are the table of contents, figures, tables, and appendices. The appendices include spread sheet calculations, experimental data, instrumentation, and material data sheets.

CHAPTER 2. LITERATURE REVIEW

2.1 Structural Insulated Panels

The concept of panel construction has been widely used in the civil engineering industry. Panel construction is where the majority of the structural components are standardized and produced in plants located away from the construction site, before being transported on-site for assembly. This system reconstructs the entire conventional construction process by enabling interaction between the design phase and production planning. It allows the use of mass production industrial methods to produce a large number of standard buildings in a short period at a low cost (Brzev,2010). There are many types of panel construction available in the market, like structural insulated panels (SIP), precast concrete, metal panels, and other composite panels.

Composite sandwich structures are materials that are fabricated by attaching two thin layers of stiff faces to a low-density thick core. Figure 2-1 provides a general cross-section for a composite sandwich material. The load-bearing layers in a sandwich structure generally consist of a high-strength material like metal, glass laminates or fiber-reinforced thermos plastics. Whereas the core is generally made up of open or closed lightweight, low-strength materials like polystyrene foam, honeycombs or balsa wood.

Before 1960, the greatest breakthrough of the sandwich system was only in aerospace applications specifically in the development of Mosquito aircraft during World War II. But after 1960, diverse uses of sandwich technology were witnessed in other industries such as automobiles, ship buildings, and building construction. (Zenkert, 1993).

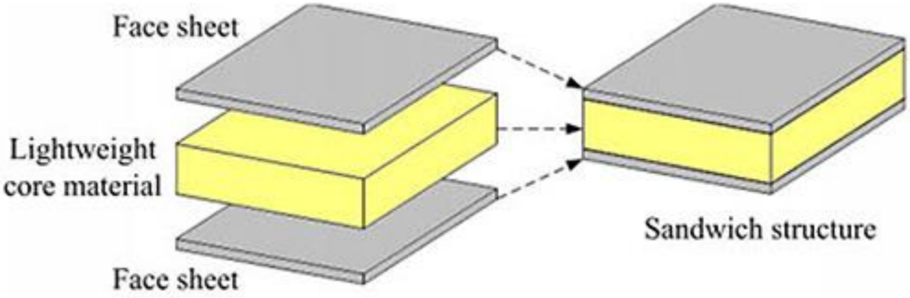

Figure 2-1 Cross-section for a composite sandwich structure (Key to Metals AG, 2019)

Utilizing the concept of composite sandwich panel construction Structural Insulated Panels (SIP) was first investigated in the Forest Production Laboratory in Madison, Wisconsin by an architect named Frank Lloyd Wright in the early 1930s. His prototype used three layers of plywood and two layers of tar paper for the structural elements. Although his design was able to incorporate beauty and simplicity into a relatively low-costing home, his prototype lacked insulation and was never produced on a large scale. His idea of SIP took a major leap when one of Wright's students and the son of the founder of the Dow Chemical Company Alden B. Dow created the first foam core SIP in 1952. These panels were then used to build the first SIP homes in Midland, Michigan (Morley, 2000). Today many variations of SIPs are available in the market. Although the traditional OSB (Oriented Strand Board) / plywood SIPs are the most common type, other variations like the Structural Concrete Insulated Panel and Metal Insulated Panels are gaining popularity. Figure 2-2 provides a detailed cross-section for a traditional OSB SIP.

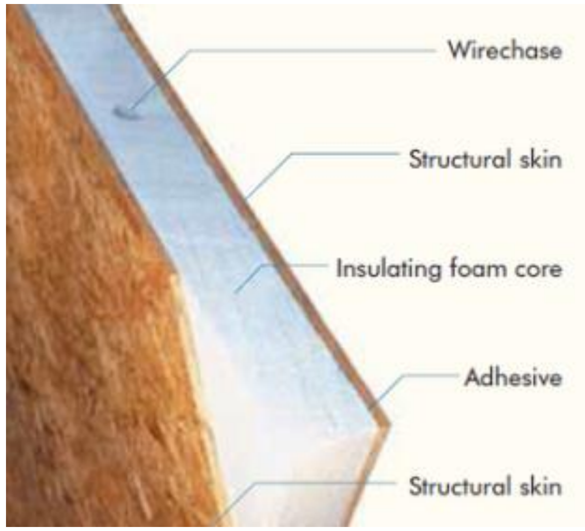

Figure 2-2: Labeled cross-section for SIP with OSB skin (Modular Homes, 2019)

Structural Concrete Insulated Panels (SCIPs) is a variation of Structural Insulated Panels (SIP) where reinforced concrete is used instead of plywood to provide the two load-bearing faces, which is held together using a complex shear transfer system. SCIPs can be used as both load-bearing and non-load-bearing walls, roof, and floors ideal for urban low-rise structures. Urban low-rise structures generally consist of buildings ranging from one to 10 stories high. The SCIP technique was originally called thin shell sandwich panel construction and was first developed and patented in the late 1960s by Victor Weismann in Pasadena, California (Mashal, 2014). Structural Concrete Insulated Panels are three-dimensional concrete panels consisting of an Expanded Polystyrene Styrofoam EPS core sandwiched between two cold-rolled steel wire mesh which held together using a diagonal transversal truss connector. The assembly then receives a layer of concrete or high-strength cementitious mortar on either side (El Demerdash, 2013). The two most commonly available commercial SCIPs in the US are MetRock panels and Tridipanels.

2.1.1 Tridipanels

Tridipanels is a variation of Structural Concrete Insulated Panel (SCIP) that are also referred to as three-dimensional EVG panels. This system was created in Austria by the EVG Company. The Tridipanel core consist of a super-insulated energy-efficient core of rigid expanded polystyrene (EPS) sandwiched between two sheets of eleven-gauge steel wire-mesh that are welded together with the aid of 9-gauge cross wires that are pierced diagonally through the polystyrene core. The wire mesh consists of a two-inch square pattern of longitudinal and transverse wires. The cross-wire truss diagonally penetrates the interior foam to form a triangulated truss system to create a single monolithic structure. The diagonal cross-wires are positioned four inches on center. The EPS core is held ½ or ¾ inches from the welded wire fabric to permit the wire to be embedded on the application of approximately one to two-inch concrete. After the panels are erected and positioned a one to two inches layer of concrete is applied to both sides by either hand application or via shotcrete (Tridipanel, 2019).

Tridipanel is manufactured using a fully automatic welding line that assembles the three major components: welded mesh, truss spacer wires, and insulation core. Details of a typical Tridipanel panel are provided in Figure 2-3. The diagonal truss wire, as well as the manufacture of the welded wire mesh, conforms with ASTM A82. The insulation core is a Type I expanded polystyrene (EPS) that complies with ASTM A82 (El Demerdash, 2013).

Figure 2-3: Cross-section for EVG Three-Dimensional Panel (Tridipanel, 2019)

2.1.2 MetRock SCIP

The MetRock Structural Concrete Insulated Panel or MetRock Panels is a modular version of SCIP. Unlike the conventional SCIP that are generally fabricated in the production plants and are transported as solid panels to the construction site, MR panels are generally transported as individual elements that can be assembled into panels using a portable hydraulic jig press and a pneumatic hollow ring fastener. An assembled MR panel consists of an Expanded Polystyrene Styrofoam block core flanked by a 14-gauge galvanized wire mesh on both sides, connected with a 3/16-inch galvanized diagonal steel wire trusses spaced at six inches. The insulation core blocks are six inches wide, four inches thick and can be up to ten feet in length. Figure 2-4 provides the details for a typical MetRock SCIP core. After the panels are positioned, the assembly is coated with a one-inch layer of concrete on either side to provide the load-bearing faces. (MetRockSCIP, 2019). Details regarding the manufacturing and product description for MR panels are provided in CHAPTER 3.

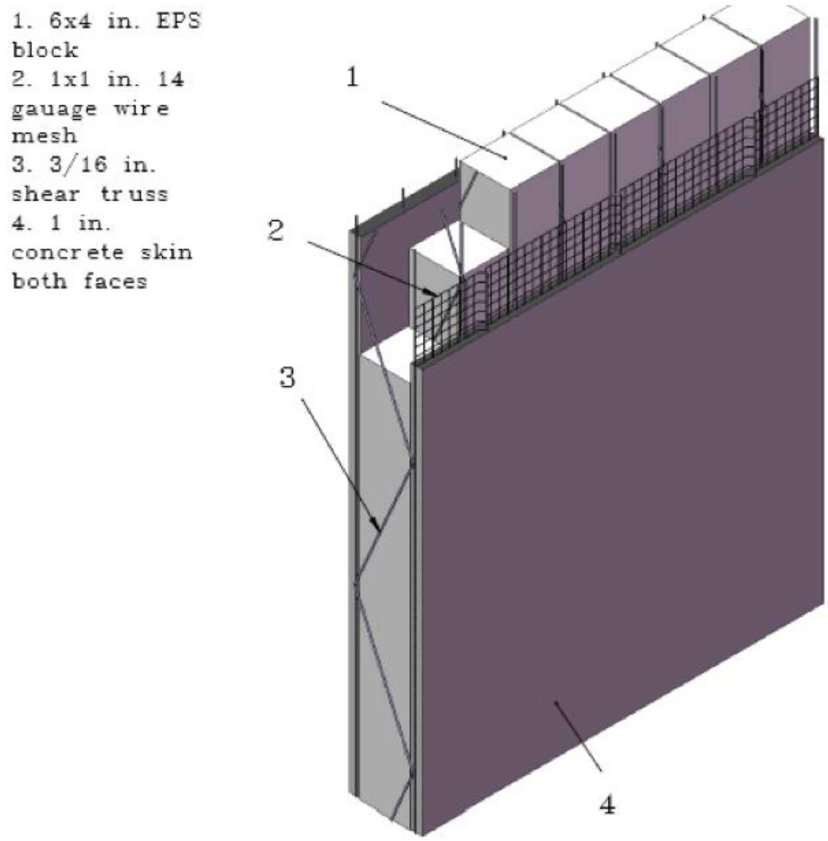

Figure 2-4: Details for typical MetRockSCIP (MetRockSCIP, 2019)

2.2 Benefits of using Structural Concrete Insulated Panel system

Due to its unique design, Structural Concrete Insulated Panels have the potential to offer structures that have many benefits. A few of its key benefits are listed in this section.

2.2.1 Fast and economical construction system.

For cost and time-efficient construction, panel construction is widely used for residential structures (Brzev,2010). Using panels not only reduces the build time but also ensures a more standardized construction since most of the structural components are produced in a controlled plant and then transported to the site for assembly. The use of panels reduces the need for intermediate beams and columns. The length and width of the panels can be changed on-site to meet the design requirements. According to Brzev, unlike traditional cast-in-place concrete where the concrete requires a form to set in; for SCIPs the concrete is directly applied to the panels, so no formwork is required. Due to the ease of handling and assembly, a faster erection of the structure is possible with minimum equipment and no skilled labor. Electric and water conduits can be accommodated directly inside the panel core. Reduction in construction time, building equipment, concrete formwork and skilled labor results in a very economical and rapid construction (El Demerdash, 2013).

2.2.2 Energy efficient structure.

The use of Expanded Polystyrene Styrofoam (EPS) core provides the SCIP structures with superior thermal insulation by reducing the thermal bridging of the interior and exterior walls. This results in a significant reduction in energy consumption for heating and cooling (Baginski, 2006). A report on the heat transfer properties of SCIPs showed that panels with a five-inch insulation core had an overall R-value of 26.8 which was significantly higher than a typical wood-frame structure with an R-13 mineral fiber insulation that had an R-value of 11.3 (Hubbell, 2006). Along with providing thermal insulation using EPS, also provides great sound insulation. Sound Attenuation Classification (STC) for these sandwich panels ranges from STC 50 to STC 33. The rating depends on different parameters including the concrete face thickness, the overall thickness of the wall or floor and the density of the foam core (Hicks, 2008).

2.2.3 Structurally sound buildings.

If designed and constructed properly SCIP elements tend to have superior structural properties. A case study conducted by Advanced Structure Panel Industry (ASPI, 2008) of a home built using SCIPs in Crystal Beach, Texas, withstood large magnitudes of lateral loading produced by high winds and tidal surges during Hurricane Rita and Ike and sustained very little damage. Figure 2-5 shows the aerial view of the crystal beach area before and after Hurricane Ike. Results from numerous studies both analytical and experimental suggest that SCIP structures are ideal for a seismically active area like Afghanistan and Iran (Kabir, 2007; Mustafa, 2011). A full-scale dynamic test of a three-dimensional concrete sandwich panel structure conducted in the Amirkabir University of Technology in Iran showed a considerable level of resistance to a high level of earthquake vibrations (Kabir, 2007).

Figure 2-5: Aerial photograph of the crystal beach and after hurricane Ike (ASPI, 2019)

2.2.4 Sustainability

Since the EPS core and the galvanized steel reinforcement are enveloped by concrete, they are not susceptible to moisture, fire, or physical damage. This results in a significant increase in the structure's service life and also decreases maintenance cost (Tapia, 2010). An ICC-ES evaluation report for SCIP with a concrete facing thickness of two inches shows a fire-resistance rating of two hours. Although the damage to the inner core of the structure due to excessive heat was not mentioned in the report, the structural integrity of the wall was still intact (ICC-ES, 2013).

Using SCIP for construction also delivers structures that are more durable and environmentally friendly than timber construction (El Demerdash, 2013). All the major components used in the SCIPs are either recycled or are commonly available. For example, the insulated core is made up of recycled expanded polystyrene foam, recycled steel from the auto industry is used for the mesh and the shear connectors and the concrete used to coat the panels are readily available in the market. (Biginski, 2006).

2.3 Structural Mechanics of SCIPs

A typical SCIP core consists of a welded–wire space frame integrated with polystyrene insulated core held together using a galvanized diagonal steel truss system. The breakdown and explanation of each material that constitutes the sandwich panels are provided in the following section.

2.3.1 Expanded Polystyrene (EPS) Core.

The insulation core serves two main purposes in a sandwich structure. Firstly, it provides separation for the two load-carrying skins. This process of separating the load-carrying faces from the center significantly increases the moment of inertia of the section. This results in a section with low density and high flexural strength and rigidity (Naji, 2015). This concept is similar to the "I" profile that is widely used in the steel industry. Figure 2-6 provides a visual comparison between an I-beam and a sandwich panel. Secondly, the core also provides the panels with the needed insulation thus reducing the heating and cooling energy requirements (Hubbell, 2006). The EPS core is used for properties like low density, good resistance to temperature fluctuation and moisture change, durability and good resistance to chemical breakdown over time (Themal Gurdaian, 2019).

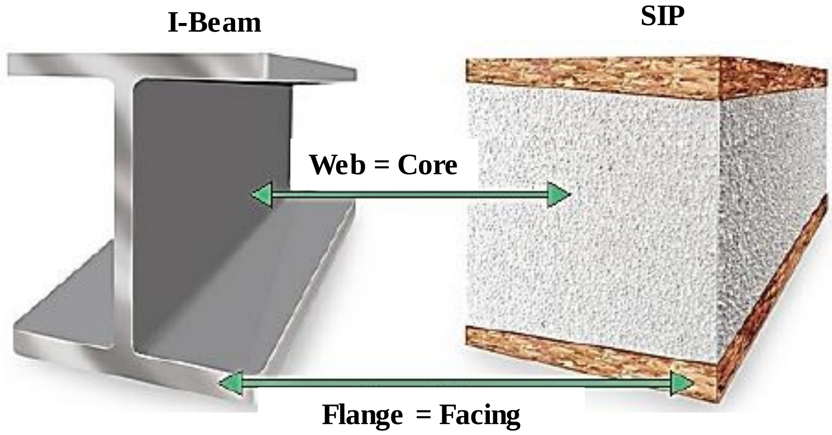

Figure 2-6: Basic concept of sandwich panel construction (Tanguayhomes, 2019)

2.3.2 Cold rolled galvanized steel mesh.

The steel mesh is generally what provides SCIP its tensile reinforcement. Most mesh reinforcements consist of cold-rolled galvanized wire mesh in a squares grid configuration. The longitudinal and transverse wires are welded together using a spot weld. In a typical SCIP mesh, the wires vary from a 14 gauge (0.08-inch diameter) to an 11 gauge (0.12-inch diameter). The wires are galvanized to provide the steel additional protection from corrosion. According to most SCIP specifications, the mesh consists of a cold rolled galvanized welded wire fabric that complies with the ASTM A185 standards. Minimum spacing between the EPS core and the mesh is maintained to achieve at least ½ inch embedment of the mesh in the concrete.

2.3.3 Diagonal steel shear truss.

The diagonal shear truss system is what connects the two-load-bearing concrete Wythes through the insulation layer. The connectors can be concrete web, steel elements or plastic ties (El Demerdash, 2013). For a sandwich panel to achieve its full load-carrying capacity the presence of a proper system of shear connectors is essential. This enables sufficient transfer of the longitudinal shear between the two load-bearing faces. A panel is said to be composite when the entire cross-section of the panel acts as one unit. Studies have shown that a fully composite panel has similar flexural properties as a traditional reinforced concrete slab (McCormac, 2016). Depending on the degree of composite action achieved a sandwich panel can be divided into three categories: fully composite, partially composite and non-composite. A panel is considered to be fully a composite section when 100% of the longitudinal shear is transferred between the two load-bearing faces. On the other hand, if there is no transfer of shear in between the two faces, the section is considered to be non-composite. Lastly, a panel is considered to be partially composite when the shear connectors transfer only a fraction of the longitudinal shear (Naji, 2015). Figure 9 shows the stress and strain distribution of a composite, partially composite and a non-composite case.

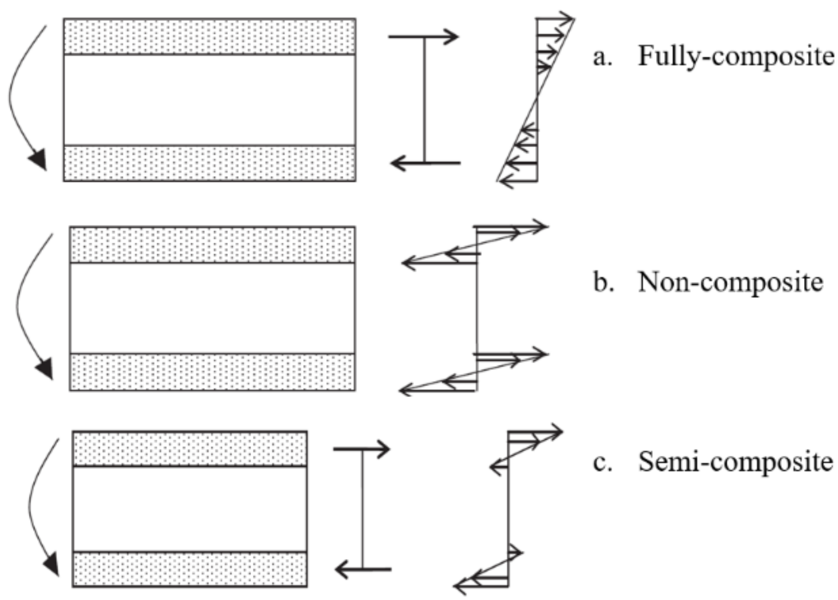

Figure 2-7 Stress-Strain distribution for fully, partially composite panels (Naji, 2015)

SCIPs typically use cold rolled diagonal shear connectors to hold its two faces together. The connectors generally integrated with the EPS core. For instance, in Tridipanels the diagonal bars pierce through the EPS core and are welded to the wire mesh. Whereas, in the MetRock SCIP the bars are sandwiched between the EPS blocks and are tied to the mesh using a hog ring ties. Figure 2-8 show the difference between diagonal connectors in grid panels and MetRock SCIPs.

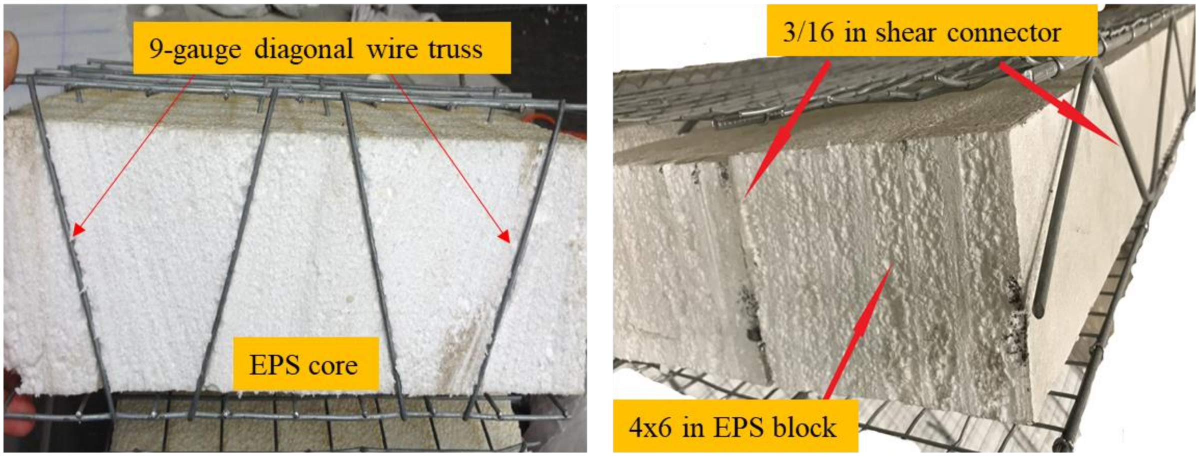

Figure 2-8: Diagonal connector for Tridipanel and MetRockSCIPs

2.3.4 *Concrete layers 'Wythes'.*

After the panels are erected on site, a layer of concrete that is one to two-inch is applied to each side of the panel. The two concrete skins in SCIPs are generally referred to as 'wythes' (McCormac, 2016). The concrete along with the welded wire mesh make up the load-bearing faces for the SCIP. The concrete wythes also provide confinement to the insulation core, and protect it from external elements such as fire, moister and impact loading. The concrete can be applied using various methods, two of the most commonly used methods are hand application and pneumatic application. The pneumatic method is also known as shotcrete, in which the concrete is sprayed on the panels using a low-velocity pump. A concrete mix with a minimum compressive strength of 3000 psi is specified for most load-bearing Structural Concrete Insulated Panels (El Demerdash, 2013). The compressive strength of the concrete can be determined using the ASTM C 109 testing standards.

2.4 Test Methodologies for Full-Scale Panels

For the experimental testing of the MR panels, two testing methodologies were selected. The first series of testing was conducted on the panels that were used as floor and roof slabs whereas the second set of testing was conducted on the panels used as structural walls.

The ASTM E 72 *Standard Test Method of Conducting Strength Test for Panels for Building Construction* provides a systematic basis for obtaining engineering data on structural panels used as floor and roof slabs (ASTM, 2005). This experiment is intended for the testing of wooden panels. However, due to the absence of a specific ASTM designation for the testing SCIPs, the ASTM E 72 standard was closely followed for the test setup and the loading protocol to experimentally quantify the out-of-plane flexural properties of SCIPs. Section 11 in the ASTM E 72 specifies the test setup, loading protocol, data collection and presentation for a transverse loading of horizontal of the panels. The transverse testing of panels can be used to study the out-of-plane flexural behavior of panels. The test setup provided in the ASTM E 72 is shown in Figure 2-9. As shown in the test setup, a loading device with the combination of a stiff spreader beam and two rollers were used to apply the loading on the slab specimen. The loading is applied at quarter span marks. The panels rest on top roller bars with plates to form a simply supported span. A quasi-static load is applied to ensure no dynamic inertia effects. The specimen is loaded until failure. Before testing, two deflection gauges (precision up to 0.01 inches) are attached to the mid-span of the specimen (one on each side) to collect the midpoint deflection. The values are averaged during the data analysis.

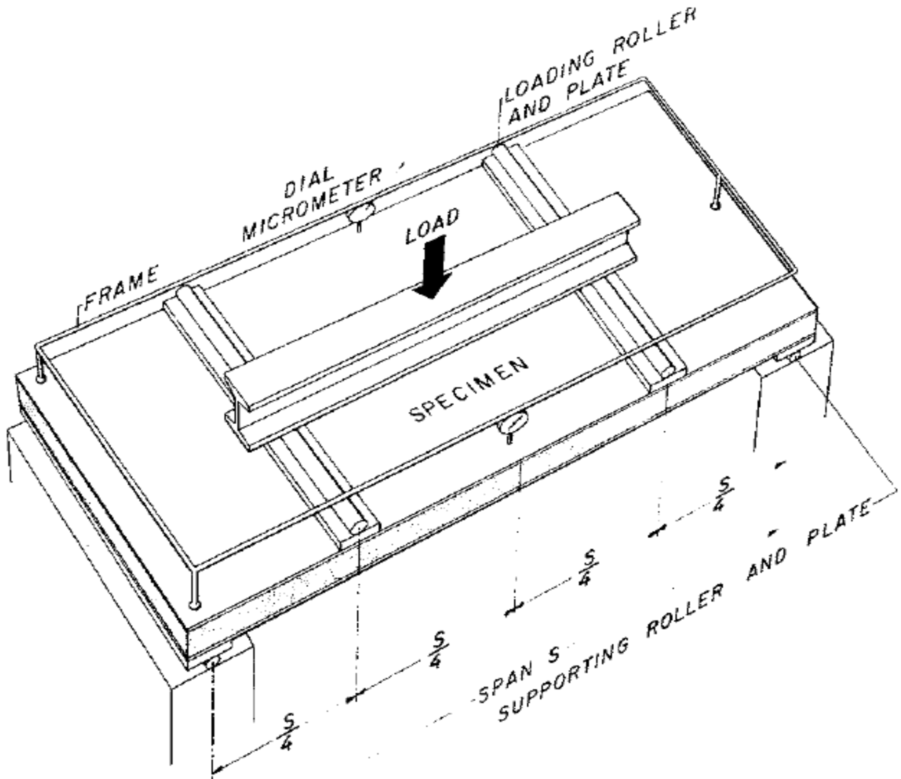

Figure 2-9: Transverse loading test setup (ASTM, 2005)

The American Concrete Institute ACI 374.2R-13 is a guide for testing of a reinforced concrete structural element that is part of the lateral force-resisting system, under slowly applied simulated seismic loading. This type of loading is also referred to as "quasi static cyclic loading." This testing is primarily intended for assessing strength, stiffness, and deformability crack/failure pattern of a structural wall element under cyclic lateral loading. It emphasizes on the correlation of test data and predetermined structural performance levels to enable a performance-based design practice for construction technology.

According to the ACI standards, a displacement-controlled load protocol is generally used for this type of testing. The drift ratio, which is a ratio of the lateral deflection to the overall height of the wall is used as the primary performance indicator. The loads intervals are applied at an increment of the yield drift ratio φ_y. The yield drift ratio φ_y is the estimated drift ratio at which the structure yields. The displacement-based design procedure can be used to calculate the yield drift ratio for the shear wall (Priestley et.al, 2007). A standard loading protocol from ACI 374 2Ris shown in Figure 2-10.

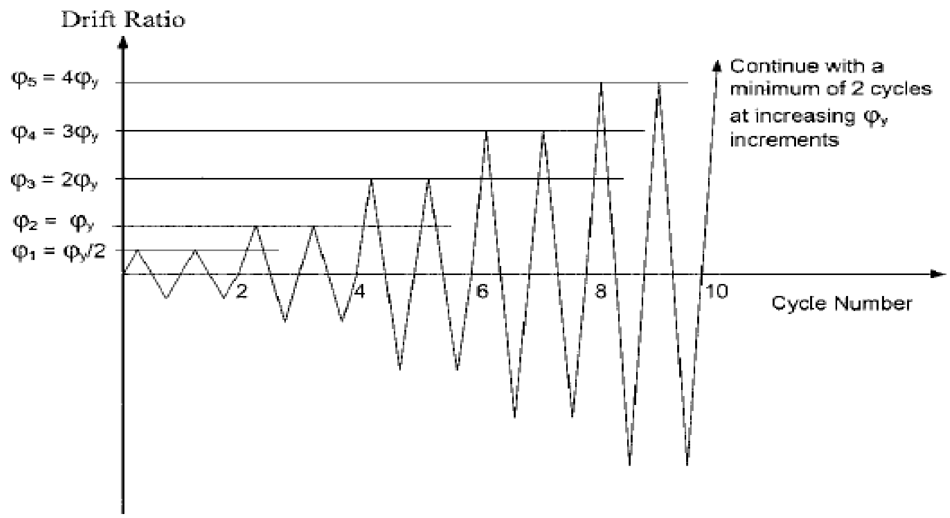

Figure 2-10: Loading protocol for unidirectional load reversals (ACI, 2013)

2.5 Previous Tests Performed on Sandwich Panels

Despite the advances in computational techniques and increased computational power, available analytical approaches and computational models based on the principles of mechanics are not sufficient and accurate for the design (ACI 347.2 R-13, 2013). Hence full-scale testing of SCIPs structure is essential to further understand and predict its structural behavior. Over the years many large-scale tests have been conducted on different types of sandwich panels. This section summarizes a few of the previously conducted tests.

2.5.1 The Behavior of MetRock Sandwich Panel in Flexural (Fouad et al, 2008)

This study of the flexural property of MetRock SCIP had both experimental and analytical components. For the experimental program, ten full-scale specimens were tested in flexural. All the specimens used for this experiment were 24 inches wide with a varying span to depth ratio. All the tests were conducted in following ASTM E72-05. The panels were quasistatically loaded at an increment of 1000 pounds which was continued until failure. Since the panels tested for this study did not have side and end confinement the edge trusses had an in-plane buckling, but due to the redundancy in the shear connectors, the specimens continued to resist more load. Although at ultimate load capacity, all the specimens had a horizontal shear failure at the end region, which is not the desired mode of failure (very brittle), however, the results showed that the panels were relatively ductile with a fairly large range of non-linear behavior. The load-deflection graph for a six-inch thick specimen is illustrated in Figure 2-11. Figure 2-11 shows the premature mode of failure observed for two specimens. The study concluded that the panels behaved as a semi-composite element suggesting that designing these panels as non-composite as specified in ACI 318 greatly underestimates their load-carrying capacity.

Figure 2-11: Modes of failures for MetRock SCIP slabs (Fouad et al, 2008)

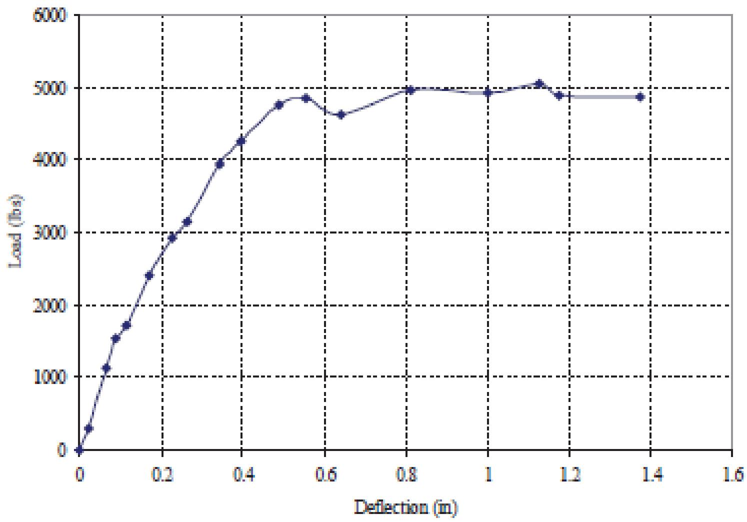

Figure 2-12: Average load Vs deflection for the MetRock SCIP slabs (Fouad et al, 2008)

2.5.2 Structural Evaluation of 3-D Sandwich Panel System (El Demerdash, 2012)

In this study, the structural property of the Tridipanel was investigated through a series of large-scale testing. This research included both analytical and experimental components for the Tridipanel used as shear walls. In this study, numerical models of the SCIP shear wall was created using the finite element method. The properties of the model were then compared to the results from the full-scale testing of the walls. The experimental program consisted of cyclic racking shear test on 10 wall specimens that were connected to the footing using dowel connections. All the walls were eight feet long and seven inches thick but with a varying aspect ratio. The ACI ITG 5.1 loading protocol was used to test the wall specimens (ACI ITG 5.1, 2008). The specimens were tested to failure to determine the ultimate load-carrying capacity, cracking pattern and hysteric response under cyclic loading. Most of the specimens demonstrated combined shear and flexural mode of failure. Figure 2-13 shows pictures of the two failure modes observed during testing. The maximum moment capacity of the walls with the aspect ratio 1 was, between 70 kip-ft and 83 kip-ft depending on the strength of the concrete used. The Finite Element (FE) models generated for this research provided similar results to the actual test results.

Figure 2-13: Failure modes for cyclic racking shear testing (El Demerdash, 2013)

2.6 Analytical Seismic Evaluation of Three-Dimensional Construction System.

This section summarizes the seismic evaluation of 3D concrete panels conducted by Mashal and Filiatrault (2012) “Quantification of seismic performance factor for building incorporating three-dimensional construction system” utilizes FEMA P695 Methodology to evaluate and predict the seismic performance for 3D panel construction system .The FEMA P695 Methodology is intended for design of new structural systems and provides a rationale method of evaluating the seismic performance factors (SPFs) such as the response modification coefficient (R-factor), the system overstrength factor (Ω_0), and deflection amplification factor (C_d). It uses a nonlinear analysis techniques to characterize nonlinear static and dynamic behavior of a proposed seismic-force-resisting system (FEMA, 2009). The definition of the SPFs are provided in Figure 2-14

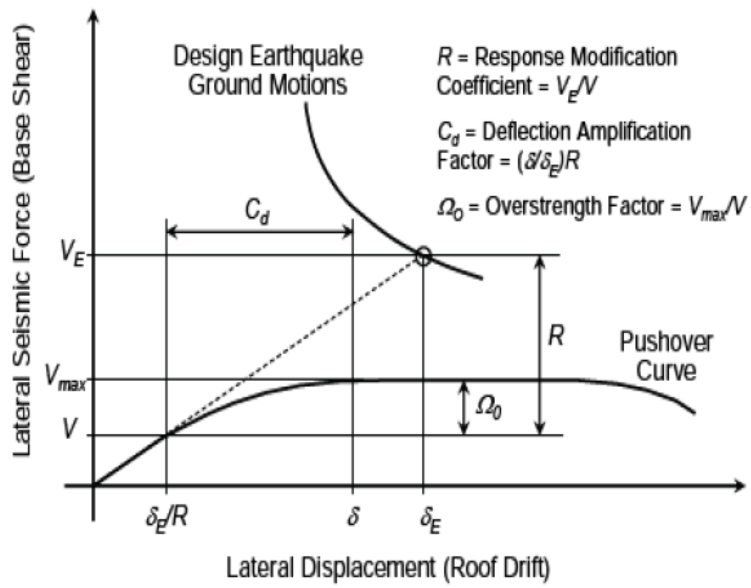

Figure 2-14: Illustration of seismic performance factor as defined by FEMA P695 (FEMA, 2009)

In this investigation the behavior of the 3D panel's seismic resisting system was investigated through the use of an *archetype,* which is a prototypical representation of a seismic force-resisting system. The authors conducted more than 5,000 dynamic and pushover analysis using SAP 2000. The development of the design requirements were conducted within the context of the seismic provision of the ASCE/SEI 7-05. The results of the nonlinear static and dynamic analysis were used to evaluate the seismic performance of the 3D panels. The final recommended values for the SPFs for one and two-story 3D panel buildings were as follows: R = 3.5, C_d = 3.5, Ω_0 = 3.0 (Mashal & Filiatrault 2012).

2.7 Conclusion

The literature review was conducted to examine past research conducted on SCIP structures. A summary of the key findings from the literature review are as follows:

1. SCIP utilizes the concept of sandwich technology that offers elements that have high flexural stiffness with relatively low unit weight.

2. Originally Structural Insulated Panels only utilized wooden sheets as its load-bearing faces, SCIPs use two thin reinforced concrete faces, commonly referred to as “wythes” for load-bearing, the two wythes are connected with shear connectors that are referred as “trusses”.
3. The Expanded Polystyrene Styrofoam (EPS) core in the SCIP is intended to provide thermal and sound insulation as well as separating the concrete wythes to increase the moment of inertia of the panel section. It also reduces the overall weight of the panel which is an important parameter for buildings located in seismic zones. Past experimental testing show that EPS core could provide a thermal R-value of 26 and a sound insulation coefficient of STC 50 to STC 33
4. Advantages of SCIPs over a traditional wood frame and masonry construction include faster construction, use of readily available an off-the-shelf materials, cost-efficiency, higher durability, cost savings in labor and construction time, better thermal and sound insulations, smaller self-weight, better fire-resistance, and easier construction which does not require highly skilled labor.
5. The current ACI 318 standard require insulated sandwich panels to be designed as non-composite structures. This is a very conservative approach in the case of SCIPs and greatly underestimates the flexural capacity of the panels. Experimental testing of SCIPs by other researchers have shown that with proper shear transfer mechanism between the two wythes, the panels behave more as partially composite elements.
6. The unconfined sides result in the out-of-plane buckling of the edge diagonal trusses. Hence confinement of panel edges is essential to prevent premature failure and to define the true out-of-plane capacity of the panels.

7. Results from a full-scale racking shear test showed that SCIP have high in-plane moment capacity making them a great alternative for the construction of shear walls.
8. Testing of the wall panels showed that the type of dowel connection used altered the overall performance of the wall. Hence using dowel connection is not an effective approach to define the true in-plane capacity of the wall panels.
9. The seismic evaluation conducted using the FEMA P695 Methodology showed that the 3D panels had a response modification coefficient (R-factor) of 3.5, a system overstrength factor (Ω_0) of 3.0, and a deflection amplification factor (C_d) of 3.5.

CHAPTER 3. Construction Technology

3.1 General

This chapter introduces the MetRock SCIP construction technology. The details regarding the fabrication of the MR panel and how they can be used for the construction of a residential building are described in this chapter. All information provided regarding the fabrication of MR panels and its construction methodology are derived from MetRock SCIP construction catalog and from visiting the production plant in Anniston, AL. Lastly, the alternative precast approach used to produce the test specimens for the experimental program are also described.

3.2 Fabrication of MetRock SCIP core

A typical MetRock SCIP core constitutes of a welded–wire space frame integrated with a polystyrene insulated core. The two layers of mesh are held together using a galvanized diagonal steel truss system. MR SCIP cores are generally two to four feet wide, three to eight inches thick, and can be up to 10 feet long. They are produced using a portable hydraulic jig press and a pneumatic hog rig tie. All elements required to manufacture the MR panel are modular off the shelf materials that are readily available. The key elements consist of a recycled Expanded Polystyrene Styrofoam (EPS) core, cold rolled galvanized steel mesh, and diagonal truss connector. Information regarding the description and function of each element can be reviewed in Section 2.3.

MetRock SCIPs utilizes Type I Expanded Polystyrene Styrofoam for its insulation core. The EPS are manufactured by the Carpenter Insulation Company and comply with the ASTM C 78. According to the product data sheet the average density of the core is 1.0 pound per cubic foot and has a modulus of elasticity of 180 psi. The product data sheet is provided in Appendix A. The blocks of EPS used to produce MetRock SCIPs are generally six inches wide and 10 feet long and have a varying thickness from 3 to 11 inches. Two EPS blocks can be combined to produce cores that were longer than 10 feet. A pile of typical EPS blocks used in the MR panels is shown in Figure 3-1.

Figure 3-1: Type I EPS core used in MetRock SCIPs

The EPS core is flanked on both sides using a one by one-inch cold rolled 14-gauge galvanized wire mesh. The mesh used to produce the MR panels follow the ASTM A82 standard. Additionally, the wire mesh in MR panels has a unique patented screed system (Patent No.: US 8,122,622 B2) installed in them that allows for an easy application of the concrete. To ensure that a uniform layer of concrete is applied on the panels, the wire mesh has two specially designed screed ribs 12 inches off center on both sides. Figure 3-2 shows the details of the screed system used in the MR panels. A spacing of half inch is maintained in between the EPS and the mesh to ensure that sufficient concrete embedment and cover is achieved by the mesh.

The two layers of mesh are held together using a 3/16-inch galvanized steel wire truss that are commonly referred to as ‘K-bars.’ The truss connectors used to fabricate the MR panels meet the 120 (SHD) Lox-all truss type wall reinforcement specifications. Although the 120 truss connectors are typically used for horizontal mortar joints for masonry walls, they act as excellent shear connectors for the MR panels. The diagonal bars transfer the longitudinal shear stress in between the two-load-bearing faces. The shear trusses are paced every six inches and are sandwiched in between two EPS blocks. They are then tied to the mesh using a pneumatic hog ring tie. Figure 3-3 shows the diagonal truss connectors used to manufacture the MR panels.

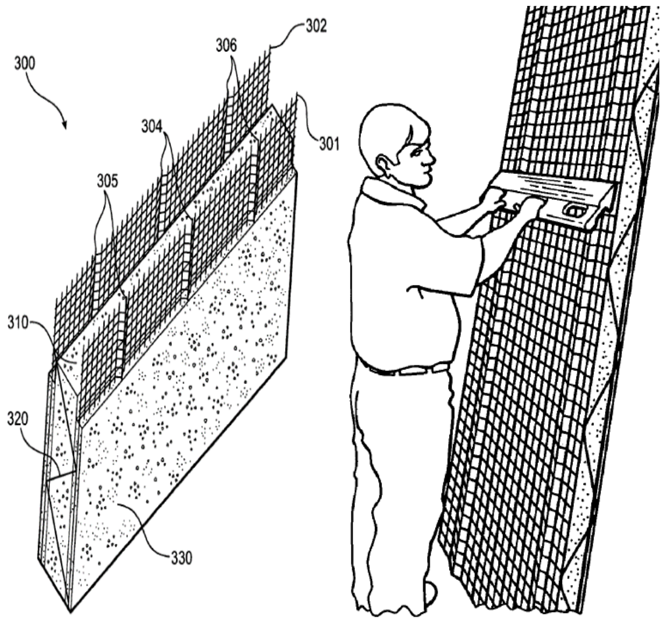

Figure 3-2 MetRock SCIP screed system (MetRock SCIP, 2012):

Figure 3-3: 3/16-inch diagonal shear connector

A portable hydraulic jig press is used to assemble the EPS, steel mesh, and the truss to produce a completed MetRock SCIP core. A standard portable jig press has the capacity to produce panels that are two to four feet wide, 10 to 18 feet long, and six to 13 inches thick. The assembly process of a typical MR panel is shown in Figure 3-4.

a) Assembling the EPS core and truss

b) Securing the truss to the mesh

c) Finished MR panel

Figure 3-4: Assembly of MetRock SCIP panel

3.3 Construction using MetRock SCIPs

Before starting the construction, the panel cores are delivered to the construction site on flatbed trucks. Standard panels having a width of two to four feet are commonly used for the ease of transportation and handling, but wider panels are sometimes designed to accommodate for door and window openings. Once the panels arrive on the construction site, they can be stored for weeks on a flat surface. The construction with MetRock SCIPs starts with the installation of a strip footing. The strip footings have starter bar (usually # 3) placed at every 12 inches. The starter bars are alternated between the inner and outer walls. Alternatively, holes also can be drilled on the footing in line with the walls where the bars can be installed and grouted in place. After the footing is prepared, panel cores are placed such that the starter bars can slide in between the mesh and the EPS core. The erecting of walls always starts from the corner; this is necessary to give the construction enough rigidity. Standard quick tie wires are then used to secure the bars to the mesh. It helps prevent the uplift of the panels before the application of the base coat. A minimum embedment of 18 inches is recommended to achieve proper connection strength. Adjacent panels are then clamped together using pneumatic ties. Splices and seams between two panels are reinforced by overlapping mesh at the splices and corners. Construction details provided in the design manual for an EVG 3D SCIP system is provided in Figure 3-5

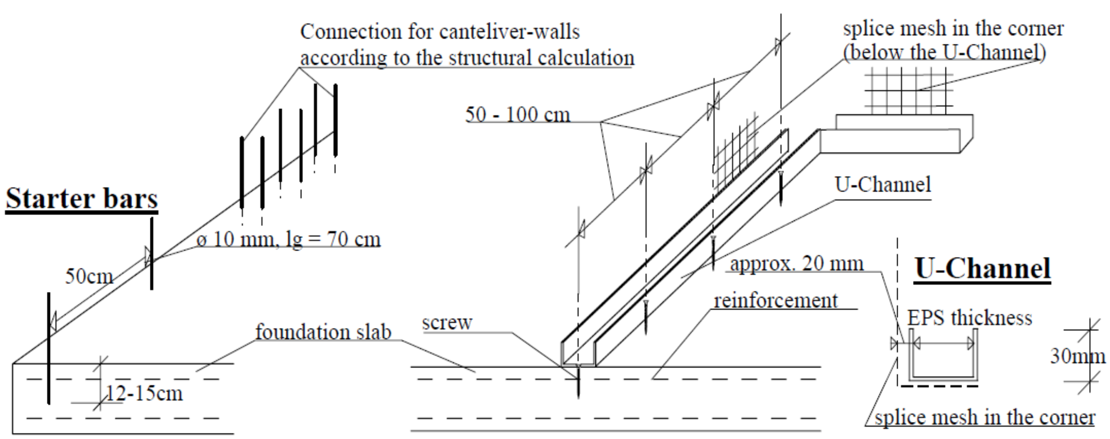

Figure 3-5: Connection for footing EVG 3D system

Required openings for doors and windows can be cut before or after the erection of the panels. Regular hand saws can be used to make these adjustments to the panels. The openings must be engineered to ensure that the structural integrity is not jeopardized. If necessary, sections of pressure treated lumber can be used to reinforce the openings. Special L and U-shaped mesh are used to confine the corners and edges of the walls. Utility conduits can also be accommodated in the gap between the foam and the wire mesh; if more space is required, parts of the foam can be cut off or burned. Once all the wall panels are placed and secured, the cores for the floor and the roof slabs are then installed. The connections between the wall and the slab require special reinforcing details and should be specified by the design engineer. Figure 3-6 illustrate a typical connection detail used for SCIP construction.

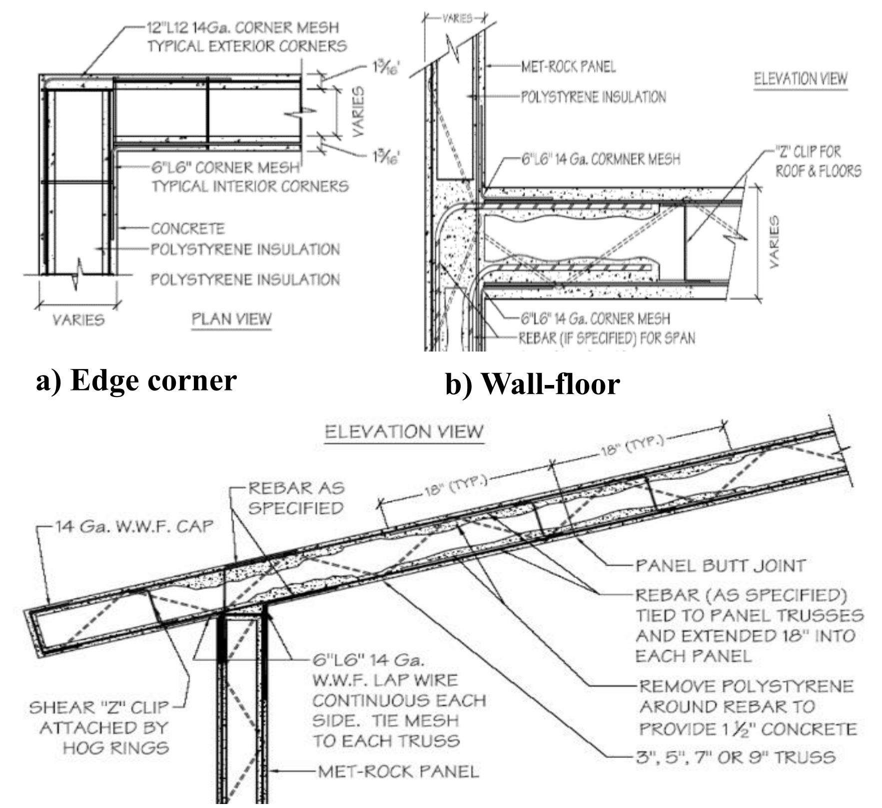

c) Wall to roof

Figure 3-6: Typical connection details for SCIPs construction

After all the panels are assembled, the required bracings are provided to the wall and floor panels. Diagonal braces are used for the walls and intermediate props are used to shore the slabs. This is flowed by the application of the concrete skins. The concrete is generally applied to using a low velocity shotcrete. A typical dry mix shotcrete procedure is shown in Figure 3-7.

Generally, for the MetRock construction, the thickness of the shotcrete ranges from 1 to 1.25 inches. All shotcrete mix design and application should be in accordance with the ACI 506R "Guide to Shotcrete." Additionally, hand application can also be used in lieu of shotcrete. For a typical dry-mix the water to cement ratio normally falls within a range of 0.3 to 0.5 and the 28 days compressive strength should be within the range of 3000-8000 psi. Admixtures can be used in the shotcrete mix design to enhance certain properties. For instance, air entertainers are commonly used to avoid freeze thaw damage, increased workability, and to reduce rebound during shotcrete. A detailed step by step construction procedure using MetRock SCIPs is provided in Figure 3-.

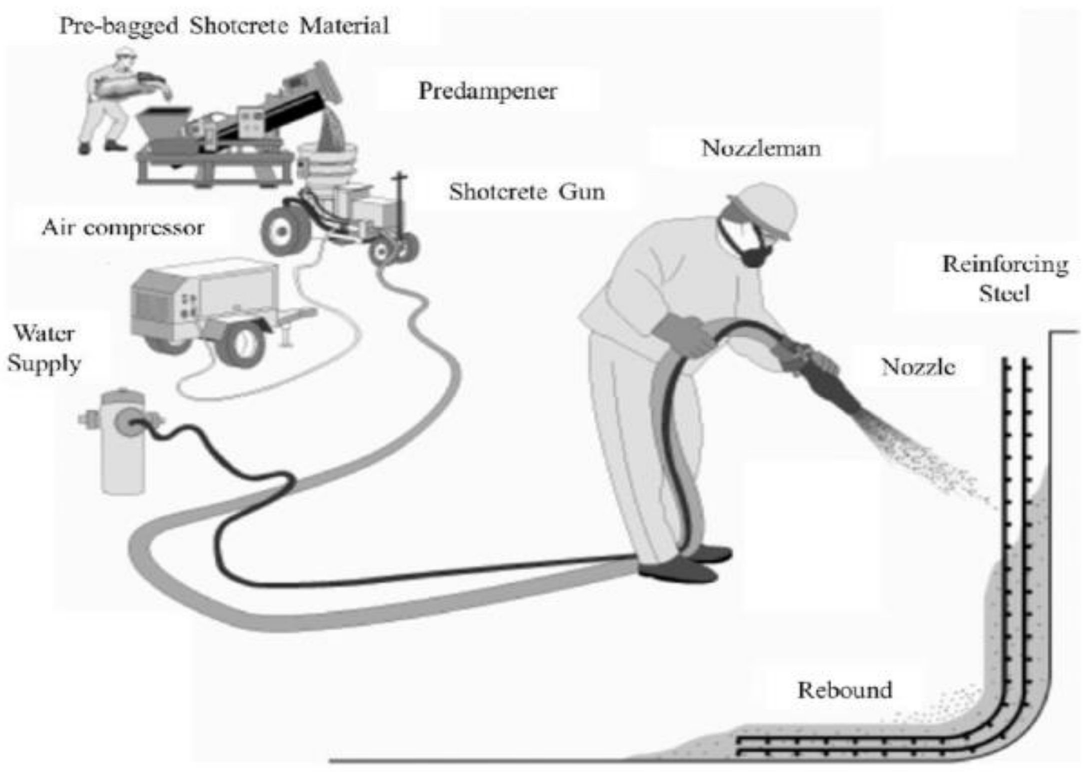

Figure 3-7: Typical dry mix shotcrete procedure

a) Transporting SCIP

b) Storage of panels on site

c) Formwork for strip footing

d) Strip footing with starter bars

i) Placement of panels on footing

j) Opening for a window

Figure 3-8: Details for the construction process using MetRock SCIPs

k) Utility conduit installed in the panel

l) Installation of first floor slabs

m) Erecting first floor walls

n) Applying shotcrete on exterior walls

o) Backfilling of basement walls

p) Applying shotcrete on interior walls & floors

Figure 3-7: Details for the construction process using MetRock SCIPs

3.4 Alternative precast approach for construction MetRock SCIPs

Instead of using the traditional shotcrete process, an alternative precast approach was used to produce the full-scale slab and wall specimens for the experimental investigations. This section discusses the construction process used to fabricate the test specimens. In total, 11 full-scale slab specimens and three wall specimens with socket connection were constructed in house at Idaho State University. All the specimens were prepared using a typical four feet wide MetRock SCIPs. The cores were produced at the Blastcrete Equipment Company in Anniston, AL and were shipped on a flatbed truck. Table 3-1 provides descriptions of the specimens.

Table 3-1: Details for large-scale specimens

Specimen Type	Specimen ID	Specimen Dimension	Date Prepared
Short span slab	A-1	123in. x 49in. x 6in.	11/15/2018
	A-2		11/19/2018
	A-3		11/28/2018
Medium span slab	B-1	171in. x 49in. x 6in.	12/18/2018
	B-2		1/11/2019
	B-3		1/14/2019
Long span slab	C-1	219in. x 49in. x 6in.	1/23/2019
	C-2		1/28/2019
	C-3		2/1/2019
Modified long span slab	S-1	219in. x 49in. x 6in.	4/25/2019
	S-2		5/21/2019
Wall	A-4	123in. x 49in. x 6in.	12/3/2018
	A-5		12/6/2018
	A-6		12/13/2018

3.4.1 Preparing panel specimens

Unlike the traditional MetRock SCIPs construction procedure where the concrete layers are applied using shotcrete, a precast approach was used for this study. A Self-Consolidating Concrete (SCC) mix was designed and produced using the ACI absolute volumetric method. Type I Portland cement and Navajo fly ash were used for the cementitious material. A mixture of crushed sand and extra fine pea gravel were used for the aggregates. The mix had a cement to water ratio of 0.4 and fly ash to cement ratio of 0.2. To achieve high workability without compromising the strength, High Range Water Reducer Agent (Master Glenimum 1466) was used. The details of the mix design are provided in Table 3-2. Additional information about the mix design procedure and material data sheet are attached in Appendix A. The mix used to produce the specimens had an average spread of 23.5 inches and an air content of 4.5% with an average density of 144.7 lb/ft^3.

All the raw materials required for the concrete were batched in buckets a day prior to the pour as shown in Figure 3-8 a. Two 1.5-gallon capacity drum mixers were used to mix the concrete needed to fabricate the specimens. Figure 3-8 b shows the concrete mixer used to mix the concrete.

a) Materials batching   b) 1.5.ft^3 concrete mixer

Figure 3-8: Material batching and concrete mixer

Table 3-2: Mix design used for Self-Consolidating Concrete

SCC Mix Design					
Cement	729.0	lb/Yd^3	Spread	23.5	in
Fly ash	183.2	lb/Yd^3	Air Content	4.5	%
Coarse sand	1701.0	lb/Yd^3	W/Cm	0.40	
Fine pea grave	810.0	lb/Yd^3	F/Cm	0.20	
Water	364.5	lb/Yd^3	Unit Weight (ɣ)	144.7	lb/ft^3
HRWRA	10.4	fl.oz/cwt			

The precast bed was constructed using standard 3/4-inch plywood and two by four lumber. The base for the bed was 20 feet long and five feet wide. A modular six-inch walls were then screwed on to the bed. The modular wall setup allowed for the precast bed to be adjustable to accommodate varying specimen sizes and aided in the ease of removal of the specimens. A plastic liner was installed in the bed before pouring the concrete. This was done in order to extend the service life of the bed and to achieve a proper sealed system. Figure 3-9 shows the construction of the precast bed.

a) Base for precast bed

b) Installing modular walls

c) Application of plastic liner

Figure 3-9: Details for the precast bed

The concrete layers for the specimen were applied in two lifts. First, the bottom layer was poured onto the precast bed. A hand trowel was used to spread the concrete and achieve a uniform one-inch layer. A one-inch depth indicator was also used to ensure a uniform layer of concrete before installing the panel. Figure 3-10 shows how the bottom layer was poured.

a) Pouring the bottom layer b) Spreading the bottom layer

Figure 3-10: Pouring the bottom concrete layer

After the bottom layer was poured, the MetRock SCIP was placed inside the precast bed. The core was lifted manually and was moved into place; sufficient pressure and lateral movement had to be applied to ensure that a uniform one-inch bottom layer was achieved. The one-inch guide ribs installed in the panels made this process very easy. The guides basically acted as a seat for the panel. Figure 3-11 shows how the panels were placed inside the precast bed.

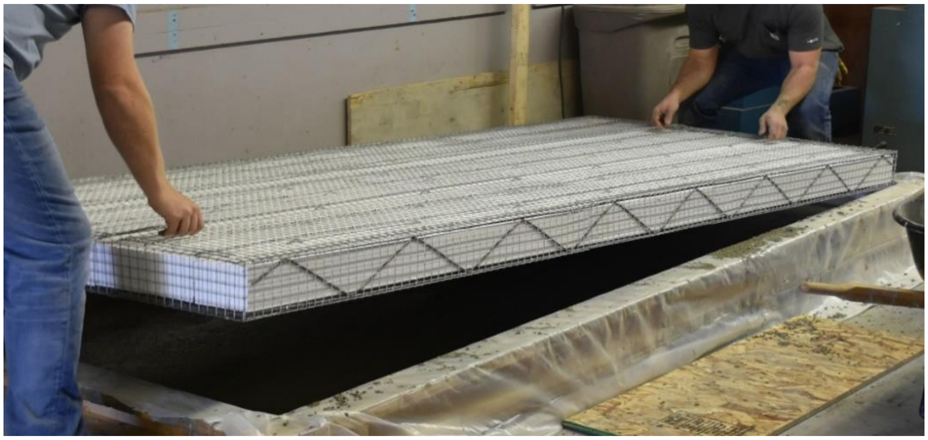

a) Lifting the MR panel into the precast bed

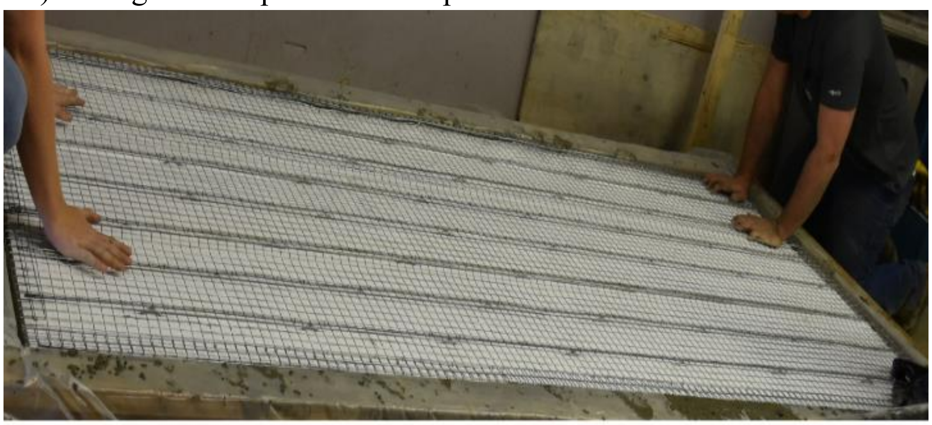

b) Moving the panel in place

Figure 3-11: Placing MetRockSCIP core inside the precast bed

After the panel was properly placed inside the precast bed, the top layer of concrete was poured in a manner identical to the bottom layer. After sufficient SCC was poured on top of the panel, hand trowels were used to evenly spread the concrete. The ribs in the mesh were helpful to maintain a uniform thickness of concrete. Additionally, a flat plate was used to rod the sides and ends of the panel. This was done to ensure an even layer of concrete cover was achieved around all the edges. Figure 3-12 shows the details for the application and finishing of the top layer.

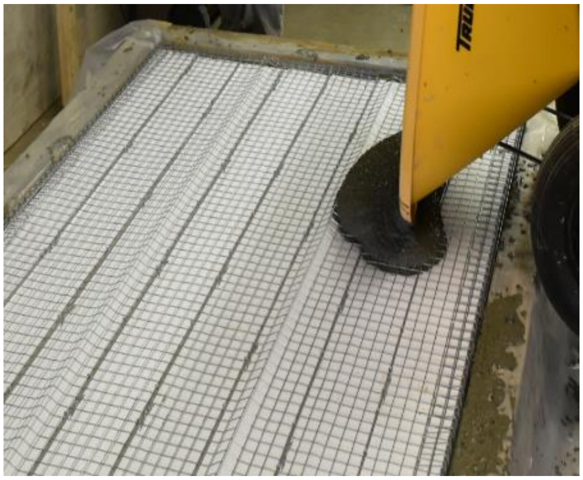

a) Pouring top layer of concrete

b) Spreading concrete on the panel

c) Using screed rib as a guide

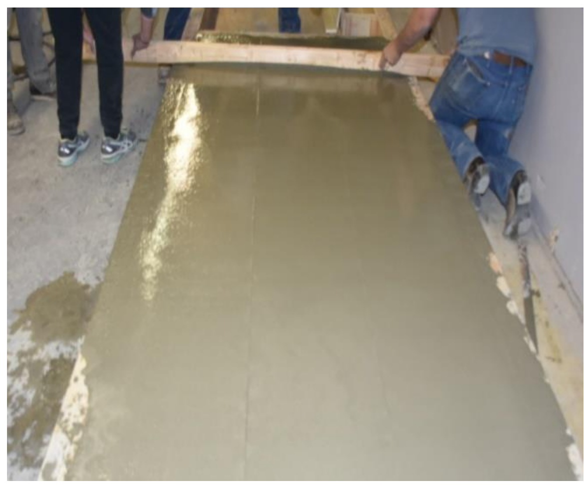

d) Finishing the top layer

Figure 3-12: Application and finishing of the top concrete layer

After the concrete was poured on the specimen, a plastic liner was used to cover the concrete. The specimen was cured inside the bed for three days using a wet burlap. The strength of the concrete for all specimens was checked before removing the panel from the bed. The specimens were moved out of the bed and on to flat roller carts. They were then transported to the curing rack where a long spreader steel beam and construction grade straps were used to lift the panels up on its side. The specimens were cured using moist burlap that was covered with a plastic wrap for 28 days. The average self-weight of the panel after the application of the concrete was 34 lb/ft^2.

a) Removal of modular wall

b) Transferring the specimen onto carts

c) Lifting the specimen using forklift

d) Moist curing for 28 days

Figure 3-13: Removal of specimen form precast bed and curing process

3.4.2 Preparing socket footing for wall specimen

A socket footing was designed and constructed to provide the fixed connection required for a cantilevered wall specimen. The socket connection used for this research consisted of a reinforced concrete strip footing that was 30 inches wide, seven feet long, and 17 inches deep . The footing had a 7x50 inch opening in the middle that was 15 inches deep. Six ducts were installed in the footing that were later used to tie the footing to the strong floor. Details for the socket footing are provided in Figure 3-14.

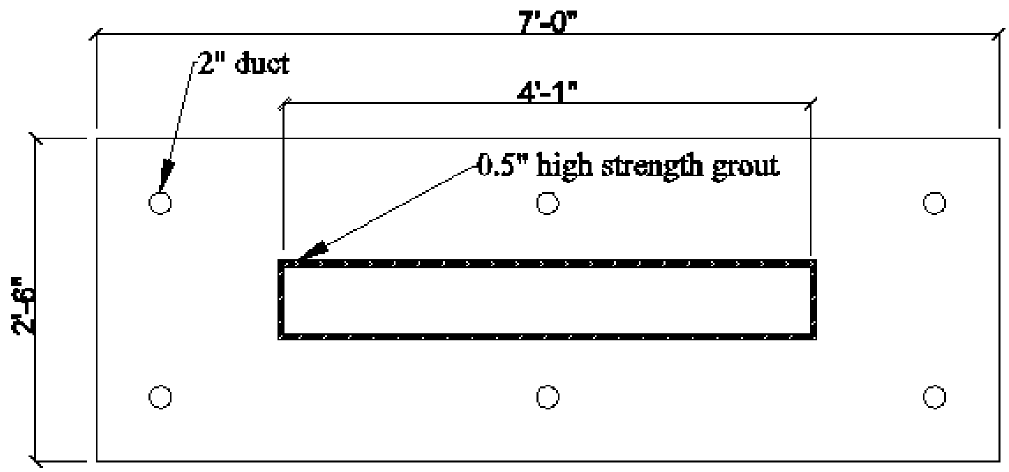

Figure 3-14: Details for socket footing

The reinforcement system used for footing consisted of two layers of longitudinal reinforcements (# 6 bars placed at 3 in O-C). The construction details used to prepare the reinforcement cage are shown in Figure 3-15. A typical two layered reinforcement cage was used, the layers of longitudinal reinforcement were placed 15 inches apart. Specially designed stirrups made from #4 bars were used to provide confinement to the footing; the stirrups were placed 12 inches on center. Similarly, confinement for the socket opening in the middle was provided using hairpin stirrups. After the reinforcement cage was assembled, six galvanized pipes were welded to the cage. These pipes were installed as ducts for the high strength post-tensioned anchor rods. Figure 3-15 shows the reinforcing used for the footings. After the reinforcement cage was completed, the remaining formwork was assembled and, a high strength concrete was poured in the formwork, details for this process is shown in Figure 3-17. The concrete was cured inside the formwork for 28 days prior to being moved to the laboratory.

a) Assembling the rebar cage

b) Finished reinforcing cage with ducts

c) Footing ready for concrete

Figure 3-15: Reinforcement detail for socket footing

a) Delivery of ready-mix concrete

c) Vibrating the concrete

b) Filling formwork with concrete

Figure 3-16: Preparation of socket footing

3.4.3 *Assembly of the shear wall test specimen*

A precast construction technique was used to assemble the prefabricated panel to the socket footings. First, the socket footings were transported from the precast bed to the structural lab. They were then secured to the strong floor with the aid of six post-tensioned high strength anchor rods. Once the footings were in place, the panels were stood up vertically using a tilt-up system. The tilt-up system required the panel to be backed up against stiff support; using a forklift. Extra care was taken for this process to induce minimum stress on the panel. The tilt-up process is shown in Figure 3-17.

After the panels were erected, they were clamped using a setup fabricated using two angled steel sections with a pair of post tensioned rods. The panels were then lifted using a forklift and were place placed inside the socket footing. The panels were then grouted in place using Dayton 1107 high strength non shrink grout. The product data sheet for the grout is provided in the Appendix A. The details for the assembly process are shown in Figure 3-18.

Figure 3-17: Tilt up a process for wall panels

a) Clamping of panel

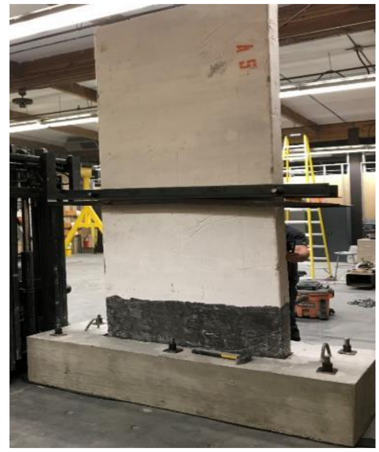

b) Placement of the panel

c) Mixing of the grout

d) Application of the grout

Figure 3-18: Assembly of wall specimen

CHAPTER 4. Experimental Testing of Slab Panels

4.1 General

This chapter presents the development and testing of MR SCIP used as slab panels. Three different spans of slabs were tested. The slab specimens were prepared using a four feet wide MR SCIP with a four-inch insulation core. The slabs were fabricated using a precast approach. The details for the fabrication of the slab specimens are provided in Section 3.3. The goal of this experiment was to study the out-of-plane flexural behavior of MR panels when subjected to transverse loading. Furthermore, the performance of the panels used as floor and roof slabs for residential structure are also assessed using the code requirements stated in the ACI 318-14 and ASCE7-16. The results obtained from the full-scale testing of the slabs are presented and analyzed in this chapter.

For this part of the research a total of 12 full-scale slab specimens were prepared and tested. To accurately study the flexural behavior of the panel, three different spans of slabs were tested. Each span had three identical specimens to avoid any outliers. The three spans used in this experiment were 10, 14, and 18 feet. Additionally, two modified 18 ft with extra splice reinforcement were also tested. A four-point bend test was conducted on all the specimens in close accordance with the ASTM E72 (ASTM, 2005). All the testing for experiment were conducted at the structural laboratory at Idaho State University.

4.2 Test specimen description

This section provides details of the test specimen used for the four-point bend test. Following the guidelines in the ASTM E72, three identical specimens for each span was produced and tested. A detailed cross-section of the MR slab specimen used for this experiment is provided in Figure 4-1. All the panels used in this study had side and end confinements. The edges of the panels were confined using a special U mesh with half inch of concrete. The details for the edge confinement are shown in Figure 4-2. The edge confinement was used to avoid premature failure caused by the out-of-plane buckling of the diagonal bars (Fouad et al, 2008). Figure 4-3 shows the three different types of panels used for the fabrication of the slab specimens.

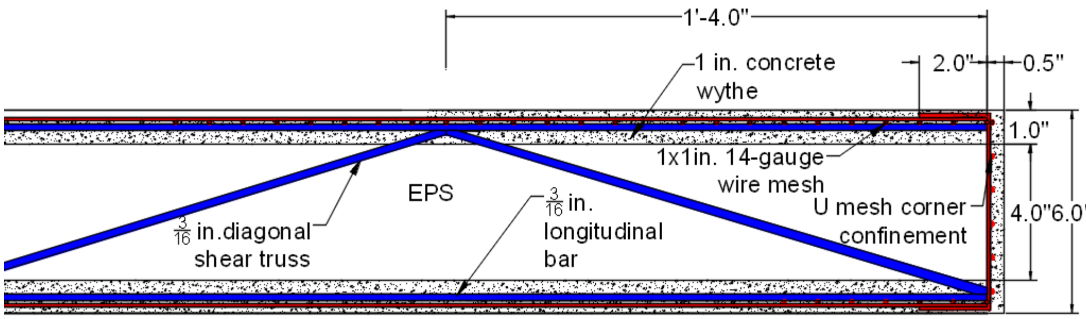

Figure 4-1: Cross-section of a MR SCIP slab specimen

Figure 4-2: Edge wall confinement for panels

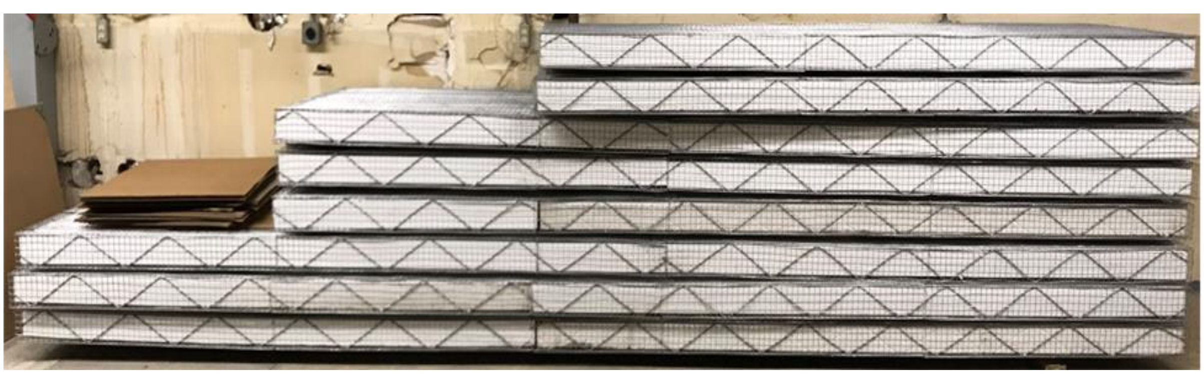

Figure 4-3: MR SCIP slabs specimens prior to concrete application

4.3 Material properties

All the slab specimens were fabricated using a typical four feet wide MR SCIP. The panel consisted of an EPS core that was flanked on both sided using two galvanized 14-gauge cold rolled steel wire mesh. The layers of mesh were held together using 3/16-inch diagonal steel shear trusses. The diagonal truss were placed at every six inches and were sandwiched in between the EPS block and were tied to the mesh using a hollow ring tie. The assembly was then completed by applying a thin layer of self-consolidating concrete on both sides. A summary of the material characterization of the MR slabs are as follows.

4.3.1 Steel Reinforcement

The tensile reinforcement system for a typical MR panel comprises of two major components: the 14-gauge cold rolled galvanized steel wire mesh and the 3/16-inch longitudinal steel bars. The two reinforcement layers were separated by a four-inch-thick EPS insulation core and were held together using shear trusses. The 14-gauge wire mesh utilized a one-inch square grid pattern. The distance between the two opposite mesh was 5 inches. Similarly, the steel mesh also had a special one-inch guide ribs installed in them. The guide ribs allowed for an easy application of the concrete layers. A spacing of half-an-inch was maintained in between the mesh and the EPS core to ensure that the mesh achieved sufficient embedment and cover. Figure 4-4 shows the actual tensile reinforcement system for the MR SCIP.

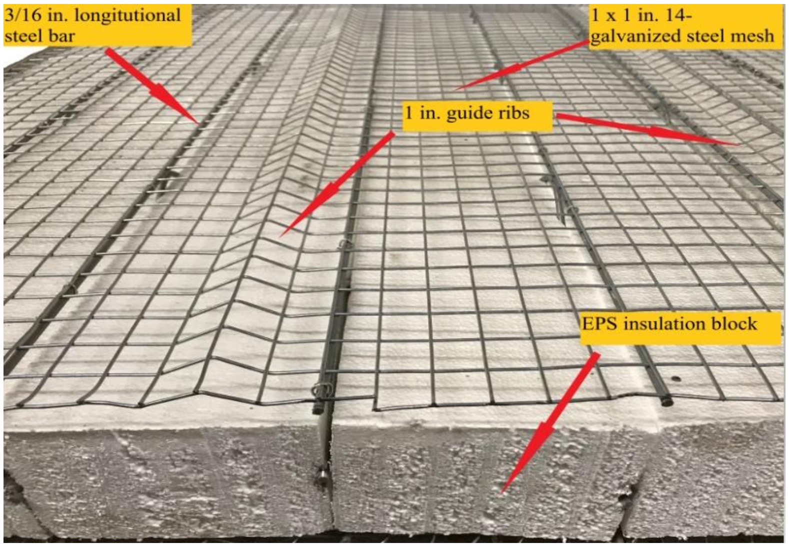

Figure 4-4: Details of tensile reinforcement for MR SCIP

The shear trusses were used to transfer the longitudinal shear stresses between the two-load-bearing faces. The MetRock panels utilized 3/16-inch diagonal shear connectors that were placed 6 inches on center and were sandwiched in between the EPS blocks. The arrangement of the shear trusses is shown in Figure 4-5.

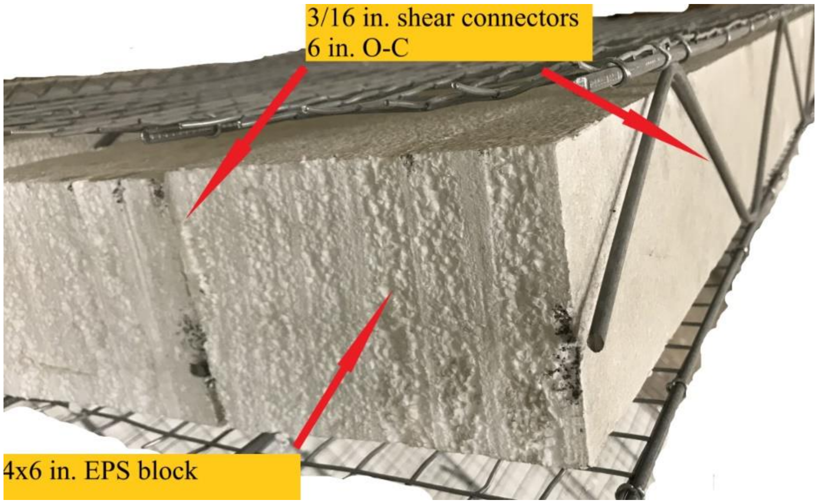

Figure 4-5: Image of diagonal shear connectors in MR SCIP

The reinforcement system for panel consisted of the mesh and the longitudinal truss bars. According to the product data sheet, the production of both the mesh and the trusses complied with the ASTM A-641 and the ASTM A-82. The average reinforcement ratio for the panels was 0.035%. This exceeded the minimum reinforcement ratio requirement for RC slabs as stated in the ACI 318-14 section 21.9.1. According to the ACI standard a minimum reinforcing ratio of 0.025% is required for a typical RC slab (ACI, 2014).

As a part of the material characterization a tensile coupon testing of the mesh and the longitudinal bars were performed. A series of uniaxial tensile tests (ASTM E-08) were performed on various 14-gauge mesh wire and the 3/16-inch longitudinal bar samples. Figure 4-6 shows the test setup and the failure modes for the wires and the bar specimens. The average ultimate strength for the 3/16 inch longitudinal bar was 81.9 ksi. Whereas, the ultimate strength for the mesh wire was 70.3 ksi. Test results from the tensile testing are provided in Table 4-1 and 4-2.

Table 4-1: Tensile test results for 3/16-inch longitudinal bar

Specimen	I	II	III	Average
Diameter (in)	0.190	0.189	0.190	0.190
Area (in^2)	0.0284	0.0281	0.0284	0.0283
Yield force (lb)	2050	2040	2090	2060
Ultimate force (lb)	2370	2310	2290	2323
Yield strength (psi)	72303	72714	73714	72910
Ultimate strength (psi)	83589	82338	80768	82232

Table 4-2: Tensile test results for 14-gauge mesh

Specimen	I	II	III	Average
Diameter (in)	0.080	0.079	0.080	0.080
Area (in^2)	0.0050	0.0049	0.0050	0.0050
Ultimate force (lb)	357	360	340	352
Ultimate strength (psi)	71023	73444	67641	70703

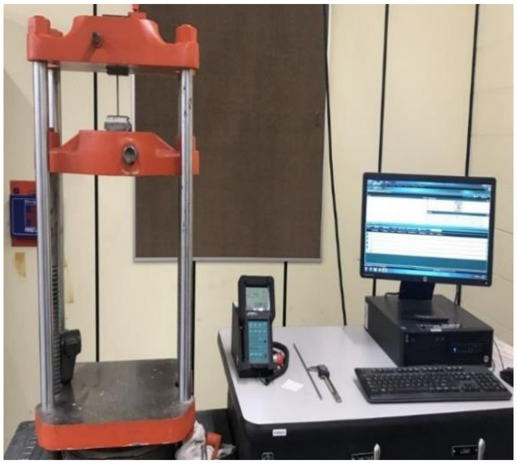

a) Tensile testing of truss bar

b) Failure of truss bars

c) Tensile testing of mesh wire

d) Failure of wire mesh

Figure 4-6: Uniaxial tensile coupon testing for SCIP reinforcing

4.3.2 Expanded Polystyrene Styrofoam (EPS) Insulation Core

For the insulation the MetRock panel utilizes Cellofoam Type I EPS insulation blocks. The panels used for this experiment used EPS blocks that were four inches thick, six inches wide, and 10 feet long. The product data sheet for the EPS core is provided in Appendix A. According to the datasheet, the EPS core has an average density of 0.95 pcf with an average thermal conductivity K factor of 0.24 and thermal resistance R-value of 4.12 per inch (ASTM C 177). The stated modulus of elasticity for the EPS core ranges in between 180-220 psi. They have a shear modulus of 280-320 psi. The EPS cores have absorption of four percent and are resistant to fungus and bacteria.

4.3.3 Self-Consolidating Concrete

As stated in chapter 3 a precast approach was used to apply the two load-bearing skins on the panels. The self-consolidating concrete used to cast the specimens was designed and mixed in-house using two 1.5 ft^3 drum mixers. To maintain the standard of the concrete used for each pour, a spread test following the ASTM 1611 was conducted for each batch (ASTM, 2012). Along with that, six standard compression cylinders were also prepared at random using the ASTM C31. Pictures for the spread test and the preparation of the concrete cylinders are shown in Figure 4-7.

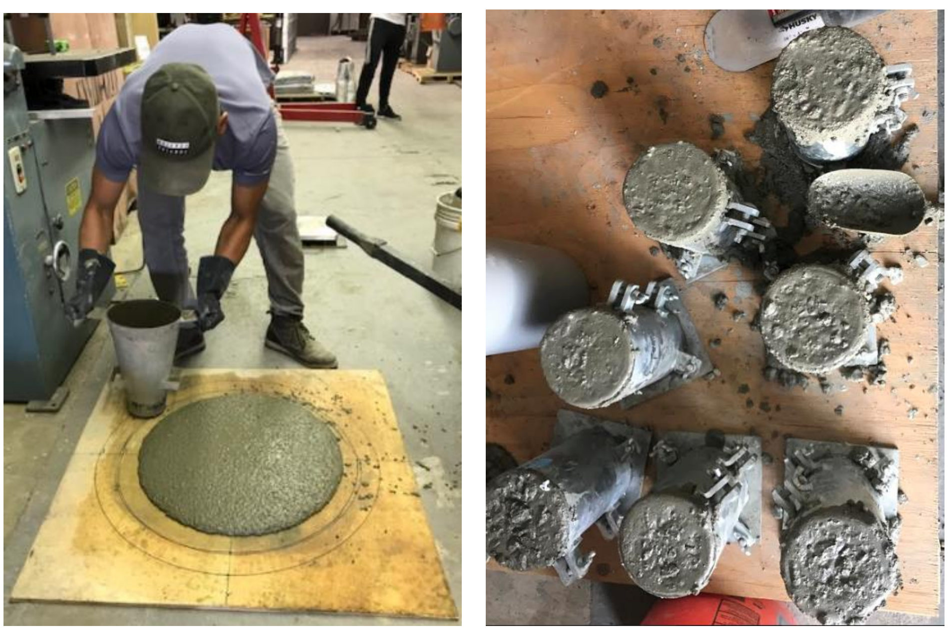

a) Spread test b) Casting test cylinders

Figure 4-7: Slump test and preparation of concrete cylinders

The concrete test cylinders were cured in a water bath prior to being tested at various stages. All the concrete specimens were tested in accordance to the ASTM C 39 and C 498 (ASTM, 2012). The strength properties of the design mix are provided in Table 4-3. Testing of the compression cylinders showed that the average 28 days strength for the mix was 8491 psi. Additionally the split cylinder testing showed that the mix had a tensile strength of 436 psi. Figure 4-8 shows the test setup for the compressive strength test and split cylinder test of the concrete specimens. The strength properties for the design mix are provided in Table 4-3.

Table 4-3 Strength properties for design SCC mix

Compressive Strength						
Sample	Diameter (in)	Height (in)	Area (in²)	Max load (lbs)	Compressive strength (psi)	Days
I	4.02	8.0	12.7	53370	4205	3
II	4.00	8.0	12.6	54980	4375	3
Average					4290	
III	3.99	8.0	12.5	77330	6185	7
IV	3.97	8.0	12.4	83120	6715	7
Average					6450	
V	4.01	8.0	12.6	112200	8895	28
VI	4.00	8.0	12.6	109310	8699	28
VII	4.01	8.2	12.6	104750	8284	28
Average					8491	
Tensile Strength						
A	6.0	12.0	28.3	42980	380	28
B	5.9	11.8	28.2	53810	492	28
Average					436	

a) Standard compression **b) Standard split cylinder**

Figure 4-8: Concrete cylinder testing for SCC design mix

4.4 Test set up

This section provides information on the testing arrangement for the MR slab specimens. The four-point bend test used for this experiment corresponded to a transverse out-of-plane loading of the MR panels. All tests for this experiment were conducted according to section 4 of the ASTM E72-05 “Standard Testing Method of Conducting Tests of Panels for Building Construction.” (ASTM E72, 2005). All tests were conducted horizontally where the slabs were simply supported in between two rollers and was loaded using two-point loads at quarter span. Figure 4-9 provides the schematics for the test setup. The actual test set up is shown in Figure 4-10.

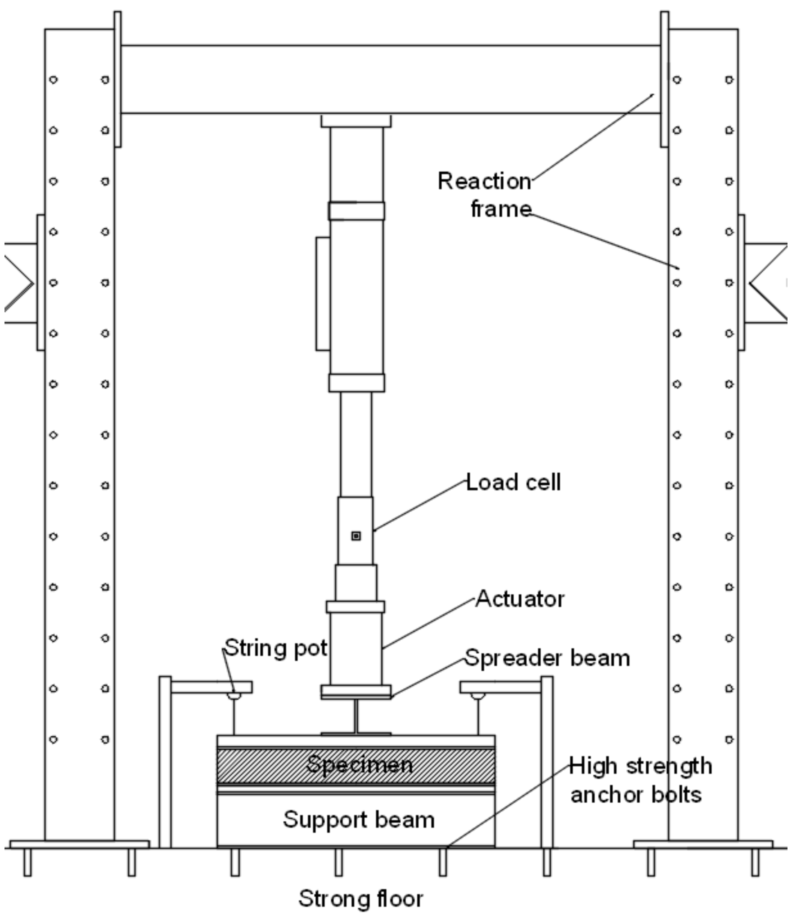

Figure 4-9: Schematic of a four-point bend test

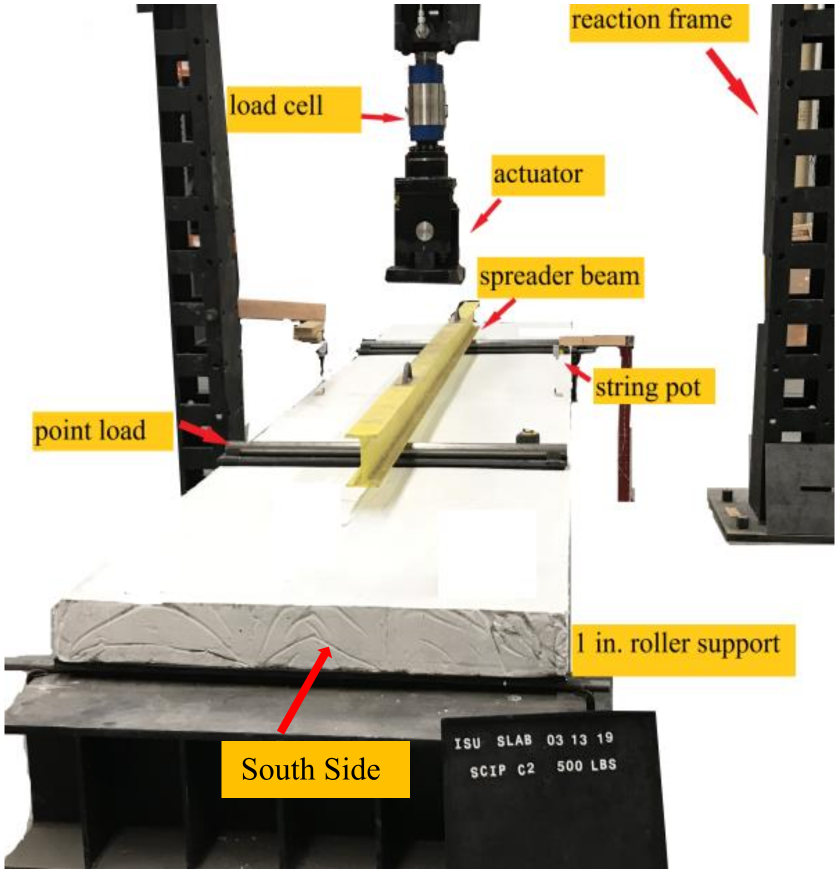

Figure 4-10: Test setup used to conduct the flexural test of slab specimen

All the specimens used for this experiment were cured for at least 28 days. Once the specimens were cured, they were moved into the structural lab on carts and were lifted on to the supports using a spreader beam and a forklift. Five construction grade straps were tied around the panels and were used to set the specimen in place for testing. The average weight for a long span specimen was about 2400 pounds therefore, extra care was taken during the transport process to ensure minimum stresses were induced on the specimen prior to testing. The transportation process used to set up a specimen is shown in Figure 4-11.

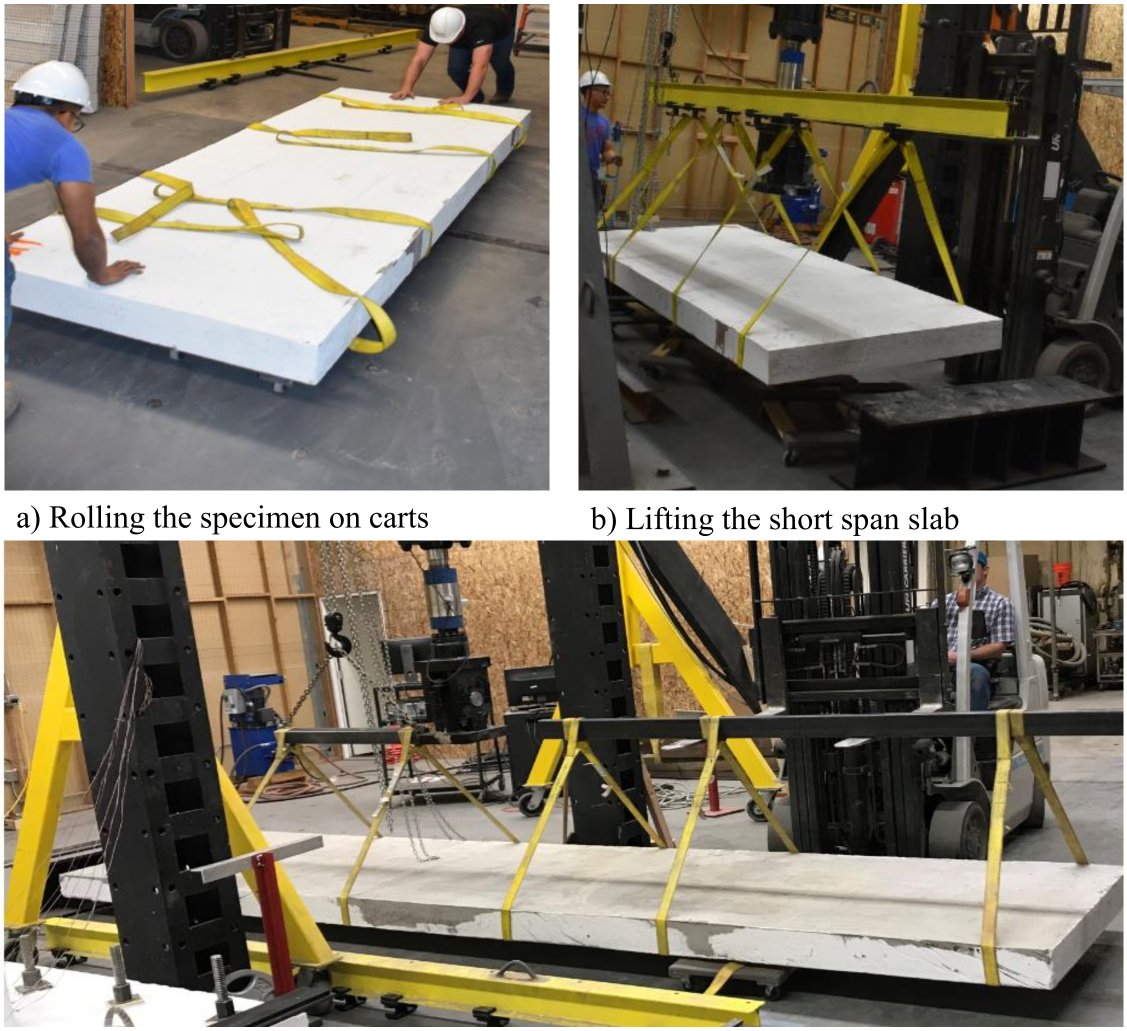

a) Rolling the specimen on carts

b) Lifting the short span slab

c) Lifting the long span slab

Figure 4-11: Setting up a slab specimen for four-point bent test

4.4.1 Support conditions

All the slab specimens were oriented horizontally and were seated on a stiff steel beam using a roller that was one-inch in diameter. Additionally a half-inch steel plate with a rubber mat was installed in between the specimen and the rollers to avoid any bearing failure. The details for the end support conditions are provided in Figure 4-12

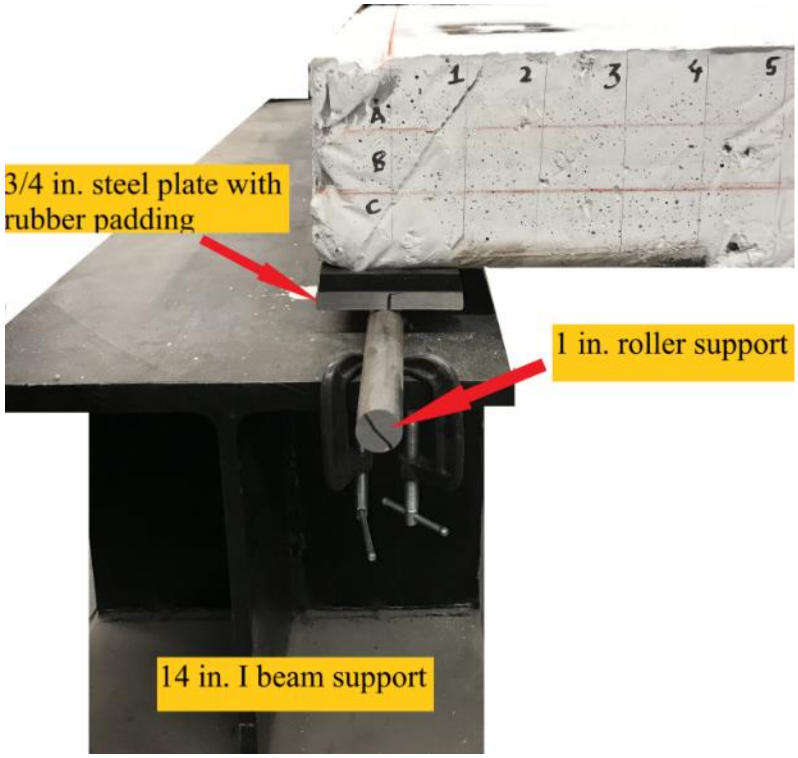

Figure 4-12: End support details for flexural test

4.4.2 Loading apparatus

The loads were applied using a 160-kip capacity displacement control servo-hydraulic actuator pushing against a reaction frame; the frame was tied down to the strong floor using high-strength threaded rods. Figure 4-10 show how the actuator and the reaction frame were setup. The load from the actuator was then divided into two-point loads at the quarter span of the specimen using a stiff steel spreader beam seated on two roller plates with 3/4-inch steel bearing plates and rubber padding. Figure 4-13 shows how the point loads were applied

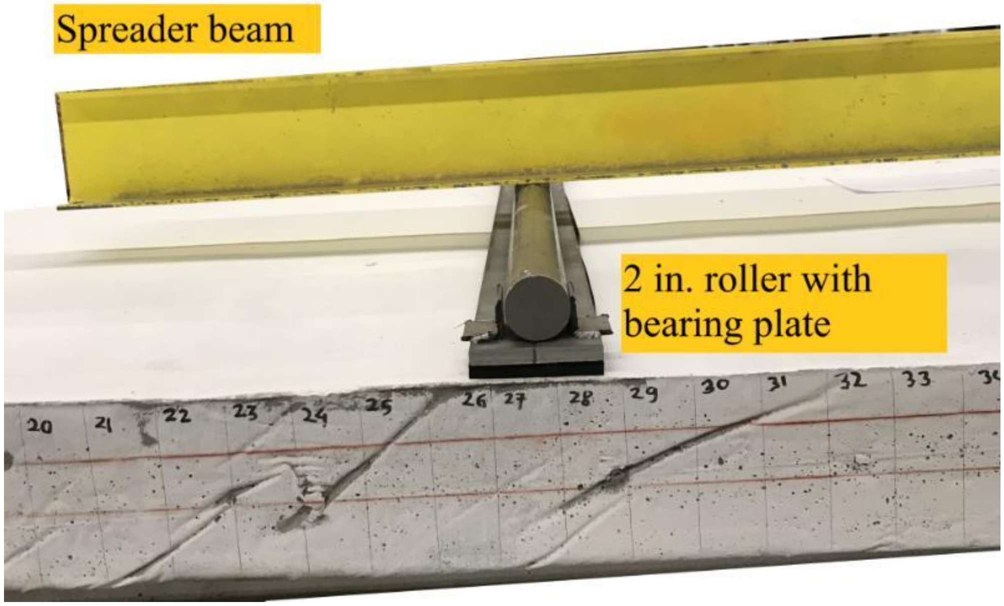

Figure 4-13: Point loading detail for flexural test of slab specimen

4.4.3 Measurement devices and instrumentation

The Campbell Scientific data acquisition system (DAQ) was used to simultaneously monitor and record the loads and the midpoint deflections during the tests. The rate of data collection for the test was set at one hertz. The loads were recorded using a 225 kip capacity load cell that was attached to the head of the actuator. The vertical midpoint deflections of the specimen were measured using two 50 inch stroke sting pots that were placed at the centerline of the specimen and were attached at the edges. The string pots were mounted on two isolated stands. The mid-span deflection was calculated as the average of the two measurements.

4.4.4 Experimental observations

The data collected for each tests was supplemented by observations at different stages of testing. A crack propagation analysis was conducted on each specimen to assess the propagation of damage and the overall specimen performance visually. The location, type, and size of cracks were noted throughout the test for this purpose.

4.5 Loading protocol

A monotonic quasi-static loading protocol in accordance with ASTM E72 was used to load the specimen for this test. A quasi-static protocol refers to loading where the inertial dynamic effects are negligible. The loading cycle for the flexural tests was applied at an increment of 500 pounds and was continued until failure. The rate of advancement for the actuator was set at one millimeter per second, and the loading intervals were applied manually. At each load increment, the maximum load was held constant for at least five minutes to allow time to mark the cracks and to make any observations. Following each increment, the load was slowly removed, and the specimen was allowed to stabilize for about five minutes.

4.6 Experimental results

This section discusses the test results and observations made during the testing of the slab panels. Each specimen was tested up to failure to determine the ultimate load capacity, yield moment capacity, failure modes, and the maximum deflection. All tests that were conducted are summarized and the results are presented graphically in this section.

4.6.1 Short span slab specimen

Three identical 10 feet slabs were tested under a four-point bend test with point loads at quarter point spans for this part of the experiment. The three specimens that were tested were labeled A-1, A-2, and A-3. All the specimens were 123 inches long, 49 inches wide and six inches thick and had a simply supported span of 119 inches. A detail test setup for the short span specimen is illustrated in Figure 4-14: . The actual test-set up of the short span specimen is shown in Figure 4-15.

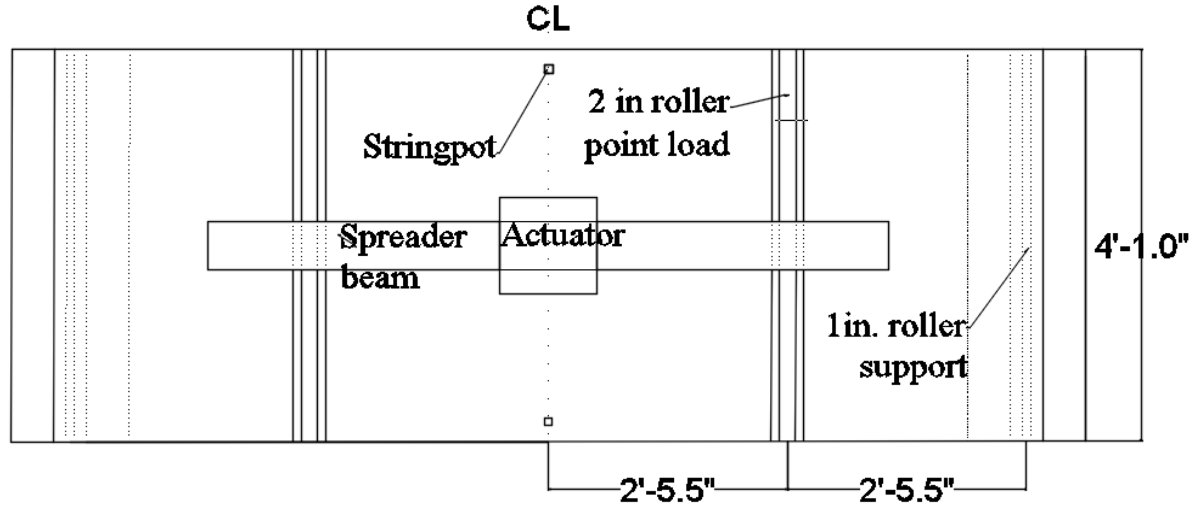

Figure 4-14: Details for short span slab testing

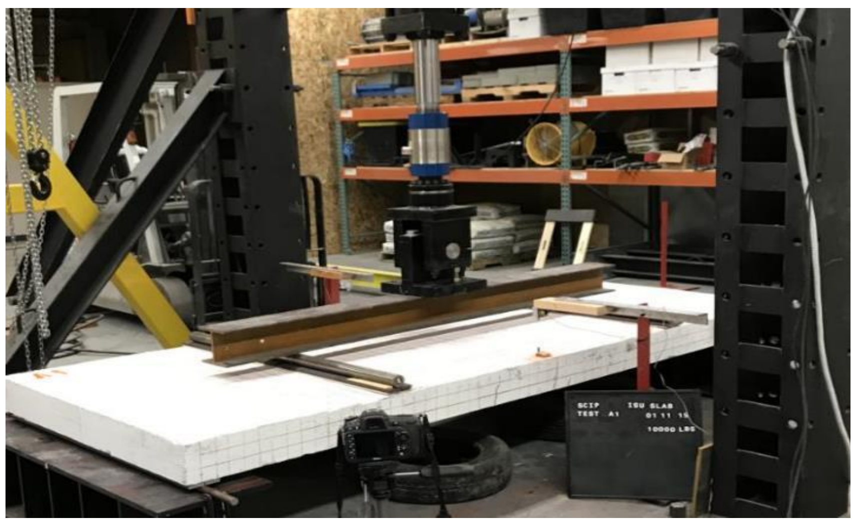

Figure 4-15: Experimental test setup for A-1

Specimen A-1 was prepared on 11/15/2018 and was tested on 01/11/2019. The concrete strength of the specimen at transfer was 3185 psi, and the test day strength was 8657.7 psi. The raw load versus midpoint deflection data collected during the testing of A-1 are provided in Figure 4-16. The peak load and its corresponding mid-span deflection from the raw data were utilized to determine the backbone curve for the specimen. This was done with the aid of a MATLAB code, the code used for this study in attached in Appendix E. The backbone load-deflection curve generated using the raw test data and the MATLAB code for specimen A-1 is provided in Figure 4-17. The corresponding moment deflection curve is also included as a secondary axis in Figure 4-17. During the testing the first cracks were observed between the load cycles of 6.5 kips and 7 kips. This can also be observed in the load-deflection curve as a bend-over point at a load of 6.37 kips. Prior to cracking, the linear stiffness of the specimen was 68.5 kip/in which reduced significantly after the yield point. The ultimate load sustained by A-1 was 12.8 kips; at which point, the average mid-span deflection was 2.28 inches. The ultimate applied moment was 15.9 kip-ft, which corresponds to an equivalent area load of 317 psf. The equivalent area load represents the amount of uniformly distributed area load required to produce the same amount of moment sustained by the panel during the test. Eq.(4.1) was used to calculate the equivalent area loads (Hibbeler, 2012).

Equivalent area load

$$A = \frac{8.M_{ult}}{L^2} * b \qquad (4.1)$$

Where,

A = Equivalent area load (psf)

M_{ult} =Ultimate applied moment (lb-ft)

L = Simply supported span (ft)

b = Width of panel (ft)

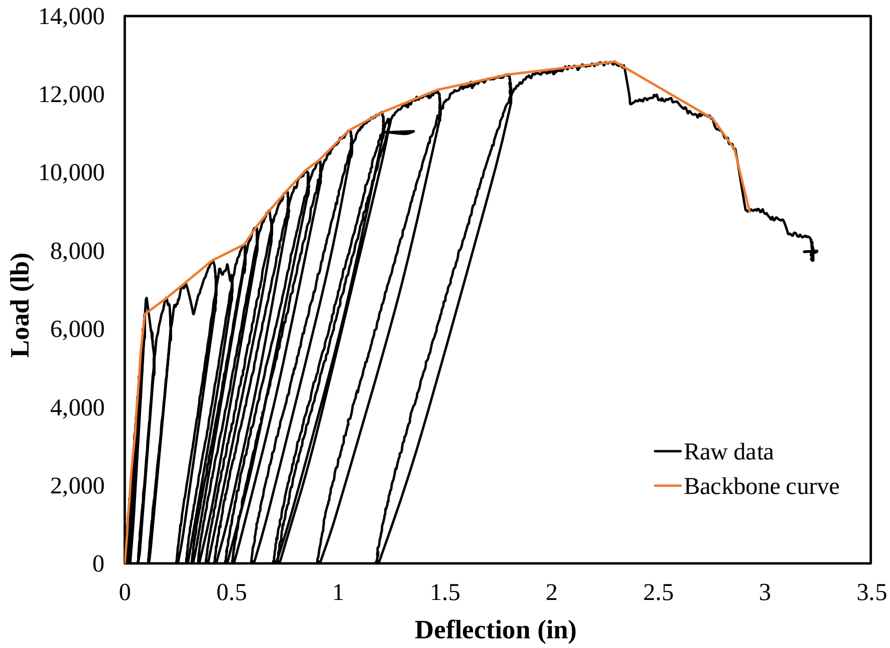

Figure 4-16: Raw flexural test data for specimen A-1

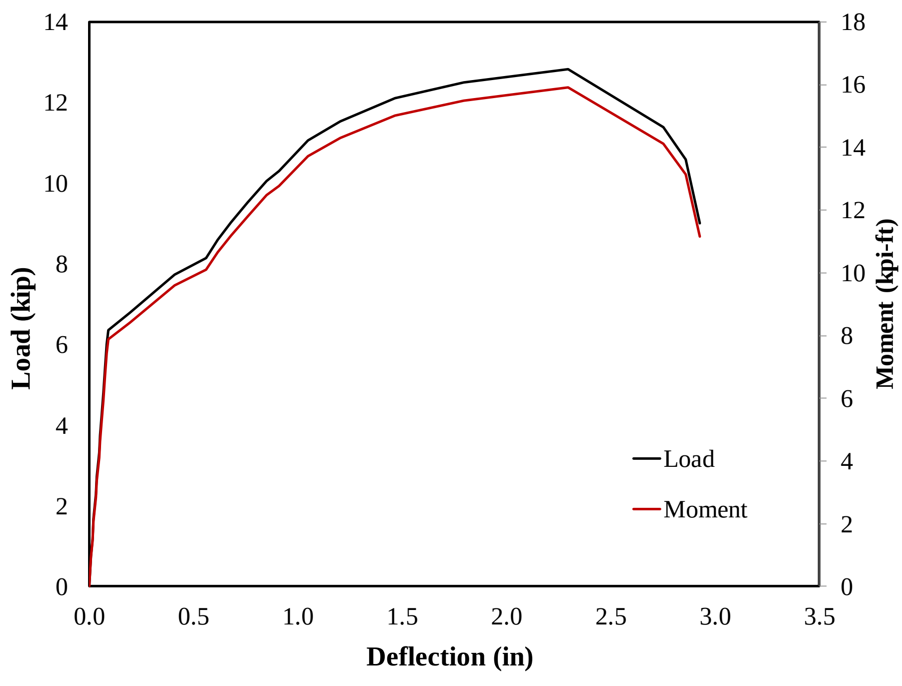

Figure 4-17: Load and moment versus deflection Curve ‘A-1’

Specimen A-2 was prepared on 11/19/2018 and was tested on 01/16/2019. The concrete strength of the specimen at transfer was 4063 psi and the test day strength were 8346.1 psi. The raw load versus midpoint deflection data collected during the testing of A-2 is provided in Figure

4-18. The load/moment versus deflection backbone curve for specimen A-2 is provided in Figure 4-17. The first cracks for A-2 were observed between the load cycles of 6.5 kips and 7 kips. This can also be observed in the load-deflection curve as a bend over the point at a load of 6.82 kips. The linear stiffness for A-2 prior to cracking 70.3 kip/in. This was reduced significantly after the yield point. The ultimate load sustained by A-2 was 13.4 kips at which point the average mid-span deflection of 3.32 inches. The ultimate applied moment was 16.6 kip-ft which corresponded to an area load of 331 psf.

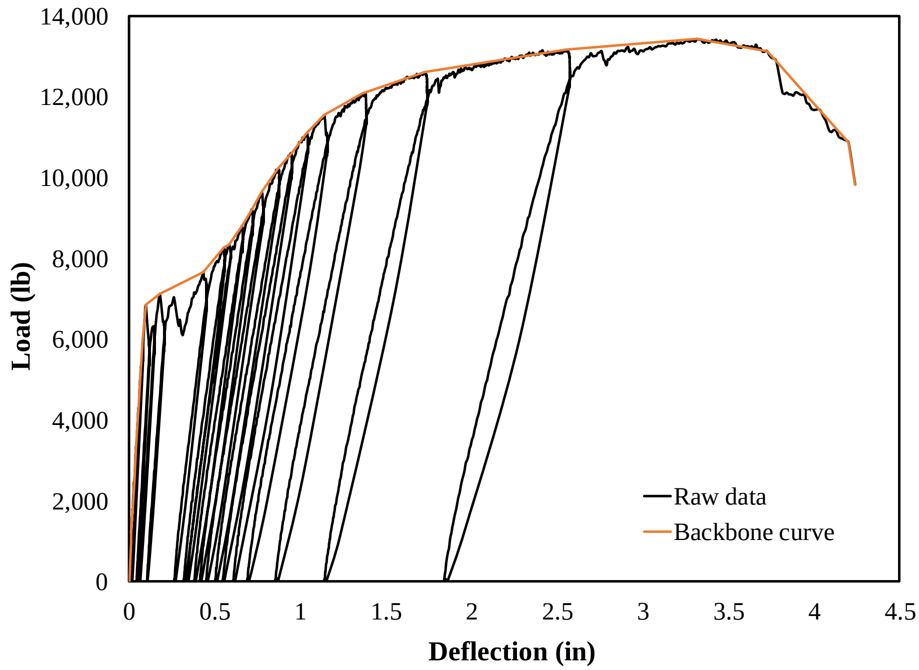

Figure 4-18: Raw flexural test data for specimen A-2

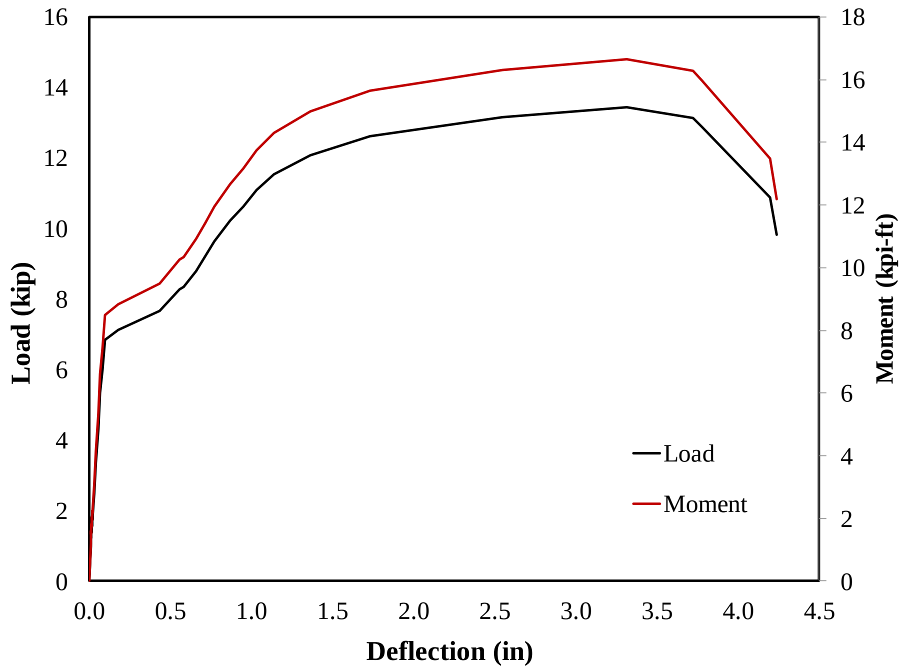

Figure 4-19: Load and Moment versus deflection Curve ‘A-2’

Specimen A-3 was prepared on 11/28/2018 and was tested on 01/20/2019. The concrete strength of the specimen at transfer was 4050 psi and the test day strength was8732.3 psi. The raw load versus midpoint deflection data collected during the testing of A-3 is provided in Figure 4-20. The load/moment versus deflection backbone curve for specimen A-3 is provided in Figure 4-21. The first cracks were observed between the load cycles of 6.5 kips and 7.0 kips. The initial linear stiffness for A-3 was 37.5 kip/in which was reduced significantly after the yield point. This can also be observed in the load-deflection curve as a bend over the point at a load of 7.04 kips. The ultimate load sustained by A-3 was 13.2 kips at an average mid-span deflection of 2.65 inches. The ultimate applied moment was 16.3 kip-ft which corresponed to an area load of 325 psf.

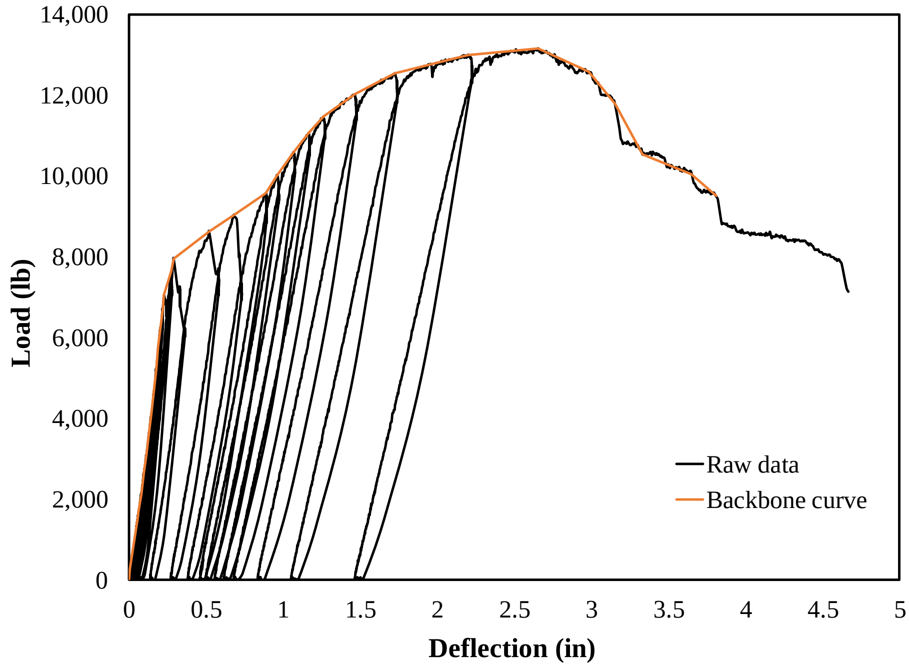

Figure 4-20: Raw flexural test data for specimen A-3

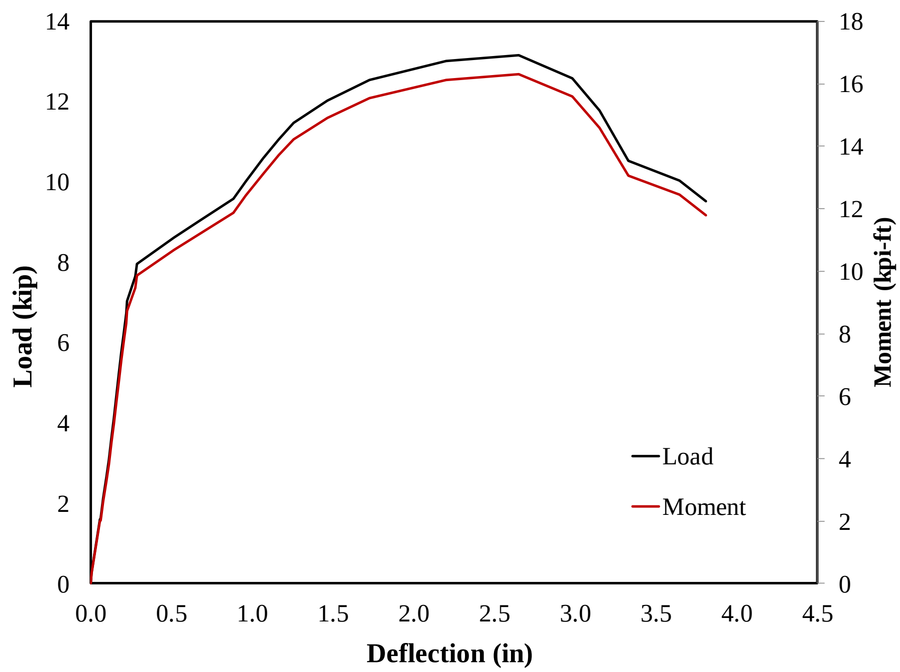

Figure 4-21: Load and moment versus deflection curves ‘A-3’

The mode of failure for all the short span specimens was flexural dominated failure that occurred inside the two-point loads. The first hairline cracks (<0.4mm) were formed on the bottom wythe of the specimen close to the mid-span. With the load increment past the initial cracking, more hairline cracks were formed inside the critical moment region (in between the two-point loads) which in the later stages propagated outside towards the supports. All the cracks that were formed during the testing were flexural cracks; the cracks went straight across the width of the slab on the bottom wythe and continued on to the edge walls. Figure 4-22 shows some of the flexural cracks observed during testing. Several new hairline cracks were formed before the specimens started to yield. Post yielding of the specimen, very few new cracks were formed and the existing cracks started to get wider. This continued until a dominant crack was formed that eventually caused the failure. The snapping of the wires and the longitudinal bars were heard towards the end of the experiment. The rupture of the reinforcement can also be observed as small drops in the raw load-deflection data. Although no specimen failed exactly at the mid-span, all failure occurred inside the critical moment region. Post failure analysis of the specimens showed no signs that indicated buckling of the diagonal bars. Table 4-4 provides the details for the modes and locations of failure for each specimen.

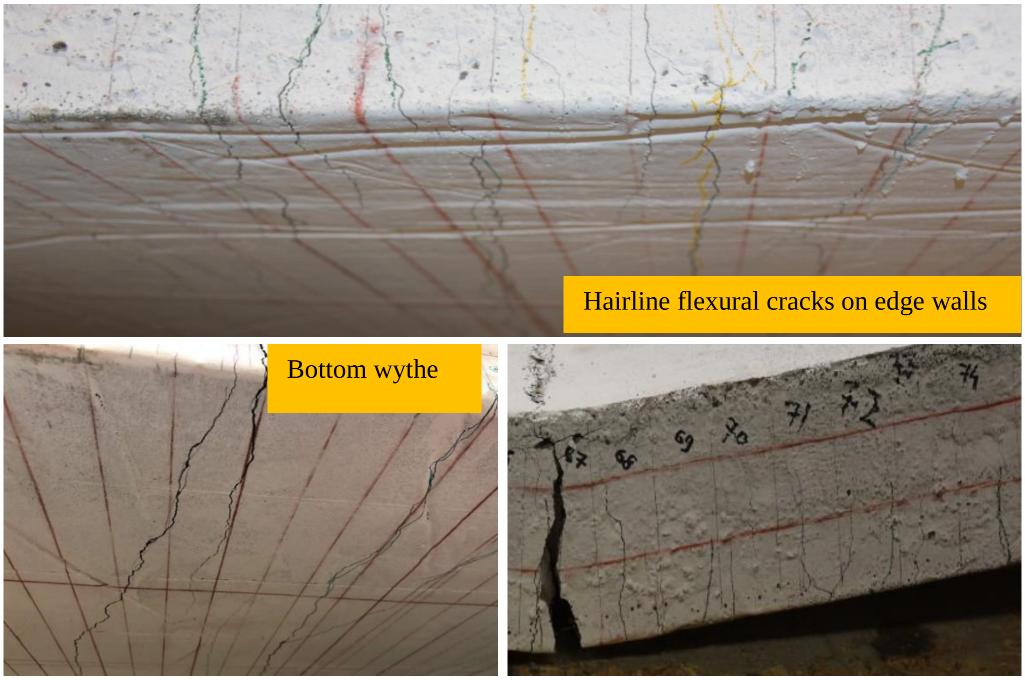

Figure 4-22: Flexural cracks on bottom wythe and edge walls

Table 4-4: Failure mode for short span slab specimens

Specimen	Mode of failure	Location of failure	Description
A-1	Ductile flexural dominated failure	12.5 inches north of the centerline	Figure 4-22 a) failure of the specimen. b) west edge wall. c) east-edge wall
A-2	Ductile flexural dominated failure	12.8 inches south of the centerline	Figure 4-23 a) failure of the specimen. b) west edge wall. c) east-edge wall
A-3	Ductile flexural dominated failure	13.5 inches North of the centerline	Figure 4-24 a) failure of the specimen. b) west edge wall. c) east-edge wall

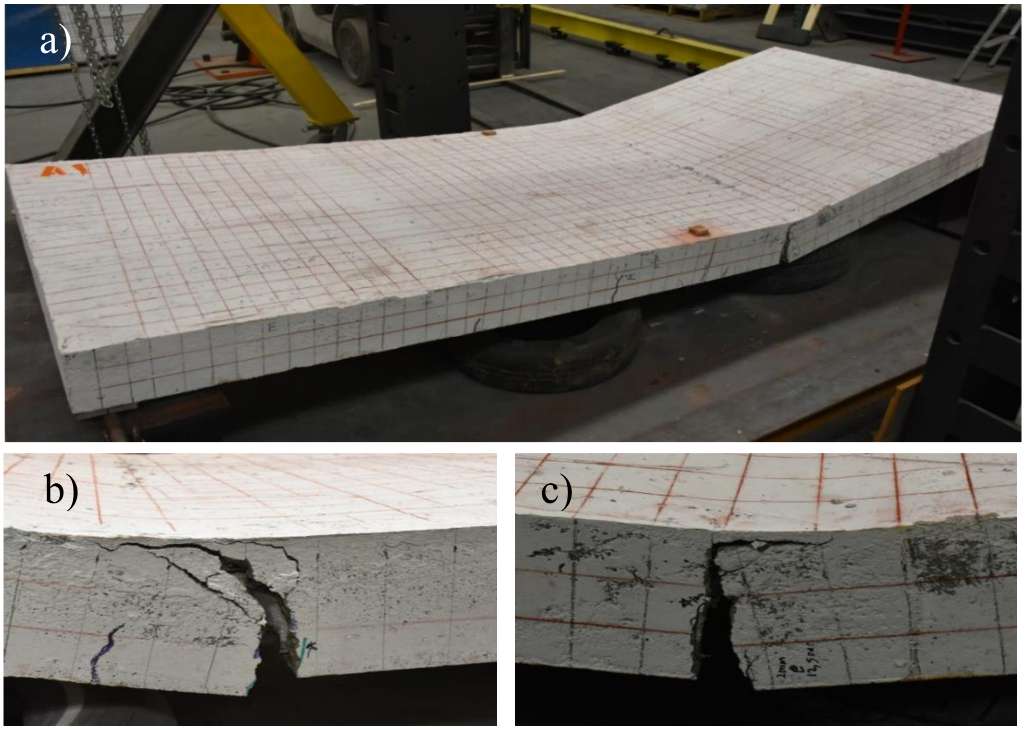

Figure 4-23: Failure mode ‘A-1’

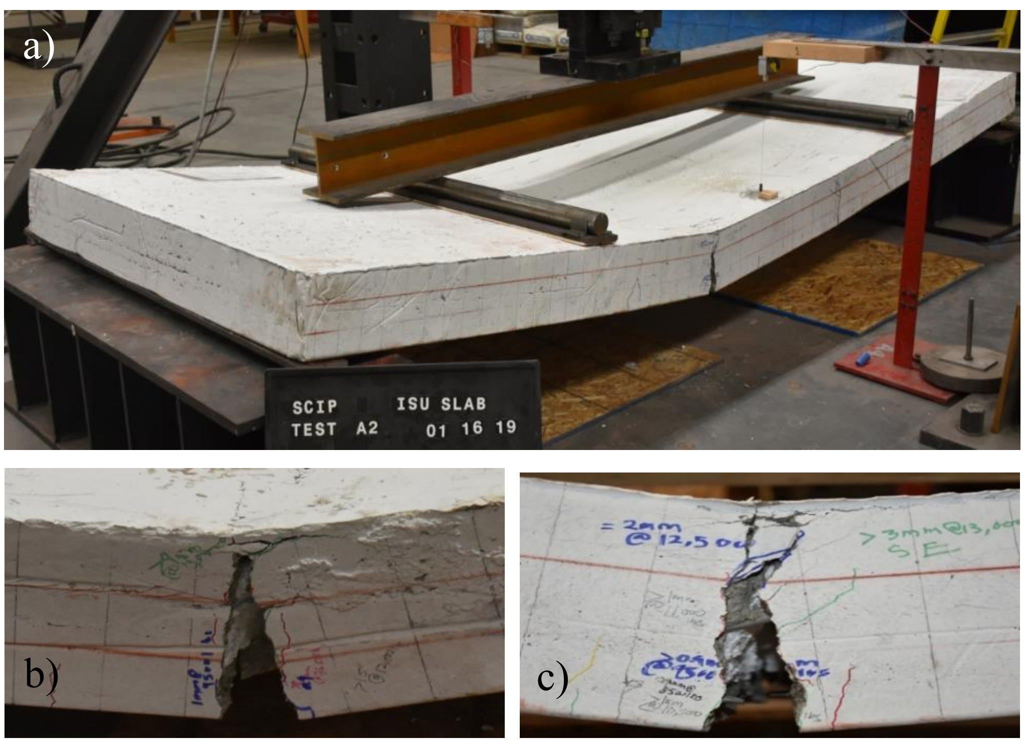

Figure 4-24: Failure mode ‘A-2’

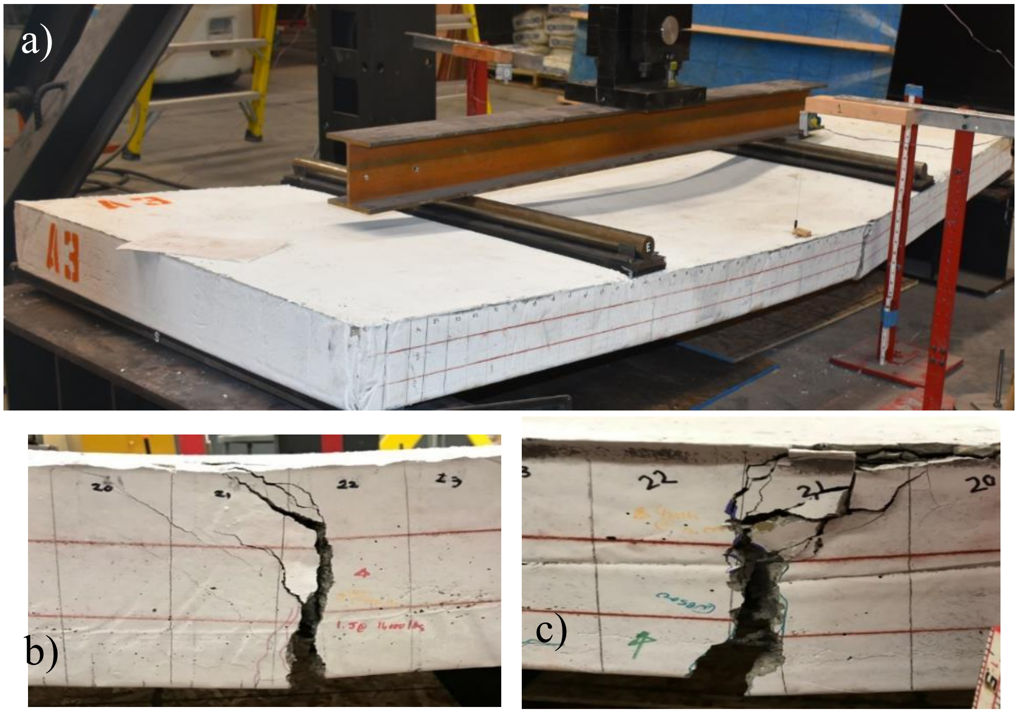

Figure 4-25: Failure mode ‘A3’

Overall the short span slabs exhibited a very ductile behavior when subjected to out-of-plane flexural loading. The test summary for all three short span specimens is provided in Table 4-5. The back bone load-deflection curves for the three specimens are provided in Figure 4-26. A regression analysis was conducted to produce the average load-deflection curve for the short span specimens. The average curve is illustrated in Figure 4-54.

According to the average data curve, the short span slabs behaved linearly with an elastic stiffness of 56.8 kip/in prior to cracking. After the yielding of the specimen, the stiffness dropped significantly and started to have inelastic behavior before failing. On average, all three specimens had a high range of inelastic behavior prior to failing. A large number of flexural cracks were formed on the bottom wythe and the edge walls before failing; this suggests that the specimens were able to properly redistribute the stress and achieve a good amount of energy dissipation

The maximum permissible deflection for one-way concrete slabs according to the ACI 318 is L/240 (ACI, 2014). Since the clear span of the short specimen was 119 inches, the maximum allowable deflection would be 0.50 inches. According to the ASCE7, the minimum live load per area for a residential structure is 40 psf. With a live load factor, the minimum allowable live load becomes 64 psf. (ASCE7, 2016). This corresponded to an equivalent test loading of 2592 pounds at which load the average deflection was 0.044 inches. This is well below the maximum allowable deflection. Hence, the panels satisfy the code requirement for a residential floor slab.

Table 4-5: Test summary for short span specimen

Specimen	Concrete strength (psi)	Elastic stiffness (lb/in)	Cracking moment (lb-ft)	Ultimate moment (lb-ft)	Ultimate deflection (in)	Ultimate load carrying capacity (psf)
A-1	8657	68475	7893	15914	2.30	317.0
A-2	8346	70329	8495	16659	3.32	331.9
A-3	8732	37046	7715	16320	2.65	325.0
Average	8578	58617	8034	16297	2.76	325

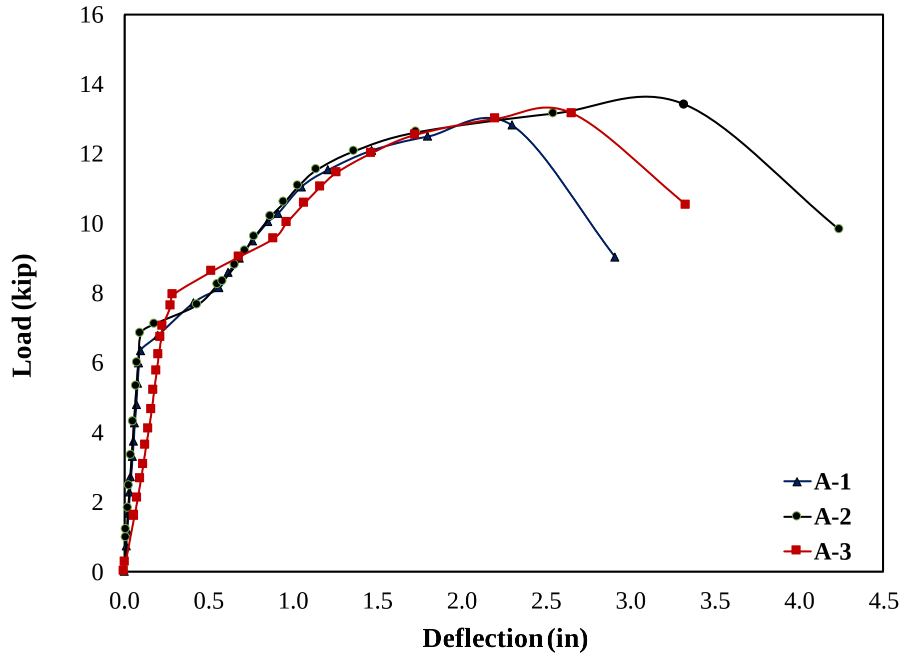

Figure 4-26: Load-deflection curve for short span slabs

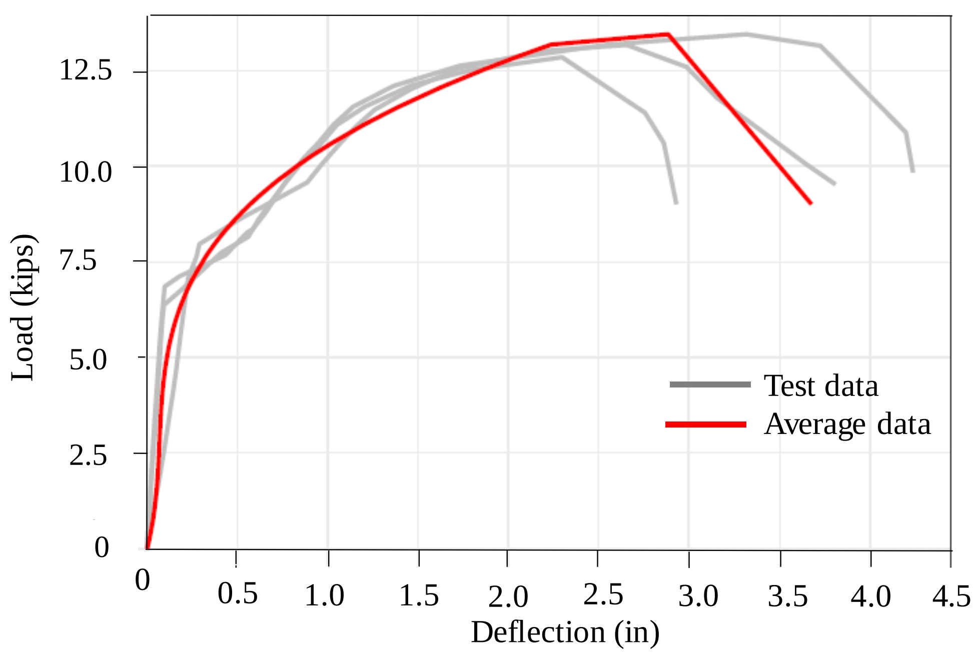

Figure 4-27: Average load-deflection curve for short span slab

4.6.2 Medium span slab specimen

Three identical 14 feet long slabs were tested under a four-point bend test with point loads at quarter point spans to determine the out-of-plane flexural behavior of the MR SCIP slabs with medium span. The three specimens that were tested were labeled B-1, B-2, and B-3. All the specimens were 171 inches long, 49 inches wide and six inches thick. The slabs had a simply supported span of 167 inches. The average self-weight of a medium span slab specimen was 1900 lbs.

Unlike the short span specimens that were fabricated using continuous sections of EPS, mesh, and diagonal trusses, the longer span slabs had a splice that was located at the center of the panels. Since all the raw material used to fabricate the MR panels came in 10 feet sections, two slices were formed at in the middle of the panel. A typical splice reinforcement technique of overlapping the mesh at splice region was used to reinforce the splice region. The two splice plans are illustrated in Figure 4-28 and are labeled A and B. The schematics for the testing of the medium span slabs are shown in Figure 4-28, which is followed by a picture of the actual test setup in Figure 4-29.

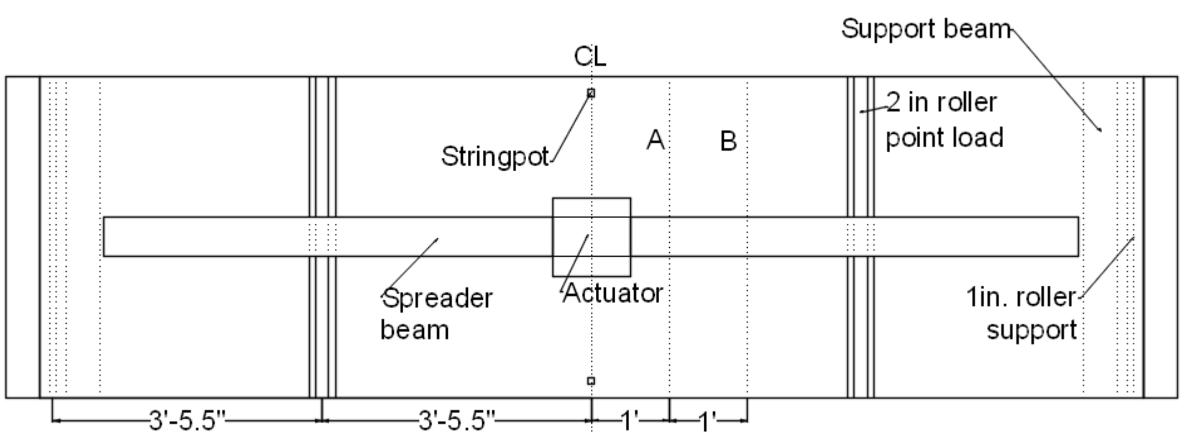

Figure 4-28: Details for flexural testing of medium span slab specimens

Figure 4-29: Test setup for medium-span slab specimen

Specimen B-1 was prepared on 12/03/2018 and was tested on 02/04/2019. The concrete strength of the specimen at transfer was 3268 psi and the test day strength was 7453 psi. The raw load versus midpoint deflection data collected during the testing of B-1 are provided in Figure 4-30. The load/moment versus deflection backbone curve for specimen B-1 is provided in Figure 4-31. The first cracks were observed between the load cycles of 2 kips and 2.5 kips. This can also be observed in the load-deflection curve as a bend over the point at a load of 2.58 kips. The linear stiffness of the specimen was 17.2 kip/in which reduced significantly after the yield point. The ultimate load sustained by B-1 was 5.41 kips at which point the average mid-span deflection was 1.96 inches. The ultimate applied moment was 9.4 kip-ft. which corresponded to an area load of 95.2 psf.

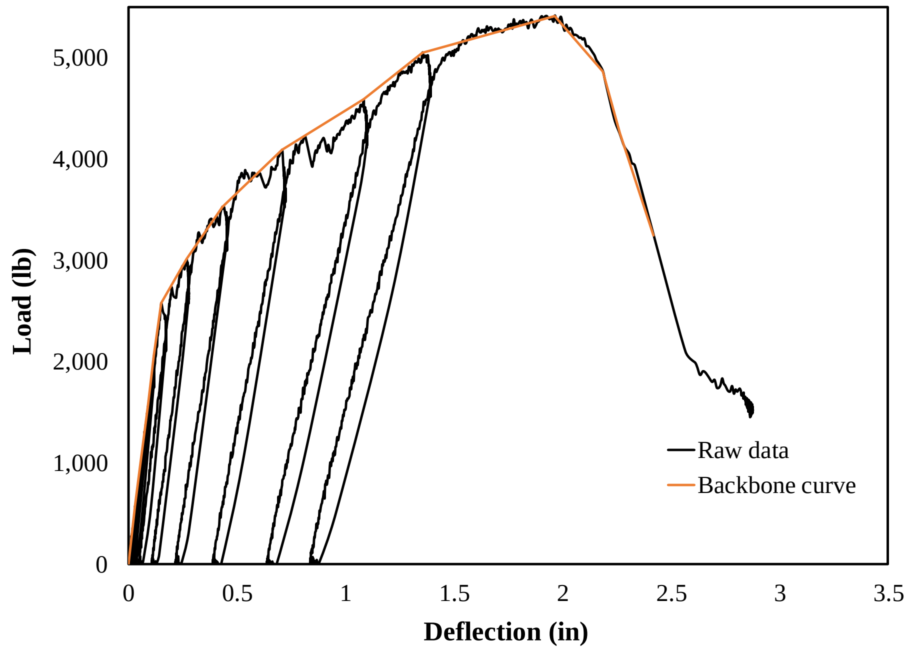

Figure 4-30: Raw flexural test data for specimen ‘B-1’

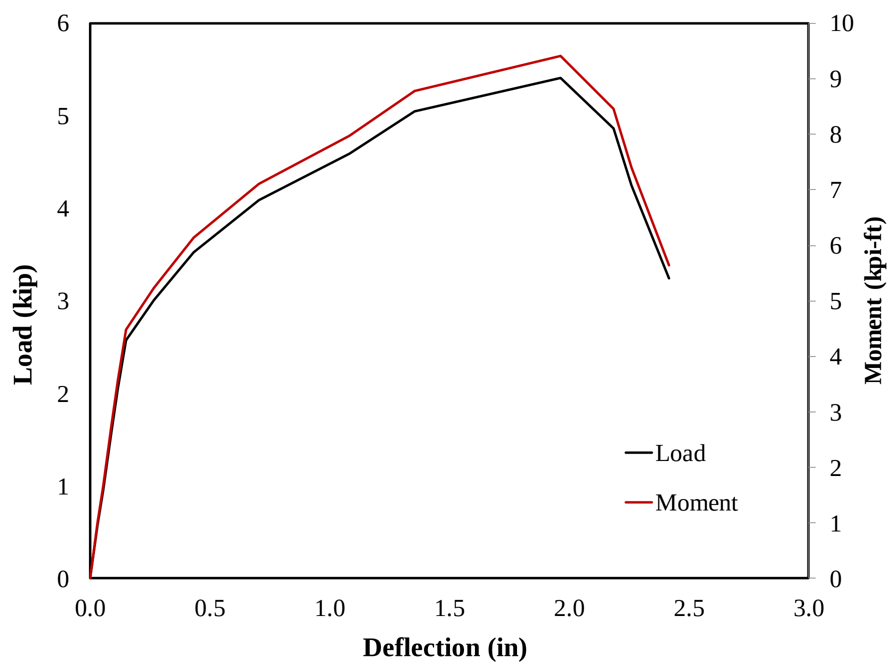

Figure 4-31: Load and moment versus deflection Curve ‘B-1’

Specimen B-2 was prepared on 02/06/2018 and was tested on 03/05/2019. The concrete strength of the specimen at transfer was 4123 psi and the test day strength was 7159 psi. The raw load versus midpoint deflection data collected during the testing of B-2 are provided in Figure 4-32. The peak load and its corresponding mid-span deflection from the raw data were then used to determine the backbone curve for the specimen. The load/moment versus deflection backbone curve for specimen B-3 is shown in Figure 4-33. The first cracks for this specimen were observed between the load cycles of 2 kips and 2.5 kips. This can also be observed in the load-deflection curve as a bend over the point at a load of 2.56 kips. The linear stiffness of the specimen was 13.3 kip/in which reduced significantly after the yield point. The ultimate load sustained by B-2 was 5.5 kips at which point the average mid-span deflection was 1.98 inches. The ultimate applied moment was 9.6kip-ft which corresponded to an area load of 97.3 psf.

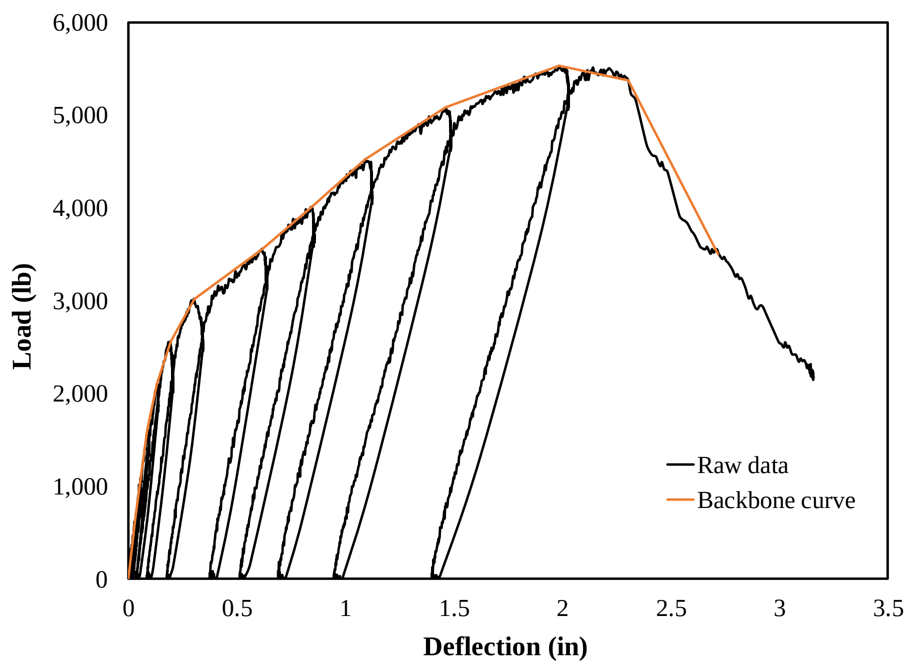

Figure 4-32: Raw flexural test data for specimen 'B-2'

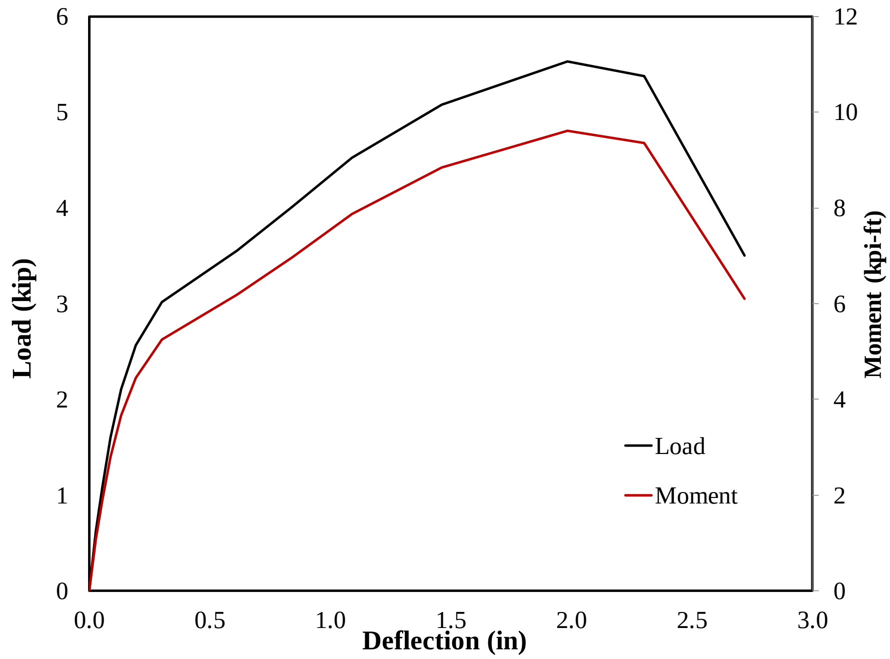

Figure 4-33: Load and moment versus deflection Curve ‘B-2’

Specimen B-3 was prepared on 12/13/2018 and was tested on 03/07/2019. The concrete strength of the specimen at transfer was 4123 psi and the test day strength was 7159 psi. The raw load versus midpoint deflection data collected during the testing of B-2 are provided in Figure 4-34. The peak load and its corresponding mid-span deflection from the raw data were then used to determine the backbone curve for the specimen. The load/moment versus deflection backbone curve for specimen B-3 is shown in Figure 4-35. The first cracks for this specimen were observed between the load cycles of 2 kips and 2.5 kips. This can also be observed in the load-deflection curve as a bend over the point at a load of 2.6 kips. The linear stiffness of the specimen was 14.1 kip/in which reduced significantly after the yield point. The ultimate load sustained by B-3 was 5.6 kips at which point the average mid-span deflection was 1.93 inches. The ultimate applied moment was 97.6 kip-ft which corresponded to an area load of 98.7psf.

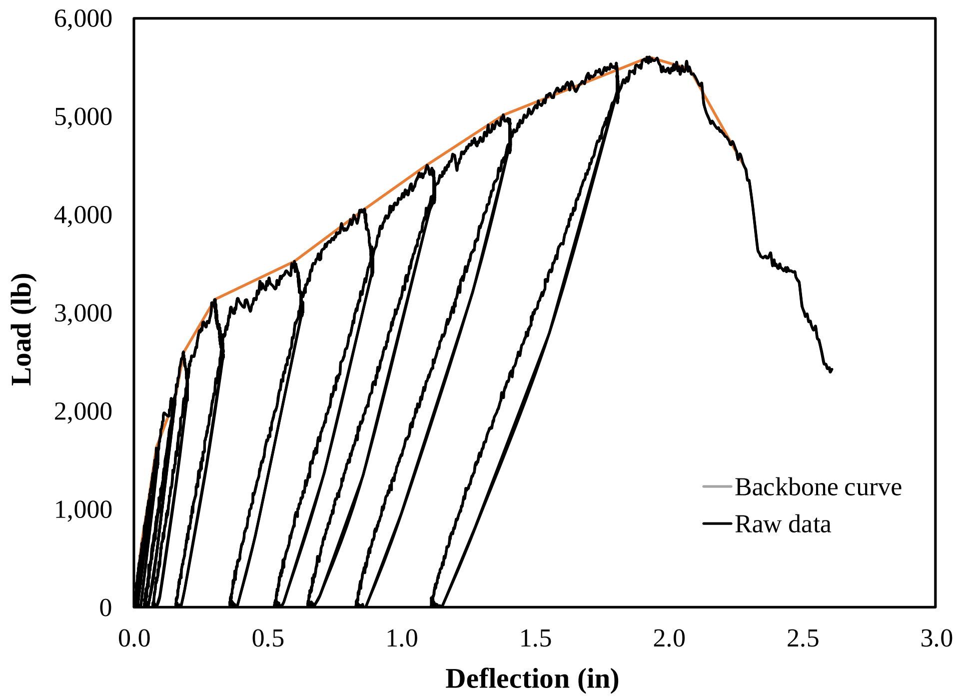

Figure 4-34: Raw flexural test data for specimen ‘B-3’

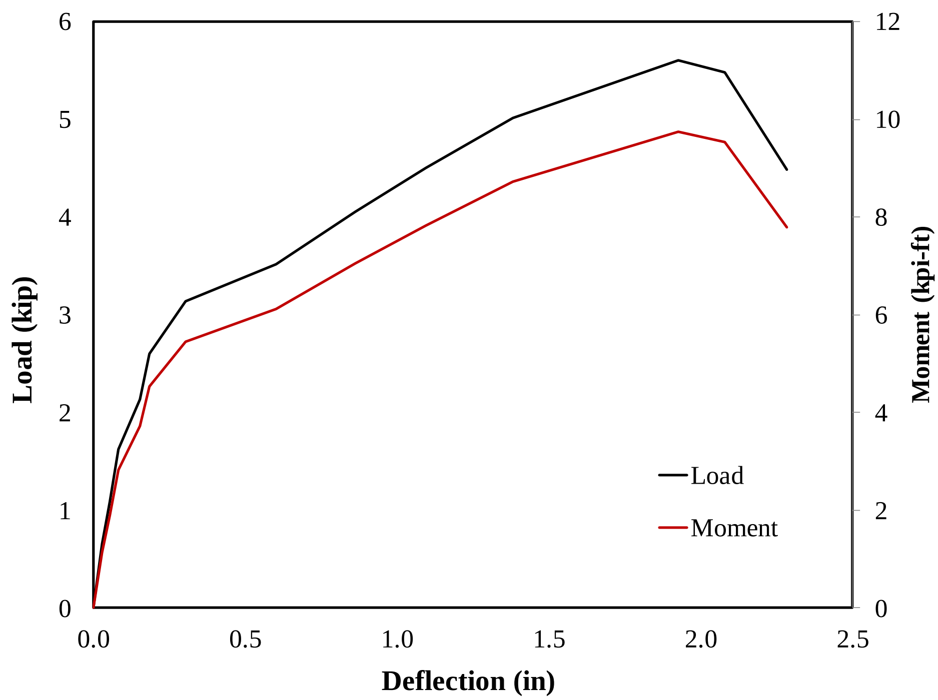

Figure 4-35: Load and moment versus deflection Curve ‘B-3’

The mode of failure for all the medium span slab was a flexural dominated brittle failure at the splice plane. The first hairline cracks (<0.4mm) were formed on the bottom wythe of the specimens close to the mid-span. After the formation of the first cracks, the specimen yielded and did not return to its initial position even after the removal of the load. With the load increment past the initial cracking more hairline cracks were formed inside the critical moment region (in between the two-point loads). Unlike the short span specimen, comparatively fewer number of cracks were formed prior to failing. After yielding of the specimen, no new cracks were formed and the existing cracks started to get wider, this continued till a dominant crack was formed at the location of the splice and caused a sudden failure. Since insufficient reinforcement was provided at the splice, a premature failure occurred prior to reaching the true capacity of the panels. The ultimate failure at the splice for specimen B-2 is shown in Figure 4-36. Table 4-6 provides the details for the modes and locations of failure for all three medium span specimens.

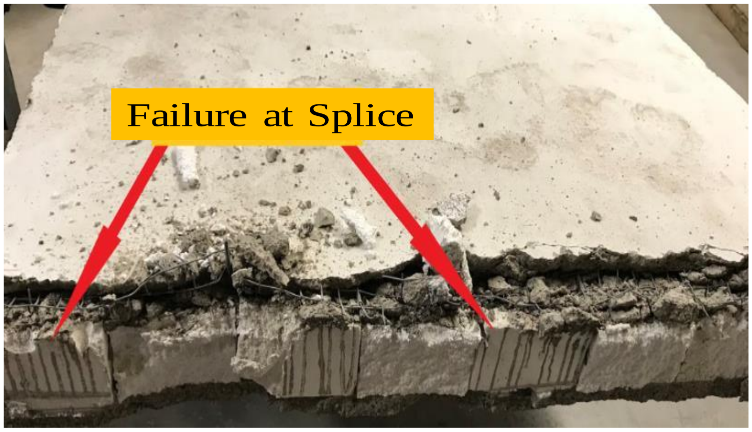

Figure 4-36: Failure at splice for slab specimen B-2

Table 4-6: Failure modes for medium-span specimens

Specimen	Mode of failure	Location of failure	Description
B-1	Brittle flexural failure at splice	12inches south of the centerline at the splice	Figure 4-37 a) failure of the specimen. b) west edge wall. c) east-edge wall
B-2	Brittle flexural failure at splice	12. inches south of the centerline at the splice	Figure 4-38 a) failure of the specimen. b) west edge wall. c) east-edge wall
B-3	Brittle flexural failure at splice	36.8 south of the centerline at the splice	Figure 4.39 a) failure of the specimen. b) west edge wall. c) east-edge wall

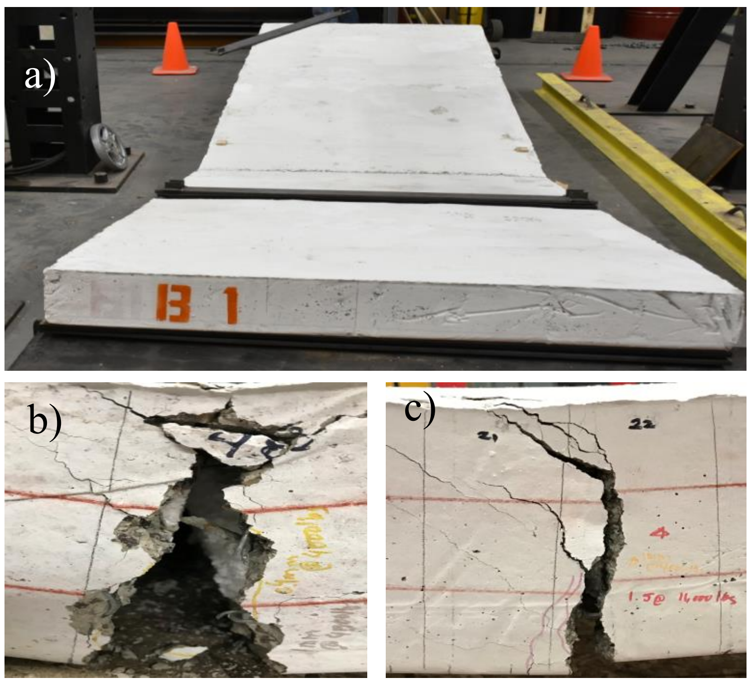

Figure 4-37: Failure mode ‘B-1’

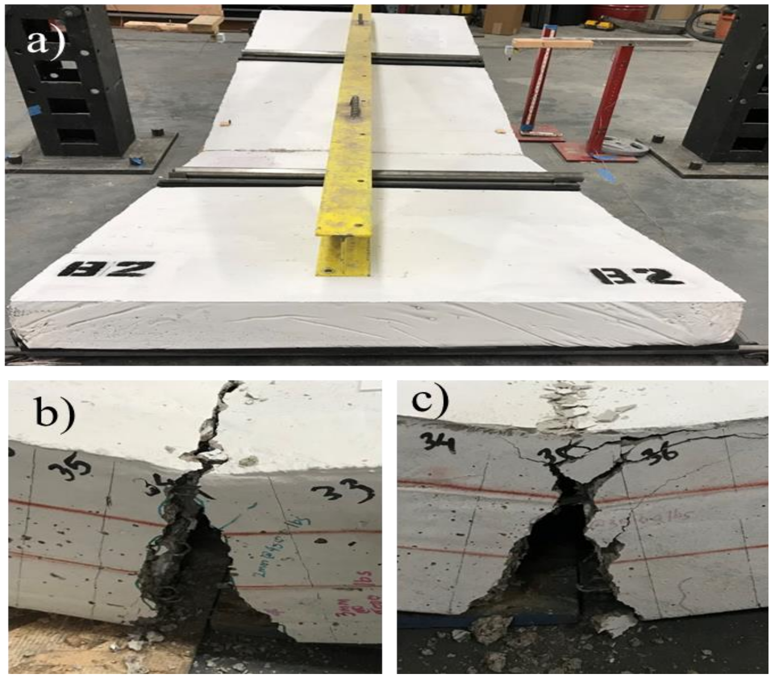

Figure 4-38: Failure mode ‘B-2’

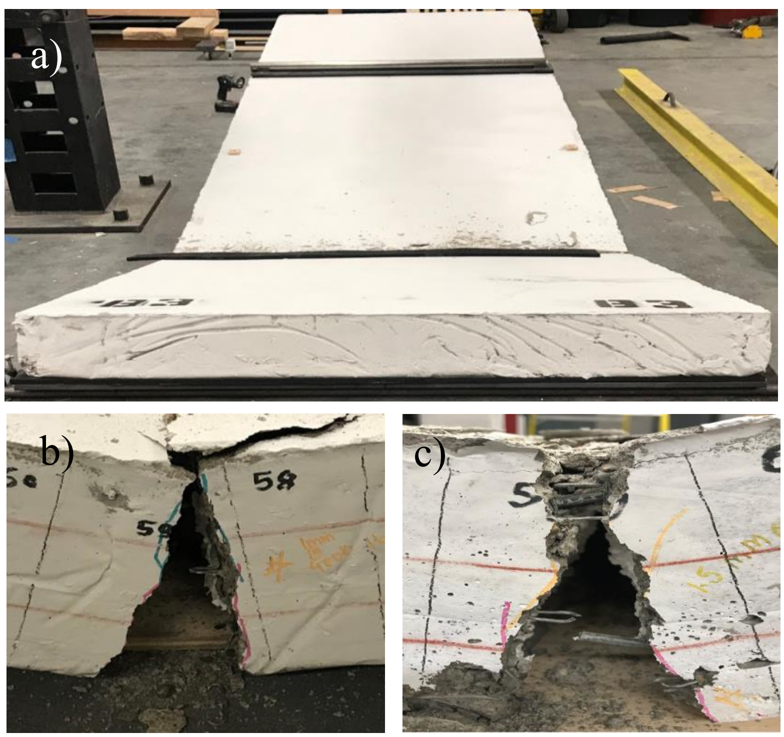

Figure 4-39: Failure mode ‘B-3’

The medium span specimen exhibited fairly ductile behavior when subjected to out-of-plane flexural loading. The lack of adequate reinforcement at the splice region caused a premature failure. Compared to the capacity of the short span specimens there was a significant loss in the ultimate load carrying capacity of the panel. The test summary for all three medium span specimens is provided in Table 4-7. The load-deflection backbone curves for all three medium span specimens are provided in Figure 4-40. A regression analysis was conducted to produce the average load-deflection curve for the short span specimen, the average curve is illustrated in Figure 4-41. The average elastic stiffness of the medium span specimen was14.8 kip/in. After the yielding of the specimen, the stiffness dropped significantly. The specimens started to exhibit an inelastic behavior before having a sudden failure. All three specimen had relatively low range of inelastic behavior prior to failing. Although these specimens suffered a premature failure, the specimens exhibited some degree of stress redistribution in the form of flexural cracks.

Table 4-7: Test summary for medium-span specimen

Specimen	Concrete strength (psi)	Elastic stiffness (lb/in)	Cracking moment (lb-ft)	Ultimate moment (lb-ft)	Ultimate deflection (in)	Ultimate load carrying capacity (psf)
B-1	7453	17158	4484	9419	1.97	95.3
B-2	7160	13269	4455	9620	1.99	97.3
B-3	7647	14057	4526	9755	1.93	98.7
Average	7420	14828	4489	9598	1.96	97

The maximum permissible deflection for a one-way concrete slabs according to the ACI-318 is L/240 (ACI 318, 2014). Since the clear span of the medium specimen was 167 inches the maximum allowable deflection was 0.7 inches. According to the ASCE 07, the minimum floor live load for a residential structure is 40 psf. With a 1.6 live load factor, the minimum allowable load becomes 64 psf (ASCE 7, 2016). This load corresponds to 3637 pounds at which load the specimens had already yielded. Hence without any additional splice reinforcement, the medium span slabs were did not meet the requirement for a residential floor.

Similarly, according to the ASCE 7, the minimum roof live load for a residential structure is 20 psf. With a live load factor of 1.6, the minimum allowable load becomes 32 psf. This load corresponds to an equivalent loading of 1818 lbs. At which point the slab is still within the elastic limit and has a deflection of 0.12 inches which is less than the allowable deflection of 0.7 inches. Although the medium span slabs meet the requirements for construction of roofs, additional splice reinforcement is highly recommended for this length for efficient results.

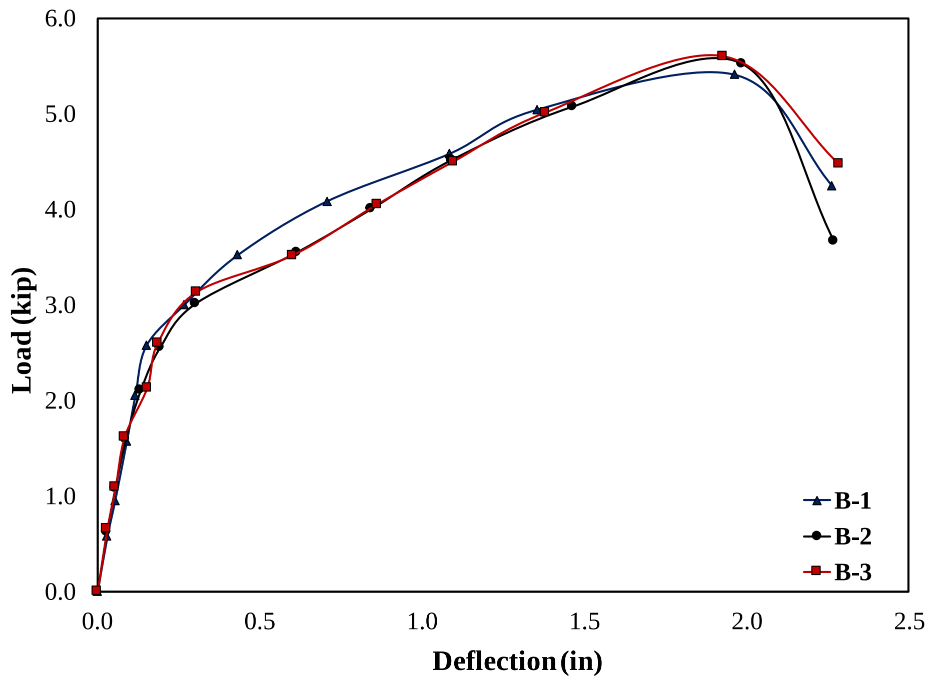

Figure 4-40: Load-deflection curve for medium-span slab specimens

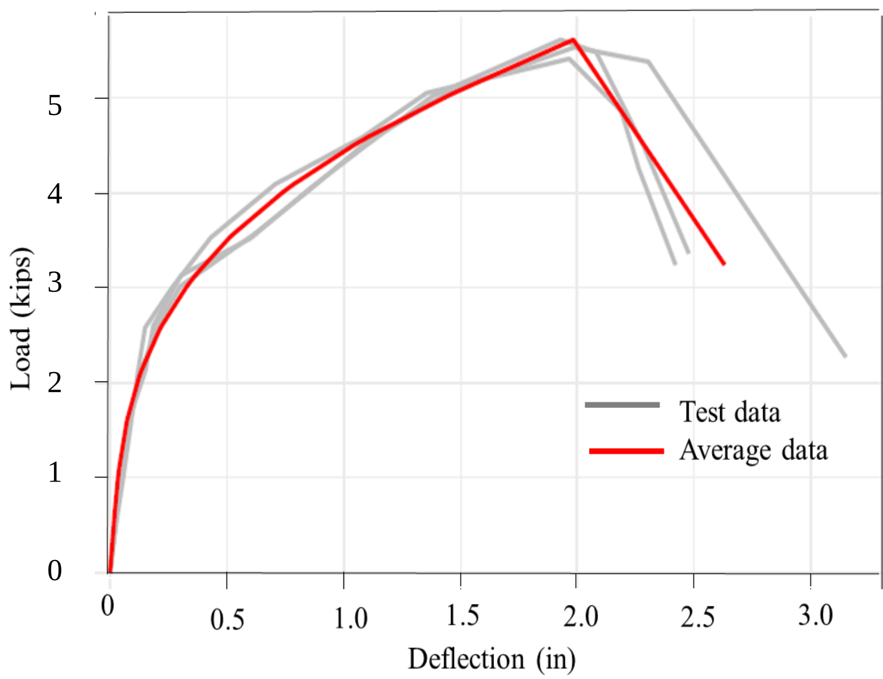

Figure 4-41: Average load-deflection curve for medium-span slabs

4.6.3 Long span slab specimen

Three identical 18 feet long slabs were tested under a four-point bend test to determine the out-of-plane structural behavior for the long span MR slab panels. The three long-span specimens that were tested were labeled C-1, C-2, and C-3. All the specimens were 219 inches long, 49 inches wide and six inches thick and had a simply supported span of 215 inches. The average self-weight of a long span specimen was 2400 lbs. The details and the actual test setup for the long span specimens are illustrated in Figure 4-14: and Figure 4-43.

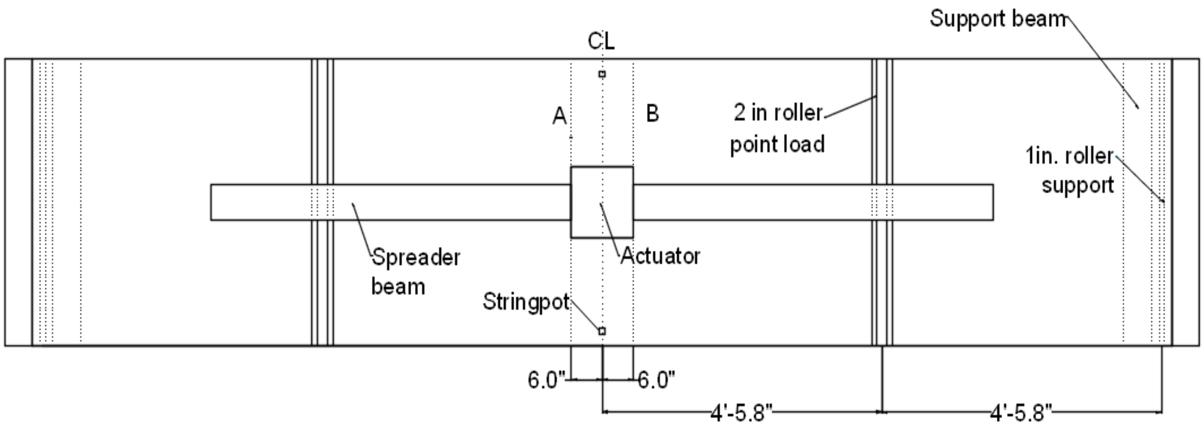

Figure 4-42: Details for flexural testing of long span slab specimens

Figure 4-43: Test setup for long span slab specimen

Specimen C-1 was prepared on 12/18/2018 and was tested on 03/15/2019. The concrete strength of the specimen at transfer was 3340 psi and the test day strength was 8183 psi. The raw load versus midpoint deflection data collected during the testing of C-1 are provided in Figure 4-44. The load/moment versus deflection backbone curve for specimen C-1 is provided in Figure 4-45. The first cracks were observed between the load cycles of 1 kip and 1.5 kips. This can also be observed in the load-deflection curve as a bend over the point at a load of 1.55 kips. The stiffness of the specimen was 9.43 kip/in which reduced significantly after the yield point. The ultimate load sustained by C-1 was 3.6 kips at which point the average mid-span deflection was

2.87 inches. The ultimate applied moment was 8.0 kip-ft which corresponded to an area load of 49 psf.

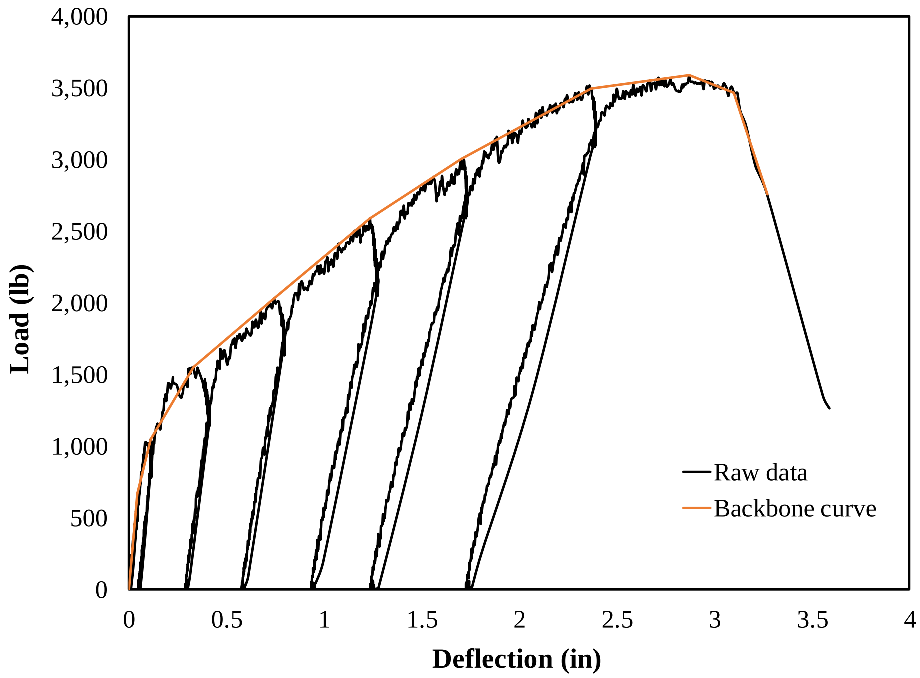

Figure 4-44: Raw flexural test data for specimen 'C-1'

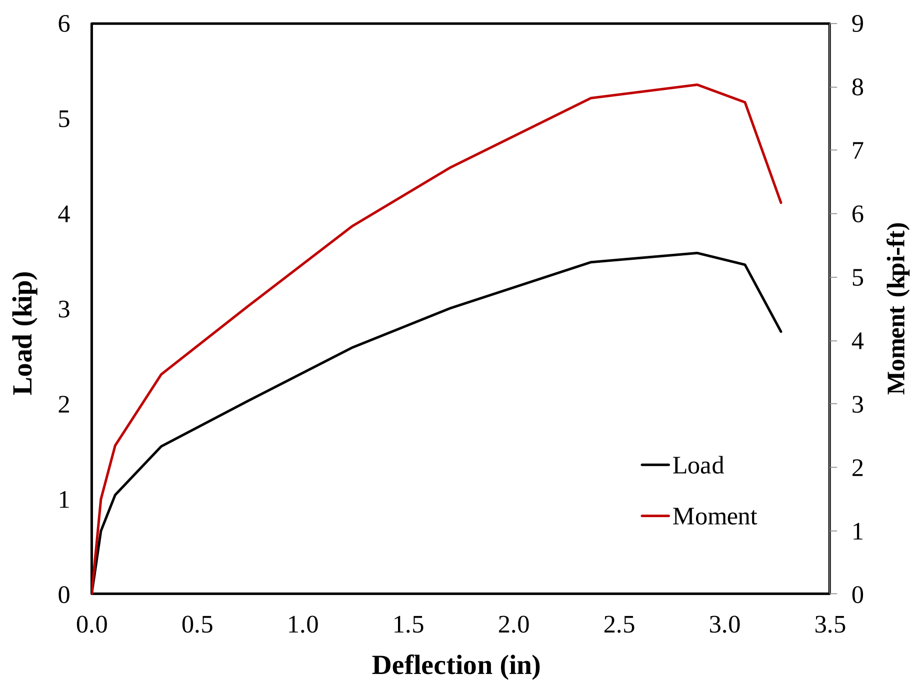

Figure 4-45: Load and moment versus deflection Curve 'C-1'

Specimen C-2 was prepared on 01/11/2019 and was tested on 03/13/2019. The concrete strength of the specimen at transfer was 2832 psi and the test day strength was 7098 psi. The raw load versus midpoint deflection data collected during the testing of C-2 are provided in Figure 4-46. The load/moment versus deflection backbone curve for specimen C-2 is provided in Figure 4-47. The first cracks were observed between the load cycles of 1 kip and 1.5 kips. This can also be observed in the load-deflection curve as a bend over the point at a load of 1.56 kips. The stiffness of the specimen was 9.85 kip/in which reduced significantly after the yield point. The ultimate load sustained by C-2 was 3.98 kips at which point the average mid-span deflection was 3.36 inches. The ultimate applied moment was 8.9 kip-ft. which was equivalent to a surface area load of 54 psf.

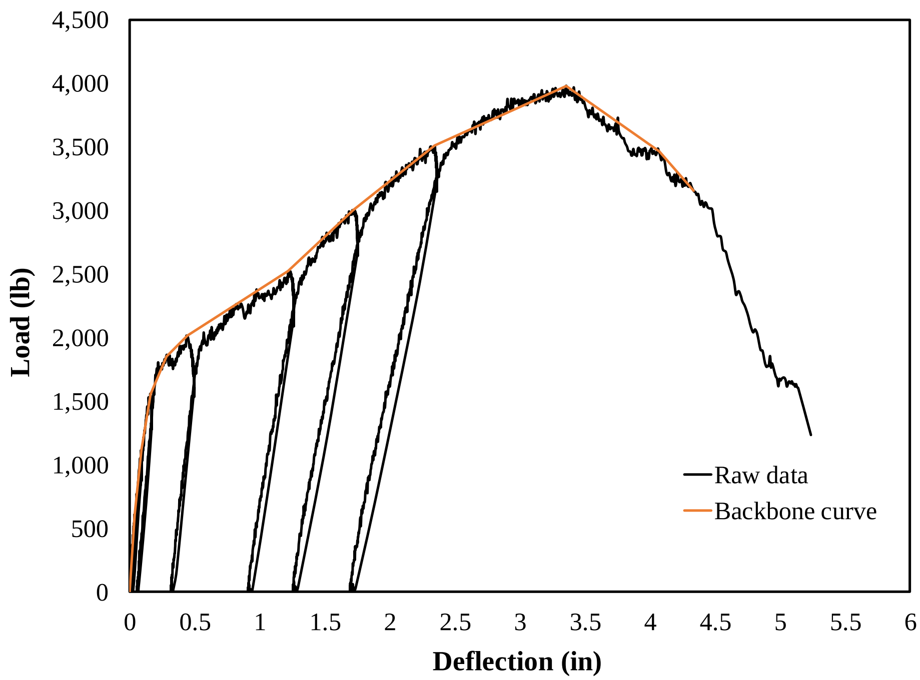

Figure 4-46: Raw flexural test data for specimen ‘C-2’

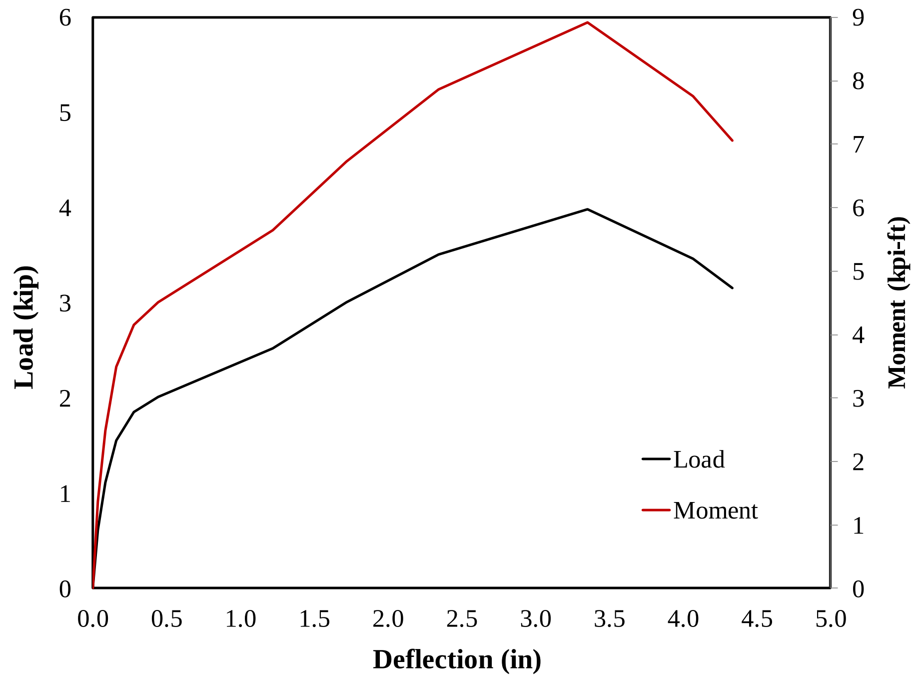

Figure 4-47: Load and Moment versus deflection Curve ‘C-2’

Specimen C-3 was prepared on 01/14/2019 and was tested on 03/11/2019. The concrete strength of the specimen at transfer was 3043psi and the test day strength was 6093 psi. The raw load versus midpoint deflection data collected during the testing of C-3 are provided in Figure 4-48. The peak load and its corresponding mid-span deflection from the raw data were then used to determine the backbone curve for the specimen. The load/moment versus deflection backbone curve for specimen C-3 is provided in Figure 4-49. The first cracks were observed between the load cycles of 1 kip and 1.5 kips. This can also be observed in the load-deflection curve as a bend over the point at a load of 1.60 kips. The elastic stiffness of the specimen was 9.07kip/in. The stiffness reduced significantly after the yield point. The ultimate load sustained by C-3 was 3.8 kips at which point the average mid-span deflection was 3.44 inches. The ultimate applied moment was 8.6 kip-ft which corresponded to an area load of 52 psf.

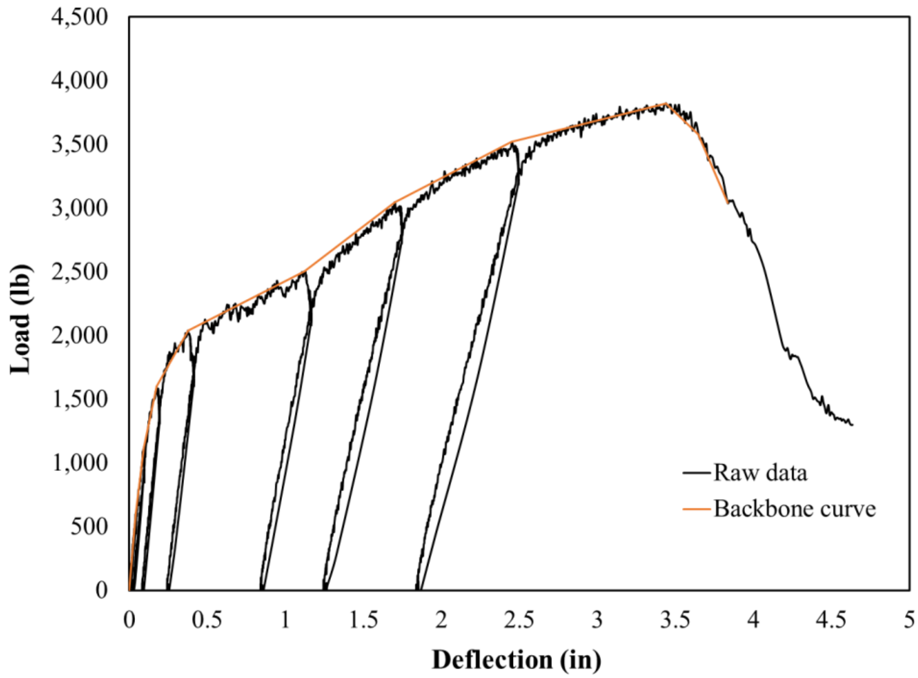

Figure 4-48: Raw flexural test data for specimen ‘C-3’

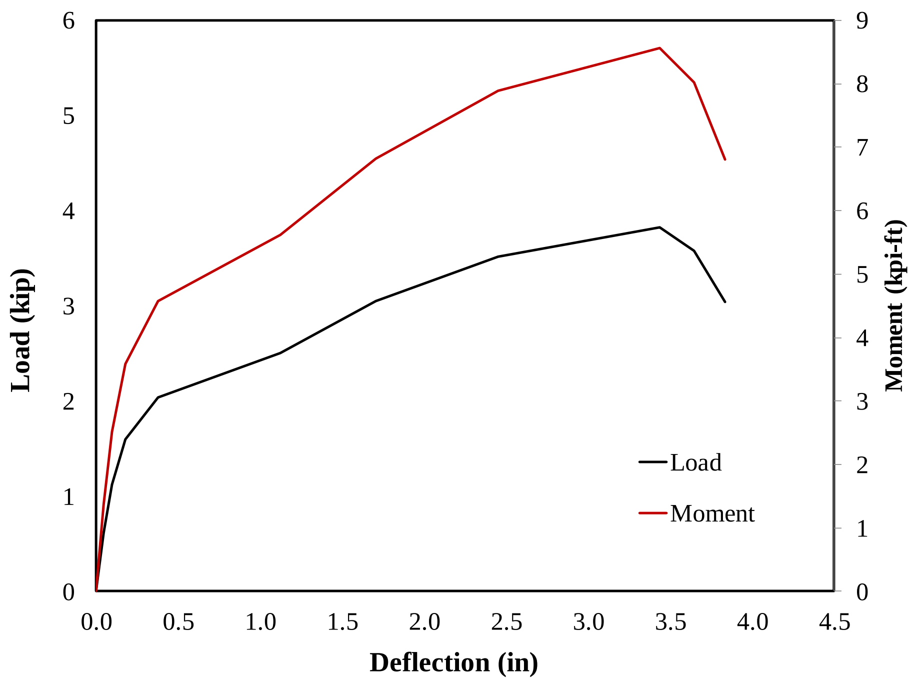

Figure 4-49: Load and Moment versus Deflection Curve ‘C-3’

The mode of failure for all the long span18 feet specimen was similar to the medium span specimens. All three specimens failed prematurely at the splice due to the inadequate amount of splice reinforcement that was provided. Table 4-8 provides the details for the modes and locations of failure for each long span specimen.

Table 4-8: Failure modes for long span slab specimen

Specimen	Mode of failure	Location of failure	Description
C-1	Brittle flexural failure at splice	12.1 inches on N side of the centerline	Figure 4-50: a) Failure of the specimen. b) West edge wall. c) East- wall
C-2	Brittle flexural failure at splice	12 inches on S side of the centerline	Figure 4-51: a) Failure of the specimen. b) West edge wall. c) East- wall
C-3	Brittle flexural failure at splice	12.5 inches on N side of the centerline	Figure 4-52: a) Failure of the specimen. b) West edge wall. c) East- wall

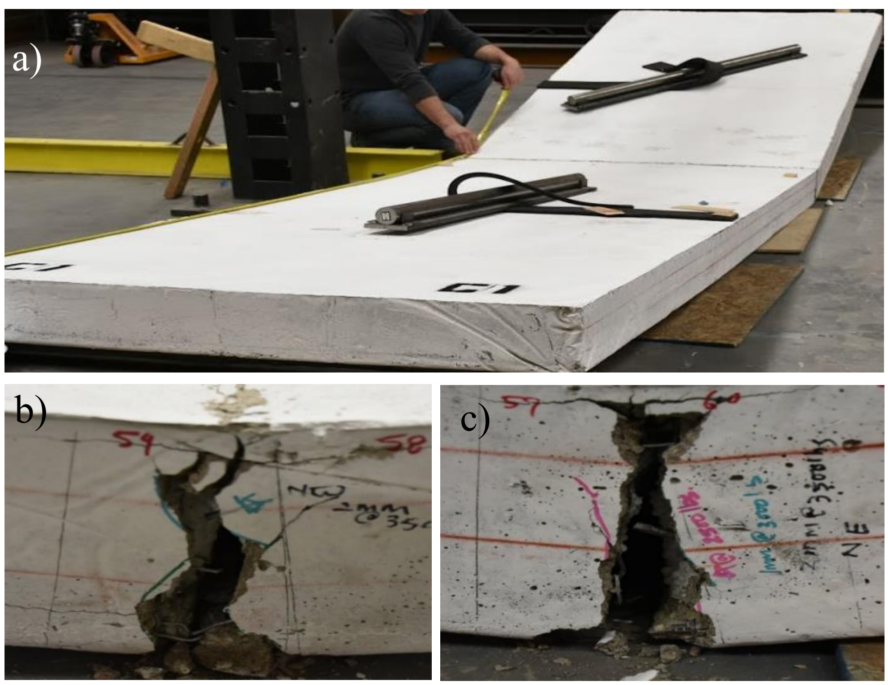

Figure 4-50: Failure mode ‘C-1’

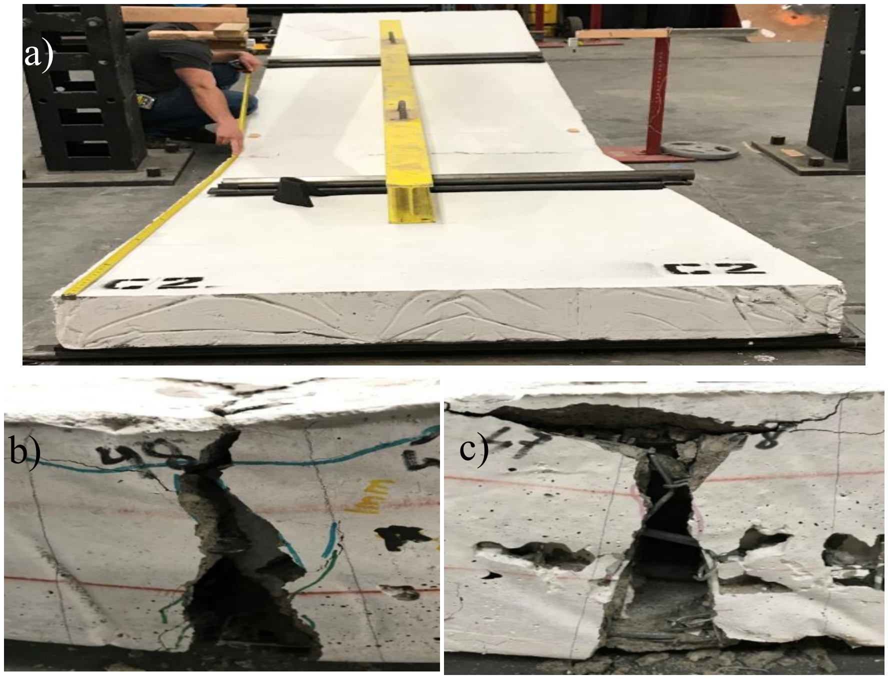

:

Figure 4-51: Failure mode ‘C-2’

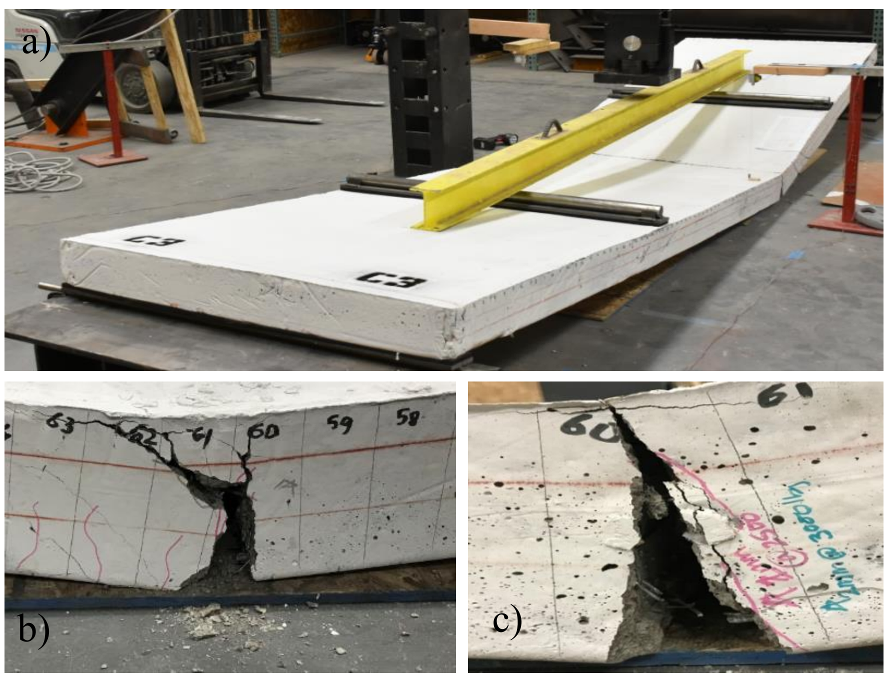

Figure 4-52: Failure mode ‘C-3’

The long span specimen exhibited a relative ductile behavior followed by a sudden failure when subjected to out-of-plane flexural loading. Compared to the ultimate capacity of the short span specimens they had a premature failure at the spliced region. The summary from the long span specimen is provided in Table 4-9. The load-deflection curve for the three long-span specimens is provided in Figure 4-53. A regression analysis was performed to produce the average load-deflection curve for the long span specimen, the average load-deflection curve for the long span slabs is illustrated in Figure 4-54. Prior to yielding the average elastic stiffness of the specimen was 9.45kip/in.

Table 4-9: Test summary for long span specimens

Specimen	Concrete strength (psi)	Elastic stiffness (lb/in)	Cracking moment (lb-ft)	Ultimate moment (lb-ft)	Ultimate deflection (in)	Ultimate load carrying capacity (psf)
C-1	8184	9436	2341	8037	2.87	49.1
C-2	7098	9851	3488	8916	3.36	54.4
C-3	7109	9073	3586	8565	3.44	52.3
Average	7464	9453	3138	8506	3.22	52

The maximum permissible deflection for a one-way concrete slabs according to the ACI-318 is L/240. Since the clear span of the medium specimen was 215 inches the maximum allowable deflection was 0.9 inches. According to the ASCE 07, the minimum live load per area for a residential structure is 40 psf. With a 1.6 live load factor, the minimum allowable load becomes 64 psf. This load corresponds to 4682 pounds. At this load the slabs are past their yield point hence the linear stiffness cannot be used to compute the average deflection. This result shows that the 18 feet MR SCIP slab specimens without reinforcement do not meet the ACI 318 standards. Hence two additional long span specimens with reinforced splice regions were tested.

Again, according to the ASCE 07, the minimum roof live load for a residential structure is 20 psf. With a live load factor of 1.6, the minimum allowable load becomes 32 psf. This load corresponds to an equivalent loading of 2341 lbs. At which point the slab has cracked but the average deflection is 0.75 inches and is still under the limit of 0.9 inches therefore it satisfies the criteria for a residential roof.

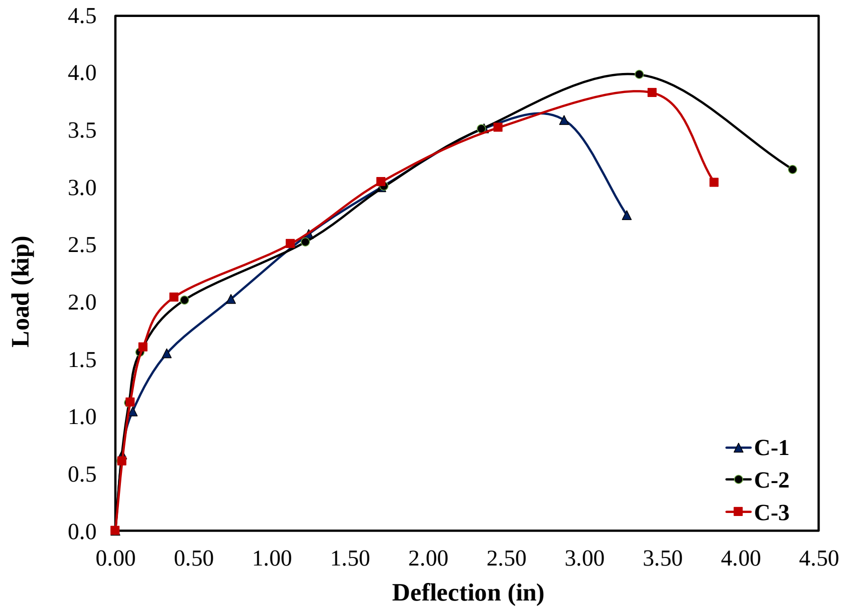

Figure 4-53: Load-deflection curves for long span slab specimens

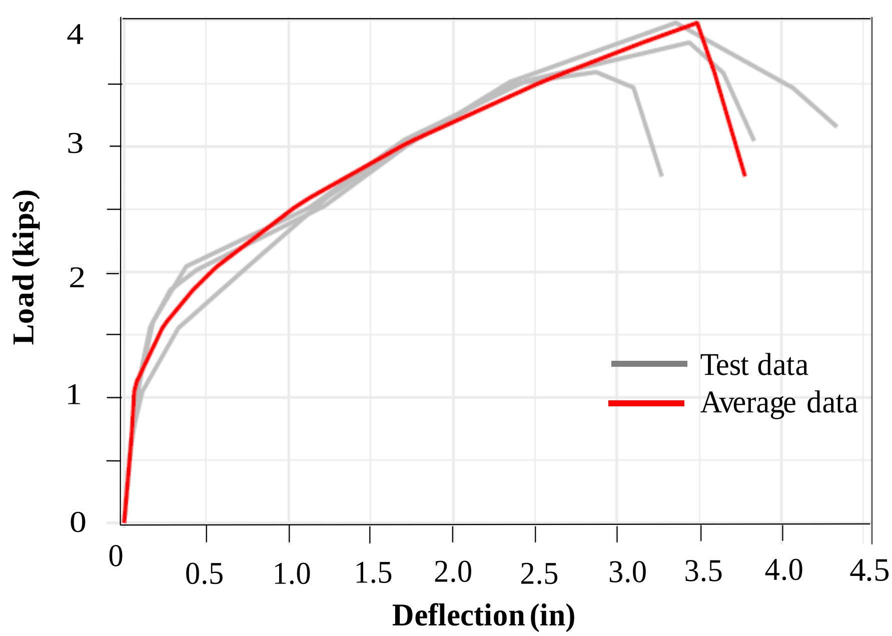

Figure 4-54: Average load-deflection curve for long span slab

4.6.4 Modified long span slab specimen

Due to the premature failure at the splice observed in the medium and the long span slab specimens, two additional long span specimens with reinforced splice region were prepared and tested. Figure 4-56 and Figure 4-57 show the typical splice reinforcement detail used in the long span specimen. The reinforcement was provided by overlapping the mesh over the splice region.

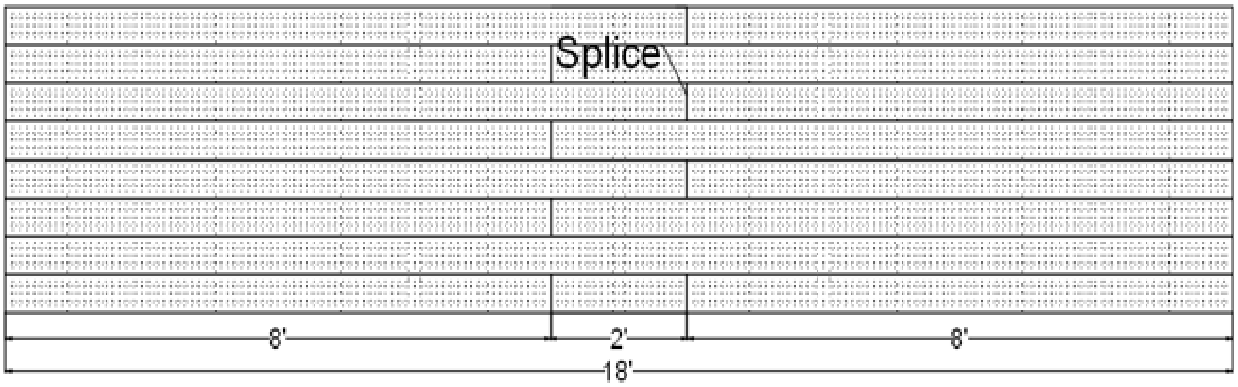

Figure 4-55: Splice location for MetRock SCIP

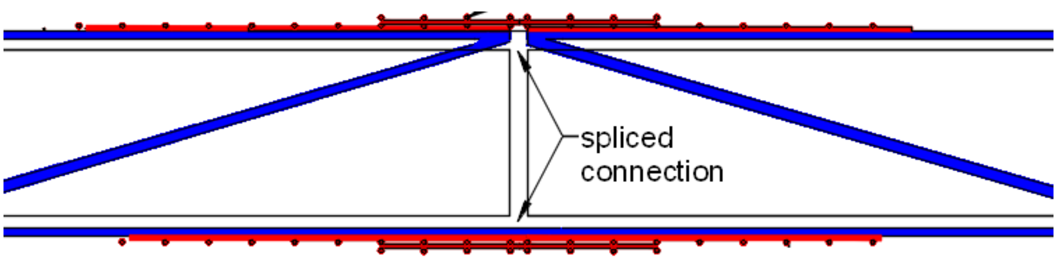

Figure 4-56: Splice detail for a typical 18 feet MetRock SCIP

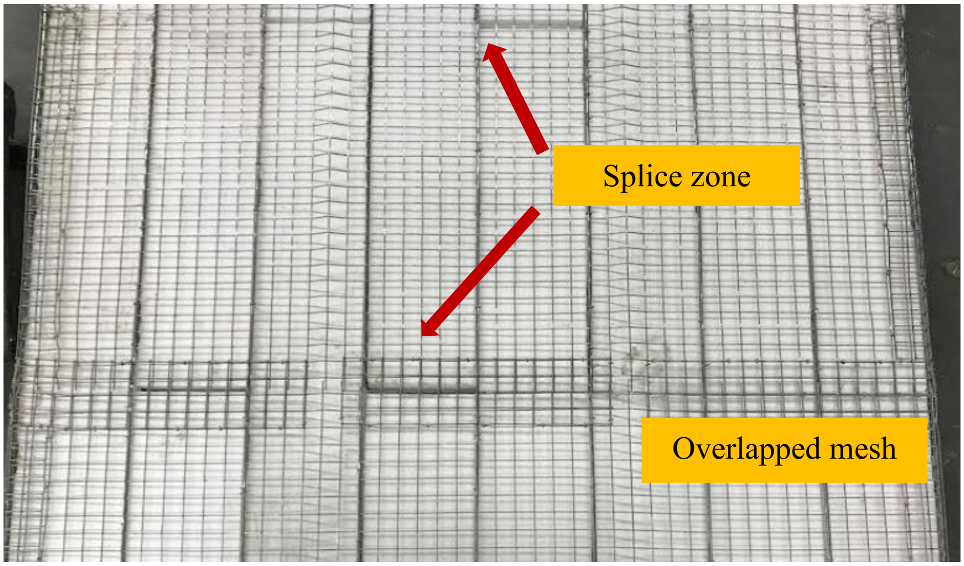

Figure 4-57: Elevation view of the splice region

The goal for this experiment was to avoid premature failure in the splice zones by providing additional splice reinforcement and to cause the failure to occur outside the splice zones. Two full-scale specimens with varying splice details were prepared and tested to fulfill these goals. The specimens used for this investigation were labeled S-1 and S-2. Grade 60 number 3 bars were used to provide the additional reinforcement at the splice.

4.6.4.1 Splice reinforcement design

The ultimate moment capacity of the short span specimen was used to determine the amount of additional tensile reinforcement required for this study. To ensure that the failure did not occur at the splice, additional reinforcement had to be used to increase the moment capacity at the splice region. The ACI 318 flexural analysis assuming a fully-composite section was conducted to determine the additional amount of reinforcement required. The spread sheet of the calculation are provided in Appendix D. According to the calculation, six number 3 bars were more than enough to push the failure outside the splice region.

ACI development length calculation was conducted to find the minimum development required to avoid a pullout of the rebar before achieving their full capacity (ACI 318-14). The calculation is provided in Appendix D. Eqn. (4.2) was used to calculate the minimum required development length of 11.3 inches for a number 3 bar (ACI, 2014). Hence, a development length of 12 inches was used for both specimens. The number 3 bars were tied in between the mesh and the EPS core as shown in Figure 4-56: Detail for reinforced splice.

$$l_d = \frac{3 f_y c_b d_b \psi_t \psi_e \psi_s}{40\lambda\sqrt{f'c}\frac{c_b}{d_b}} \quad (4.2)$$

Where,

l_d = development length (in)

f_y = yield of steel (psi)

f'c = compressive strength of concrete (psi)

cb = cover distance =0.5 in; db = diameter of bar = 0.375 in

ψt = reinforcement location = 1 ; ψe = coated factor = 1;

ψs= size factor = 0.8; λ = 1

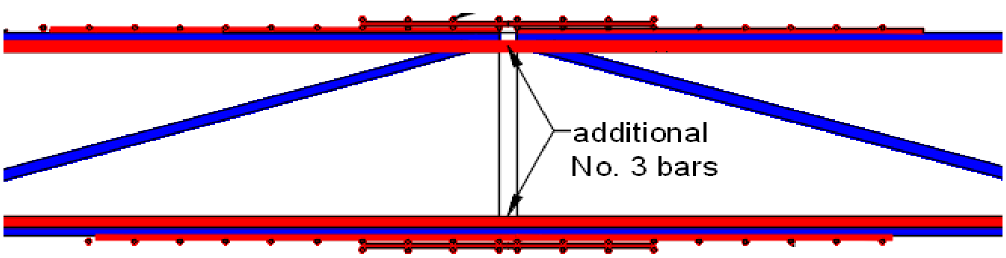

Figure 4-56: Detail for reinforced splice

4.6.4.2 Test specimen description

Specimen S-1 was prepared on 04/25/19 and was tested on 03/15/2019. For this specimen six #3 was placed at 8 inches on center. The bars used were four feet in length and were tied in between the mesh and EPS core. The reinforcement detail for S-1 is provided in Figure 4-57.

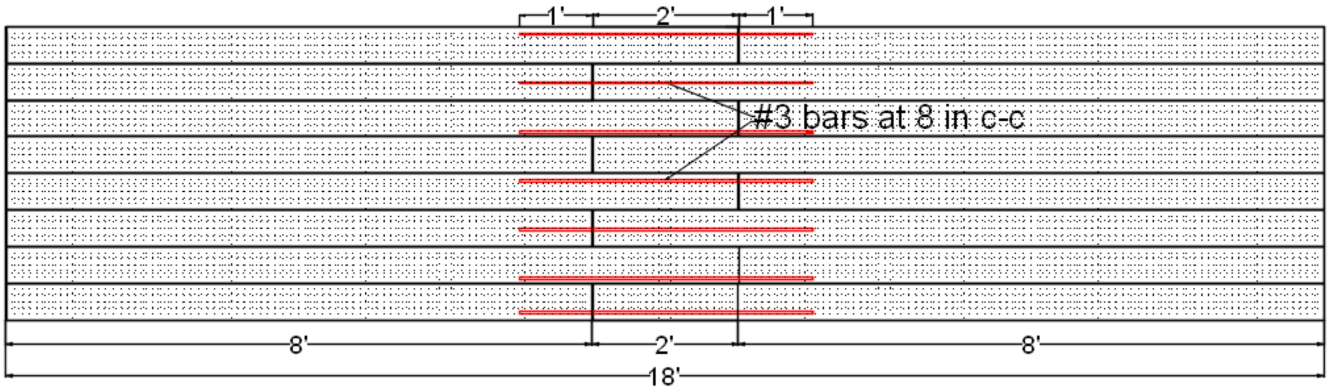

Figure 4-57: Splice reinforcement detail for specimen ‘S-1’

Figure 4-58: Splice reinforcement used in ‘S-1’

Specimen S-2 was prepared on 04/25/2019 and was tested on 03/15/2019. For this specimen, nine # 3 bars were placed in a staggered orientation at 6 inches on center. The bars used were two feet in length and were tied in between the mesh and EPS core. The details of the splice reinforcement for S-2 is provided in Figure 4-59.

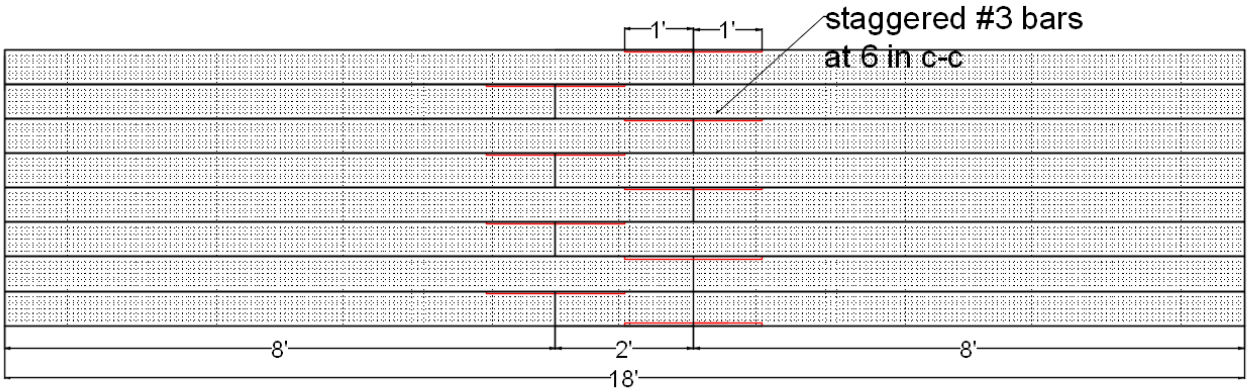

Figure 4-59: Splice reinforcement detail for specimen ‘S-2’

Figure 4-60: Splice reinforcement used in ‘S-2’

4.6.4.3 Experimental result.

The concrete strength of the specimen S-1 at transfer was 4072 psi and the test day strength was 6431 psi. The raw load versus midpoint deflection data collected during the testing of S-1 are provided in Figure 4-61. The peak load and its corresponding mid-span deflection from the raw data were then used to determine the backbone curve for the specimen. The load/moment versus deflection backbone curve for specimen S-1 is provided in Figure 4-62. The first cracks were observed between the load cycles of 1.5 kip and 2.0 kips. This can also be observed in the load-deflection curve as a bend over the point at a load of 2.0 kips. The stiffness of the specimen was 10.9 kip/in at the first bend over point. Unlike the other long span specimen, S-1 had a second linear portion from 2.0 kips to 5.1 kips. The second linear portion had a stiffness of 11.34 kip-in. The ultimate load sustained by S-1 was 6.8 kips at which point the average mid-span deflection was 8.84 inches. The ultimate deflection was 79% higher than the average unreinforced long span specimen. The ultimate applied moment was 15.2 kip-ft which corresponds to an area load of 92.6 psf.

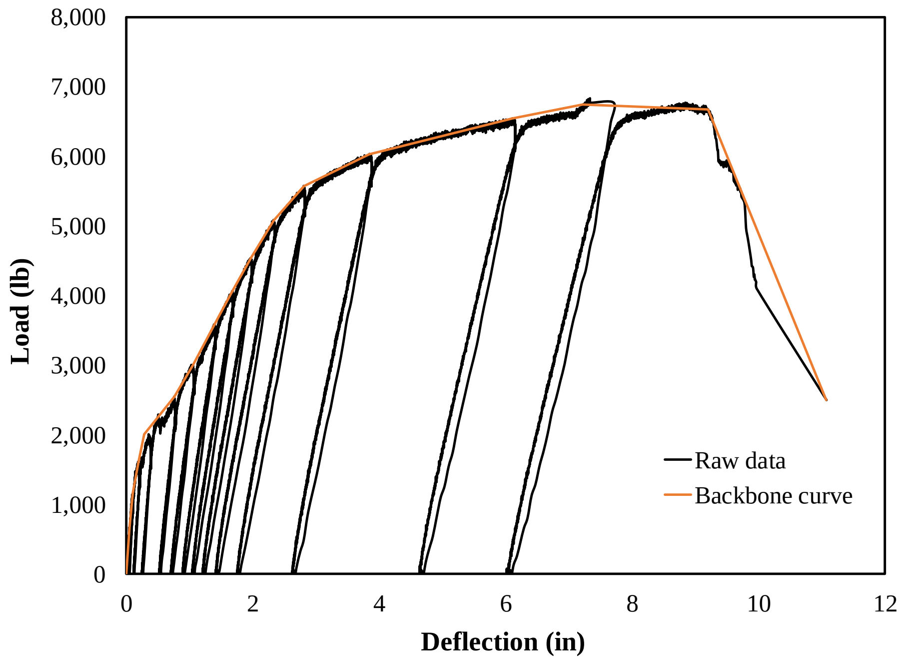

Figure 4-61: Raw flexural test data for specimen ‘S-1’

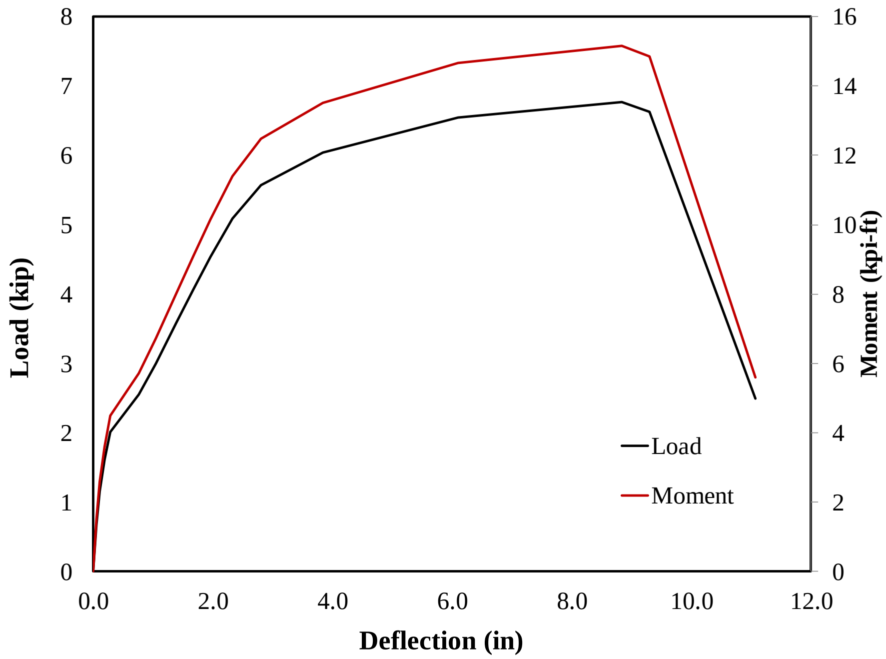

Figure 4-62: Load and moment versus deflection curve 'S-1’'

The mode of failure specimen S-1 was a flexural dominated failure. The splice reinforcement provided in S-1 was successful in shifting the failure plane away from the splice zone. The first hairline cracks (<0.4mm) were formed on the bottom wythe of the specimens close to the mid-span. With the load increment past the initial cracking, more hairline cracks were formed inside the moment region (in between the two-point loads) which in the later phases shifted out towards the supports. All the cracks that were formed during the testing were flexural cracks. Many cracks were formed before the specimen started to yield; the numbers of cracks observed in this test was significantly more than the unreinforced long span specimens. After yielding, no new cracks were formed and few of the existing cracks started to get wider, this continued till a dominant crack and caused the failure. The failure plane was 24 inches away from the mid-span. This interface was where the additional rebars ended. The failure mode and location can be observed in Figure 4-63. The failure was very ductile with significant deflection before the failure of the bottom reinforcements

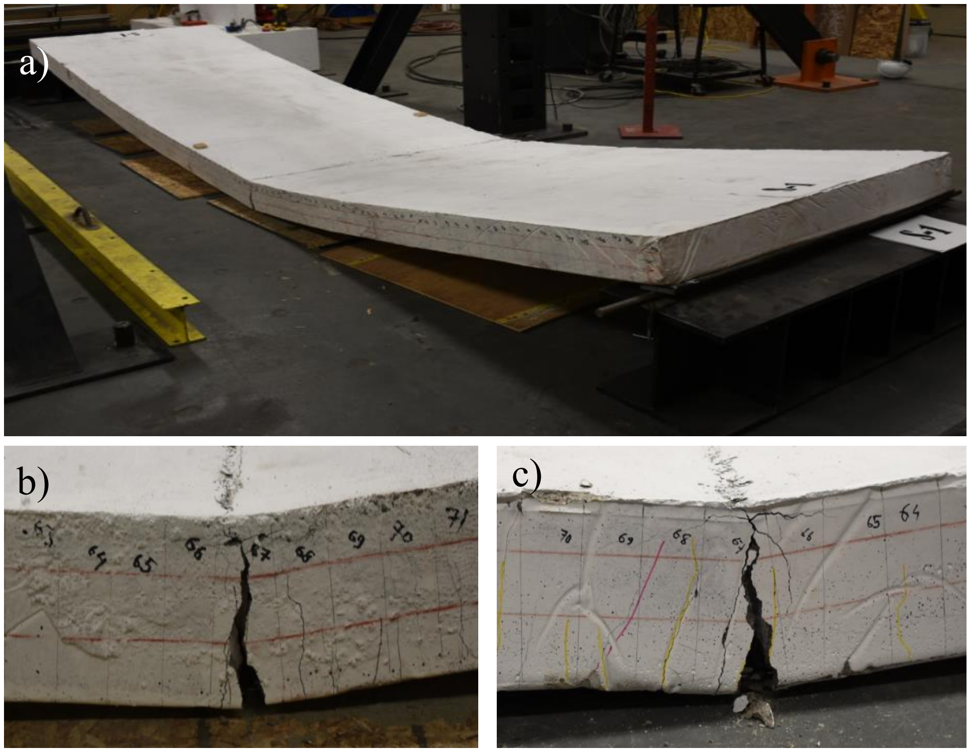

Figure 4-63: Failure mode S-1

The concrete strength of the specimen S-2 at transfer was 4123 psi and the test day strength was 7109 psi. The raw load versus midpoint deflection data collected during the testing of S-2 are provided in Figure 4-64: Raw flexural test data for specimen ‘S-2’. The peak load and its corresponding mid-span deflection from the raw data were then used to determine the backbone curve for the specimen. The load/moment versus deflection backbone curve for specimen S-2 is provided in. The first cracks were observed between the load cycles of 1.5 kip and 2.0 kips. This can also be observed in the load-deflection curve as a bend over the point at a load of 1.6 kips. The stiffness of the specimen was 9.0 kip/in at the first bend over point. The ultimate load sustained by S-2 was 6.1 kips at which point the average mid-span deflection was 6.4 inches. The ultimate applied moment was 13.5 kip-ft which corresponded to an area load of 82.6 psf.

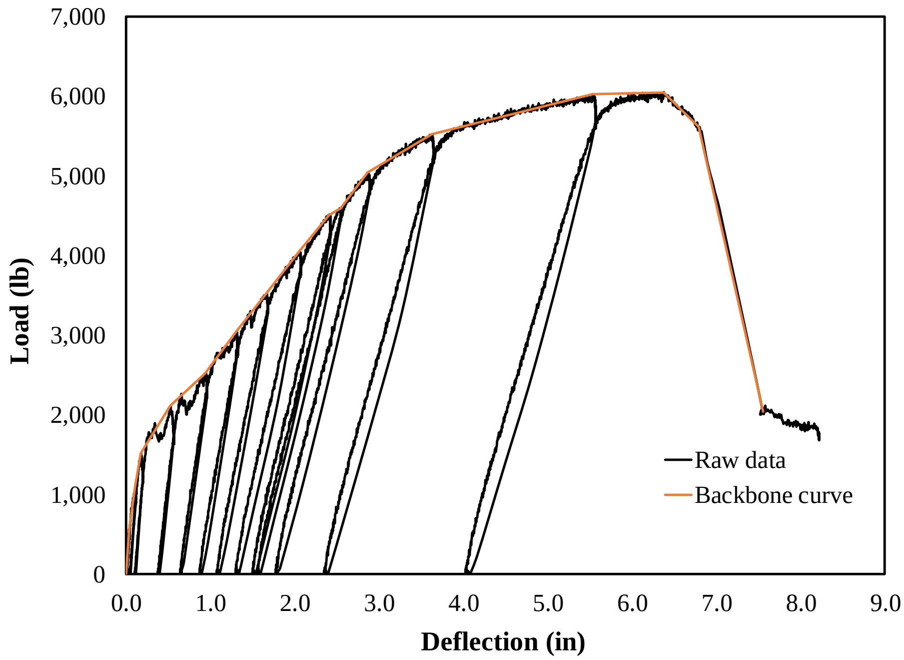

Figure 4-64: Raw flexural test data for specimen ‘S-2’

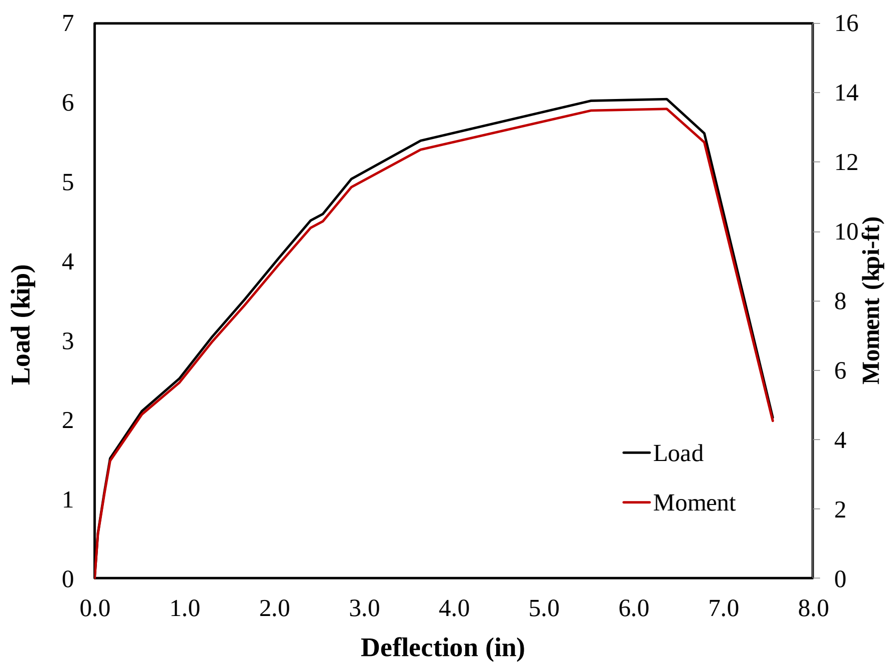

Figure 4-65: Load and moment versus deflection curve 'S-2'

The mode of failure for specimen S-2 was a flexural dominated failure. The splice reinforcement provided in S-2 was successful in shifting the failure plane away from the splice zone. The first hairline cracks (<0.4mm) were formed on the bottom wythe of the specimens close to the mid-span. With the load increment past the initial cracking, more hairline cracks were formed inside the moment region (in between the two-point loads) which in the later phases shifted out towards the supports. All the cracks that were formed during the testing were flexural cracks. Many cracks were formed before the specimen started to yield. After yielding no new cracks were formed and few of the existing cracks started to get wider, this continued until formation of a dominant crack that caused the failure. Two dominant cracks were formed 12 inches apart in the west edge wall, whereas on the east edge wall there was only one dominant crack formed. The failure plane was 12 inches north from the mid-span. The mode and location of failures in S-2 can be observed in Figure 4-66. Since the rebars in S-2 were staggered unlike S-1 where they were placed uniformly, the failure path could not find a straight line casing the two dominant cracks in the west wall. The failure occurred 12 inches to the north of the centerline. The failure was very ductile with significant deflection before the failure of the bottom reinforcements

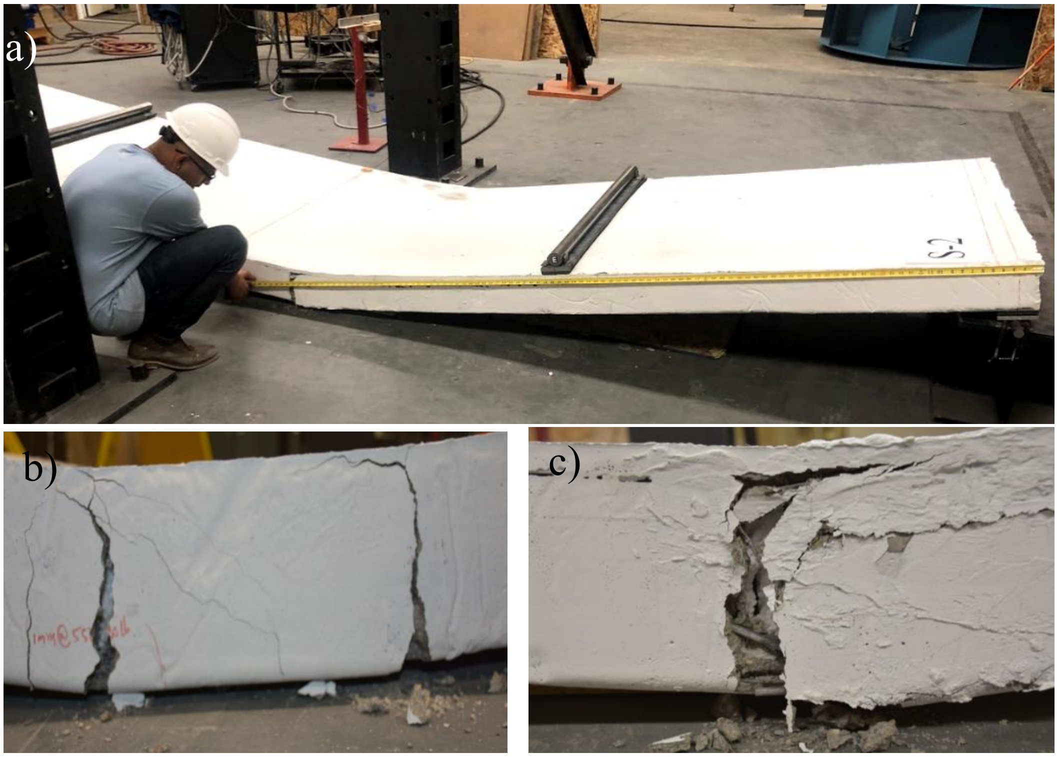

Figure 4-66: Failure mode S-2

The additional slice reinforcements successfully managed to prevent the premature failure of the panels. Unlike the original long span specimens that had a fairly brittle failure, both modified specimens had a very ductile failure. This led to a significant increase in the ultimate load carrying capacity of the long span slab specimens. The average ultimate moment capacity for the modified specimen was14.3 kip-ft which was 46% higher than the original long span specimens. Splice detail S-1 that had 4 feet # 3 bars placed uniformly at 8 inches on center exhibited a higher ultimate capacity than S-2 that had 2 feet # 3 bars that had a staggered orientation at 6 inches on center. Although the nonlinear behavior of the slabs increased significantly, there was no noticeable change in the linear behavior. The average elastic stiffness was 10.8 kip-in and the cracking moment was 3502 lb-ft. The test summary for the modified long span specimens is provided in Table 4-10.

Table 4-10: Test summary long modified long span slab specimens

Specimen	Concrete strength (psi)	Elastic stiffness (lb/in)	Cracking moment (lb-ft)	Ultimate moment (lb-ft)	Ultimate deflection (in)	Ultimate load carrying capacity (psf)
S-1	6432	11344	3612	15166	8.84	92.6
S-2	7109	10243	3393	13541	6.38	82.6
Average	6771	10793	3502	14354	7.61	88.0

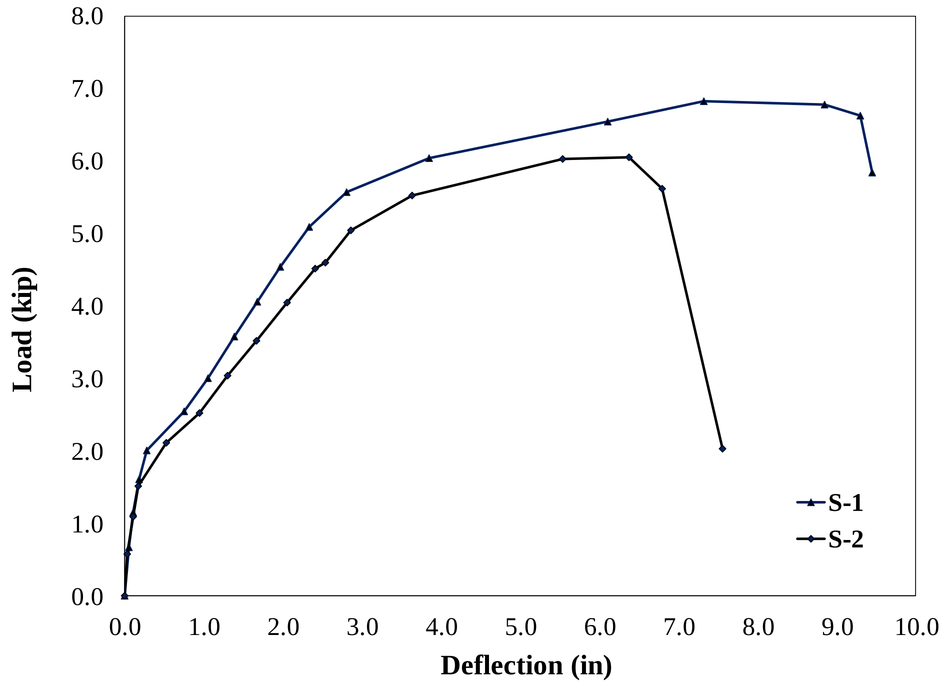

Figure 4-67: Load-deflection curve for modified long span slab specimen

To check if adding reinforcements to the long span specimens increased the total moment capacity of the slabs, the total moment capacities for each span was calculated. The total moment for each span was calculated as the sum of the moment caused by the self-weight of the slabs and the average applied moments. An average self-weight of 135 lb/ft was assumed for all spans. The results for the total moment capacities of the slabs are provided in Table 4-11 and are also displayed as a bar graph in Figure 4-68. The total moment capacity for the short span specimen was 17.9 kip-ft. Compared to the capacity of the short span, it can be observed that there was a significant reduction in the total moment capacity for the unmodified medium and long span specimens. This was caused due to the premature failures at the splices. Whereas the total moment capacity for the modified long span specimen was slightly higher than that of the short span specimen. This was due to the additional reinforcement that was provided for these specimens.

Table 4-11: Total moment capacities for slab specimens

Specimen	Self-weight moment (kip-ft)	Applied moment (kip-ft)	Total moment (kip-ft)
Short	1.7	16.2	18.0
Medium	3.3	9.6	12.9
Long	5.4	8.5	13.9
S-1	5.4	15.2	20.6
S-2	5.4	13.5	18.9

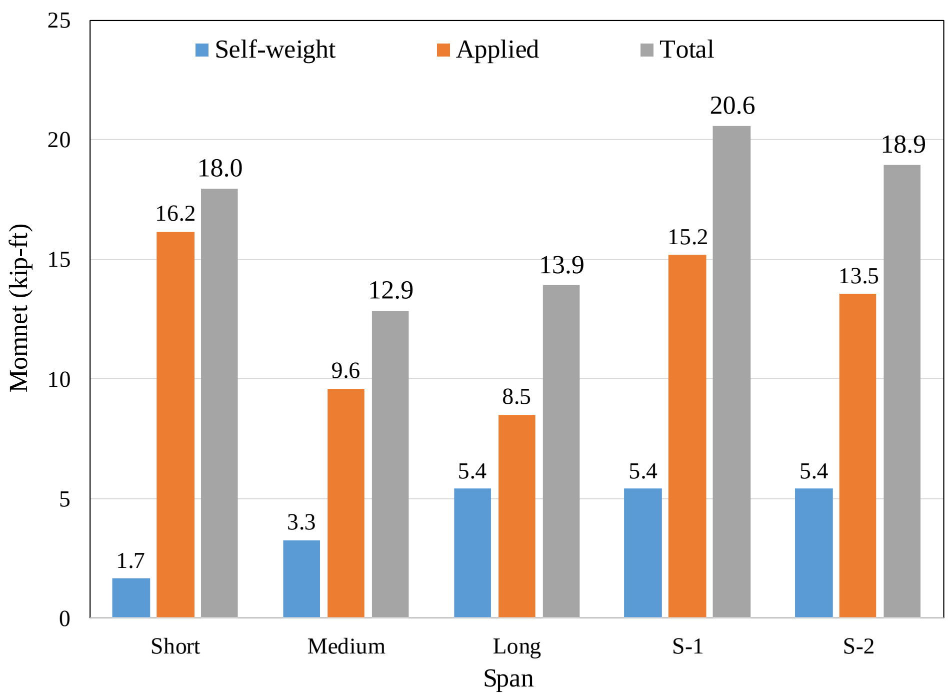

Figure 4-68: Total moment capacities for different span slabs

4.7 Summary

1. The short span (10 feet) slab specimens exhibited a very ductile behavior when subjected to out-of-plane flexural loading. The failure mode was a flexural-controlled failure with the formation of many hairline cracks before failing.
2. The average elastic stiffness for the short span slabs was 58.6 kip/in. The average cracking moment was 8.1 kip-ft, with a corresponding midpoint deflection of 0.13 inches. The ultimate moment capacity was 16.3 kip-ft. with a corresponding midpoint deflection of 2.76 inches
3. The short span MR panels satisfy ACI 318 deflection criteria under the ASCE7 load requirements for a residential concrete floor and roof slabs. The average load carrying capacity for the short span slabs was 167 psf.
4. The medium (14 feet) and the long span (18 feet) slab specimens exhibited a fairly ductile behavior followed by a very sudden failure at the splice location. The insufficient reinforcement of the splice was what caused the premature failure and prevented the panels from achieving their full capacity.
5. The average elastic stiffness for the medium span slabs was 14.8 kip/in. The average cracking moment capacity 4.5 kip-ft, at a mid-point deflection of 0.18 inches. The ultimate moment capacity was 9.6 kip-ft. at a deflection of 1.96 inches.
6. The average elastic stiffness for the long span slabs was 9.45 kip/in. The average cracking moment capacity 3.2 kip-ft, with a corresponding midpoint deflection of 0.15 inches. The ultimate moment capacity was 8.5 kip-ft with a corresponding midpoint deflection of 3.0 inches.

7. The medium and the long span slabs did not meet the ACI 318 deflection requirement for a residential floor. However, they were able to meet the requirement for a residential roof slab.
8. Current splice detail of overlapping the mesh at the spice region is not adequate and requires additional reinforcement to prevent a premature brittle failure and to achieve the full capacity of the panels
9. Both modified long span specimens were successful in transferring the failure location away from the splice region. This significantly increased the ultimate moment capacity of the panels and caused a ductile failure. The average ultimate moment capacity of the modified specimens was 12.4 kip-ft which was 46% more than the capacity for the unmodified long span specimen. The average ultimate mid-point deflection of the modified panels was 7.6 inches, which was 138% more than the unmodified long span specimens.
10. The spice detail used in S-1 had the higher moment capacity of the two modified specimens.

CHAPTER 5. Linear Flexural Analysis for Slab Panels

5.1 General

In this chapter, a simple model was developed to predict the flexural capacity of the MetRock SCIP slab. The MR panels were analyzed using the flexural analysis for a one-way slab stated in ACI 318 (ACI,2014). Although sandwich panels are different from conventional solid reinforced concrete slabs, they can still be analyzed using a similar process based on the degree of composite action achieved by the panels. Unlike traditional insulated panels that only rely on the insulation core for the transfer of shear in between the two load-bearing faces, the MR panels have a truss shear transfer mechanism installed in them. This includes a series of diagonal steel connectors that are placed at every six inches and are connected to the two layers of mesh using hog ring ties. This enables MR panels to achieve significant level of composite action. Generally based on the degree of composite action achieved, a sandwich panel can be classified into three possible types: fully composite, semi-composite, and non-composite. The description for each type of panel is as follows

5.1.1 Fully composite panel

A panel is assumed to be a fully composite section if 100% of the longitudinal shear produced during loading is successfully transferred in between the two load-bearing faces. In order to achieve this degree of shear transfer, a panel must have well established arrangement of shear connectors. In a fully composite panel, the two concrete wythes resist the applied flexural loads as if they were an integral section. This allows the panel to be designed as a solid reinforced concrete slab having the same cross-section as the panel. The sandwich panels that have proper and sufficient shear transfer mechanism, are said to be fully composite panels.

Figure 5-1 shows how the stresses is transferred in between the two load-bearing faces in a fully composite panel.

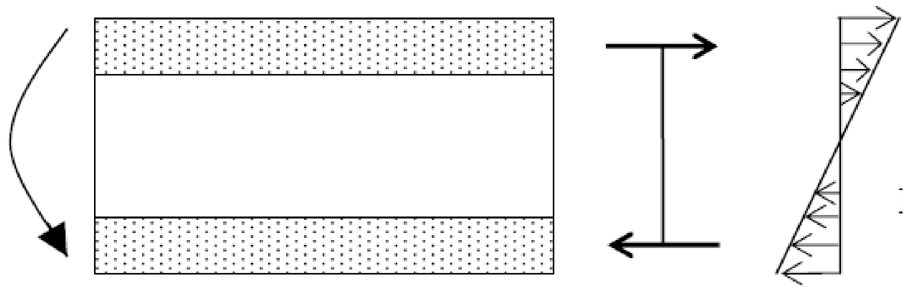

Figure 5-1: Flexural stress distribution for a fully composite section

5.1.2 Non-composite panel behavior

The panel is said to be non-composite if there is very little to no longitudinal shear transfer in between the two-load-bearing faces. Most traditional insulted panels i.e. wooden and metal that rely only on the insulation core for shear resistance behave as a non-composite section. In a non-composite panel, the two load-bearing faces resist the applied flexural loads as individual slabs. This greatly reduces the moment of inertia of the section hence, causing a significant loss in the overall flexural capacity. The flexural design for a non-composite section is identical to that of a solid reinforced concrete slab that has the same cross-section of one of the concrete wythe. Figure 5-2 shows how the stresses is transferred in between the two load-bearing faces in a non-composite section.

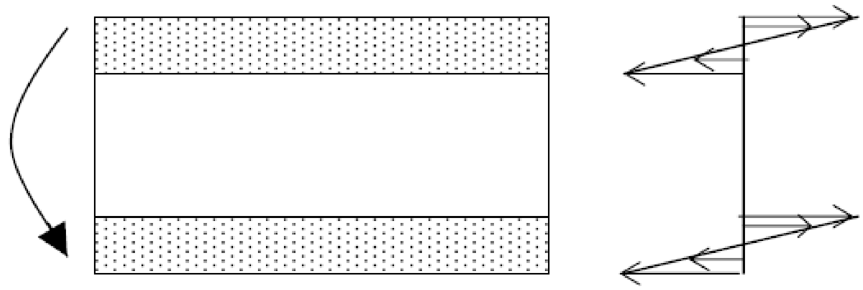

Figure 5-2: Flexural stress distribution for non-composite section

5.1.3 Partially composite panel behavior

The sandwich panels that are able to achieve some degree of shear transfer in between the two load-bearing faces are assumed to be semi-composite sections. For a semi-composite section, the shear connectors could have the capacity to transfer 0 to 100 percent of the longitudinal shear produced by the flexural loads. Generally, most SCIPs fall in this category and their capacity is calculated as a percent of the fully composite section. That being said, although most SCIPs exhibit a semi composite behavior, according to ACI 533R “Guide for precast sandwich panels”, all insulated panels are designed as non-composite sections (ACI, 2012). Figure 5-3 illustrates how the stresses is transferred in between the two load-bearing faces in a semi-composite section.

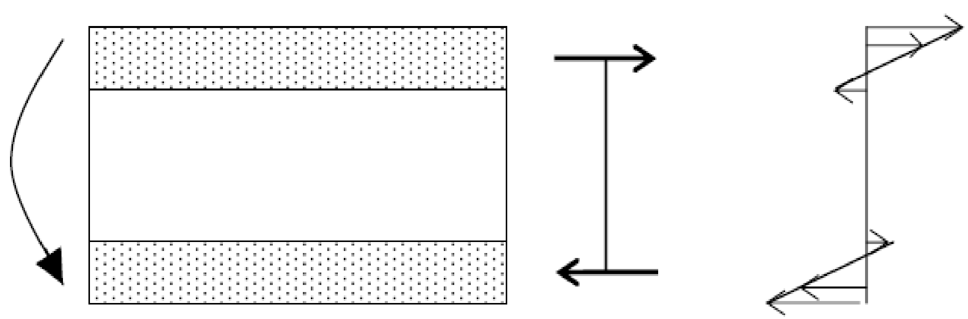

Figure 5-3: Flexural stress distribution for partially composite section

5.2 ACI 318 flexural calculation

In this section, the flexural capacity of the short span MR slab was analyzed as a fully composite section and a non-composite section. The actual flexural capacity of the panels obtained from the experimental program were then used to determine the degree of composite action achieved by the MR panels.

The calculations used in this analysis were governed by the ACI 318 section 9.2.1 (ACI, 2014). The actual dimensions and details of the short span specimen from the experimental program was used for the analysis. The slabs were analyzed as a simply supported component that resists an out-of-plane bending moment produced by its self-weight and the applied normal loads. In actual construction, slabs are generally subjected to flexural loading in the form of concentrated or distributed area loads. For this analysis, it was assumed that the bottom wythe was in tension and the top wythe was in compression. It was also assumed that all the compressive stresses were resisted by the top wythe, whereas the tensile stresses were resisted by the reinforcing in the bottom wythe. Similarly, all the shear stresses were mainly resisted by the two layers of concrete and the diagonal steel connectors. Although the EPS core do have some shear resistance, their contribution is generally not taken into consideration.

Since the experimental test results showed that no specimens had a shear failure at the supports, the minimum shear capacity of 6.6 kips ($P_{max}/2$) is assumed for the panels. The average compressive strength of concrete was assumed to be 8000 psi in the calculations, this was based on the average concrete strength of the panels on the testing day. Although the hard-drawn mesh and the longitudinal bars had a slightly higher yield strength as shown by the coupon testing, the yield strength of the reinforcement was conservatively assumed to be 60 ksi in the calculations. The area of steel in the mesh and the longitudinal bars were accounted for flexural reinforcement. The clear span of the slab for the analysis was assumed to be 119 inches. The slabs were assumed to be 49 inches wide and 6 inches thick. The self-weight of 33 lb/ft^2 was also considered in the calculations.

5.2.1 Flexural analysis assuming fully composite section

For this part of the analysis the specimen was assumed to be a fully composite section. According to the ACI 318, a fully composite panel can be designed as a solid reinforced concrete slab. Hence, for this analysis the cross-section of the panels was assumed to be a solid reinforced concrete slab with two layers of reinforcement. The mesh and the bars in the bottom wythe were considered to be the tensile steel, and the reinforcements in the top face was assumed to be compression steel. The total area of steel in each wythe was 0.52.in^2. The cross-section used in the analysis is shown in Figure 5-4. The nominal moment capacity was calculated using the effective moment equation stated in the section 10.2 of ACI 318. The equation for the nominal moment capacity for the fully composite section is provided in Eqn. (5.1).

The analysis showed that total moment capacity for a fully composite section was 13.7 kip-ft. The moment caused by the self-weight of the panel was then subtracted to calculate the effective moment capacity. The self-weight of the panel was assumed to be a uniformly distributed line load of 131 lb/ft. The net effective moment capacity was 12.2 kip-ft, which corresponded to an equivalent test load of 9.86 kips. Detailed calculations for this analysis are provided in Appendix D.

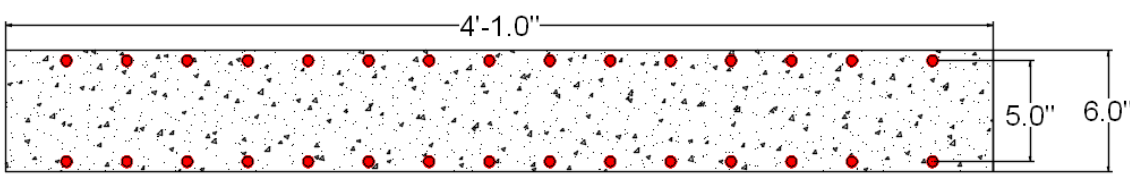

Figure 5-4: Cross section for fully composite flexural analysis

$$\phi M_n = 0.85\, f'a * b(d - \frac{a}{2}) + A's * f's(\text{d-d'}) \tag{5.1}$$

Where,

As= Area of tensile steel (in^2)

A's =Area of compression steel (in^2)

d = distance to tension steel (in)

d' = distance to compression steel (in)

f_y = yield strength for steel (psi)

f'_s = stress in compression bars (psi)

f'_c =compressive strength of concrete (psi)

a = distance to the neutral axis (in)

5.2.2 Flexural analysis assuming a non-composite section

For this part of the analysis, a non-composite section was assumed for the sandwich panel. Since for a non-composite section there is no transfer of stresses in between the two wythes, the wythes resist the flexural loads as two individual sections. The cross-section area used for this analysis was similar to that of just one individual wythe. The cross-section used for this analysis is provided in Figure 5-5. Unlike the analysis for a fully composite section where both the compression and tension steel were used, for this analysis, only one layer of tensile reinforcement was considered. The equation used to calculate total moment capacity for the non-composite section is provided in Eqn. (5.2)

The analysis showed that, total moment capacity for the non-composite section was 2.4 kip-ft. Similarly, the net effective moment capacity was 1.35 kip-ft, which corresponded to an equivalent test load of 1.09 kips. Detailed calculation for flexural strength are provided in Appendix D

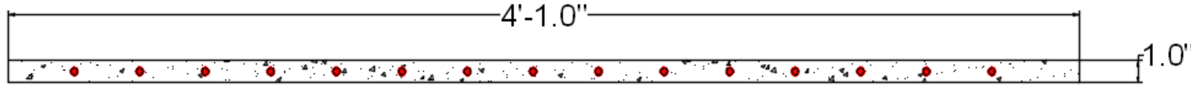

Figure 5-5: Cross section for non-composite section

$$\phi M_n = 0.85\, f' a * b(d - \frac{a}{2}) \quad (5.2)$$

Where,

As = Area of tensile steel (in^2)

d = distance to tension steel (in)

f_y = yield strength for steel (psi)

f'_s = stress in compression bars (psi)

f'_c =c ompressive strength of concrete (psi)

a = distance to the neutral axis (in)

5.3 Composite behavior for MetRock SCIP slab panels

In this section, the effective moment capacity of the short span MR slabs obtained from the experimental program is compared to the capacities of the fully composite and the non-composite panels that were calculated in the earlier sections. These values are compared to determine the composite action achieved by the MR panels.

Results from the ACI flexural analysis, assuming a fully composite section showed that the panels would have an effective moment capacity of 12.2 kip-ft, which corresponded to an equivalent test load of 9.86 kips. Similarly, the capacity for the non-composite section was 1.35 kip-ft; which corresponded to an equivalent test load of 0.98 kips. Test results showed that the average effective moment capacity for the short span specimens was 8.03 kip-ft with an equivalent test load of 6.76 kips.

The average load-deflection curve obtained from the testing of the short span panels along with the calculated capacity of fully composite and non-composite sections are illustrated in Figure 5-6. From the load graph, it can be observed that the capacity of the MR panel falls in between the capacities of fully composite and the non-composite sections. The capacity of the panels is closer to the fully composite section than a non-composite section. Hence the MR panels can be classified as a partially composite section. Calculations show that average effective moment capacity for the MR panels was 66% of the effective capacity of a fully composite section.

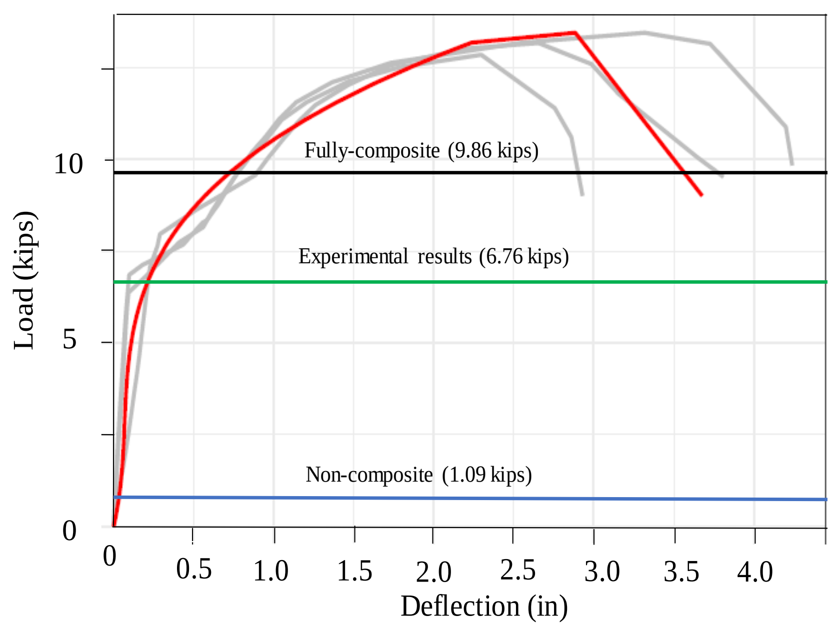

Figure 5-6: Load-deflection curve for partially composite MR panels

CHAPTER 6. Experimental Testing of Wall Panels

6.1 General

This chapter presents the development and testing of the MetRock SCIPs used as structural walls for the construction of low-rise buildings. This part of the experimental program was conducted with the aim to study the in-plane flexural properties of the MR panels subjected to lateral loading. Additionally, this investigation was also used to assess the seismic performance of the MR wall panels. Three slender cantilevered wall specimens were prepared using the standard 4ft x10ft MR SCIP with a 4-inch insulation core. Fabrication details of the wall specimens are provided in Section 3.4. All three walls were tested until failure under a quasi-static cyclic lateral loading protocol. The results obtained from the testing of the walls are presented and analyzed in this chapter. The strength properties such as the in-plane elastic stiffness and drift ratio limits of the MR walls are documented and presented. Furthermore, the nonlinear properties such as the damage propagation, energy dissipation and the modes of failures observed during the testing are also discussed.

6.2 Test specimen description

The wall specimens used for this investigation were fabricated using the standard short span MR panels. The specimens were prepared using a precast approach where two layers of SCC was poured over the panels. The fabrication process for the wall panel was identical to that of the slab specimens, details from the fabrication process can be reviewed in Chapter 3. The wall specimens used for this experiment were labeled A-4, A-5, and A-6. All three specimens were cantilever walls that had an overall height of 125 inches. A reinforced concrete socket footing was used to provide the fixed base for the specimens. The footing was tied down to the strong floor using high strength threaded anchor rods. The distance from the base to the top of the wall was 108 inches. Specimen A-5 is shown in Figure 6-1.

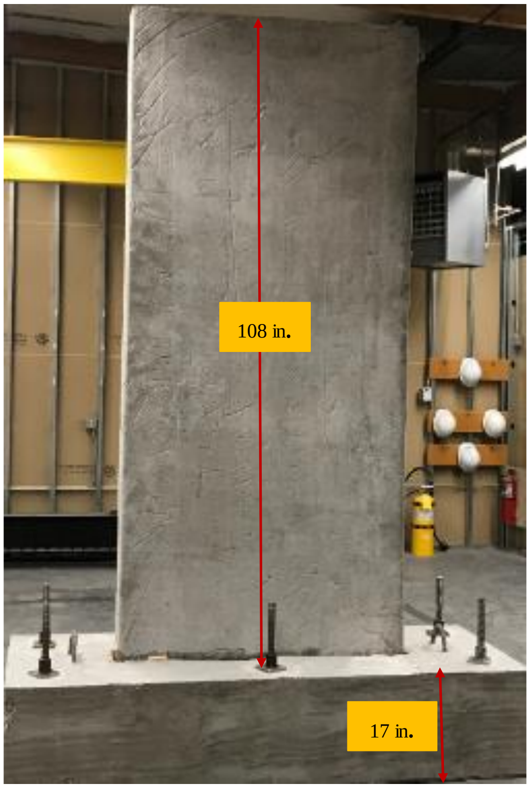

Figure 6-1: MR SCIP wall specimen

To investigate the actual in-plane capacity of the panels, a socket connection was used for the panel to footing connection. This type of connection is not typical in residential construction but are frequently used for retaining walls. The socket connection was 7 feet long, 30 inches wide and 17 inches deep reinforced concrete strip footing with a 7 in x50 in recess in the middle that was 15 inches deep. The socket was slightly wider than the panel to ensure that a uniform half-inch gap was maintained in between the panel and the socket. Construction details for the socket footing are discussed in Section 3.4.2. Additionally, six one-inch ducts were installed inside the footing before the concrete was poured. These ducts were then used to anchor the footing to the strong floor with the aid of six high strength threaded anchor rods. Details for the socket footing is provided in Figure 6-2.

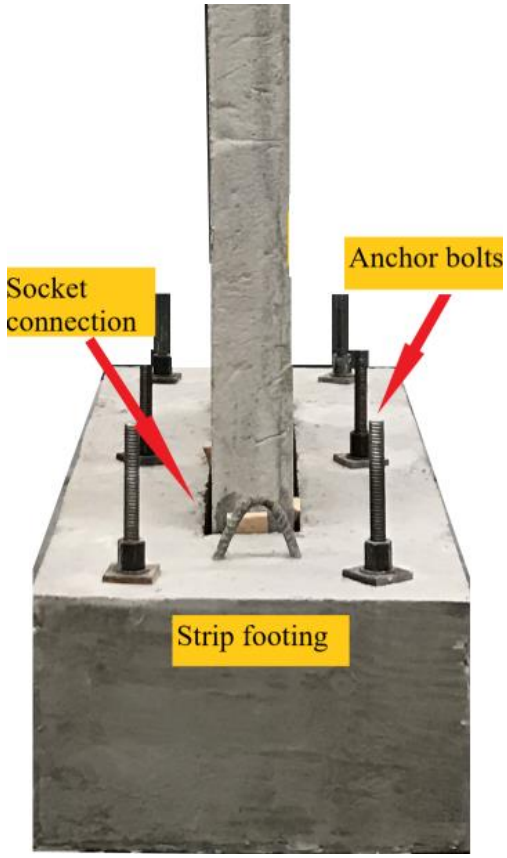

Figure 6-2: Detailed socket wall footing

A precast approach was used to assemble the prefabricated panel to the socket footing. First, the footing was transported from the precast bed to the structural lab. They were then secured to the strong floor using high strength anchor rods. Once the footing was in place, the panel was stood up vertically using a tilt-up system. The panel was then clamped and placed inside the footing using a forklift. After the panel was set inside the socket, it was grouted in-place using a fluid high-strength non-shrink Dayton 1107 advanced grout. The product data sheet for the grout is provided in the Appendix A. The grout was applied in the half inch gap that was maintained in between the panel and the footing. Details for the assembly of the wall specimen are provided in Section 3.4.3. Six standard two-inch grout cubes were prepared for each wall specimen. These cubes were used to determine the test day compressive strength of the grout.

The ASTM C109 (Standard Compressive Strength of Hydraulic Cement Mortar) was used to test the grout cubes. Figure 6-3 show the pictures form testing of grout cubes.

a) Preparing grout cubes b) Testing grout cubes c) Failure modes

Figure 6-3: Testing of grout cubes for wall specimen

6.3 Test setup

This section provides information on the testing arrangement of the MR wall specimens. The testing protocol for this experiment was drafted according to the ACI 374.2R "Guide for Testing Reinforced Concrete Structural Elements under Slowly Applied Simulated Seismic Loads" (ACI, 2013). The test setup, boundary conditions, and loading protocol stated in the guide were used to properly execute the experiment. All the tests were performed at the structural lab at Idaho State University. The schematics for the wall test setup is shown in Figure 6-4. The actual test setup is presented in Figure 6-5.

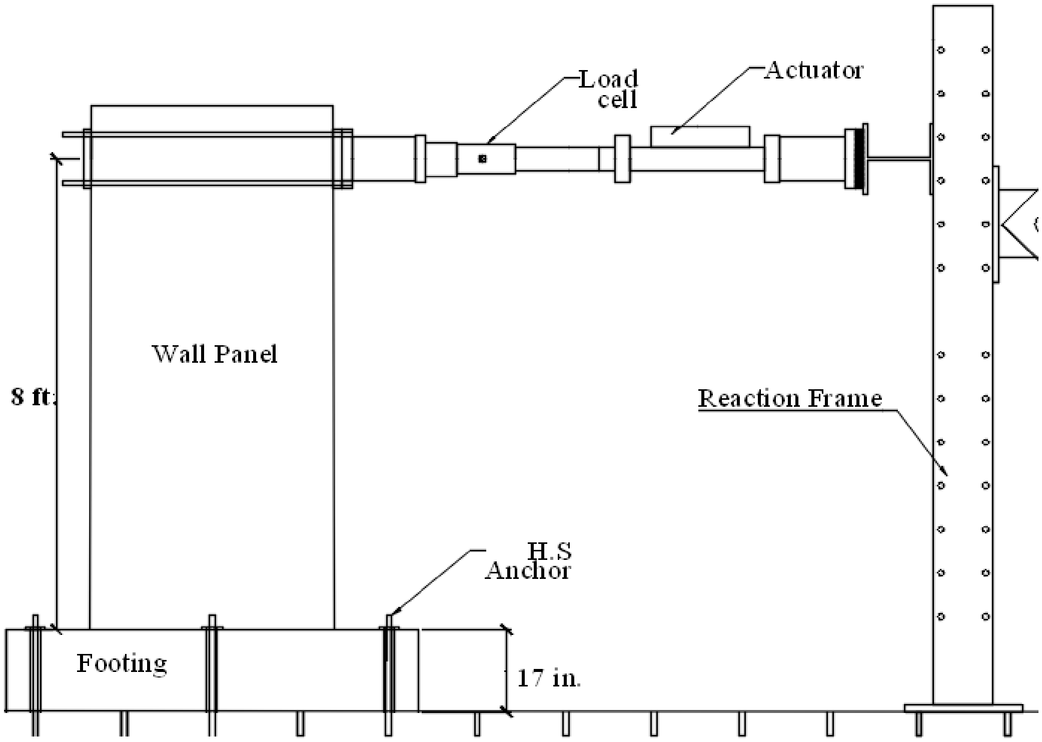

Figure 6-4: Schematics for wall test setup

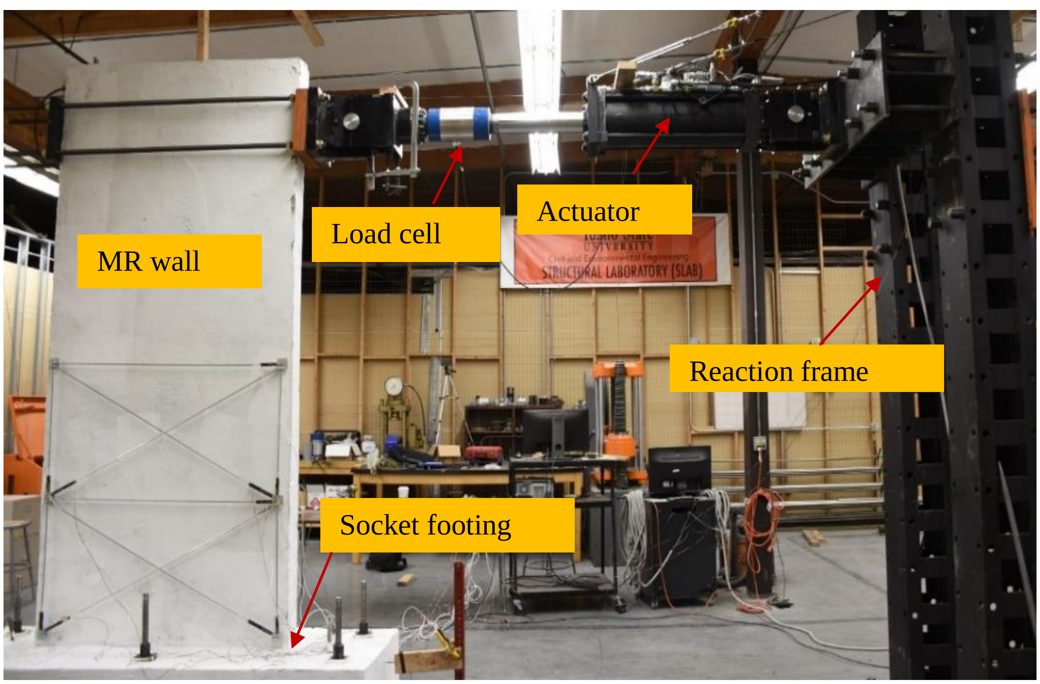

Figure 6-5: Wall test setup

6.3.1 Support conditions

As mentioned in Section 6.1, the specimens used for this experiment were cantilever walls that had a fixed connection at the base. The height from the base of the wall to the center of the actuator was eight feet.

6.3.2 Loading apparatus

The lateral in-plane loading was applied to the specimen by a 160-kip capacity displacement controlled servo-hydraulic actuator. The actuator was pushing against a reaction frame that was tied down to the strong floor using high strength threaded rods. The head of the actuator was attached to the top of the specimen using four high strength threaded rods and two 1.5-inch steel bearing plates. The top of wall was clamped to the actuator to achieve both push and pull loading intervals.

6.3.3 Measurement device and instrumentation

Campbell Scientific data acquisition system was used to continuously record and report all necessary information from the instruments attached to the specimen during testing. The logger system comprised of a separate computer which was intended to record the data from the instruments mounted on the specimen and the load cells at each step of time during testing. Each instrument was calibrated to a channel in the logger computer. There was a trigger set for the logger system which was designed to get a reading from all instruments mounted on the specimen, which then transferred the data to the logger computer at one hertz sampling rate. The instrumentation details for are presented Figure 6-6. The label, description, and the function of each instrument used are provided in Table 6-1.

Table 6-1: Instrumentation for testing of wall specimens

Label	Description	Function
IPT	50-inch capacity string potentiometer	Measured the in-plane deflection of the wall
OPT	50-inch capacity string potentiometer	Measured the out-of-plane deflection of the wall
IPF	2-inch stroke potentiometer	Measured the in-plane deflection of the footing
OPF	2-inch stroke potentiometer	Measured the out-of-plane deflection of the footing
V (1-8)	2-inch stroke potentiometer	Measured the curvature of the specimen with respect to the footing
H (1&2)	2-inch stroke potentiometer	Measured the horizontal cracking of the wall
D (1-4)	4-inch stroke potentiometer	Measured the diagonal cracking of the wall

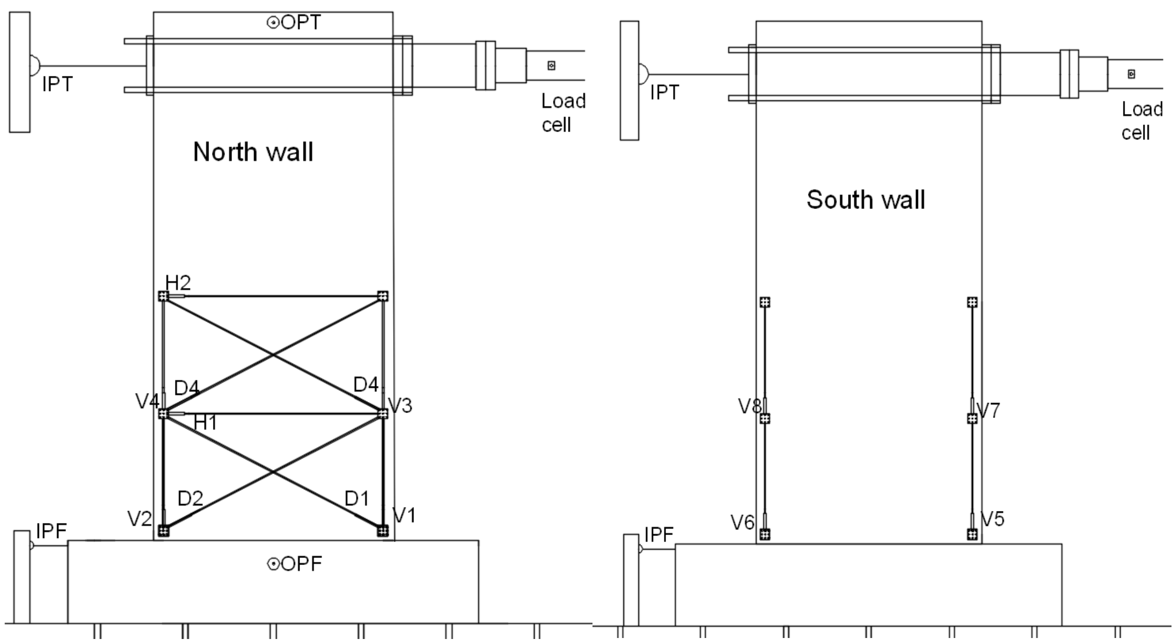

Figure 6-6: Schematics for instrumentation of wall specimen

The lateral loads were recorded using a 225-kip capacity two-way load cell that was installed at the head of the actuator. Figure 6-7 shows the load cell setup.

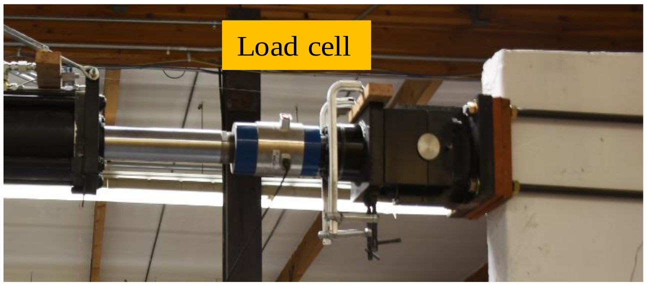

Figure 6-7: Instrumentation for wall testing (load cell)

The in-plane lateral displacement of the wall was measured at two locations using a set of string potentiometers that were mounted to an independent frame. The string potentiomentrs were used to measure the in-plane displacement at the top and at the base of the wall. Similarly, the out-of-plane motion of the wall and the base were also monitored using the same setup. Figure 6-8 show the setup for the potentiometers used to the record the in-plane and out-of-plane displacements of the specimen.

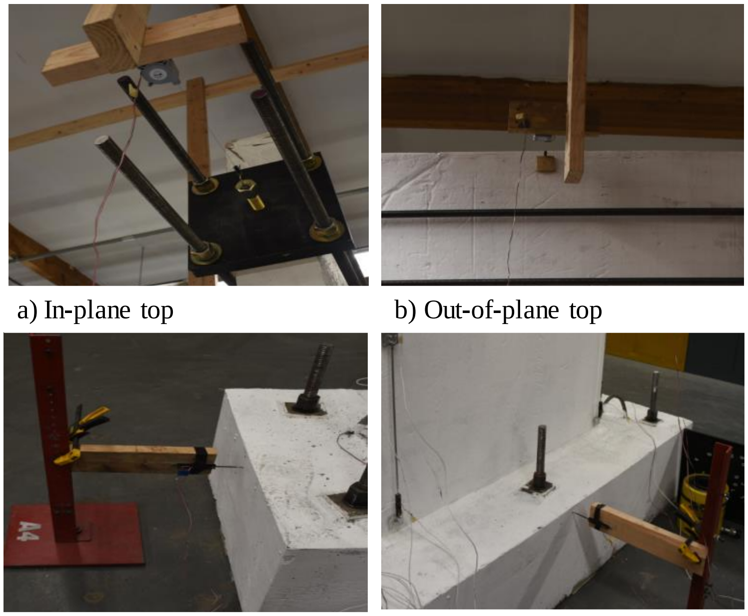

a) In-plane top

b) Out-of-plane top

c) In-plane footing

d) Out-of-plane footing

Figure 6-8: Instrumentation for wall panel testing (in-plane and out-of-plane deflection)

Flexural and shear deformations of the wall were measured using vertical, horizontal and diagonal array of rod end potentiometers (pots). The pots were directly mounted on both faces of the wall. The pots were attached to the wall using studs with aluminum brackets that were drilled and epoxied into the concrete wythe. The vertical pots (V) were used to measure the curvature of the wall with respect to the footing while the horizontal and the diagonal pots (H and D) measured shear deformation. The arrangement of the potentiometers is provided in Figure 6-9.

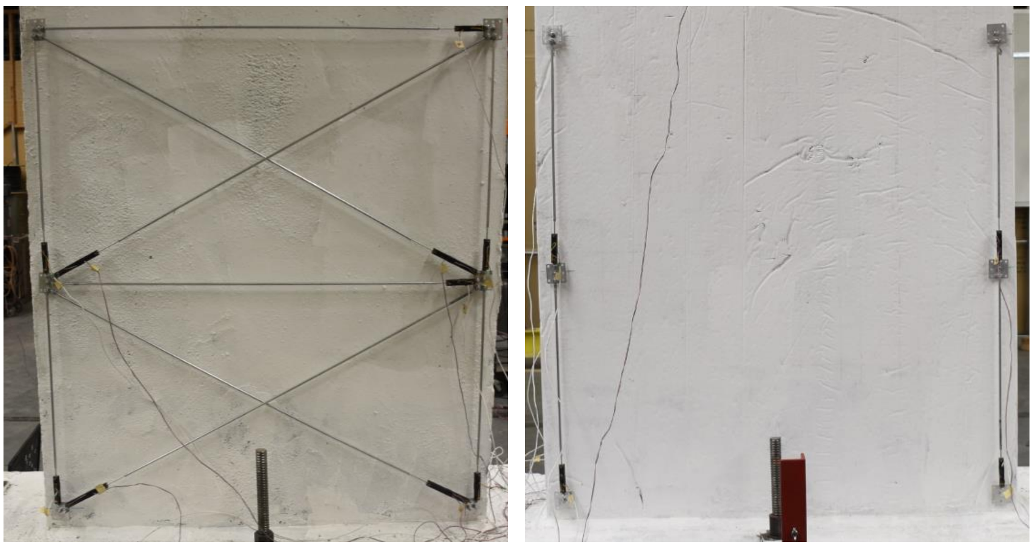

Figure 6-9: Instrumentation for testing of wall (potentiometers)

6.3.4 Experimental observations

The test data collected for each test was supplemented by observations made during different stages of testing. A crack propagation analysis was conducted for each test to assess the progression of damage and the overall specimen performance. The location, type, and size of cracks were noted at each cycle for this purpose. The cracks formed during the pull and the push cycles were marked with green and red colors, respectively.

6.4 Loading protocol

A displacement controlled loading protocol was used for this testing. A quasi-static reverse cyclic lateral loading was applied at increasing displacements. The loading rate of one millimeter per second was used to eliminate the dynamic inertial effects on the specimen. The loading sequence at each drift ratio consisted of two cycles with the same drift ratio. Each interval started at a pull which was followed by a push cycle. This type of loading protocol was adopted from the ACI recommendations (ACI Innovation Task Group, 2007).

The drift ratio was selected as the control parameter for progressive. Drift ratios are calculated as the ratio of the lateral displacement at the top of the structure to the overall height. The loading intervals for this experiment were set using an estimated yield drift ratio φ_y. The estimated yield drift ratio was calculated using the yield displacement equation for structural walls provided in Priestley's "Displacement-based seismic design of structures" (Priestley et al, 2007). The yield deflection was calculated using Eqn. (6.2). The estimated drift ratio calculated for this test was 0.32 inches. The targeted drift ratios selected for the loading intervals were based on the estimated yield drift ratio. The loading history used for this experiment are provide in Table 6-2. The loading profile is shown in Figure 6-10. In all three testing, positive values were assigned to the push cycles and negative values were assigned to the pull cycles. The testing was stopped after 50 percent strength loss.

$$\Delta_{yi} = \frac{\epsilon_y}{b} H_i^2 \left(1 - \frac{H_i}{3H_n}\right) \qquad (6.1)$$

Where,

ϵ_y = Yield strain for steel (in/in)

b = Width of the wall (in)

H_i = Height of i^{th} wall (in)

H_n= Total height pf structure (in)

Table 6-2: Drift targets for reverse cyclic lateral loading protocol

Cycle	Δ (in)	Drift (%)
1/4 φy	0.08	0.08
1/2 φy	0.16	0.16
3/4 φy	0.24	0.24
1 φy	0.32	0.32
1.5 φy	0.47	0.48
2 φy	0.63	0.64
2.5 φy	0.79	0.80
3 φy	0.95	0.97
4 φy	1.26	1.29
5 φy	1.58	1.61
6 φy	1.89	1.93
7 φy	2.21	2.25

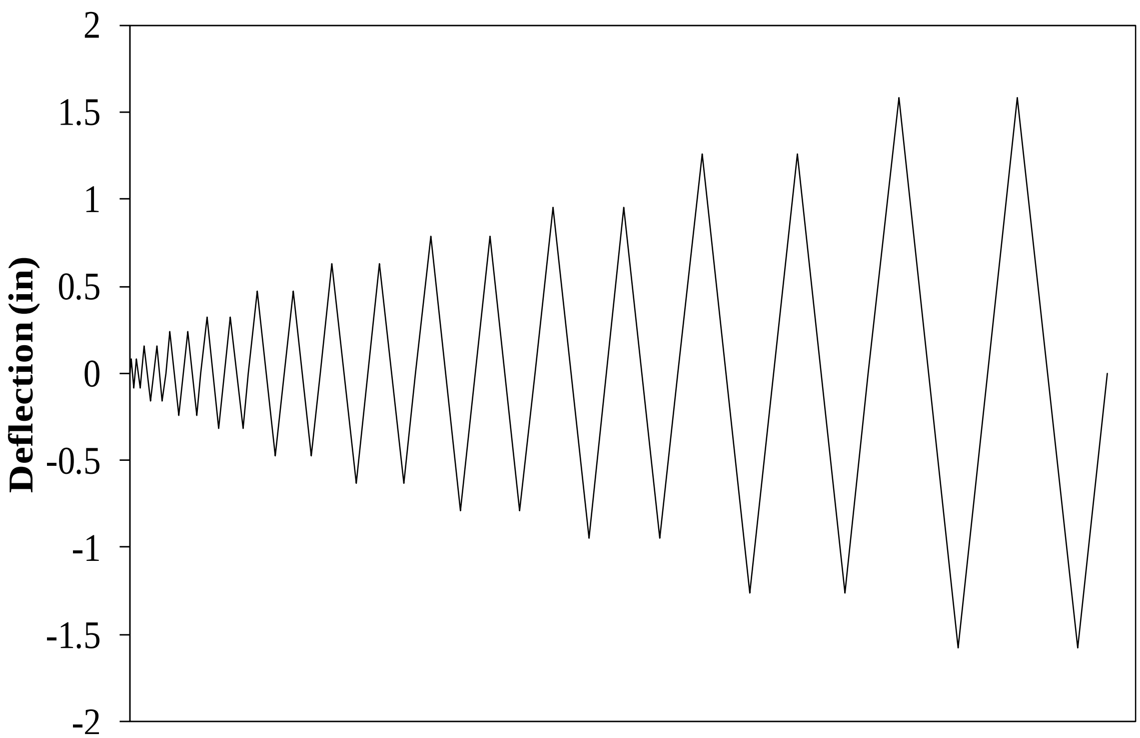

Figure 6-10: Loading protocol for reverse cyclic lateral loading

During testing no axial gravity load was applied on the specimen. Although the application of gravity load is recommended by ACI 374.2R, section 4.5 mentions that the gravity loads are required only if their effects are deemed important (ACI, 2015). For a typical MR SCIP construction, all the walls in the building are load-bearing walls. This causes the gravity load to be distributed evenly among all the walls, which significantly reduces the amount of gravity load applied on an individual section. Additionally, similar cyclic testing conducted by El Demerdash showed that the application of gravity load did not change the overall the performance of the walls (El Demerdash, 2012)

6.5 Experiment results

This section discusses the results and observations obtained from the testing of the full-scale MR wall specimens. All three specimens were tested up to a 50% strength degradation to define the in-plane structural properties of the MR panels. Each test is summarized, and the results are presented graphically in this section. The raw displacement and load data collected during the tests were used to generate the load-deflection hysteresis for each specimen. The backbone data was then used to generate the load-drift ratio curve, and to calculate the moment capacity and the elastic in-plane stiffness of the panels.

The curvature of the wall was also measured during the tests. This was done using the data recorded by the vertical potentiometers that were placed in the plastic hinge zone. The curvature was calculated as the average slope of the deflection in the compression and the tension region. The raw data were processed using a MATLAB code to produce the backbone curve.

The energy dissipation obtained by each specimen prior to failing was also analyzed for this investigation, the envelope areas inside the load-deflection curves were used to compute the energy dissipation at each drift interval. The dissipated energy was calculated using numerical integration of the area enclosed inside the load-displacement hysteresis loop for each cycle The MATLAB code used to compute the envelope area is attached in Appendix E.

Specimen A-4 was prepared on 12/03/2018 and was tested on 5/29/19. The concrete strength of the wall panel at transfer was 3681 psi and the test day strength were 8584.5 psi. The average compressive strength on the test day for the footing and the grout was 10,800 psi and 5682 psi respectively.

The raw load defection hysteresis for A-4 is provided in Figure 6-11. The backbone load drift ratio curve derived from the test data is illustrated in Figure 6-12. The test results showed that the hysteresis for A-4 was fairly symmetric. The first yielding of the specimen occurred during the pull cycle at a deflection of 0.068 inches with a yield force of 8.13 kips. The drift ratio at yielding was 0.07% which corresponded to a moment of 65 kip-ft. Similarly, for the push cycle, the specimen yielded at a deflection of 0.065 inches with a yield force of 8.57 kips. The drift ratio at yield was 0.07% with a moment of 68.5 kip-ft. The ultimate force for the pull cycle was 18.9 kips at a drift ratio of 0.78% whereas the ultimate force for the push cycle was 17.4 kips with at a drift ratio of 0.804%. The moment capacity for the specimen in pull was 151.1 kip-ft. whereas in the push cycle it was 139 kip-ft. Due to slight deflection in the reaction frame, the push and t6he pull cycles were slightly different from each other. The moment-curvaturegraph for A-4 is provided in Figure 6-13.

The energy dissipated per loop at each cycle for A-4 is presented in Figure 6-14. In this figure, the energy per loop at each loading interval is displayed in a histogram plot where the cumulative dissipated energy during testing is shown on the secondary axis of the graph. Data from Figure 6-14 show that the inside the hysteretic loop was small in the initial loading intervals and gradually increased increasing drift ratios. Also, within the two cycles of the same loading interval, the first cycle dissipated more energy than the second. This indicated that the specimen experienced strength/stiffness degradation during the cycles. The total amount of energy dissipated during the test was 13.2 KJ, and the maximum energy dissipation was experienced during the 10th cycle.

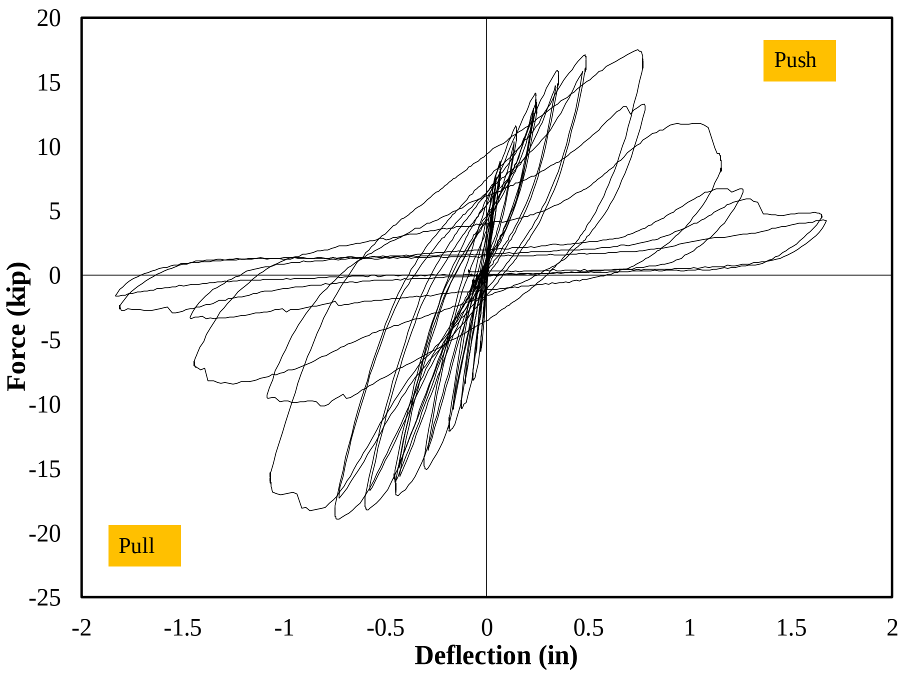

Figure 6-11: Load-deflection hysteresis for specimen A-4

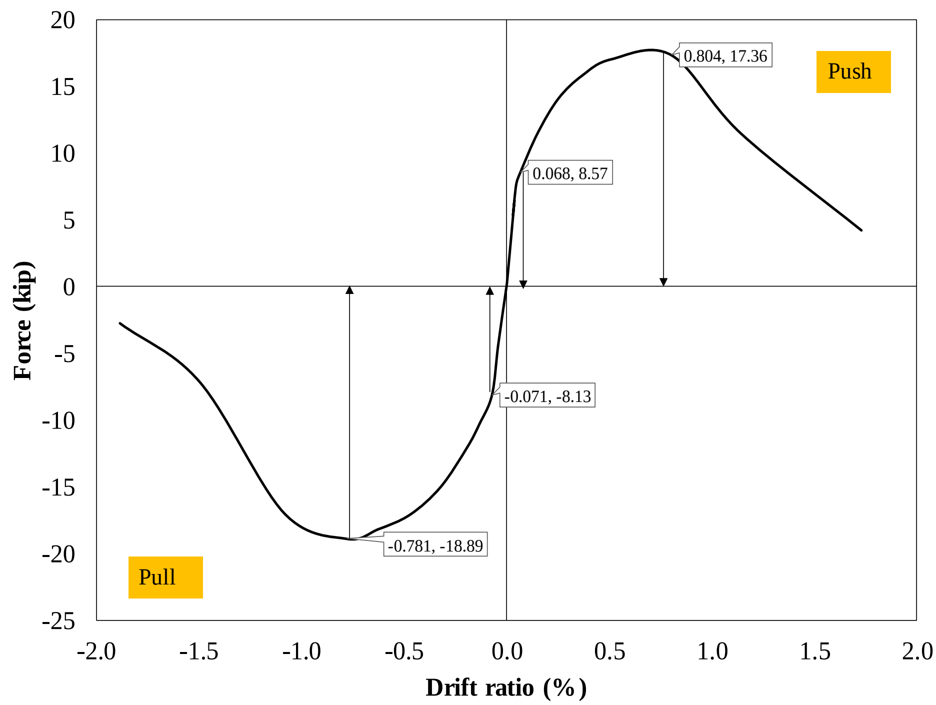

Figure 6-12: Force-drift ratio backbone curve for A-4

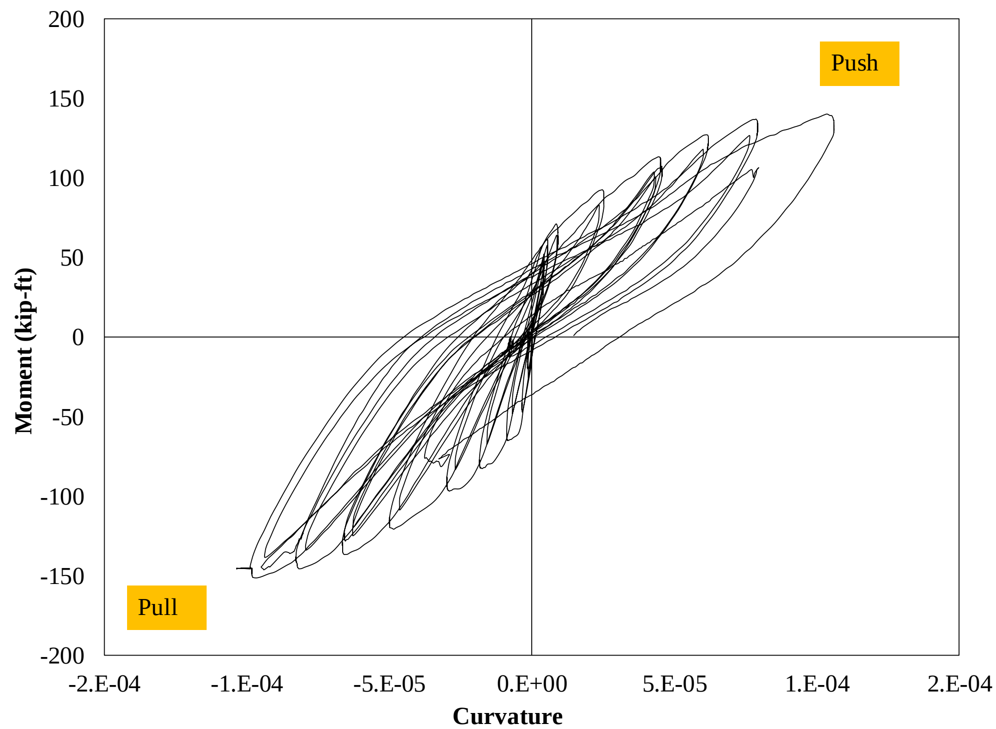

Figure 6-13: Moment-curvature for specimen A-4

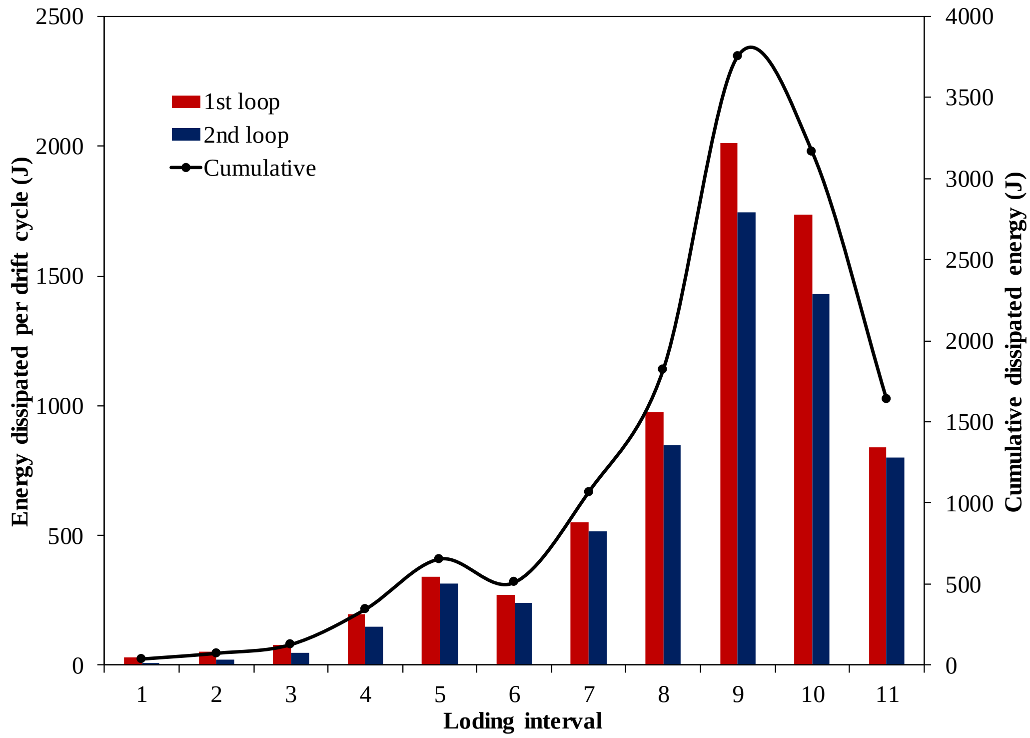

Figure 6-14: Energy dissipation plot for specimen A-4

Specimen A-5 was prepared on 12/06/2018 and was tested on 5/22/19. The concrete strength of the wall panel at transfer and on test day were 3613 psi and 7309 psi respectively. The average compressive strength for the footing and the grout were 10,800 psi and was 5781psi respectively.

The raw load-defection hysteresis for A-5 is provided in Figure 6-15. The load-drift ratio backbone curve derived from the raw test data is provided in Figure 6-16. The test results showed that the hysteresis for A-5 was fairly symmetrical. The yielding of the specimen occurred in the pull cycle at a deflection of 0.081 inches with a yield force of 7.71 kips. The drift ratio at yielding was 0.085% with a moment of 61.7 kip-ft. Similarly, for the push cycle, the specimen yielded at a deflection of 0.08 inches and the yield force was 8.4 kips. The drift ratio at yield was 0.083% with a moment of 67.7 kip-ft. The ultimate force for the pull cycle was 19.5 kips that corresponded to a drift ratio of 1.1%. The ultimate force for the push cycle was 17.4

kips at a drift ratio of 0.84%. The moment capacity for the specimen in pull was 156.5 kip-ft. whereas in the push cycle it was 139.2 kip-ft. The moment-curvature graph for A-5 is provided in Figure 6-17.

The energy dissipated per loop at each interval for A-5 is presented in Figure 6-18. Similar to A-4 the dissipation graph for A-5 shows that the enclosed area loops was small during the initial cycles and gradually increased with increasing drift ratios. This indicated that the specimen experienced strength/stiffness degradation during the cycles. The total energy dissipated during the testing of A-5 was 18.8 KJ, and the maximum energy dissipation was attained in the 10th loading interval where the dissipated energy was 6.2 KJ.

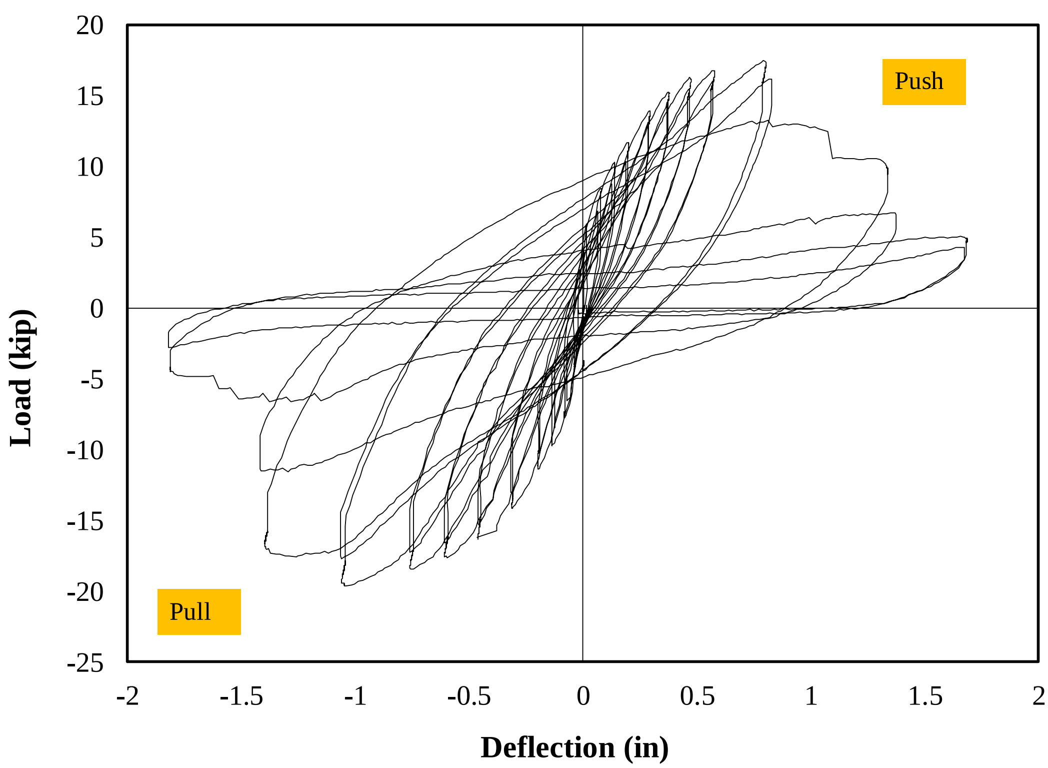

Figure 6-15: Load-deflection hysteresis for specimen A-5

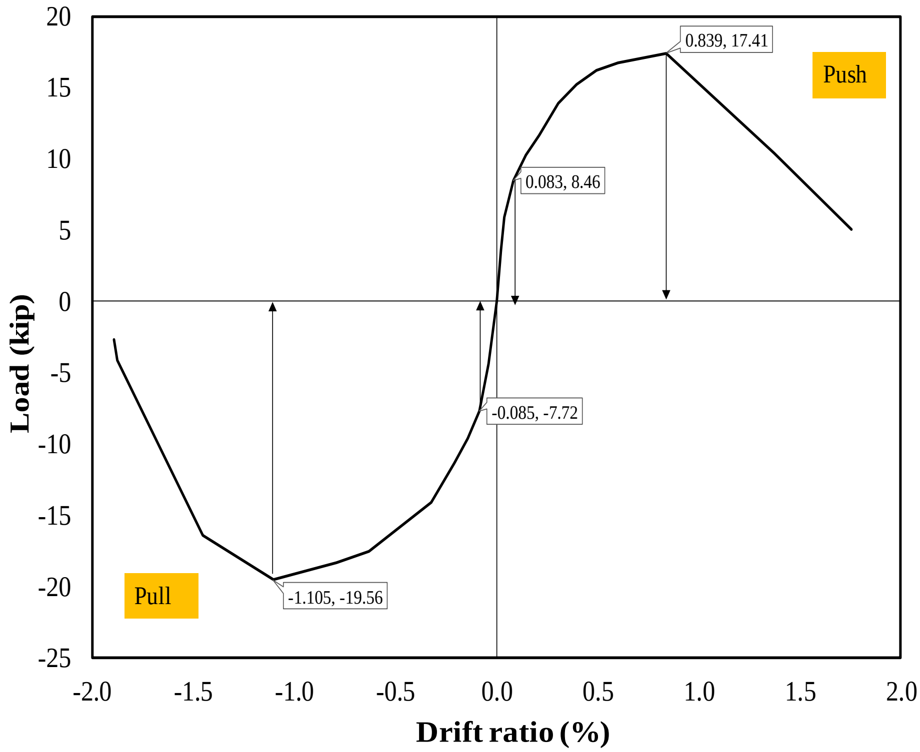

Figure 6-16: A-5: Backbone load-drift ratio curve A-5

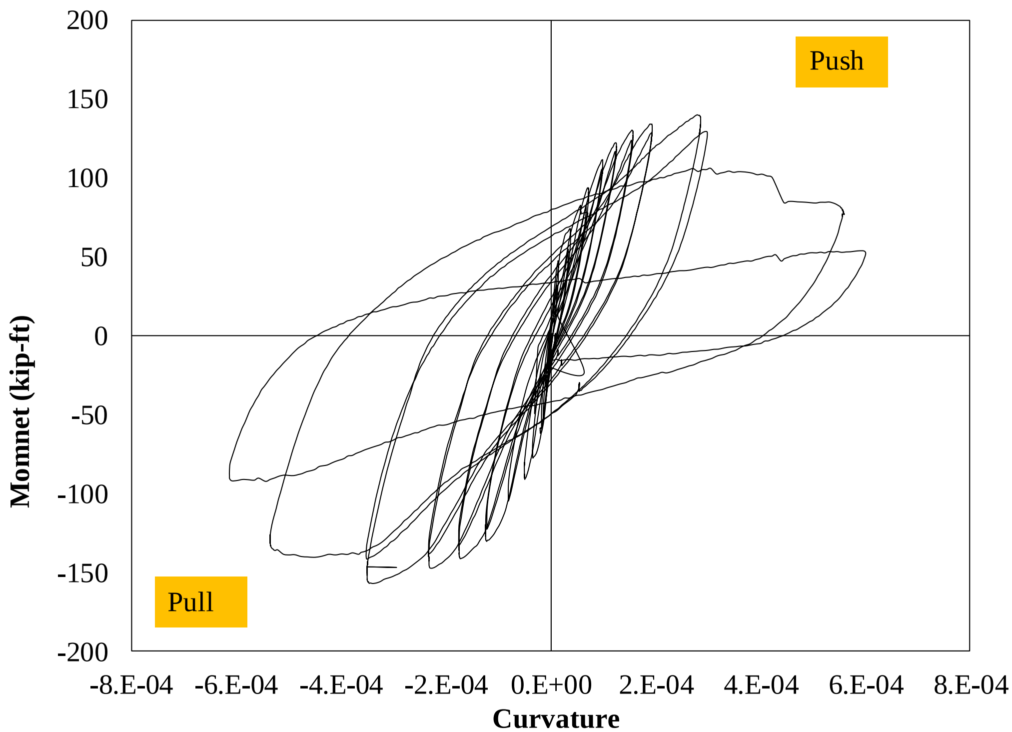

Figure 6-17: Moment-curvature for A-5

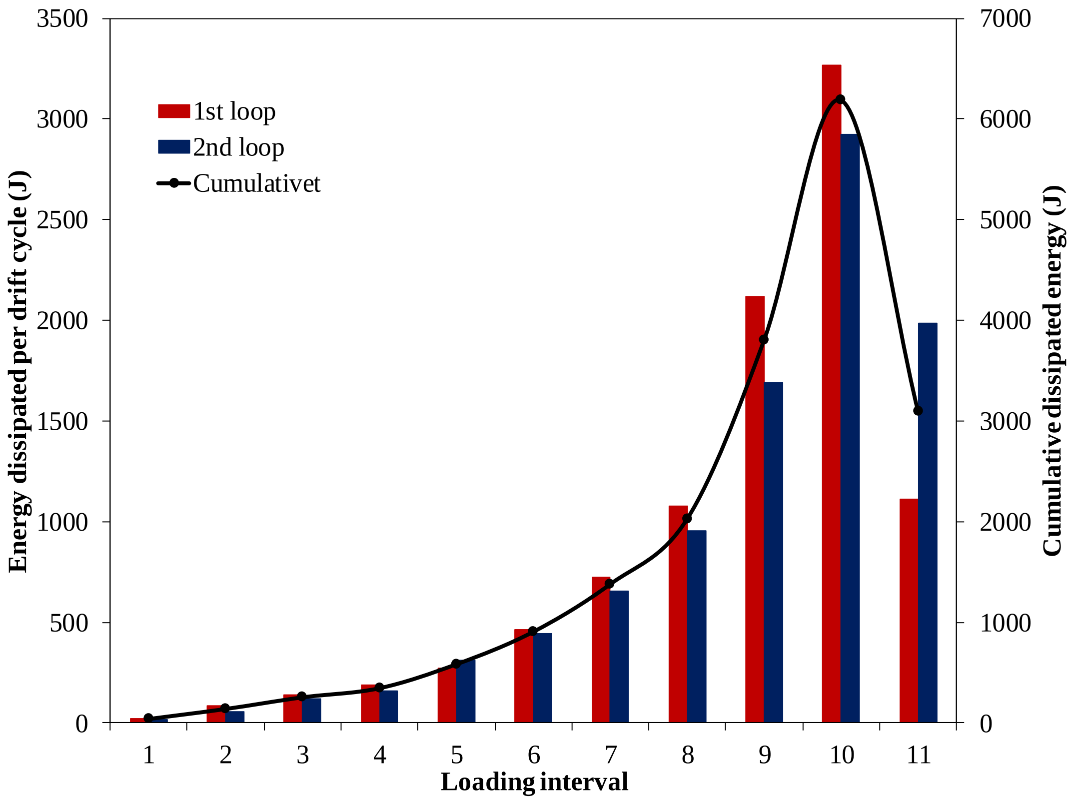

Figure 6-18: Energy dissipation for specimen A-5

Specimen A-6 was prepared on 12/132018 and was tested on 5/10/19. The concrete strength of the wall panel at transfer and on test day were 3013 psi and 7564 psi respectively. The average compressive strength for the footing and the grout were 10,800 psi and was 6295psi respectively.

The raw load-defection hysteresis for A-6 is provided in Figure 6-19. The load-drift ratio curve derived from the test data is provided in Figure 6-20.The test results showed that the hysteresis for A-6 was fairly symmetrical. The yielding of the specimen occurred in the pull cycle at a displacement of 0.094 inches with a yield force of 7.3 kips. The drift ratio at yielding was 0.094% with a moment of 58.8 kip-ft. Similarly, for the push cycle, the specimen yielded at a deflection of 0.084 inches and the yield force was 7.25 kips. The drift ratio at yield was 0.087% at a corresponding moment of 58kip-ft. The ultimate force for the pull cycle was 19.2 kips with a at a drift ratio of 0.93%. The ultimate force for the push cycle was 18.3 kips with a corresponding drift ratio of 0.76%. The moment capacity for the specimen in pull was 153 kip-ft. whereas in the push cycle it was 146.8 kip-ft. The moment-curvature graph for A-5 is provided in Figure 6-21.

The energy dissipated each drift interval for A-6 is presented in Figure 6-22. The graph shows that the area enclosed inside the loops was small in the initial cycles, and gradually increased with every drift ratio. This indicates that the specimen experienced strength/stiffness degradation during the cycles. Similar to A-4 and A-5 prior to reaching the ultimate capacity, for the same targeted drift interval more energy dissipation occurred in the first cycle than the second. The total energy dissipated during the testing of A-6 was 17.0 KJ. The maximum energy dissipation was attained in the 9h loading interval where the dissipated energy was 5.2 KJ.

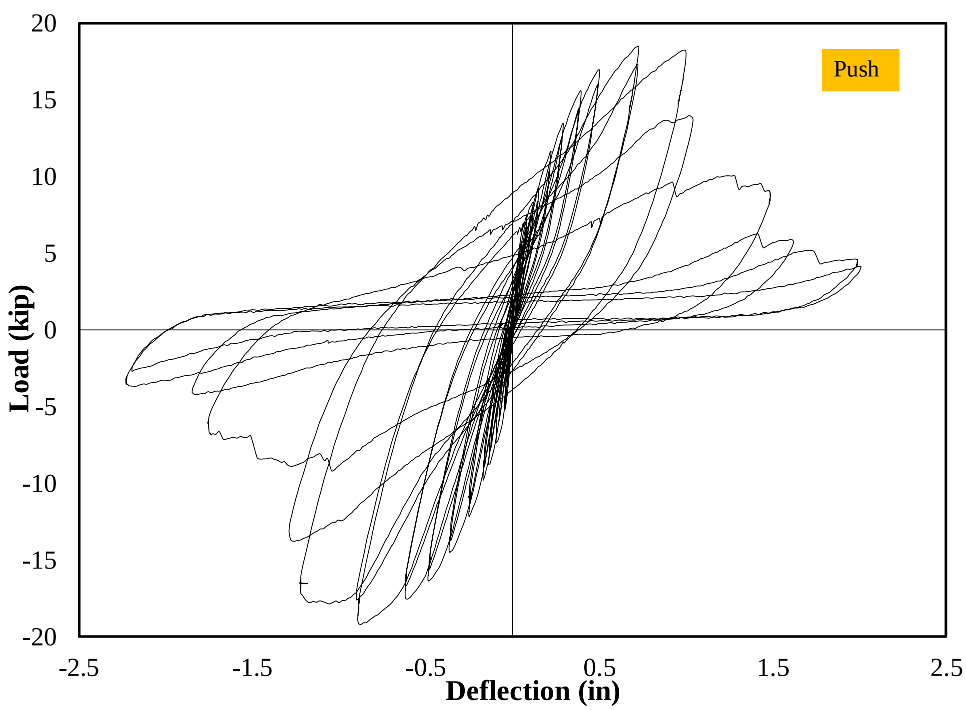

Figure 6-19: Load-deflection hysteresis for specimen A-6

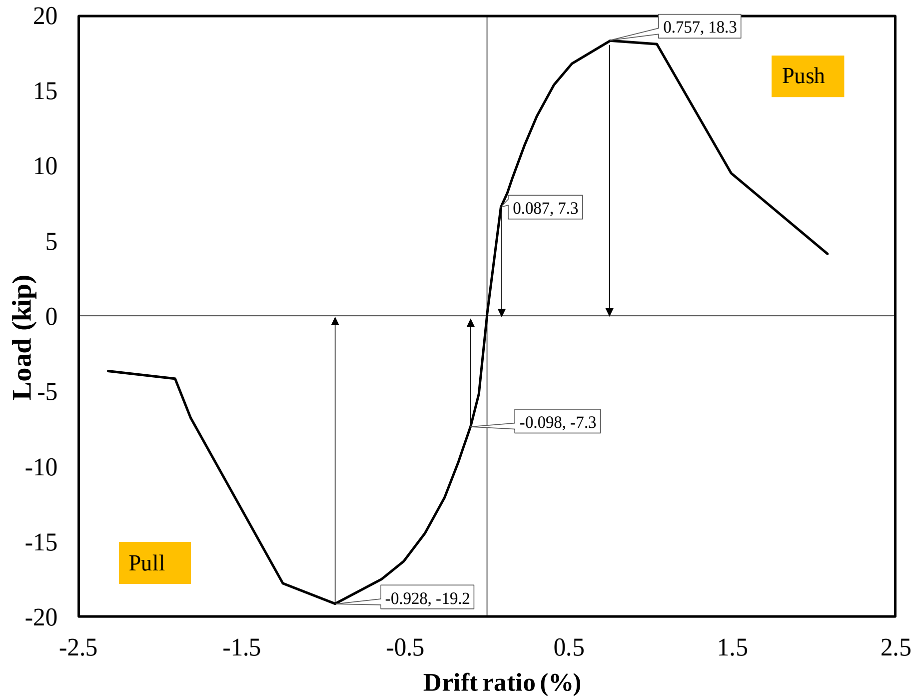

Figure 6-20: Backbone load-drift ratio for specimen A-6

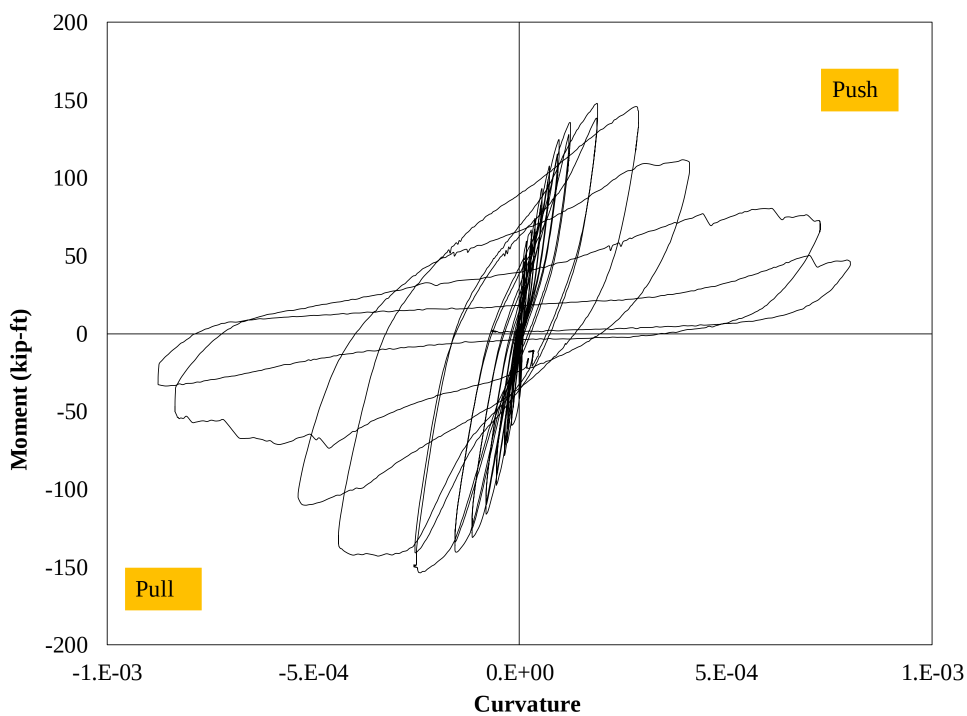

Figure 6-21: Moment-curvature for specimen A-6

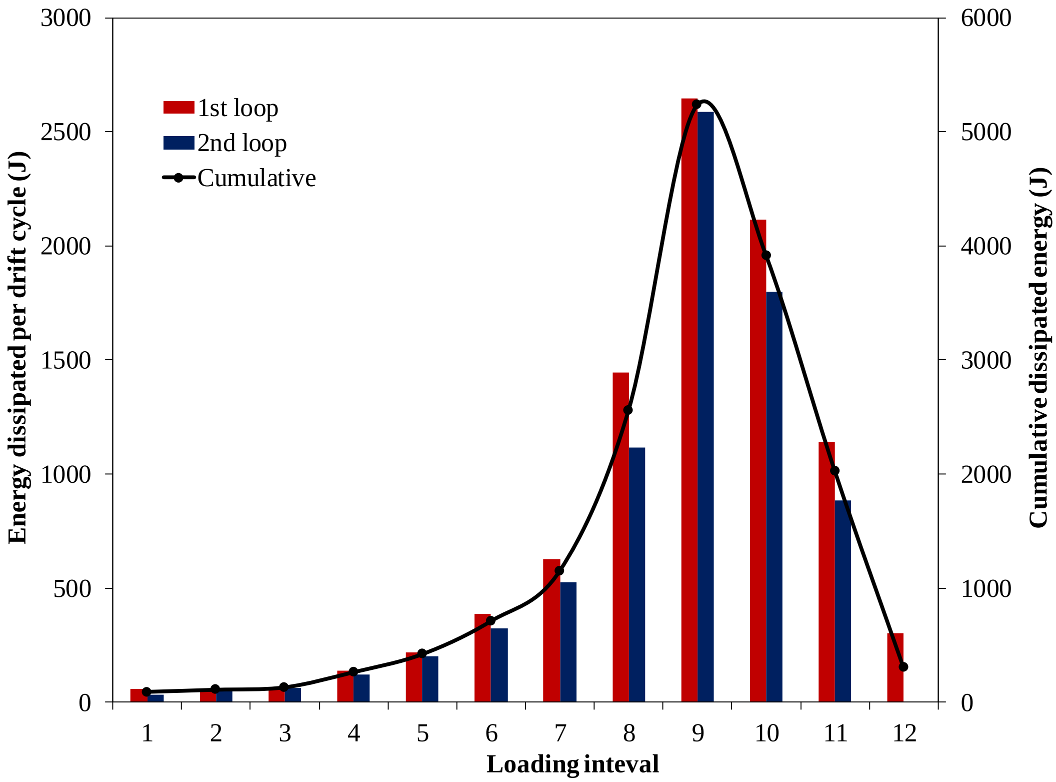

Figure 6-22: Energy dissipation plot for specimen A-6

The overall test summary for the in-plane cyclic testing of the MR wall specimens are presented in Table 6-3. The average yield drift ratio for the specimens was 0.082%. The average yield force was 7.91 kips which corresponded to an average moment capacity of 63.2 kip-ft. The average in-plane elastic stiffness for the specimens was 102.7 kip/in. The average ultimate moment capacity of the specimen was 148 kip-ft and was reached at a drift ratio of 0.89%.

Table 6-3: Test summary for in-plane cyclic loading of MR wall specimens

Specimen	Cycle	Yield drift ratio (%)	Yield moment (kip-ft)	In-plane stiffness (kip/in)	Ultimate drift ratio %	Ultimate moment capacity (kip-ft)	Energy dissipated (K.J)
A-4	Pull	0.071	65.0	119.5	0.781	151.1	13.2
	Push	0.068	68.5	131.8	0.804	138.9	
A-5	Pull	0.085	61.7	95.3	1.105	156.5	18.8
	Push	0.083	67.7	105.7	0.839	139.2	
A-6	Pull	0.098	58.8	78.1	0.928	153.2	17.0
	Push	0.087	58.0	86.3	0.757	146.8	
Average		0.082	63.3	102.8	0.869	147.6	16.3

The load-deflection data obtained from the experiment were also used to define two important seismic parameters for the MR panels. The overstrength factor (Ωo) and the ultimate ductility (μ_T) for the panels were calculated using the methodology stated in FEMA P695. FEMA P695 provides a rational method of evaluating the seismic performance factors for various seismic force resisting systems (FEMA, 2009). The idealized non-linear static push over (backbone) curve used for this analysis is illustrated in Figure 6-21. Eqns. (6.2) and (6.3) were used to calculate the overstrength factor and the ultimate ductility. The calculated overstrength factors for the three specimens are summarized in Table 6-4. Similarly, the values for the ultimate displacement ductility for the three specimens were calculated and are presented in Table 6-5. Testing results showed that the average calculated overstrength factor for the MR panel was 2.5, and the total ductility was 16.3.

$$\Omega o = Vu/Vy \tag{6.2}$$

Where,

Ωo = Overstrength factor

Vy = Base shear at yield (kip)

Vu = Ultimate base shear (kip)

$$\mu_T = \delta ult/\delta y \tag{6.3}$$

Where,

μ_T= Ultimate ductility

δy = Deflection at yield (in)

δu= Deflection at the point of 20% strength loss (in)

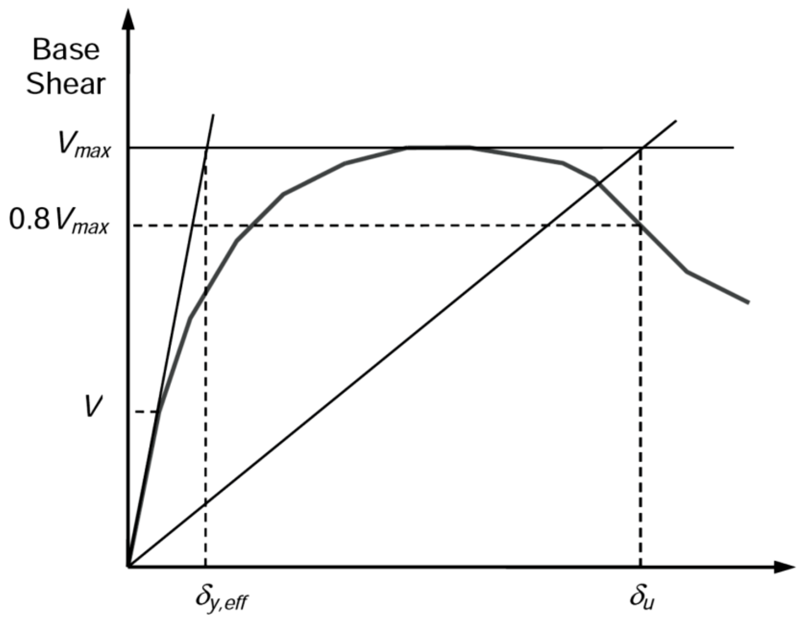

Figure 6-21: Idealized nonlinear static push over curve (FEMA, 2009)

Table 6-4: Overstrength factor for wall panels

Specimen	Base shear (kip)		Overstrength factor (Ω_o)
	V_y	V_u	
A-4	8.1	18.9	2.3
A-5	7.7	19.6	2.5
A-6	7.3	19.3	2.6
Average	7.7	19.3	2.5

Table 6-5: Ultimate ductility values for wall specimens

Specimen	Deflection (in)		Ultimate ductility (μ)
	δ_y	δ_u	
A-4	0.068	1.13	16.62
A-5	0.081	1.48	18.27
A-6	0.094	1.31	13.94
Average	0.08	1.31	16.28

As part of the nonlinear analysis of the walls, the strength degradation, damage propagation, and the modes of failure for all three specimens were recorded during the testing. The strength degradation for all three specimens followed a typical four-line stiffness degradation model represented by cracking, yield, ultimate and failure points. The dominant mode of failure observed for the three specimens was a flexural-controlled failure that occurred at the base of the wall. At failure, the specimens were riddled with many flexural cracks that were mostly concentrated inside the plastic hinging region. Although the exact locations of the failure are different for all three specimens, all failure occurred within the plastic hinge region close to the base of the walls.

The degradation process for the specimens started with the development of flexural cracks at the bottom of the wall which slowly propagated upwards toward the upper half of the walll. With the increase in the drift ratio past initial cracking, greater number of hairline cracks were formed. Significant number of cracks were observed on both wythes and at the edge walls. Once the specimen yielded, fewer number of cracks appeared and the existing cracks, especially in the plastic hinge region started getting wider. This continued till a dominant crack was formed and caused the specimen to fail. The failure was caused by the crushing of the concrete cover at the edges which was followed by the rupture of the reinforcement during the subsequent cycle. The damage progression observed at the edge of the walls can be observed in Figure 6-23 through 6-65. In these figures the strength degradation at 0.08%, 0.4%, 0.65%, 1%, 1.6% and 2% targeted drift ratios are labeled ‘a’ through ‘f’, respectively. The details and description of the modes of failure for each wall specimen are summarized in Table 6-4.

Table 6-4: Modes of failure for wall specimens

Specimen	Mode of failure	Location of failure	Description
A-4	Flexural dominated toe failure	6 inches above the base in push and 2 inches above in the pull cycle	Figure 6-24;6-25
A-5	Flexural dominated toe failure	2 inches above the base in push and 6 inches above it in the pull cycle	Figure 6-26;6-27
A-3	Flexural dominated toe failure	10 inches above the base in push and 6 inches above it in the pull cycle	Figure 6-28;6-29

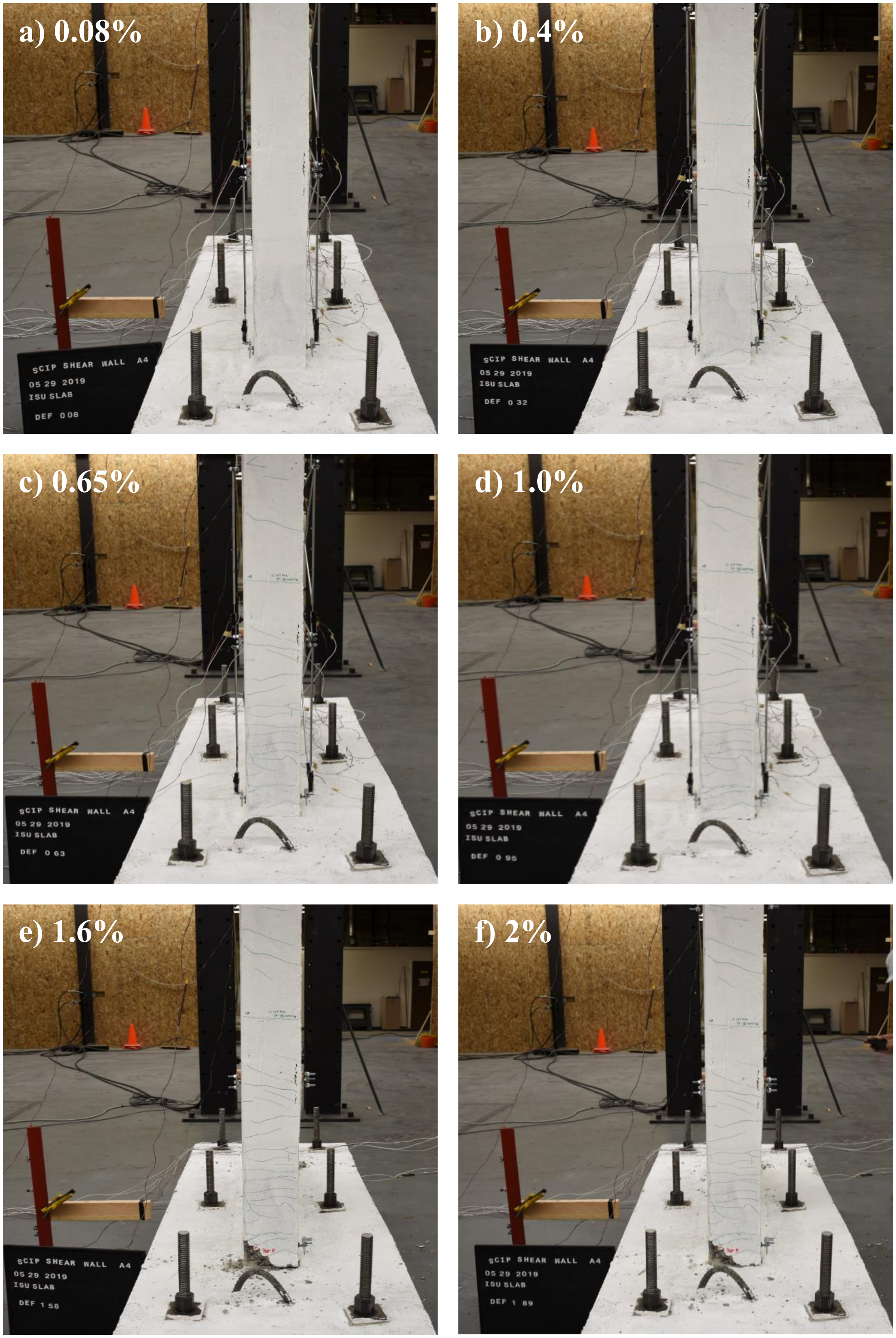

Figure 6-23: Damage progression ‘A-4’

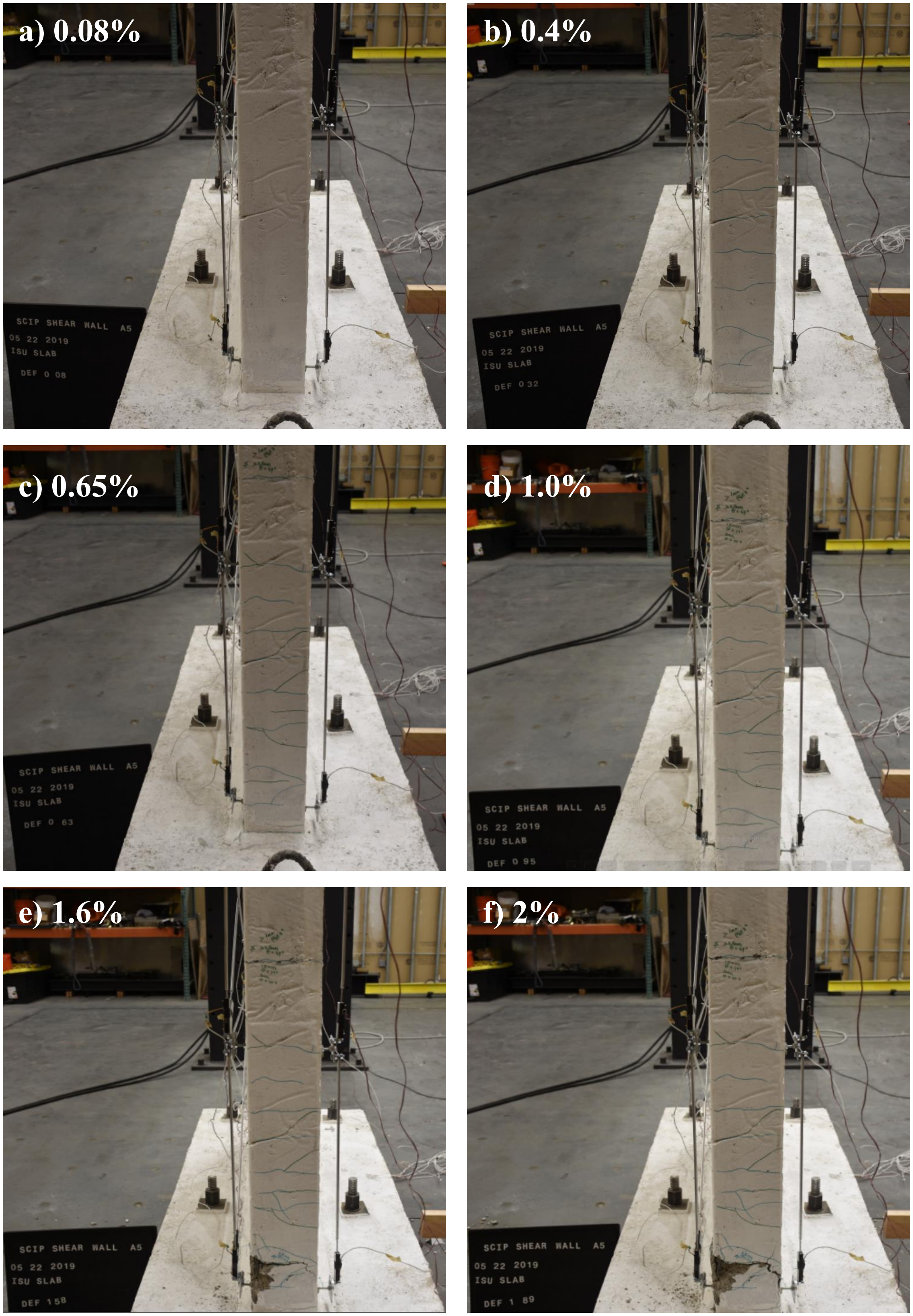

Figure 6-24: Damage progression ‘A-5’

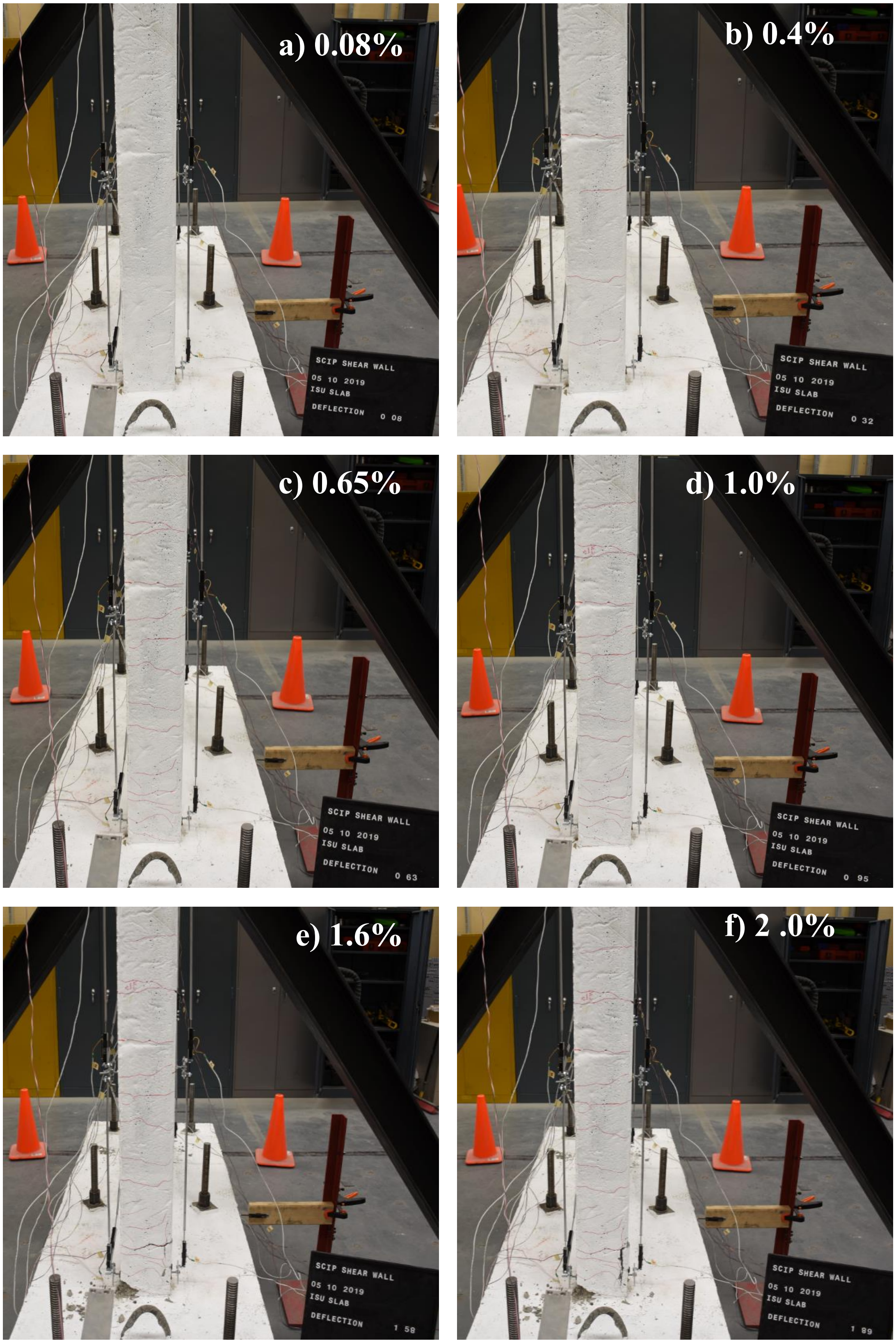

Figure 6-25: Damage progression ‘A-6’

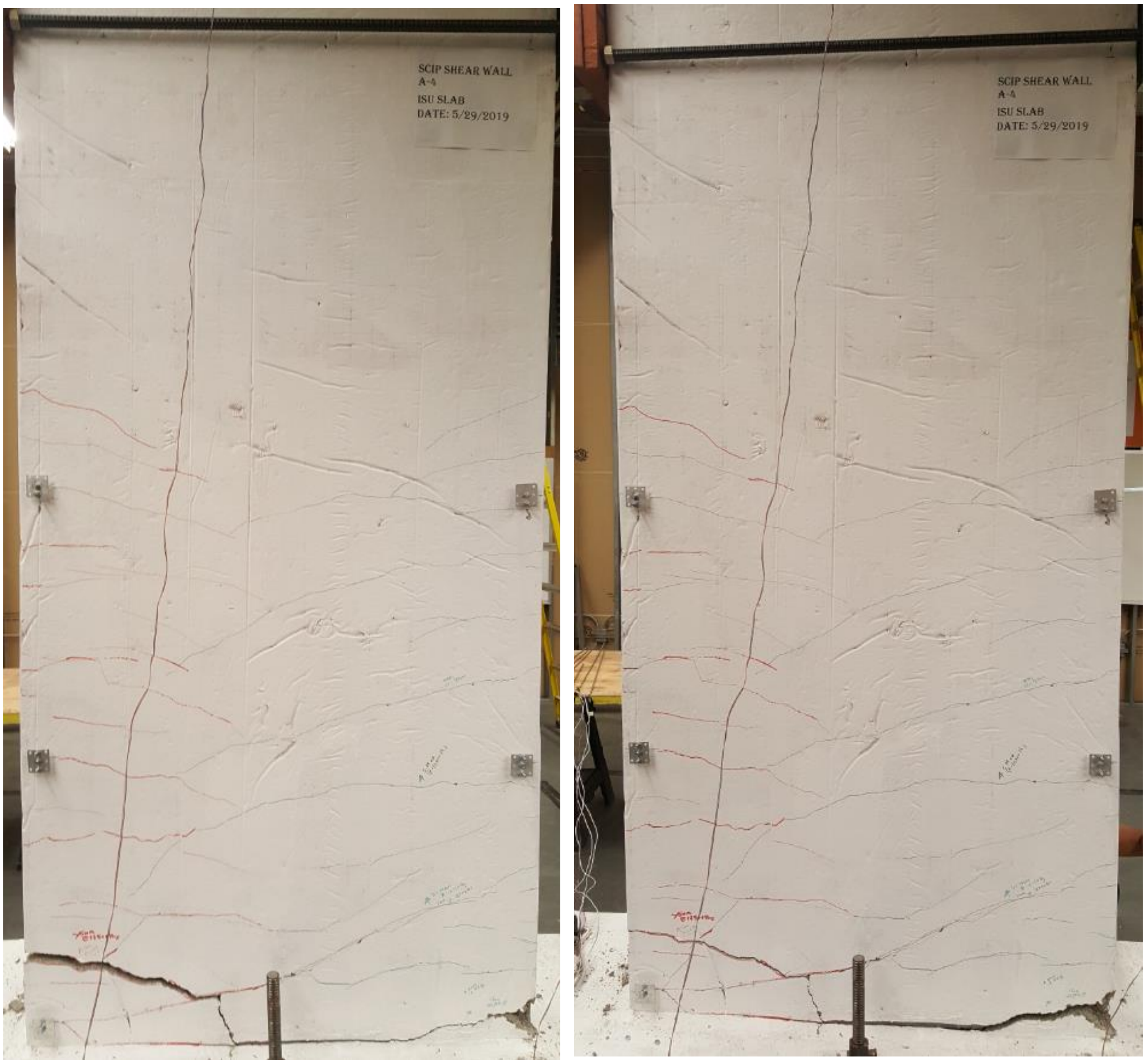

a) Failure push cycle b) Failure pull cycle

Figure 6-26: Failure mode for specimen ‘A-4’

a) West edge wall push cycle

b) East edge wall pull cycle

c) North wall push cycle

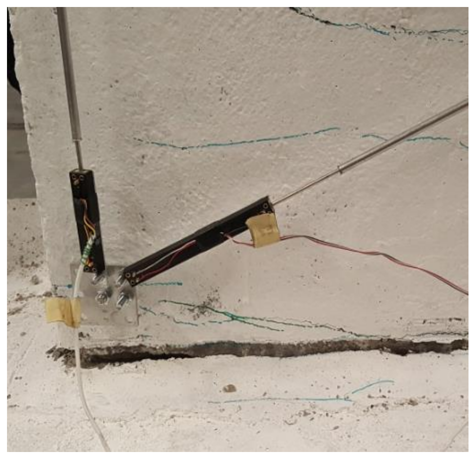

d) North wall pull cycle

e) South wall push cycle

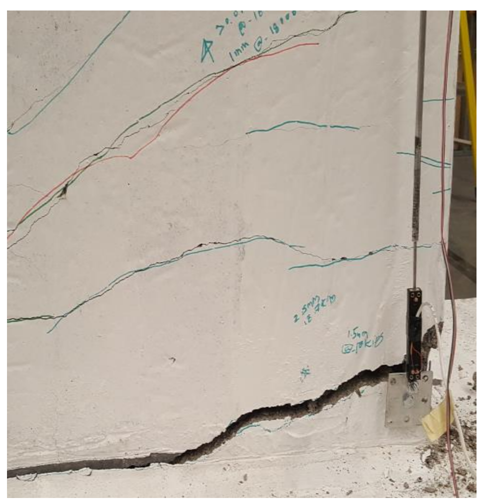

f) South wall pull cycle

Figure 6-27: Failure mode for specimen 'A-4'

a) Failure push cycle

b) Failure pull cycle

Figure 6-28: Failure mode for specimen ‘A-5’

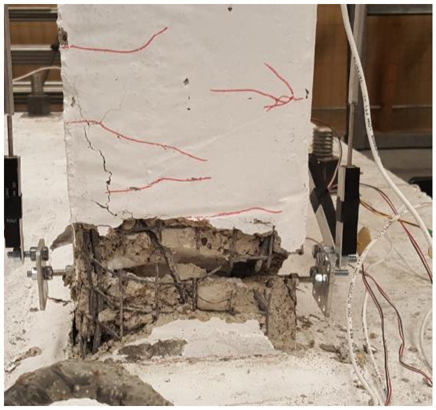

a) West edge wall push cycle

b) East edge wall pull cycle

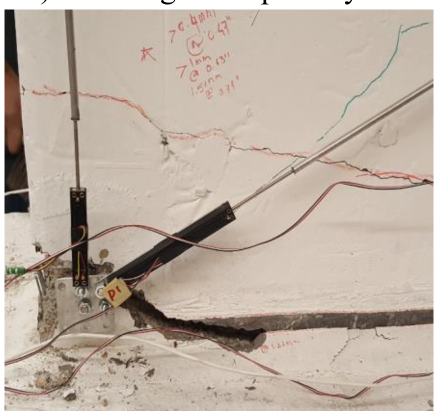

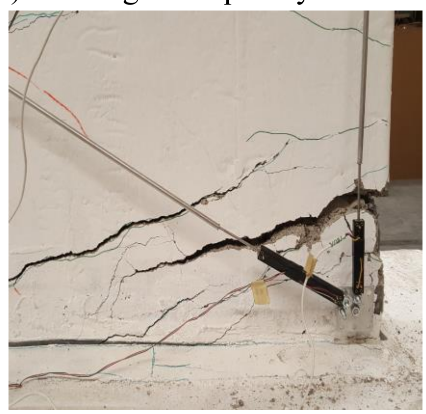

c) North wall push cycle

d) North wall pull cycle

e) South wall push cycle

f) South wall pull cycle

Figure 6-29: Failure mode for specimen ‘A-5’

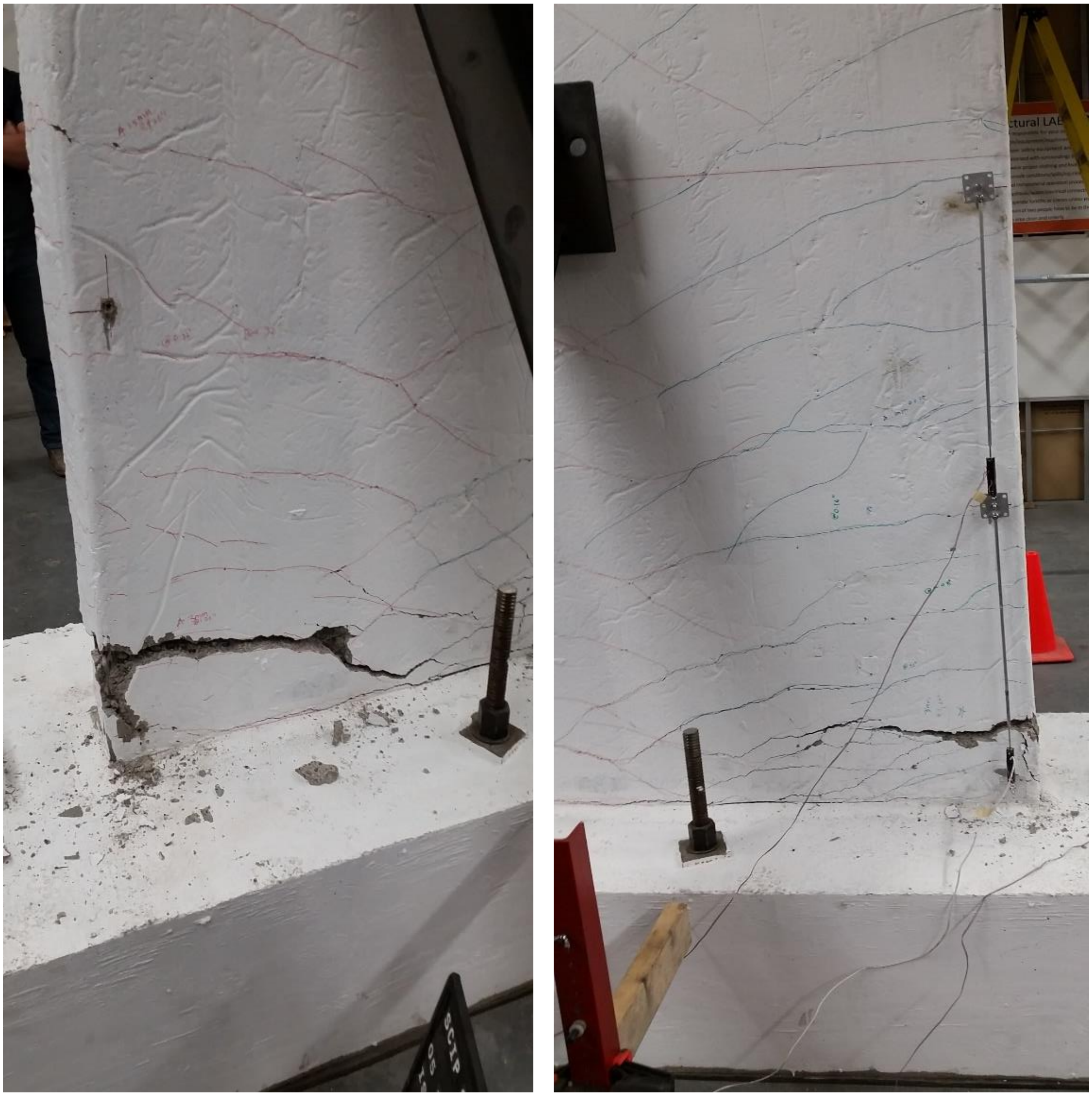

a) Failure push cycle b) Failure pull cycle

Figure 6-30: Failure mode for specimen ‘A-6’

a) West edge wall push cycle

b) East edge wall pull cycle

c) North wall push cycle

d) North wall pull cycle

e) South wall push cycle

f) South wall pull cycle

Figure 6-31: Failure mode for specimen ‘A-6’

6.6 Summary

1. Three MR wall specimens were successfully tested using ACI 374.2R-13 "Guide for Testing Reinforced Concrete Structural Elements under Slowly Applied Simulated Seismic Loads."
2. The load-deflection hysteresis and the moment-curvature for all three walls were fairly symmetrical.
3. The average yield drift ratio for specimen A-4 was 0.07% and the yield moment capacity was 66.8 kip-ft. Similarly, the ultimate moment capacity was 145 kip-ft and drift ratio at the ultimate capacity was 0.79%. The elastic in-plane stiffness of the specimen was 125.6 kip/in.
4. The overstrength factor (Ω_o) for A-4 was 2.3 and ultimate ductility (μ_T) was 16.6.
5. The average yield drift ratio for specimen A-5 was 0.084% and the yield moment capacity was 64.7 kip-ft. Similarly, ultimate moment capacity was 147.8 kip-ft and drift ratio at ultimate capacity was 0.97%. The elastic in-plane stiffness of the specimen was 100.4 kip/in.
6. The overstrength factor (Ω_o) for A-5 was 2.5 and the ultimate ductility (μ_T) was18.3.
7. The average yield drift ratio for specimen A-6 was 0.092% and the yield moment capacity was 58.4 kip-ft. Similarly, the ultimate moment capacity of the specimen was 150. kip-ft and drift ratio at ultimate capacity was 0.84%. The elastic in-plane stiffness of the specimen was 82.2 kip/in.
8. The overstrength factor (Ω_o) for A-6 was 2.6 and the total ductility (μ_T) was 13.9.
9. The strength degradation for all three specimens followed a typical four-line stiffness degradation model represented by cracking, yield, ultimate and failure.

10. Considerable amount of energy dissipation was achieved through the formation of flexural cracks before failure.
11. The average energy dissipated by the MR wall specimen was 16.3 K.J.
12. A stiffness degradation was observed during the testing, this was confirmed by the uniform increase in energy dissipation throughout the testing.
13. The failure for all three specimens was caused by the toe-crushing at the base of the wall was followed by horizontal shear failure.

CHAPTER 7. CONCLUSIONS

The purpose of this research was to introduce MetRock Structural Concrete Insulated Panels and to investigate their in-plane and out-of-plane structural properties. Two types of full-scale experimental testing were conducted. The tests conducted were: 1) out-of-plane flexural testing of MR panels used as floor/roof slabs. 2) in-plane cyclic testing of MR panels used as walls under seismic loading. The testing was successfully conducted at the structural lavatory at Idaho State University. The summaries from the testing are presented in this section along with conclusions, detailing considerations and recommendations for future research

7.1 MetRock SCIPs used as floor/roof slabs

1. Eleven MetRock SCIP slab specimens were constructed and tested under four-point flexural test. The tests were conducted in accordance with ASTM E72-05.
2. The short span (10 feet) slab specimens exhibited very ductile behavior when subjected to out-of-plane flexural loading. The failure mode was a flexural-controlled failure with significant energy dissipation in the form of many hairline flexural cracks prior to failing.
3. The average elastic stiffness for the short span slabs was 58.6 kip/in. The average applied cracking moment capacity was 8.1 kip-ft. The ultimate moment capacity was 16.3 kip-ft., which corresponded to an ultimate load carrying capacity of 324.6 psf.
4. Since none of the specimens failed in shear nor were there any shear cracks observed at the end supports, it can be assumed that the minimum shear capacity of the panels was 6.6 kips ($P_{max}/2$).
5. The short span MR panels satisfied the ACI 318-14 and ASCE 07 code requirements for a residential concrete floor and roof slabs. The average distributed load carrying capacity for the short span slabs was calculated to be 167 psf.

6. The short span specimens behaved as a partially composite section and achieved 66% flexural capacity of a fully composite section that was analyzed using the ACI flexural analysis.
7. The medium (14 feet) and the long span (18 feet) slab specimens exhibited fairly ductile behavior followed by a very sudden failure at the splice location. The under reinforcement of the splice in the panels was what caused the premature failure and prevented it from achieving its full capacity.
8. The average elastic stiffness for the medium span slabs was 14.8 kip/in. The average cracking moment was 4.5 kip-ft. The ultimate moment capacity was 9.6 kip-ft., which corresponded to an ultimate distributed load carrying capacity of 97.1 psf.
9. The average elastic stiffness for the long span slabs was 9.45 kip/in. The average cracking moment capacity of 3.2 kip-ft. The ultimate moment capacity was 8.5 kip-ft. which corresponded to an ultimate load carrying capacity of 52 psf.
10. The medium and the long span slabs did not meet the ACI code for residential concrete floor slabs. However, they did meet the required standards for residential roof construction. It is though that providing thicker panels (e.g. thicker concrete wythes) could make the medium and long span slabs suitable for residential floor slabs. This could be done using analytical models generated from the experimental results in this thesis.
11. Due to the premature failure of the medium and the long span specimens, two additional slabs with reinforced splice regions were tested.
12. Both modified long span specimens were successful in transferring the failure plane away from the splice region, which significantly increased the ultimate moment capacity of the

panels and avoided a brittle failure. The average ultimate moment capacity of the modified specimens was 12.4 kip-ft. This was which 46% more than the capacity for the unmodified long span specimen. The ultimate distributed load carrying capacity of the modified specimen was 88 psf.

7.2 MetRock SCIPs used as wall panels

1. Three MR wall specimens were constructed and tested under lateral loads in accordance with the ACI 374.2R-13 "Guide for Testing Reinforced Concrete Structural Elements under Slowly Applied Simulated Seismic Loads."
2. The large-scale tests were performed to quantify the in-plane flexural capacity and the failure pattern of the MR panels used as structural walls under seismic loading.
3. Significant energy dissipation and ductility were achieved by all three specimens prior to failing. The average energy dissipated during the tests was 16.3 K.J.
4. The strength degradation for all three specimens could be represented using a typical four-line stiffness degradation model represented by cracking, yield, ultimate, and failure.
5. The failure for all three specimens was caused by toe crushing at the base of the wall.
6. The load-deflection hysteresis and the moment-curvature for all three walls were relatively symmetric.
7. The average in-plane elastic stiffness for the wall specimens was 102.8 kip/in.
8. The average yield moment capacity for the walls was 63.3 kip-ft which was attained at a drift ratio of 0.082%.
9. The ultimate moment capacity for the specimens was 146.8 kip-ft. at a drift ratio of 0.9%.

10. The overstrength factor for the MR walls was 2.5.

7.3 Conclusion and Recommendations

In conclusion, a series of full-scale testing of MetRock SCIPs were conducted to define their structural performance and viability for residential construction. The experimental testing showed that MR SCIPs performed well as building slabs and wall. Since the MR panels are monolithically poured reinforced concrete structures that utilize an EPS core, they can be used to construct structurally sound buildings that are economical, sustainable, efficient and durable.

Test results showed that the short span panels could be used for constructing floor and roof slabs for residential structures. The load carrying capacity of the short span slabs exceeded both ACI 318-14 and ASCE 07 code requirements for a residential floor and roof slab. An integral finding of this research was that due to the complex arrangement of the diagonal shear connectors in the MR panels, the slabs were able to achieve significant shear transfer between the two load-bearing faces when subjected to out-of-plane flexural loading. The panels behaved as a partially composite section and achieved 66% capacity of a fully composite section. Hence designing MR SCIPs as a non-composite section as specified in ACI 374.2R would largely underestimate their load carrying capacity. The slab specimens exhibited a wide range of nonlinear behavior, and redistribution of stresses was successfully achieved through the formation of many hairline flexural cracks prior to failing.

Although the medium and long MR panels did not satisfy the code requirements for a residential floor, they can still be effectively used as residential roof slabs. Testing of the longer span slabs showed that they meet the deflection requirements stated in ACI 318 under a standard ASCE7 residential roof live load. However, that being said, test results showed that just relying on the mesh for the splice reinforcement was not sufficient and caused a premature failure.

Hence, to achieve the full capacity of the longer span slabs additional splice reinforcements are recommended. Standard grade 60 #3 bars can be used to reinforce the splice and significantly increase the slabs' ultimate load carrying capacity. The reinforcement detail used for specimen S-1 is recommended for the most effective result.

Another key detail in avoiding premature failure of the slabs was the edge confinement provided to the panels. For the test specimens the confinement was provided using a special "U-mesh" with a half inch of concrete cover. The confinement of the edges prevented the out-of-plane buckling of the diagonal trusses and significantly increased the load-carrying capacity of the panels. Although during real-world construction "U mesh" are not applied to the panels, the cores may achieve adequate lateral confinement by clamping adjacent panels together. This prevents the edge trusses from out-of-plane buckling and ensures that the panels achieve their full capacity.

Additionally, due to their high in-plane elastic stiffness, MR panels can be effectively used as shear walls for residential buildings located in coastal areas that are prone to high lateral wind loads. Additionally, the cyclic testing of MetRock walls showed that the panels were able achieve an adequate amount of energy dissipation prior to failure. The walls exhibited fairly ductile nonlinear behavior past the yield drift ratio of 0.08%. At the ultimate drift ratio of 0.9%, all three wall specimens failed by toe crushing followed by horizontal shear. The ultimate ductility (μ_T) exhibited by the MR panels was 16.3. Test results also showed that the MR walls had an over strength factor (Ω_o) of 2.5 which was equal to the value stated in the ACI 318 for a normally reinforced concrete wall. Since the MR walls displayed a relatively high overstrength factor.

The alternative precast approach used to fabricate the slabs and walls used in this research is different from traditional construction of MR SCIPs, this method could be an efficient construction technique. All of the precast specimens were relatively easy to produce, handle, and assemble. They did not require specialized labor; thereby providing a relatively economical and easy construction option. Furthermore, the precast approach could be a great alternative to applying shotcrete to the floor and roof slabs. Applying shotcrete to the slabs can be a complicated process due to the difficulty in application and the rebound of the shotcrete, especially for the bottom half of the slabs. Therefore, instead of using shotcrete, the bottom layer of the slabs can be poured in a precast bed prior to being installed and the top layer can be poured in-place.

7.4 Future work

By successfully executing a full-scale experimental program, this research has laid a solid foundation for many possible future studies on SCIPs in general. The elastic strength properties obtained from the test results can be used to for the structures incorporating MetRock SCIPs. It can also be used to verify the results obtained from numerous analytical and numerical predicting models. Experimental results in this thesis could be used to develop analytical finite element and simplified models for MR panels with various span lengths and thicknesses. Design charts can be developed for wider application of this technology. The models can then be used to produce proper performance-based design guidelines for the MetRock SCIP construction technology. With the aid of proper design, manual engineers will no longer hesitate to use MR panels in their designs and can produce efficient residential structures. Also, the narrow scope of this study of just one type of Structural Concrete Insulated Panel can be used as a blueprint to test various similar sandwiched panels.

REFERENCES

Alagusundaramoorthy, P., Joseph, J. D., & Prabakar, J. (2018). Flexural behavior of precast concrete sandwich panels under different loading conditions such as punching and bending. *Alexandria Engineering Journal, 57(1),* 309-320. doi:10.1016/j.aej.2016.11.016

American Concrete Institute 533R-11. (2012). Guide for precast concrete wall panels. Farmington Hills, MI: American Concrete Institute.

American Concrete Institute 374.2R-13. (2013). Guide for testing reinforced structural elements under slowly applied simulated seismic loads. Farmington Hills, MI: American Concrete Institute.

American Standard Testing and Material E72-06 (2005). Standard tests of panels for building construction. West Conshohocken, PA: American Standard Testing and Material

ASTM. (2005). "Standard Test Methods of Conducting Strength Test of Panels for Building Construction." *ASTM E72-05*, West Conshohocken, PA.

ASTM. (2007). "Standard Specification for Steel Wire, Plain, for Concrete Reinforcement." *ASTM A82/A82M-07*, West Conshohocken, PA.

ASTM. (2007). "Standard Specification for Steel Welded Wire Reinforcement, Plain, for Concrete ." *ASTM A185/A185M-07,* West Conshohocken, PA.

ASTM. (2016). "Standard Test method for Compressive Strength of Hydraulic Cement Mortars (Using 2-in. or [50-mm] Cube Specimens)." *ASTM C109/ C 109M – 16a*, West Conshohocken, PA.

ASTM. (2018). "Standard test Method for Flexural Strength of Concrete (Using Simple Beam with Third-Point Loading)." *ASTM C78 / C78M-18*, West Conshohocken, PA.

ASTM. (2014). “Standard Specification for Zinc-Coated (Galvanized) Carbon Steel Wire.” *ASTM A641 / A641M – 09a (2014),* West Conshohocken, PA.

ASTM. (2008). “Standard test Methods for Tension Testing of metallic Materials.” *ASTM E8/ E8M – 08,* West Conshohocken, PA.

ASTM. (2018). “Standard Test Method for Slump Flow of Self-Consolidating Concrete.” *ASTM C1611 / C1611M – 18,* West Conshohocken, PA.

ASTM. (2019). “Standard Test Method for Steady – State Heat Flux Measurements and Thermal Transmission Properties by Means of the Guarded- Hot – plate Apparatus.” *ASTM C177 – 19,* West Conshohocken, PA.

ASTM. (2018). “Standard Test Method for Compressive Strength of Cylindrical Concrete Specimens.” *ASTM C39 / C39M – 18,* West Conshohocken, PA.

ASTM. (2017). “Standard Test Method for Splitting Tensile Strength of Cylindrical Concrete Specimens.” *ASTM C496 / C496M – 17,* West Conshohocken, PA.

ASTM. (2016). “Standard Test Method for Compressive Strength of Hydraulic Cement Mortars (Using 2-in. or [50-mm] Cube Specimens).” *ASTM C109 / C109M -16a,* West Conshohocken, PA.

ASTM. (2018). “Standard Test Method for Flexural Strength of Advanced Ceramics at Ambient Temperature.” *ASTM C1161 – 18,* West Conshohocken, PA.

ASTM. (2017). “Standard Practice for Making Test Cylinders and prisms for Determining Strength and Destiny of Preplaced-Aggregate Concrete in the Laboratory.” *ASTM C943-17,* West Conshohocken, PA.

ASTM. (2010). “Standard Practice for Making Test Cylinders and Prisms for Determining Strength and Density of Preplaced-Aggregate Concrete in the Laboratory.” *ASTM C943 - 10*, West Conshohocken, PA.

Brzev, S., & Teresa G. (2010). *Precast concrete construction.* British Columbia Institute of Technology, Canada

Che, J., P Deng, M., Liang, X. & Yang, (2013). Seismic Behavior of High-Strength Concrete Structural Walls with Edge Columns. *ACI Structural Journal, 110(06)*, 953-964. doi:10.14359/51686151

Culp, D. G., Einea, A., Salmon, D. C. & Tadros, K. M. (1997). Full-Scale Testing of Precast Concrete Sandwich Panels. *ACI Structural Journal, 94(4)*.doi: 10.14359/486.

Daczko, J. A. (2012). *Self-consolidating concrete: Applying what we know*. London: Spon Press

El Demerdash, I. M. (2013). *Structural evaluation of sustainable orthotropic three-dimensional sandwich panel system*. Retrieved from ProQuest Dissertations & Theses Global. doi:1491849596

Farrell, J., Fouad, F. H., Heath, M., Shalaby, A., & Vichare, A. (2009). The behavior of the MR Sandwich Panel in Flexural. *ACI Special Publication, 260*, 73-88. doi:10.14359/56626

FEMA, 2009, Quantification of Building Seismic Performance Factors, FEMA P695, prepared by the Applied Technology Council for the Federal Emergency Management Agency, Washington, D.C

Hicks, R. (2008). UCI Draft Structural QTP for IBC 2006 Compliance. *Thermal Guardian*. Retrieved from http://www.spa-mart.com/hot-tub-spa-covers/insulating-spa-cover/lf_spaCover_foamCores.cfm

Kabir, M. Z. (2005). Structural Performance of 3-D Sandwich Panels under Shear and Flexural Loading. *Scientia Iranica 12 (4)*, 402-408

Key to Metals AG. (2019). Sandwich steel panels. *Total Material.* Retrieved from https://www.totalmateria.com/page.aspx?ID=CheckArticle&LN

Logan, D. L. (2012). *A first course in the finite element method* (5th ed.). Stamford, CT: Cengage Learning

Mashal, M. (2011). *Quantification of Seismic Performance Factors for Building Incorporating Three-Dimensional Construction System*. (Master's thesis, State University of New York, Buffalo, NY. Retrieved from Research gate (26806036)

Mashal, M. and Filiatrault, A. (2012). Quantification of Seismic Performance Factors for Buildings Incorporating Three-Dimensional Construction System. Proceedings of the 15th World Conference on Earthquake Engineering, Lisbon, Portugal.

MetRockSCIP. (n.d). Retrieved 2019, from https://www.metrockscip.com/

McCormac, J. C., & Brown, R. H. (2016). *Design of reinforced concrete* (10th ed.).Hoboken, NJ: John Wiley & Sons, Inc.

Michael, M (2000). Building with Structural Insulated Panels (SIPs): *Strength and Energy Efficiency through Structural Panel Construction*. Newtown, CT: Taunton Press, Inc.

Modular Homes (2019). What are SIPS. *Green Galaxy Homes.* Retrieved from http://www.greengalaxyhomes.com/structural-insulated-panels

Naji, B.,& Toubia, E. A. (2015). *Flexural Analysis and Composite Behavior of Precast Concrete Sandwich Panel*. Retrieved from fib symposium

Priestley M J N,, Calvin G M., & Kowalsky M J. (2007) *Displacement-Based Seismic Design of Structures.* IUUSS Press, Pavia, Italy

Tapia, W.T (2010). *Regionalism and the design of low-rise building envelope systems* (Master's thesis, Massachusetts Institute of Technology, Cambridge, MA. Retrieved from CORE (4423497)

Tridipanel Tech Specs. (n.d). Retrieved 2019, from https://tridipanel.com/tec-specs/

Vespa, J., Armstrong, D. M., & Medina, L. (2018). Demographic Turning Points for the United States: Population Projections for 2020 to 2060. *United States Census Bureau P25-1144*

Xianyoung,N , Shaungyin, C, Shaungyin,Y & Liang Shuai (2018) *Stiffness degradation of shear walls under cyclic loading: Experimental study and modeling* Bulletin of Earthquake Engineering

Zenkert, D. (1993). *An introduction to Sandwich Construction*. Department of Lightweight Structures, Royal Institute of Technology, Stockholm, Sweden

APPENDICES

Appendix A. Material Datasheet

ASH GROVE

ASH GROVE CEMENT COMPANY
WESTERN REGION
33060 SHIRTTAIL CREEK ROAD
P.O. BOX 287
DURKEE, OREGON 97905
(541) 877-2411

Durkee Plant
Mill Test Report

Mill Analysis No. 17-5
Bin No. 2,3,4,D

Cement Type II-V L.A.
Production Period February 1 thru February 28, 2017

Date 03-07-2017

STANDARD REQUIREMENTS
ASTM C150

CHEMICAL

Item	Spec. Limit	Test Result
SiO_2 (%)	A	22.3
Al_2O_3 (%)	6.0 max.	3.4
Fe_2O_3 (%)	6.0 max.	3.1
CaO (%)	A	64.3
MgO (%)	6.0 max.	2.3
SO_3 (%)	D	2.5
Loss On Ignition (%)	3.0 max.	0.88
Na_2O (%)	A	0.22
K_2O (%)	A	0.47
TiO_2 (%)	A	0.25
P_2O_5 (%)	A	0.12
Mn_2O_3 (%)	A	0.06
Insoluble Residue (%)	0.75 max.	0.34
CO_2 (%)	A	0.36
Limestone %	5.0 max.	0.89
$CaCO_3$ in Limestone	70 min.	91.85
$C_3S + 4.75C_3A$	100 max.	76
Potential Compounds (%)	C	
C_3S	A	57
C_2S	A	21
C_3A	5 max.	4
C_4AF	A	9
$C_4AF+2(C_3A)$	25 max.	17

PHYSICAL

Item			Spec. Limit	Test Result
Air Content of Mortar (volume %)				
C185			12 max.	6.2
Fineness (m^2/kg)				
C204	(Air permeability)		260 min.	375
Autoclave Expansion (%)			0.80 max.	0.05
C151				
Compressive Strength Psi (Mpa)			Min.:	
C109		1 Day	A	2120 (14.6)
		3 Days	1450 (10.0)	3920 (27.0)
		7 Days	2470 (17.0)	5160 (35.6)
		28 Days	3050 (21.0)	F
Time of Setting (minutes)				
C191	(Vicat)			
	Initial	Not less than	45	126
		Not more than	375	

OPTIONAL REQUIREMENTS
ASTM C150, (other)

CHEMICAL

Item	Spec. Limit	Test Result
Equivalent Alkalies (%)	0.60 max.	0.52
Chloride (%)	B	0.002

PHYSICAL

Item		Spec. Limit	Test Result
Time of Set - Final (minutes)	C191	B	205
False Set (%) C451		50 min.	92
Heat of Hydration (cal /g)	C186		
	7 days	B	81
Sulfate Resistance (%)	C452	0.040	0.025
Water Expasion (%)	C1038	0.020	0.016
% retain on 45µm sieve		B	1.22

A = Not applicable
B = Test results represents most recent value and is provided for informational purposes only.
C = Adjusted per A 1.6.
D = C1038 expansion in water does not exceed 0.02% at 14 days.
F = Test results for this production period not yet available.

We certify that the above described cement, at the time of shipment, meets the chemical and physical requirement of the ASTM C150-16 or AASHTO M-85 -12 Type I-II-V specification also will meet CSA A3000-13 Type GU, MS and HS.

Signature:

Title: Chief Chemist

Figure A-0-1: Portland cement datasheet

HEADWATERS RESOURCES

Materials Testing & Research Facility
2650 Old State Hwy 113
Taylorsville, GA 30178
770-684-0102

ASTM C618 / AASHTO M295 Testing of Navajo Generating Station Fly Ash

Sample Date:	2/10 - 2/13/17	**Report Date:**	3/24/2017
Sample Type:	3200-ton	**MTRF ID:**	360NV
Sample ID:	NV-014-17		

Chemical Analysis	**Results**	**ASTM Limit Class F/C**	**AASHTO Limit Class F/C**
Silicon Dioxide (SiO2)	58.96 %		
Aluminum Oxide (Al2O3)	25.10 %		
Iron Oxide (Fe2O3)	4.31 %		
Sum (SiO2+Al2O3+Fe2O3)	88.37 %	70.0/50.0 min	70.0/50.0 min
Sulfur Trioxide (SO3)	0.36 %	5.0 max	5.0 max
Calcium Oxide (CaO)	4.74 %		
Magnesium Oxide (MgO)	1.12 %		
Sodium Oxide (Na2O)	2.12 %		
Potassium Oxide (K2O)	1.21 %		
Moisture	0.06 %	3.0 max	3.0 max
Loss on Ignition	0.57 %	6.0 max	5.0 max
Available Alkalies, as Na2Oe	1.27 %	Not Required	1.5 max* *when required by purchaser
Physical Analysis			
Fineness, % retained on 45-µm sieve	21.26 %	34 max	34 max
Strength Activity Index - 7 or 28 day requirement			
7 day, % of control	80 %	75 min	75 min
28 day, % of control	83 %	75 min	75 min
Water Requirement, % control	96 %	105 max	105 max
Autoclave Soundness	0.03 %	0.8 max	0.8 max
Density	2.26		

Headwaters Resources certifies that pursuant to current ASTM C618 protocol for testing, the test data listed herein was generated by applicable ASTM methods and meets the requirements of ASTM C618.

Doug Rhodes, CET
Facility Manager

AASHTO R18

Figure A-0-2: Navajo fly-ash datasheet

BASF
We create chemistry

3	03 30 00	Cast-in-Place Concrete
	03 40 00	Precast Concrete
	03 70 00	Mass Concrete

MasterGlenium® 1466

High-Range Water-Reducing Admixture

Formerly PS1466*

Description

MasterGlenium 1466 ready-to-use high-range water-reducing admixture is a new generation, patent pending admixture based on polycarboxylate chemistry. MasterGlenium 1466 admixture is very effective in producing concretes with different levels of workability.

MasterGlenium 1466 admixture is particularly effective in improving concrete mixtures with reduced portland cement contents without compromising 28-day strength requirements. MasterGlenium 1466 admixture meets ASTM C 494/C 494M requirements for Type A, water-reducing, and Type F, high-range water-reducing, admixtures.

Applications

Recommended for use in:

- Concrete with varying water reduction requirements (5-40%)
- Concrete where high flowability, increased stability and durability are needed
- Producing self-consolidating concrete (SCC)
- Strength-on-demand concrete, such as 4x4™ Concrete
- Pervious concrete

Features

- Maximum dosage effectiveness for a given water reduction
- Controlled rheology
- Robust air-entraining admixture compatibility
- Improved strength development

Benefits

- Can be used in a wide variety of concrete mixtures as a Type A or Type F admixture
- Improved finishability and surface appearance
- Mixture development flexibility for cement reductions and/or increased use of supplementary cementitious materials

Performance Characteristics

Compressive Strength: Concrete produced with MasterGlenium 1466 admixture achieves significantly higher 28-day compressive strength compared to plain concrete and concrete mixtures containing naphthalene, melamine, and early generation polycarboxylate high-range water-reducing admixtures.

Mixture Data: Type I portland cement; Ambient Temperature, 70 °F (21 °C)

Mix 1: 620 lb/yd³ (367 kg/m³); w/c = 0.43; Conventional PC HRWR

Mix 2: 620 lb/yd³ (367 kg/m³); w/c = 0.43; MasterGlenium 1466

Mix 3: 600 lb/yd³ (356 kg/m³); w/c = 0.44; MasterGlenium 1466

Mix 4: 580 lb/yd³ (344 kg/m³); w/c = 0.46; MasterGlenium 1466

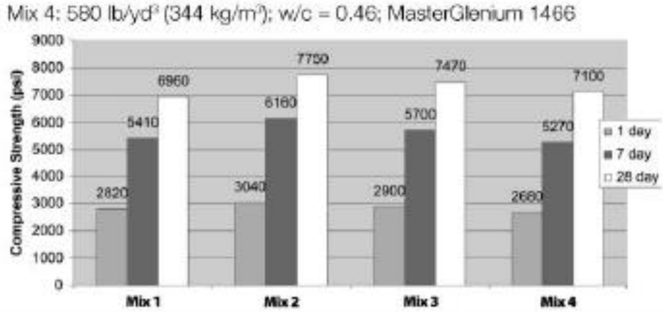

MASTER® BUILDERS SOLUTIONS

Figure A-0-3a MasterGlenium 1466 datasheet

Guidelines for Use

Dosage: MasterGlenium 1466 admixture has a recommended dosage range of 2-10 fl oz/cwt (130-650 mL/100 kg) of cementitious materials. For most applications, dosages in the range of 2-6 fl oz/cwt (130-390 mL/100 kg) will provide excellent performance. Because of variations in concrete materials, job site conditions and/or applications, dosages outside of the recommended range may be required. In such cases, contact your local sales representative.

Mixing: MasterGlenium 1466 admixture can be added with the initial batch water or as a delayed addition. However, optimum water reduction is generally obtained with a delayed addition.

Product Notes

Corrosivity – Non-Chloride, Non-Corrosive: MasterGlenium 1466 admixture will neither initiate nor promote corrosion of reinforcing steel embedded in concrete, prestressing steel or of galvanized steel floor and roof systems. Neither calcium chloride nor other chloride-based ingredients are used in the manufacture of MasterGlenium 1466 admixture.

Compatibility: MasterGlenium 1466 admixture is compatible with most admixtures used in the production of quality concrete, including normal, mid-range and high-range water-reducing admixtures, air-entrainers, accelerators, retarders, extended set control admixtures, corrosion inhibitors, and shrinkage reducers.

Do not use MasterGlenium 1466 admixture with admixtures containing naphthalene sulfonate. Erratic behaviors in slump, workability retention and pumpability may be experienced.

Storage and Handling

Storage Temperature: MasterGlenium 1466 admixture must be stored at temperatures above 40 °F (5 °C). If MasterGlenium 1466 admixture freezes, thaw and reconstitute by mechanical agitation. **Do not use pressurized air for agitation.**

Shelf Life: MasterGlenium 1466 admixture has a minimum shelf life of 6 months. Depending on storage conditions, shelf life may be greater than standard. Please contact your local sales representative regarding suitability for use and dosage recommendations if the shelf life of MasterGlenium 1466 admixture has been exceeded.

Packaging

MasterGlenium 1466 admixture is supplied in 55 gal (208 L) drums, 275 gal (1040 L) totes and by bulk delivery.

Related Documents

Safety Data Sheets: MasterGlenium 1466 admixture

Additional Information

For additional information on MasterGlenium 1466 admixture or its use in developing concrete mixtures with special performance characteristics, contact your local sales representative.

The Admixture Systems business of BASF's Construction Chemicals division is the leading provider of solutions that improve placement, pumping, finishing, appearance and performance characteristics of specialty concrete used in the ready-mixed, precast, manufactured concrete products, underground construction and paving markets. For over 100 years we have offered reliable products and innovative technologies, and through the Master Builders Solutions brand, we are connected globally with experts from many fields to provide sustainable solutions for the construction industry.

Figure A-3b MasterGlenium 1466 datasheet

Limited Warranty Notice

BASF warrants this product to be free from manufacturing defects and to meet the technical properties on the current Technical Data Guide, if used as directed within shelf life. Satisfactory results depend not only on quality products but also upon many factors beyond our control. BASF MAKES NO OTHER WARRANTY OR GUARANTEE, EXPRESS OR IMPLIED, INCLUDING WARRANTIES OF MERCHANTABILITY OR FITNESS FOR A PARTICULAR PURPOSE WITH RESPECT TO ITS PRODUCTS. The sole and exclusive remedy of Purchaser for any claim concerning this product, including but not limited to, claims alleging breach of warranty, negligence, strict liability or otherwise, is shipment to purchaser of product equal to the amount of product that fails to meet this warranty or refund of the original purchase price of product that fails to meet this warranty, at the sole option of BASF. Any claims concerning this product must be received in writing within one (1) year from the date of shipment and any claims not presented within that period are waived by Purchaser. BASF WILL NOT BE RESPONSIBLE FOR ANY SPECIAL, INCIDENTAL, CONSEQUENTIAL (INCLUDING LOST PROFITS) OR PUNITIVE DAMAGES OF ANY KIND.

Purchaser must determine the suitability of the products for the intended use and assumes all risks and liabilities in connection therewith. This information and all further technical advice are based on BASF's present knowledge and experience. However, BASF assumes no liability for providing such information and advice including the extent to which such information and advice may relate to existing third party intellectual property rights, especially patent rights, nor shall any legal relationship be created by or arise from the provision of such information and advice. BASF reserves the right to make any changes according to technological progress or further developments. The Purchaser of the Product(s) must test the product(s) for suitability for the intended application and purpose before proceeding with a full application of the product(s). Performance of the product described herein should be verified by testing and carried out by qualified experts.

*PS 1466 became MasterGlenium 1466 under the Master Builders Solutions brand, effective May 11, 2016

BASF Corporation
Admixture Systems
www.master-builders-solutions.basf.us

United States
23700 Chagrin Boulevard
Cleveland, Ohio 44122-5544
Tel: 800 628-9990 ■ Fax: 216 839-8821

Canada
1800 Clark Boulevard
Brampton, Ontario L6T 4M7
Tel: 800 387-5862 ■ Fax: 905 792-0651

Figure A-3c MasterGlenium 1466 datasheet

DAYTON SUPERIOR

1107 Advantage Grout

Cement Based Grout

TECHNICAL DATA SHEET

DESCRIPTION

The 1107 Advantage Grout is a non-shrink, non-metallic, non-corrosive, cementitious grout that is designed to provide a controlled, positive expansion to ensure an excellent bearing area. The 1107 Advantage Grout can be mixed from a fluid to a dry pack consistency.

USE

Exterior grouting of structural column base plates, pump and machinery bases, anchoring bolts, dowels, bearing pads and keyway joints. It finds applications in paper mills, oil refineries, food plants, chemical plants, sewage and water treatment plants etc.

FEATURES

- Controlled, net positive expansion
- Non shrink
- Non metallic/non corrosive
- Pourable, pumpable or dry pack consistency
- Interior/exterior applications

PROPERTIES

Corps of Engineers Specification for non-shrink grout: CRD-C 621 Grades A, B, C

ASTM C1107 Grades A, B, C

ASTM C827 - 1107 Advantage Grout yielded a controlled positive expansion

Expansion - ASTM C1090:
1 day: 0.10%
3 days: 0.11%
14 days: 0.11%
28 days: 0.11%

Time of Set per ASTM C807 (Flowable)
Initial Time Set 4 hours, 30 minutes
Final Time Set 6 hours, 05 minutes

Freeze-Thaw Resistance per ASTM C666
Durability Factor at 300 Cycles (Flowable):
Greater than 96%

Test Results

	@ 1 Day		@ 3 Days		@ 7 Days		@ 28 Days	
Fluidity	PSI	MPa	PSI	MPa	PSI	MPa	PSI	MPa
Dry-Pack	5000	34.5	7000	48.2	9000	62.0	10000	68.9
Flowable	2500	17.2	5000	34.5	6000	41.4	8000	55.1
Fluid	2000	13.8	4000	27.6	5000	34.5	7500	51.7

Note:
The data shown is typical for controlled laboratory conditions. Reasonable variation from these results can be expected due to interlaboratory precision and bias. When testing the field mixed material, other factors such as variations in mixing, water content, temperature and curing conditions should be considered.

Estimating Guide

Yield (Flowable Consistency):
0.43 cu. ft./50 lbs. (0.0122 cu. m/22.7 kg) bag
0.59 cu. ft./50 lbs. (0.017 cu. m/22.7 kg) bag extended with 25 lbs. (11.34 kg) of washed 3/8 in. (1cm) pea gravel

Packaging

Product Code	Package	Size	
		lbs	kg
67435	Bag	50	22.7
67437	Supersack	3,000	1,360.8

STORAGE

Store in a cool, dry area free from direct sunlight. Shelf life of unopened bags, when stored in a dry facility, is 12 months. Excessive temperature differential and /or high humidity can shorten the shelf life expectancy.

Surface Preparation:

Thoroughly clean all contact surfaces. Existing concrete should be strong and sound. Surface should be roughened to insure bond. Metal base plates should be clean and free of oil and other contaminants. Maintain contact areas between 45°F (7°C) and 90°F (32°C) before grouting and during curing period.

Thoroughly wet concrete contact area 24 hours prior to grouting, keep wet and remove all surface water just prior to placement. If 24 hours is not possible, then saturate with water for at least 4 hours. Seal forms to prevent water or grout loss. On the placement side, provide an angle in the form high enough to assist in grouting and to maintain head pressure on the grout during the entire grouting process. Forms should be at least 1 in. (2.5 cm) higher than the bottom of the base plate.

Water Requirements:

Desired Mix Water / 50 lbs. (22.67 kg) Bag
Dry Pack: 5 pints (2.4 L)
Flowable: 8 pints (3.8 L)
Fluid: 9 pints (4.2 L)

Visit www.daytonsuperior.com for the most up to date technical information

Page 1 of 3

File Date: 3/15/2018

Figure A-0-4a Dayton superior data sheet

DAYTON SUPERIOR

1107 Advantage Grout

Cement Based Grout

TECHNICAL DATA SHEET

Mixing:
A mechanical mixer with rotating blades like a mortar mixer is best. Small quantities can be mixed with a drill and paddle. When mixing less than a full bag, always first agitate the bag thoroughly so that a representative sample is obtained.

Place approximately 3/4 of the anticipated mix water into the mixer and add the grout mix, adding the minimum additional water necessary to achieve desired consistency.
Mix for a total of five minutes ensuring uniform consistency. For placements greater in depth than 3 in. (7.6 cm), up to 25 lbs. (11.34 kg) of washed 3/8 in. (1 cm) pea gravel must be added to each 50 lbs. (22.7 kg) bag of grout. The approximate working time (pot life) is 30 minutes but will vary somewhat with ambient conditions.

For hot weather conditions, greater than 85°F (29°C), mix with cold water approximately 40°F (4°C).
For cold weather conditions, less than 50°F (10°C), mix with warm water, approximately 90°F (29°C).
For additional hot and cold weather applications, contact Dayton Superior.

Placement:
Grout should be placed preferably from one side using a grout box to avoid entrapping air.
Grout should not be over-worked or over-watered causing segregation or bleeding.
Vent holes should be provided where necessary.
When possible, grout bolt holes first. Placement and consolidation should be continuous for any one section of the grout. When nearby equipment causes vibration of the grout, such equipment should be shut down for a period of 24 hours.
Forms may be removed when grout is completely self-supporting.
For best results, grout should extend downward at a 45 degree angle from the lower edge of the steel base plates or similar structures.

CURING

Exposed grout surfaces must be cured. Dayton Superior recommends using a Dayton Superior curing compound, cure & seal or a wet cure for 3 days. Maintain the temperature of the grout and contact area at 45°F (7°C) to 90°F (32°C) for a minimum of 24 hours.

CLEAN UP

Use clean water. Hardened material will require mechanical removal methods.

LIMITATIONS

FOR PROFESSIONAL USE ONLY

Do not re-temper after initial mixing
Do not add other cements or additives
Setting time for the 1107 Advantage Grout will slow during cooler weather, less than 50°F (10°C) and speed up during hot weather, greater than 80°F (27°C)
Prepackaged material segregates while in the bag, thus when mixing less than a full bag it is recommended to first agitate the bag to assure it is blended prior to sampling.

PRECAUTIONS

READ SDS PRIOR TO USING PRODUCT

- Product contains Crystalline Silica and Portland Cement Avoid breathing dust Silica may cause serious lung problems
- Use with adequate ventilation
  n Wear protective clothing, gloves and eye protection
  (goggles, safety glasses and/or face shield)
- Keep out of the reach of children
- Do not take internally
- In case of ingestion, seek medical help immediately
- May cause skin irritation upon contact, especially prolonged or repeated. If skin contact occurs, wash immediately with soap and water and seek medical help as needed.
- If eye contact occurs, flush immediately with clean water and seek medical help as needed
- Dispose of waste material in accordance with federal,
  state and local requirements

MANUFACTURER

Dayton Superior Corporation
1125 Byers Road
Miamisburg, OH 45342
Customer Service: 888-977-9600
Technical Services: 877-266-7732
Website: www.daytonsuperior.com

Figure A-4b Dayton superior data sheet

DAYTON SUPERIOR

1107 Advantage Grout

Cement Based Grout

TECHNICAL DATA SHEET

WARRANTY

Dayton Superior Corporation ("Dayton") warrants for 12 months from the date of manufacture or for the duration of the published product shelf life, whichever is less, that at the time of shipment by Dayton, the product is free of manufacturing defects and conforms to Dayton's product properties in force on the date of acceptance by Dayton of the order. Dayton shall only be liable under this warranty if the product has been applied, used, and stored in accordance with Dayton's instructions, especially surface preparation and installation, in force on the date of acceptance by Dayton of the order. The purchaser must examine the product when received and promptly notify Dayton in writing of any non-conformity before the product is used and no later than 30 days after such non-conformity is first discovered. If Dayton, in its sole discretion, determines that the product breached the above warranty, it will, in its sole discretion, replace the non-conforming product, refund the purchase price or issue a credit in the amount of the purchase price. This is the sole and exclusive remedy for breach of this warranty. Only a Dayton officer is authorized to modify this warranty. The information in this data sheet supersedes all other sales information received by the customer during the sales process. THE FOREGOING WARRANTY SHALL BE EXCLUSIVE AND IN LIEU OF ANY OTHER WARRANTIES, EXPRESS OR IMPLIED, INCLUDING WARRANTIES OF MERCHANTABILITY AND FITNESS FOR A PARTICULAR PURPOSE, AND ALL OTHER WARRANTIES OTHERWISE ARISING BY OPERATION OF LAW, COURSE OF DEALING, CUSTOM, TRADE OR OTHERWISE.

Dayton shall not be liable in contract or in tort (including, without limitation, negligence, strict liability or otherwise) for loss of sales, revenues or profits; cost of capital or funds; business interruption or cost of downtime, loss of use, damage to or loss of use of other property (real or personal); failure to realize expected savings; frustration of economic or business expectations; claims by third parties (other than for bodily injury), or economic losses of any kind; or for any special, incidental, indirect, consequential, punitive or exemplary damages arising in any way out of the performance of, or failure to perform, its obligations under any contract for sale of product, even if Dayton could foresee or has been advised of the possibility of such damages. The Parties expressly agree that these limitations on damages are allocations of risk constituting, in part, the consideration for this contract, and also that such limitations shall survive the determination of any court of competent jurisdiction that any remedy provided in these terms or available at law fails of its essential purpose.

Visit www.daytonsuperior.com for the most up to date technical information

Page 3 of 3

File Date: 3/15/2018

Figure A-4c Dayton superior data sheet

cellofoam®

EPS INSULATION
TECHNICAL DATA

TYPICAL PHYSICAL PROPERTIES OF EPS INSULATION
Specification Reference: ASTM-C578

Cellofoam EPS Insulation as manufactured by Cellofoam North America Inc is a modified expanded polystyrene. It is rigid, foamed plastic with resilient closed cells molded in a range of densities and sizes to meet your application specifications and requirements.

Cellofoam EPS provides all the characteristics required for long-term performance: permanent R value, inherent water resistance, excellent physical strength,and dimensional stability.

Cellofoam EPS provides a high R value at a comparatively low cost, making it the insulation choice for: Roof, Perimeter, Cold Storage, Exterior and Cavity Wall Insulation, Polyshield Fanfold, Leveling Board and Non-Structural Sheathing.

Property		Units	ASTM Test	Type I	Type VIII	Type II	Type IX
Density (Maximum)		pcf		1.0	1.25	1.5	2.0
Density (Minimum)		pcf	C303 or D1622	0.90	1.15	1.35	1.80
Thermal Conductivity K Factor	at 25F at 40F at 75F	BTU/(hr.) (sq. ft.)(F/in.)	C177 or C518	0.23 0.24 0.26	0.22 0.235 0.255	0.21 0.22 0.24	0.20 0.21 0.23
Thermal Resistance Values (R)*	at 25F at 40F at 75F	per inch	_ _ _	4.35 4.17 3.85	4.54 4.25 3.92	4.76 4.55 4.17	5.00 4.76 4.35
Strength Properties							
Compressive 10% Deformation		psi	D1621	10-14	13-18	15-21	25-33
Flexural		psi	C203	25-30	30-38	40-50	50-75
Tensile		psi	D1623	16-20	17-21	18-22	23-27
Shear		psi	D732	18-22	23-25	26-32	33-37
Shear Modulus		psi	_	280-320	370-410	460-500	600-640
Modulus of Elasticity		psi	_	180-220	250-310	320-360	460-500
Moisture Resistance							
WVT		perm. in.	E96	2.0-5.0	1.5-3.5	1.0-3.5	0.6-2.0
Absorption (vol.)		%	C272	less than 4.0	less than 3.0	less than 3.0	less than 2.0
Capillarity		_	_	none	none	none	none
Coefficient of Thermal Expansion		in./(in.)(F)	D696	0.000035	0.000035	0.000035	0.000035
Maximum Service Temperature		°F	_				
Long-term				167	167	167	167
Intermittent				180	180	180	180
Oxygen Index		Minimum %	D2863	24.0	24.0	24.0	24.0
Dimensional Stability		% Change	D2126	max. 2.0	max. 2.0	max. 2.0	max. 2.0
Bond Strength, lb/ft² shear							
with Portland Cement				830	830	830	830
with gypsum				510	510	510	510
Buoyancy, lb/ft³				60	60	60	60
Toxicity			Laboratory Reports	Approximately the same as burning wood, paper or cardboard			
Fungus & Bacterial Resistance			F.H.A. Test Procedures	Will not support bacterial or fungus growth; no food value.			

**'R' means resistance to heat flow. The higher the 'R' value, the greater the insulating power.*

Figure A-5: EPS insulation technical data sheet

HOHMANN & BARNARD, INC.
a MiTek company

Lox♦All® Truss Joint Reinforcement

120 Truss-Mesh

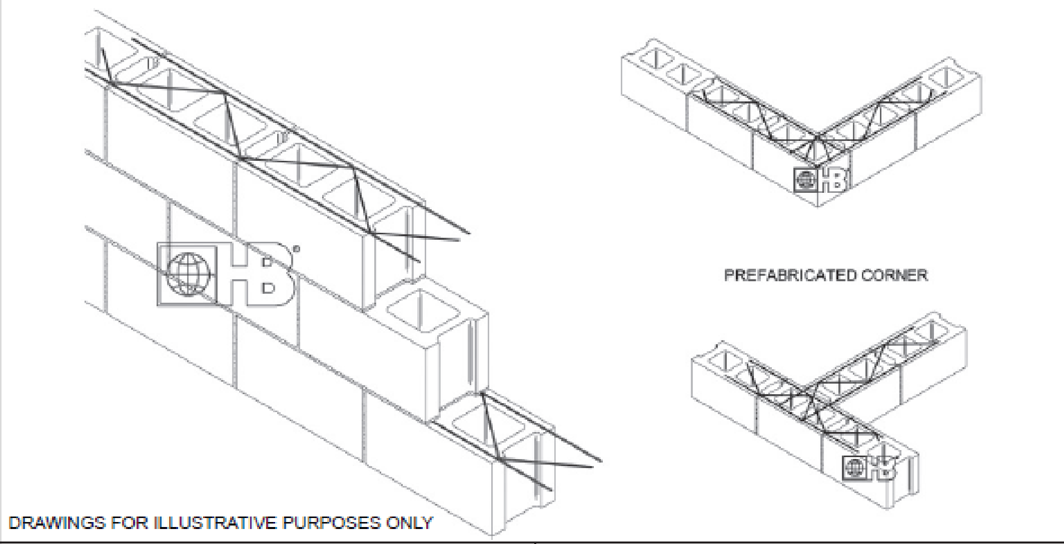

120 Truss-Mesh are continuous lengths of joint reinforcement that are embedded into the horizontal mortar joints of the masonry walls.

MATERIAL CONFORMANCE
Hohmann & Barnard joint reinforcement products conform to:
ASTM A951/A951M (Standard Specification for Steel Wire for Masonry Joint Reinforcement)
ACI / ASCE 530 (Building Code Requirements for Masonry Structures)

Wire (Carbon Steel): Prefabricated from cold-drawn steel wire conforming to **ASTM A1064/A1064M**
Tensile Strength - 80,000 p.s.i. | Yield Point - 70,000 p.s.i. minimum
Zinc Coating:
Mill Galvanized coating: **ASTM A641/A641M** (0.1 oz/ft²)
Available special order: **ASTM A641/A641M** (0.4 oz/ft²)
ASTM A641/A641M (0.8 oz/ft²)
Hot-Dip Galvanized after fabrication: **ASTM A153/A153M-B2** (1.5 oz/ft²)
Note: Hohmann & Barnard will certify to a minimum of 2.0 oz/ft²

Wire (Stainless Steel): **ASTM A580/ASTM A580M** - AISI Type 304
(Type 316 available on special order)

Wire Diameter:
9 gauge (.148" or W1.7) or 3/16"Ø (.187" or W2.8)
Side Rods and Cross Rods available in any combination of the above.
Cross Rods welded 16" O.C.

H&B manufactures steel wire products from a minimum of 95% recycled material.

Finishes:
- ☐ Mill Galvanized Coating
- ☐ Hot-Dip Galvanized
- ☐ Stainless Steel - Type 304
- ☐ Stainless Steel - Type 316

Note: **H&B recommends Stainless Steel for maximum protection against corrosion.**

Wire Size:
- ☐ (S) Standard Weight: 9 Gauge Side Rods x 9 Gauge Cross Rods
- ☐ (EH) Extra Heavy: 3/16" Side Rods x 9 Gauge Cross Rods
- ☐ (SHD) Super Heavy Duty: 3/16" Side Rods x 3/16" Cross Rods

Block Size:
☐ 4" ☐ 6" ☐ 8" ☐ 10"
☐ 12" ☐ 14" ☐ 16"

Standard Sizes: 4" wall - 16" wall. Other widths available on special request.

Note: State overall wall size and cavity or insulation thickness when ordering.

IMPORTANT: Since each construction project is unique, the appropriate selection and use of any product contained herein must be determined by competent architects, engineers and other appropriate professionals who are familiar with the specific requirements of the project in question.

HOHMANN & BARNARD, Inc.
30 Rasons Court | Hauppauge, NY 11788
CORPORATE HEADQUARTERS
T: 800.645.0616 F: 631.234.0683
www.h-b.com

Branch/Subsidiary Locations:
ALABAMA - ILLINOIS - MARYLAND
NEW YORK - PENNSYLVANIA - TEXAS
UTAH - CANADA

PRINT FORM
RESET FORM SAVE FORM
SAVE FORM LOCK & HIDE BUTTONS

Figure A-6 Lox all truss 120 truss-mesh data sheet

US008122662B2

(12) **United States Patent**
Farrell, Jr.

(10) **Patent No.:** **US 8,122,662 B2**
(45) **Date of Patent:** **Feb. 28, 2012**

(54) **LOW-COST, ENERGY-EFFICIENT BUILDING PANEL ASSEMBLIES COMPRISED OF LOAD AND NON-LOAD BEARING SUBSTITUENT PANELS**

(75) Inventor: **William J. Farrell, Jr.**, Anniston, AL (US)

(73) Assignee: **Met-Rock, LLC**, Anniston, AL (US)

(*) Notice: Subject to any disclaimer, the term of this patent is extended or adjusted under 35 U.S.C. 154(b) by 359 days.

(21) Appl. No.: **12/339,782**

(22) Filed: **Dec. 19, 2008**

(65) **Prior Publication Data**

US 2009/0094927 A1 Apr. 16, 2009

Related U.S. Application Data

(63) Continuation-in-part of application No. 10/696,583, filed on Oct. 30, 2003.

(60) Provisional application No. 60/422,089, filed on Oct. 30, 2002.

(51) **Int. Cl.**
E04B 5/00 (2006.01)

(52) **U.S. Cl.** **52/371**; 52/405.1; 52/676; 52/791.1

(58) **Field of Classification Search** 52/364, 52/366, 376, 388, 660, 676, 371, 375, 426, 52/384, 385, 386, 791.1, 405.1
See application file for complete search history.

(56) **References Cited**

U.S. PATENT DOCUMENTS

290,133 A	12/1883	Stanley	
1,597,507 A	8/1926	Benedict	
1,664,837 A	4/1928	Joseph	
1,932,276 A	10/1933	Joseph	
1,932,274 A	12/1933	Kublanow	
2,669,114 A	2/1954	Mills	
3,407,560 A	10/1968	Baumann	
4,104,842 A	8/1978	Rockstead et al.	
4,578,915 A *	4/1986	Schneller	52/309.12
4,611,450 A	9/1986	Chen	
4,660,342 A	4/1987	Salisbury	
5,540,023 A	7/1996	Jaenson	
6,272,805 B1	8/2001	Ritter et al.	
6,430,824 B1	8/2002	Smith	
6,718,712 B1 *	4/2004	Heath	52/309.12
6,820,387 B2	11/2004	Sacks et al.	

FOREIGN PATENT DOCUMENTS

JP	8-128154	5/1996

* cited by examiner

Primary Examiner — William Gilbert
(74) *Attorney, Agent, or Firm* — Cahn & Samuels, LLP

(57) **ABSTRACT**

This invention relates to building materials and methods. A building assembly for constructing a building includes load bearing structural panels joined and finished with a non-load bearing panels. The load bearing panels comprise a structural concrete insulating panel (SCIP) comprising a pair of wire mesh members sandwiching a middle member comprising polystyrene, wherein each of said wire mesh members defines two outwardly projecting screed ridges. The non-load bearing panels comprise a pair of fiber cement boards sandwiching a polystyrene core. The load bearing SCIP panel is placed in position and then the non-load bearing panel is positioned in a desirous location abutting the SCIP. The SCIP then receives a layer of cementitious material that is cut flat using the screed ridges. The assembled SCIP and non-load bearing composite is then finished with a final finishing layer so that the entire assembly has the same outer appearance.

11 Claims, 12 Drawing Sheets

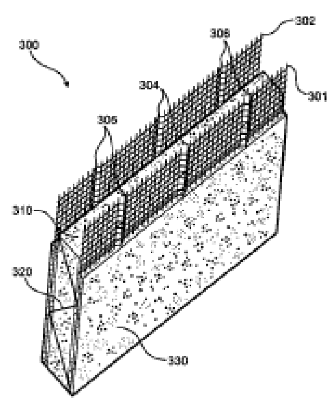

Figure A-9: Patent detail for rib guides MetRock SCIPs

Appendix B. Concrete Test Results

Table B-1: Concrete test result specimen A-1

A-1 pour (11/15/18)	I	II	III	IV	V	VI
Diameter (in)	4.01	4.01	3.97	4.00	3.99	3.98
Height (in)	7.95	7.93	7.87	7.95	8.00	7.98
Area (ft^2)	0.09	0.09	0.09	0.09	0.09	0.09
Area (in^2)	12.60	12.62	12.38	12.57	12.49	12.41
Volume (ft^3)	0.06	0.06	0.06	0.06	0.06	0.06
Weight (lbs)	7.78	7.76	8.14	7.71	7.99	8.12
Unit Weight (pcf)	134.17	134.03	144.39	133.36	138.18	141.78
Max load lbs	38270	38620	42810	106580.	102710	115000
Strength (psi)	3036	3061	3458	8481	8224	9266

Table B-2: Concrete test result specimen A-2

A-2 pour (11/19/18)	I	II	III	IV	V	VI
Diameter (in)	4.00	4.01	3.98	3.99	4.00	3.99
Height (in)	8.07	7.93	7.98	7.86	7.96	7.80
Area (ft^2)	0.09	0.09	0.09	0.09	0.09	0.09
Area (in^2)	12.55	12.63	12.41	12.51	12.59	12.50
Volume (ft^3)	0.06	0.06	0.06	0.06	0.06	0.06
Weight (lbs)	7.79	8.03	7.78	8.02	7.67	8.03
Unit Weight (pcf)	133.00	138.48	135.76	140.98	132.27	142.28
Max load lbs	53650	52810	46310	119000	93630	101100
Strength (psi)	4275	4181	3731	9514	7437	8085

Table B-3: Concrete test result specimen A-3

A-3 pour (11/28/18)	I	II	III	IV	V	VI
Diameter (in)	4.00	3.99	3.98	4.00	3.92	4.01
Height (in)	8.02	8.07	8.05	7.98	8.02	8.01
Area (ft^2)	0.09	0.09	0.09	0.09	0.08	0.09
Area (in^2)	12.57	12.47	12.44	12.57	12.04	12.63
Volume (ft^3)	0.06	0.06	0.06	0.06	0.06	0.06
Weight (lbs)	8.30	8.29	8.06	7.98	8.02	8.01
Unit Weight (pcf)	142.31	142.32	139.07	137.51	143.55	136.82
Max load (lbs)	42116	42780	66796	112680	107190	105150
Strength (psi)	3351	3430	5369	8966	8904	8325

Table B-4: Concrete test result specimen A-5

A-5 pour (12/06/18)	I	II	III	IV	V	VI
Diameter (in)	3.98	3.96	3.98	3.99	3.99	3.99
Height (in)	8.03	8.04	8.03	8.21	8.09	8.01
Area (ft^2)	0.09	0.09	0.09	0.09	0.09	0.09
Area (in^2)	12.44	12.30	12.44	12.53	12.50	12.47
Volume (ft^3)	0.06	0.06	0.06	0.06	0.06	0.06
Weight (lbs)	8.14	8.09	7.97	8.21	8.03	8.00
Unit Weight lb/ft^3	140.85	141.41	137.89	137.96	137.24	138.46
Max load lbs	45910	45400	43010	91470	91190	91420
Strength (psi)	3690	3690	3457	7302	7296	7329

Table B-5: Concrete test result specimen A-6

A-6 pour (12/13/18)	I	II	III	IV	V	VI
Diameter (in)	3.99	3.98	3.98	3.97	3.98	3.99
Height (in)	8.03	7.95	8.00	8.03	8.03	8.00
Area (ft^2)	0.09	0.09	0.09	0.09	0.09	0.09
Area (in^2)	12.50	12.44	12.41	12.38	12.42	12.51
Volume (ft^3)	0.06	0.06	0.06	0.06	0.06	0.06
Weight (lbs)	7.93	7.73	8.06	7.90	8.07	8.13
Unit Weight lb/ft^3	136.56	135.05	140.29	137.42	139.88	140.31
Max load lbs	40950	34850	36770	83610	103730	94950
Strength (psi)	3275	2801	2962	6754	8350	7588

Table B-6: Concrete test result specimen B-1

B-1 pour (12/18/18)	I	II	III	IV	V	VI
Diameter (in)	3.98	3.98	3.98	3.98	3.99	4.01
Height (in)	7.98	7.90	7.83	8.01	7.97	8.00
Area (ft^2)	0.09	0.09	0.09	0.09	0.09	0.09
Area (in^2)	12.41	12.46	12.46	12.44	12.47	12.60
Volume (ft^3)	0.06	0.06	0.06	0.06	0.06	0.06
Weight (lbs)	7.87	7.82	7.79	7.50	7.82	7.75
Unit Weight lb/ft^3	137.33	137.32	138.10	130.13	135.98	132.81
Max load lbs	43840	38140	39990	89710	93430	96510
Strength (psi)	3532	3061	3210	7210	7491	7657

Table B-7: Concrete test result specimen B-2

B-2 pour (01/11/19)	I	II	III	IV	V	VI
Diameter (in)	4.00	4.01	3.98	3.99	4.00	3.99
Height (in)	7.98	7.99	8.02	8.00	7.98	7.95
Area (ft^2)	0.09	0.09	0.09	0.09	0.09	0.09
Area (in^2)	12.57	12.60	12.45	12.50	12.57	12.50
Volume (ft^3)	0.06	0.06	0.06	0.06	0.06	0.06
Weight (lbs)	7.80	7.94	7.85	8.04	7.98	7.95
Unit Weight lb/ft^3	134.41	136.31	135.85	138.80	137.42	138.20
Max load lbs	53920	49670	51510	101160	97070	70890
Strength (psi)	4290	3942	4137	8090	7719	5669

Table B-8: Concrete test result specimen B-3

B-3 pour (01/14/19)	I	II	III	IV	V	VI
Diameter (in)	4.06	4.01	3.98	4.00	3.99	3.98
Height (in)	7.98	7.95	8.05	8.03	8.05	7.95
Area (ft^2)	0.09	0.09	0.09	0.09	0.09	0.09
Area (in^2)	12.96	12.61	12.44	12.58	12.48	12.46
Volume (ft^3)	0.06	0.06	0.06	0.06	0.06	0.06
Weight (lbs)	7.99	7.59	7.69	7.68	7.45	7.46
Unit Weight lb/ft^3	133.51	130.82	132.68	131.43	128.22	130.09
Max load lbs	38220	35270	36860	98130	89530	99300
Strength (psi)	2949	2796	2962	7799	7173	7966

Table B-9: Concrete test result specimen C-1

C-1 pour (01/23/19)	I	II	III	IV	V	VI
Diameter (in)	3.98	3.99	3.98	3.99	3.99	4.00
Height (in)	7.90	7.98	7.98	7.93	8.00	7.95
Area (ft^2)	0.09	0.09	0.09	0.09	0.09	0.09
Area (in^2)	12.47	12.52	12.47	12.50	12.49	12.57
Volume (ft^3)	0.06	0.06	0.06	0.06	0.06	0.06
Weight (lbs)	7.55	7.78	7.59	7.71	7.71	7.76
Unit Weight lb/ft^3	132.44	134.53	131.84	134.36	133.25	134.22
Max load lbs	37058	43957	44095	100710	103280	103390
Strength (psi)	2971	3510	3537	8054	8269	8227

Table B-10: Concrete test result specimen C-2

C-2 pour (01/28/19)	I	II	III	IV	V	VI
Diameter (in)	3.98	3.99	3.98	3.99	3.95	3.98
Height (in)	7.98	8.01	8.00	8.00	8.02	8.03
Area (ft^2)	0.09	0.09	0.09	0.09	0.08	0.09
Area (in^2)	12.44	12.47	12.46	12.47	12.24	12.44
Volume (ft^3)	0.06	0.06	0.06	0.06	0.06	0.06
Weight (lbs)	7.39	7.50	7.64	7.83	7.76	7.35
Unit Weight lb/ft^3	128.63	129.73	132.56	135.60	136.63	127.20
Max load lbs	34930	35870	35040	94810	95920	72840
Strength (psi)	2807.65	2875.97	2812.95	7601.65	7838.45	5854.82

Table B-11: Concrete test result specimen C-3

C-3 pour (02/01/19)	I	II	III	IV	V	VI
Diameter (in)	3.99	3.99	3.99	3.98	3.99	3.99
Height (in)	8.05	8.06	8.11	8.05	8.07	7.98
Area (ft^2)	0.09	0.09	0.09	0.09	0.09	0.09
Area (in^2)	12.49	12.50	12.50	12.41	12.47	12.49
Volume (ft^3)	0.06	0.06	0.06	0.06	0.06	0.06
Weight (lbs)	7.37	7.61	7.50	7.48	7.43	7.52
Unit Weight lb/ft^3	126.68	130.57	127.81	129.39	127.62	130.40
Max load lbs	33370	41310	39440	78380	74410	74890
Strength (psi)	2672	3303	3154	6315	5966	5996

Table B-12: Concrete test result specimen S-1

S-1 pour (04/25/19)	I	II	III	IV	V	VI
Diameter (in)	3.98	3.99	3.97	3.97	3.99	3.98
Height (in)	8.05	8.06	8.11	8.05	8.07	7.98
Area (ft^2)	0.09	0.09	0.09	0.09	0.09	0.09
Area (in^2)	12.44	12.50	12.38	12.38	12.50	12.44
Volume (ft^3)	0.06	0.06	0.06	0.06	0.06	0.06
Weight (lbs)	7.37	7.61	7.50	7.48	7.43	7.52
Unit Weight lb/ft^3	127.16	130.57	129.10	129.71	127.30	130.89
Max load lbs	48880	47200.00	55880	80050	81480	78530
Strength (psi)	3928	3774	4514	6466	6516	6312

Table B-13: Concrete test result specimen S-2

S-2 pour (04/25/19)	I	II	III	IV	V	VI
Diameter (in)	3.98	3.99	3.97	3.97	3.99	3.98
Height (in)	8.05	8.06	8.11	8.05	8.07	7.98
Area (ft^2)	0.09	0.09	0.09	0.09	0.09	0.09
Area (in^2)	12.44	12.50	12.38	12.38	12.50	12.44
Volume (ft^3)	0.06	0.06	0.06	0.06	0.06	0.06
Weight (lbs)	7.37	7.61	7.50	7.48	7.43	7.52
Unit Weight lb/ft^3	127.16	130.57	129.10	129.71	127.30	130.89
Max load lbs	48000	60170	50500	81500	79540	104300
Strength (psi)	3858	4812	4079	6583	6361	8383

Table B-14: Concrete test result for socket footing

Wall footing (03/28/19)	I	II	III
Diameter (in)	4.021	3.97235	3.97475
Height (in)	8.025	8.0251	7.975
Area (in^2)	12.69866	12.39324	12.40822
Max load lbs	132640	137940	135390
Compressive Strength (psi)	10445.19	11130.26	10911.31

Table B-15: Grout strength for specimen A-4

Grout A-4 (05/23/19)	I	II	III
Width (in)	2.030	2.040	2.080
Height (in)	2.000	2.050	2.020
Area (in^2)	4.060	4.182	4.202
Max load lbs	22190	22155	26390
Compressive Strength (psi)	5466	5298	6281

Table B-16: Grout strength for specimen A-5

Grout A-5 (04/29/19)	I	II	III
Width (in)	2.020	2.030	2.020
Height (in)	2.010	2.040	2.030
Area (in^2)	4.060	4.141	4.101
Max load lbs	23880	24430	22810
Compressive Strength (psi)	5881	5899	5563

Table B-17: Grout strength for specimen A-6

Grout A-6 (04/29/19)	I	II	III
Width (in)	2.020	2.025	2.026
Height (in)	1.979	2.025	1.979
Area (in^2)	3.998	4.101	4.008
Max load lbs	25070	24730	26390
Compressive Strength (psi)	6271	6031	6584

Appendix C. Slab Test Results

Table C-1:

A-1		A-2		A-3	
Load (lbs.)	Average mid-span (in)	Load (lbs.)	Average mid-span (in)	Load (lbs.)	Average mid-span (in)
0.0	0.00	0.0	0.00	0.0	0.00
754.7	0.01	976.2	0.01	1601.6	0.06
1189.7	0.02	1218.2	0.01	2119.6	0.08
1665.3	0.02	1815.0	0.02	2662.3	0.10
2284.7	0.03	2481.1	0.03	3086.3	0.11
2726.2	0.04	3358.5	0.04	3626.4	0.13
3319.6	0.05	4308.7	0.05	4113.2	0.14
3742.3	0.05	5335.0	0.07	4671.1	0.16
4268.8	0.06	5997.0	0.08	5220.0	0.18
4792.5	0.07	6852.9	0.10	5766.6	0.19
5415.9	0.08	7123.9	0.18	6243.6	0.20
5999.4	0.09	7667.6	0.43	6733.0	0.22
6367.5	0.09	8268.0	0.56	7045.8	0.23
6788.1	0.20	8341.6	0.58	7644.8	0.27
7740.2	0.41	8802.6	0.66	7956.7	0.29
8153.5	0.56	9223.3	0.72	8626.8	0.52
8601.9	0.62	9633.2	0.77	9043.7	0.68
9024.2	0.68	10214.5	0.87	9574.3	0.89
9521.3	0.76	10614.4	0.95	10023.0	0.96
10059.0	0.85	11087.7	1.03	10586.9	1.07
10302.5	0.91	11547.2	1.14	11066.8	1.16
11069.8	1.05	12085.7	1.36	11469.4	1.26
11545.6	1.21	12623.3	1.73	12022.0	1.47
12108.8	1.47	13167.0	2.55	12549.0	1.73
12507.7	1.80	13438.8	3.32	13005.8	2.20
12837.9	2.30	9834.5	4.24	13163.8	2.65
9040.6	2.91			10529.3	3.33

Table C-2: Backbone load-deflection data for medium span slabs

B-1		**B-2**		**B-3**	
Load (lbs.)	Average mid-span (in)	Load (lbs.)	Average mid-span (in)	Load (lbs.)	Average mid-span (in)
0.0	0.00	0.0	0.00	0.0	0.00
576.9	0.03	619.7	0.03	653.6	0.03
955.4	0.05	1085.0	0.05	1091.4	0.06
1579.6	0.09	1601.0	0.09	1620.3	0.08
2058.1	0.12	2105.0	0.13	2136.4	0.15
2577.8	0.15	2561.0	0.19	2601.9	0.19
3007.8	0.27	3019.0	0.30	3134.8	0.30
3527.1	0.43	3557.0	0.62	3521.6	0.60
4090.2	0.71	4010.0	0.84	4056.7	0.86
4587.4	1.08	4524.0	1.09	4503.7	1.10
5049.9	1.35	5081.0	1.46	5018.6	1.38
5414.3	1.97	5530.0	1.99	5607.7	1.93
4252.6	2.26	3668.0	2.27	4482.6	2.28

Table C-3Backbone load-deflection data for long span slabs

C-1		**C-2**		**C-3**	
Load (lbs.)	Average mid-span (in)	Load (lbs.)	Average mid-span (in)	Load (lbs.)	Average mid-span (in)
0.0	0.00	0.0	0.00	0.0	0.00
668.2	0.04	608.8	0.04	609.2	0.04
1045.2	0.11	1112.9	0.09	1123.7	0.10
1549.8	0.33	1557.5	0.16	1601.4	0.18
2026.9	0.74	2014.4	0.44	2041.1	0.38
2591.0	1.24	2522.7	1.22	2506.3	1.12
3002.3	1.70	3005.6	1.72	3048.1	1.70
3517.3	2.36	3509.9	2.35	3521.2	2.45
3588.7	2.87	3981.0	3.36	3824.3	3.44
2758.8	3.27	3153.3	4.34	3041.6	3.83

Table C-4: Backbone load-deflection data for modified long span slabs

S-1		**S-2**	
Load (lbs)	Average mid-span (in)	Load (lbs)	Average mid-span (in)
0.0	0.00	0.0	0.00
675.4	0.05	573.9	0.03
1157.9	0.10	1098.4	0.11
1612.7	0.18	1515.1	0.17
2007.5	0.28	2112.5	0.52
2547.5	0.76	2523.7	0.94
3004.9	1.05	3043.8	1.30
3584.4	1.39	3520.0	1.67
4064.7	1.67	4045.2	2.05
4537.7	1.96	4512.8	2.41
5085.8	2.33	4593.2	2.54
5576.0	2.80	5038.1	2.86
6034.7	3.84	5521.3	3.63
6547.0	6.11	6023.6	5.53
6819.0	8.84	6046.2	6.38
6630.0	9.30	5614.0	6.79
5844.2	9.45	2033.2	7.55
2499.3	11.08		

Table C-5: Backbone load-deflection data for wall specimen

A-4		A-5		A-6	
Deflection (in)	Load (lbs)	Deflection (in)	Load (lbs)	Deflection (in)	Load (lbs)
0	0	0	0	0	0
-0.04	-4384	-0.04	-4384	-0.04	-5181
-0.07	-8126	-0.08	-7717	-0.09	-7345
-0.13	-10309	-0.14	-9656	-0.14	-8736
-0.19	-12086	-0.20	-11334	-0.17	-9709
-0.31	-15021	-0.31	-14118	-0.25	-12067
-0.45	-17072	-0.61	-17578	-0.36	-14442
-0.60	-18176	-0.76	-18358	-0.49	-16315
-0.75	-18893	-1.06	-19561	-0.62	-17499
-1.04	-16944	-1.40	-17474	-0.89	-19155
-1.44	-7158	-1.81	-6474	-1.20	-17790
-1.81	-2772	-1.82	-2674	-1.74	-6738
0	0	0	0	-1.83	-4151
0.00	314	0.00	3590	-2.23	-3638
0.04	6433	0.02	5894	0.00	97
0.03	5344	0.08	8457	0.08	7251
0.04	7626	0.14	10248	0.12	8232
0.06	8568	0.20	11676	0.15	9174
0.15	11514	0.29	13892	0.22	11368
0.24	14112	0.38	15221	0.29	13287
0.35	15829	0.47	16202	0.39	15368
0.49	17052	0.58	16707	0.50	16791
0.77	17364	0.81	17405	0.73	18349
1.10	11507	1.34	13114	1.00	18106
1.66	4197	1.69	5031	1.43	9522
				2.00	4125

Appendix D. ACI 318-14 Calculations

Ultimate load carrying capacity for SCIP slabs
ACI 318-02
Assuming fully composite Section

Span	l =	119	in
28 days compressive strength	f'c =	8000	psi
Yield strength of steel	fy =	60000	psi
Distance to tension steel	d =	5.5	in
Distance to compression steel	d' =	0.5	in
Width	b =	49	in
Depth	h =	6	in
Modulus of Elasticity of Concrete	Ec =	5098235	psi
Modulus of Elasticity of Steel	Es =	29000000	psi
Modular ratio	n =	5.69	
Area of Tension Steel			
Diameter of 14-gauge wire mesh		0.08	in
Area of wire mesh x 49		0.246301	in^2
Diameter of longitudinal bars		0.1875	in^2
Area of 3/16" longitudinal bars.x. 9		0.276	in^2
Total area of tension steel	As =	0.522	in^2
Total area of compression steel	A's =	0.522	in^2

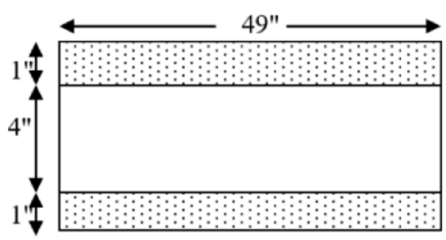

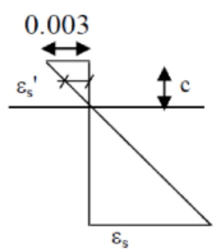

Treating the panel as a doubly reinforced beam

Compression (C)= C concrete +C steel

Where,

C concrete = 0. 85f'c.b. a — 0.85f'c.b= 333200

a = β1. c for f'c=8000psi — β1 = 0.65

C steel = A's.f's

$$\beta_1 = 0.85 - \left(\frac{f'_c - 4000 \text{ psi}}{1000}\right)(0.05) \geq 0.65$$

f's = Es. ϵ's

Assuming, the concrete cracked under compression

ϵc = 0.003 so using similar triangle:

$$\epsilon's = \frac{c-d'}{c}(0.003)$$

So, $f's = Es. ((c-d')*0.003/c)$
$C = (0.85f'c.b.a + A's.f's)$
Assuming the steel yeilds

$T = As.fy$	As.fy =	31345.04	

Now,

Equating Tension and Compression

$As.fy = 0.85.f'c.b.a + A's.f's$
$As.fy = 0.85.f'c.b.\beta1.c + (A's.Es.((c-d')*0.003/c)))$
Solving for c;

$31345.04 = 346800(0.65*c) + (0.522*29000000*((c-0.5)*0.003/c)))$

$31345.04*c = 225420*c^2 + 45414*c - 22707$
$22707 = 225420*c^2 + 14069*c$

	c =	0.292994	
	a =	0.190446	
Since ϵ's is negative the top steel is in tension too,	ϵ's =	-0.00212	
So,			
	f's =	-61467.3	psi
Moment Capacity (M)			
$0.85f'c.b.a(d-a/2)+A's*f's(d-d')$	M =	182411	lb-in
		15200.92	lb-ft
Now, subtracting the moment produced by self-weight			
Average weight for a 10' panel	Wt =	1302	lbs
Length of panel	Lp =	119	in
Average unit weight of panel per linear ft		10.94118	lb/in
		131.2941	lb/ft
Moment caused by self-weight	Msw	19367.25	lb-in
So, Effective Moment capacity:	Mn = M - Msw	163043.7	lb-in
So Effective load for a four-point bend test	Pn =	10960.92	lbs
	Pu =	9864.832	lbs

Ultimate load carrying capacity for SCIPS
ACI 318-02
Assuming non-composite Section

Span	l =	119	in
28 days compressive strength	f'c =	8000	psi
Yield strength of steel	fy =	60000	psi
Distance to tension steel	d =	0.5	in
Distance to compression steel	d' =	0	in
Width	b =	49	in
Depth	h =	3	in
Modulus of Elasticity of Concrete	Ec =	5098235	psi
Modulus of Elasticity of Steel	Es =	29000000	psi
Modular ratio	n =	5.69	
Area of Tension Steel			
Diameter of 14-gauge wire mesh		0.08	in
Area of wire mesh x 49		0.246	in^2
Diameter of longitudinal bars		0.1875	in^2
Area of 3/16" longitudinal bars.x. 9		0.276	in^2
Total area of tension steel	As =	0.522	in^2
Total area of compression steel	A's =	0.000	in^2
a=As. Fy/(0.85 f'c b)	a	0.0941	
Nominal moment for one wythe	Mn =	14198	lb-in
For two wythes	Mn =	28396	lb-in
		2366.3608	lb-ft
Now, subtracting the moment produced by self-weight			
Average weight for a 10' panel	Wt =	1302	lbs
Length of panel	Lp =	119	in
Average unit weight of panel per linear ft		10.941176	lb/in
		131.29412	lb/ft
Moment caused by self-weight	Msw =	19367.25	lb-in
So, Effective Moment capacity:	Mn = M - Msw	9029	lb-in
		752.42329	lb-ft
So, Effective load for four-point bend test	Pn=	607	lbs
	Pu =	1093	lbs

Ultimate load carrying capacity for long span SCIPs with unreinforced splice
ACI 318-02

Assuming fully composite section

Span	l =	215	in
28 days compressive strength	f'c =	8000	psi
Yield strength of steel	fy =	60000	psi
Distance to tension steel	d =	5.5	in
Distance to compression steel	d' =	0.5	in
Width	b =	48	in
Depth	h =	6	in
Modulus of Elasticity of Concrete	Ec =	5098235	psi
Modulus of Elasticity of Steel	Es =	29000000	psi
Modular ratio	n =	5.69	
Area of Tension Steel			
Diameter of 14-gauge wire mesh		0.08	in
Area of wire mesh x 49		0.246301	in^2
diameter of longitudinal bars		0.1875	in
Area of 3/16" longitudinal bars. (half the number of bars in the splice)		0.138	in^2
Total area of tension steel	As =	0.384	in^2
Total area of tension steel	A's =	0.384	in^2

Treating the panel as a doubly reinforced beam

Compression (C)= C concrete +C steel

Where,

C concrete = 0.85f'c.b.a	0.85f'c.b=	326400	
a = β1. c	β1 =	0.65	(f'c= 8000psi)

C steel = A's.f's

f's = Es. ϵ's

Assuming, the concrete cracked under compression

ϵc = 0.003 so using similar triangle:

So, f's= Es. ((c-d')*0.003/c)

C = (0.85f'c.b.a + A's.f's)

Assuming the steel yeilds

T = As.fy	As.fy =	23061.55

Now,

Equating Tension and Compression

As.fy = 0.85.f'c.b.a + A's.f's

As.fy = 0.85.f'c.b.β1.c + (A's.Es.((c-d')*0.003/c)))
Solving for c;
31345.04 = 346800(0.65*c) + (0.522*29000000*((c-0.5)*0.003/c)))
31345.04*c = 225420*c^2 + 45414*c- 22707
22707= 225420*c^2+14069*c

	c =	0.257331	
	a =	0.167265	
Since ϵ's is negative the top steel is in tension too,	ϵ's =	-0.00283	
So,			
	f's =	-82042.7	psi
Moment Capacity (M) = 0.85f'c.b.a (d-a/2)+A's*f's(d-d')		138039.5	lb-in
Total Moment capacity	Mt=	138039.5	lb-in
Now, subtracting the moment produced by self-weight			
Average weight for a 10' panel	Wt =	1302	lbs
Length of panel	Lp =	118	in
Average unit weight of panel per linear ft		11.0339	lb/in
		132.4068	lb/ft
Moment caused by self-weight	Msw	19204.5	lb-in
So, Effective Moment capacity:	Mn = M - Msw	118835	lb-in
So Effective load for a four-point bend test	Pmax	4421.767	lbs

Ultimate load carrying capacity for long span SCIP with splice reinforcement
ACI 318-02
Assuming fully composite Section

Span	l =	215	in
28 days compressive strength	f'c =	8000	psi
Yield strength of steel	fy =	60000	psi
Distance to tension steel	d =	5.5	in
Distance to compression steel	d' =	0.5	in
Width	b =	48	in
Depth	h =	6	in
Modulus of Elasticity of Concrete	Ec =	5098235	psi
Modulus of Elasticity of Steel	Es =	29E6	psi
Modular ratio	n =	5.69	
Area of Tension Steel			
Diameter of 14-gauge wire mesh		0.08	in
Area of wire mesh x 49		0.24630 1	in^2
diameter of longitudinal bars		0.1875	in
Area of 3/16" longitudinal bars. (half the number of bars in the splice)		0.138	in^2
Addition #3 rebar (7 bars)		0.770	in^2
Total area of tension steel	As =	1.154	in^2
Total area of tension steel	A's =	1.154	in^2

Treating the panel as a doubly reinforced beam
Compression (C)= C concrete +C steel
Where,

C concrete = 0.85f'c.b.a	0.85f'c.b=	326400	
a = β1. c	β1 =	0.65	(f'c= 8000psi)

C steel = A's.f's
f's = Es. ϵ's
Assuming, the concrete cracked under compression
ϵc = 0.003 so using similar triangle:
So, f's= Es. ((c-d')*0.003/c)
C = (0.85f'c.b.a + A's.f's)
Assuming the steel yields

T = As.fy	As.fy =	69261.5

Now,

Equating Tension and Compression

As.fy = 0.85.f'c.b.a + A's.f's

As.fy = 0.85.f'c.b.β1.c + (A's.Es.((c-d')*0.003/c)))

Solving for c;

31345.04 = 346800(0.65*c) + (0.522*29000000*((c-0.5)*0.003/c)))

31345.04*c = 225420*c^2 + 45414*c- 22707

22707= 225420*c^2+14069*c

	c =	0.41856	
	a =	0.27206	
Since ϵ's is negative the top steel is in tension too, So,	ϵ's =	-0.00058	
	f's =	-16927.5	psi
Moment Capacity (M) = 0.85f'c.b.a (d-a/2)+A's*f's(d-d')		378628	lb-in
Total Moment capacity	Mt=	378628	lb-in
Now, subtracting the moment produced by self-weight			
Average weight for a 10' panel	Wt =	1302	lbs
Length of panel	Lp =	118	in
Average unit weight of panel per linear ft		11.0339	lb/in
		132.406 8	lb/ft
Moment caused by self-weight	Msw	19204.5	lb-in
So, Effective Moment capacity:	Mn = M - Msw	359424	lb-in
So Effective load for a four-point bend test	Pmax	13373	lbs

Development length ACI equation 12-1	ld	11.3	in
cover distance	cb	0.5	in
	Ktr	0	
diameter of bar #3	db	0.375	
lambda	λ	1	
reinforcement location	Ψt	1	
coated factor	Ψe	1	
size factor	Ψs	0.8	

Appendix E. MATLAB Codes for Data Postpocessing

E.1. Data analysis for processing test results from slab testing

```
Function out=findlocalmaxpoint(data,load_col,exceloutputname)
%Input
%data =2D matrix
%exceloutputname = Name of excel file that output will be exported to

%Output
%load_max_value = local maximum load
%avg_midspan = average midspan
%RN
%index = index representing the datapoint with local maximum load
%matrix data = all outputs in matrix from
% 1st column = index
% 2nd column = RN
% 3rd column = load_max_value
% 4th column = avg_midspan

data_load=abs(data(:,load_col));% Choosing the column with load absolute values
dv=diff(data_load);% Taking difference between consecutive datapoints
lower_threshold=find(dv<=(-100));%Determing cutoff points where there is a maximum applied load drop off
load_lowthres=data_load(lower_threshold+1);% Extracting the load next to the drop off
upper_threshold=find(load_lowthres<=200);%Insuring the following point after the max drop off is within 100 lbs
n=length(upper_threshold);

%Pre-allocation
max_all=nan(n,1);
index_all=nan(n,1);
cutoff=zeros(n+1,1);
for k=1:n
cutoff(k+1)=lower_threshold(upper_threshold(k));
ind_range= cutoff(k)+1:cutoff(k+1);
dt=data_load(ind_range);
mv=max(dt);
ind=find(dt==mv);
max_all(k)=mv;
index_all(k)=ind_range(ind(1));
end
index_s=index_all(max_all>=500);
max_value=max_all(max_all>=500);
max_ind=find(max_value==max(max_value));
```

```
index=index_s(1:max_ind);
if max_value==max(data_load)
amax=max(data_load);
b=find(data_load==max(data_load));
beyond_b=data_load(b+1:end);
thres1=find(beyond_b<=0.80*amax);
%Output data (struct file)
out.load_max_value=[max_value(1:max_ind);beyond_b(thres1(1))];
midspan=data(b+1:end,:);
out.midspan1=[data(index,2);midspan(thres1(1),2)];
out.midspan2=[data(index,3);midspan(thres1(1),3)];
out.index=[index;b+thres1(1)];
out.matrixdata=[out.index,out.load_max_value,out.midspan1,out.midspan2];
xlswrite(exceloutputname,[{'Index','Load','MS1','MS2'};num2cell(out.matrixdata)]);
else
amax=max(data_load);
b=find(data_load==max(data_load));
beyond_b=data_load(b+1:end);
thres1=find(beyond_b<=0.80*amax);
%Output data (struct file)
out.load_max_value=[max_value(1:max_ind);amax;beyond_b(thres1(1))];
midspan=data(b+1:end,:);
out.midspan1=[data(index,2);data(b,2);midspan(thres1(1),2)];
out.midspan2=[data(index,3);data(b,3);midspan(thres1(1),3)];
out.index=[index;b;b+thres1(1)];
out.matrixdata=[out.index,out.load_max_value,out.midspan1,out.midspan2];
xlswrite(exceloutputname,[{'Index','Load','MS1','MS2'};num2cell(out.matrixdata)]);
end

end
```

E.2. Data analysis for processing test results from cyclic wall testing

```
% Data Analysis
Data2
ydata = data(:,1);
 xdata = data(:,2);

% Loop Separation:
m = 0;% Data counter for each loop
n = 1;% Loop counter
for i = 2:length(data)% Loop for all data
    if xdata(i-1)<=0 && ydata(i-1)>=0 && xdata(i)>=0% Separation loop condition
        n = n+1;% If above cond. is true, one loop will be created
        m = 0;% Reset the data counter per each loop
    end

    m = m+1;% If above cond. is true, m will be restarted from 1
    x{m,n} = xdata(i);% Saving each loop in separation column of cell variable
    y{m,n} = ydata(i);% "
end


% Plot the results:
figure
hold on
title(['F-D Hysteresis for ' num2str(n) ' loop(s)'])
ylabel('Load Per UFP')
xlabel('Displace')

for i = 1:n % Plot n loops
    plot(cell2mat(x(:,i)),cell2mat(y(:,i)))% To plot we have to change cell variable to matrix arrey
    area(i) = polyarea(cell2mat(x(:,i)),cell2mat(y(:,i)));% Using polyarea to calculate area in each
loop
    disp(['Area for loop # ' num2str(i) ': ' num2str(area(i))])% Display results in command window
    Legend{i} = ['Area for loop # ' num2str(i) ' : ' num2str(area(i))];% Saving strings for legend
    legend(Legend,'FontSize',8)% Printing strings of legend in current figure
%%%     legend(Legend,'NumColumns',2)% For upper version of MATLAB
%%%     pause(0.5)% Using some delay in each loop to observe the result grafically
end

% Plot bar chart for each area
figure% Open another figure
bar(area)
title('Area for each loop')
xlabel('Number of Loop')
ylabel('Area')
```

```
%==================================================================
===

% Finding the sharp points:
for i = 1:n
   x_up(i)   = max(cell2mat(x(:,i)));
   x_down(i) = min(cell2mat(x(:,i)));
   y_up(i)   = max(cell2mat(y(:,i)));
   y_down(i) = min(cell2mat(y(:,i)));
end
% We omit the first loop because of wrong data:
% x_down(1)=[];
% y_down(1)=[];
% Rename:
delta_m      = x_up;
F_m          = y_up;
% Integrating sharp points:
x_integrated = [x_down x_up];
y_integrated = [y_down y_up];
% Resorting data
x_integrated = sort(x_integrated);
y_integrated = sort(y_integrated);
xlswrite('Just_Data',[x_integrated' y_integrated']);
 x_fit = linspace(min(x_integrated),max(x_integrated));
y_fit = polyval(data_fit_3rd,x_fit);
figure
subplot(2,2,1)
plot(x_integrated,y_integrated,'-o')
title('Just Data')
ylabel('Load Per UFP')
xlabel('Displace')
subplot(2,2,2)
plot(x_integrated,y_integrated,'o',x_fit,y_fit)
title('Fitting a 3rd order Polynomial')
ylabel('Load Per UFP')
xlabel('Displace')
x_integrated = smooth(smooth(x_integrated));
y_integrated = smooth(smooth(y_integrated));
% Fit a third order polynomial on integrated data
data_fit_3rd = polyfit(x_integrated,y_integrated,3);
% Plot and Fit the integrated data
x_fit = linspace(min(x_integrated),max(x_integrated));
y_fit = polyval(data_fit_3rd,x_fit);
plot(x_integrated,y_integrated,'o',x_fit,y_fit)
title('Fitting a 3rd order Polynomial with Smoothing')
```

```
ylabel('Load Per UFP')
xlabel('Displace')

% Calculating Delta area Based:
delta_area_based = area ./ (2*pi * F_m .* delta_m);
subplot(2,2,4)
bar(delta_area_based)
title('\delta_a_r_e_a_-_B_a_s_e_d')

% Writing as an Excel File:
C(1,1) = {'Area'};
C(1,2) = {'Fm'};
C(1,3) = {'Delta'};
C(1,4) = {'Delta Area Based'};

for i = 1:length(area)
   C(i+1,1) = {area(i)};
   C(i+1,2) = {F_m(i)};
   C(i+1,3) = {delta_m(i)};
   C(i+1,4) = {delta_area_based(i)};
end
xlswrite('area_data',C);
% D(1,1) = {'Load per UFP'};
% D(1,2) = {'Displace'};
% D(1,3) = {'Area'};
% for i = 1:length(x)
%     D(i+1,1) = {x(i)};
%     D(i+1,2) = {y(i)};
%     D(i+1,3) = {area(i)};
% end
xlswrite('Load_Displace',[x y]);
xlswrite('Area',area');
% Creartion a Table:
Area = area';
Fm   = F_m';
Delta= delta_m';
Delta_Area = delta_area_based';
T = table(Area,Fm,Delta,Delta_Area);
disp(T)
```